

## PROMICE 2007-2010

### Final report for the establishment phase of the Programme for Monitoring of the Greenland Ice Sheet

Andreas P. Ahlstrøm, Dirk van As, Michele Citterio,  
Signe Bech Andersen, Faezeh Maghami Nick,  
Peter Gravesen, Karen Edelvang,  
Robert Schjøtt Fausto, Morten Langer Andersen,  
Steen Savstrup Kristensen,  
Erik Lintz Christensen,  
John P. Merryman Boncori, Jørgen Dall,  
Rene Forsberg, Lars Stenseng,  
Susanne Hanson, Dorthe Petersen  
& Marianne B. Wiese



## PROMICE 2007-2010

### Final report for the establishment phase of the Programme for Monitoring of the Greenland Ice Sheet

Andreas P. Ahlstrøm<sup>1</sup>, Dirk van As<sup>1</sup>, Michele Citterio<sup>1</sup>,  
Signe Bech Andersen<sup>1</sup>, Faezeh Maghami Nick<sup>1</sup>,  
Peter Gravesen<sup>1</sup>, Karen Edelvang<sup>1</sup>,  
Robert Schjøtt Fausto<sup>1</sup>, Morten Langer Andersen<sup>1</sup>,  
Steen Savstrup Kristensen<sup>2a</sup>,  
Erik Lintz Christensen<sup>2a</sup>,  
John P. Merryman Boncori<sup>2a</sup>, Jørgen Dall<sup>2a</sup>,  
Rene Forsberg<sup>2b</sup>, Lars Stenseng<sup>2b</sup>,  
Susanne Hanson<sup>2b</sup>, Dorte Petersen<sup>3</sup>  
& Marianne B. Wiese<sup>1</sup>

<sup>1</sup> GEUS – Geological Survey of Denmark and Greenland, Øster Voldgade 10, DK-1350 Copenhagen

<sup>2a</sup> DTU Space, Ørstedes Plads, Bldg. 348, DK-2800 Lyngby

<sup>2b</sup> DTU Space, Juliane Maries Vej 30, DK-2100 Copenhagen

<sup>3</sup> ASIAQ – Greenland Survey, P.O. Box 1003, Qatserisut 8, DK-3900 Nuuk, Greenland

# Contents

<b>Contents</b>	<b>3</b>
<b>Introduction</b>	<b>6</b>
<b>Automatic weather stations</b>	<b>10</b>
Purchase and calibration of instruments .....	10
Assembling and testing automatic weather stations .....	11
Development of the ablation assembly .....	15
Development of data transmission by satellite .....	18
Data transmission cost analysis .....	22
Hardware and software implementation .....	24
<b>Data</b>	<b>27</b>
Database development .....	27
PROMICE database .....	28
Data treatment and success rate .....	43
<b>Fieldwork</b>	<b>51</b>
Placing transects of automatic weather stations on the ice sheet .....	51
Performing maintenance on transects of automatic weather stations .....	53
Development of a new calving model for numerical ice flow modelling .....	56
Improvement of a new air temperature parameterization .....	60
Development of a surface melt model .....	79
<b>Optical remote sensing and glacier mapping</b>	<b>81</b>
Background .....	81
Glacier mapping overview .....	81
<b>Airborne survey of ice sheet elevation and thickness</b>	<b>92</b>
GPS data .....	93
Lidar data .....	93
Data acquisition and processing - Ice-sheet bottom echo .....	93
Ice surface elevation, ice thickness and bottom elevation .....	94
<b>Ice sheet velocity mapping</b>	<b>97</b>
Objectives and Planning .....	97
Processing chain overview .....	97
Development data set .....	99
Processing Chain Performance on the Development Data Set .....	101
Software validation .....	116
Operational measurements .....	122
Data acquisition strategy .....	128

<b>Outlet glacier monitoring</b>	<b>130</b>
Methods for monitoring glacier velocity .....	130
The EIS system in Greenland .....	131
<b>Outreach</b>	<b>135</b>
Media strategy .....	135
Webpage & online social media .....	136
E-learning initiatives .....	136
<b>Research education</b>	<b>138</b>
Abstract from PhD thesis: Robert S. Fausto .....	138
Surface melt, dynamics and seismicity at Helheim Glacier, East Greenland .....	139
Modelling Hydrology of the Greenland Ice Sheet .....	139
Mass balance on A.P. Olsen Ice Cap .....	140
Sermilik Field Course .....	140
<b>Scientific publications &amp; presentations</b>	<b>141</b>
Scientific activities .....	141
Contribution to SWIPA.....	141
<b>Collaborative activities</b>	<b>142</b>
Greenland Ecological Monitoring (GEM).....	142
Ice2sea .....	142
Stability and Variations of Land Ice (SVALI) .....	144
Greenland Analogue Project (GAP) .....	145
FreshLink.....	145
ImGlaCo.....	145
SEDIMICE .....	145
Greenland Climate Network (GC-Net) .....	146
Global Land Ice Measurements from Space (GLIMS).....	147
World Glacier Monitoring System.....	147
GlobGlacier - Glacier Monitoring Service using Data from Space.....	148
<b>Conclusion &amp; Outlook</b>	<b>149</b>
<b>References</b>	<b>155</b>
<b>Appendix A – PROMICE in the public arena</b>	<b>163</b>
<b>Appendix B – Science from the PROMICE team</b>	<b>169</b>
Scientific publications with international peer-review.....	169
Scientific presentations & abstracts at conferences .....	171
Reports .....	177



# Introduction

During the writing Fourth Assessment Report of the Intergovernmental Panel on Climate Change, observations of the most significant outlet glaciers of the Greenland Ice Sheet rapidly changed the outlook in a dramatic way (IPCC, 2007). The ice sheet models delivering the forecast on the ice sheet contribution to global sea level change proved insufficient and unable to reproduce the events taking place. The opening remarks of the chapter '4.6 Changes and Stability of Ice Sheets and Ice Shelves' in the report reveals the frustration:

*'New and improved observational techniques, and extended time series, reveal changes in many parts of the large ice sheets. Greenland has experienced mass loss recently in response to increases in near-coastal melting and in ice flow velocity more than offsetting increases in snowfall.'*

*(IPCC 2007, Ch.4.6)*

...and concluding:

*'Until recently (including IPCC, 2001), it was assumed that velocities of these outlet glaciers and ice streams cannot change rapidly, and impacts of climate change were estimated primarily as changes in snowfall and surface melting. Recent observations show that outlet glacier and ice stream speeds can change rapidly, for reasons that are still under investigation. Consequently, this assessment will not adequately quantify such effects.'*

*(IPCC 2007, Ch.4.6.1)*

Indeed, the tabulated values for the contribution of land ice masses to sea level rise were cut at the year 2003. For the ice sheet mass loss after this year, disagreement between scientists made reaching an authoritative statement impossible.

The important lesson from this is that observations prevail when it comes to increasing our understanding of a physical system as complicated as the interaction between climate and ice sheets. Observational evidence is now forcing the ice sheet modelling community to develop more advanced models for predictive purposes, eventually providing more reliable estimates of sea level change.

Lately, observations of surface melt on the Greenland Ice Sheet has provided a similar shift in our perception, showing the sensitivity of the mass loss to changing atmospheric circulation patterns that are possibly connected to the shrinking summertime extent of the sea ice in the Arctic Ocean (Box et al., 2010; Serreze et al., 2011). Again, observational evidence proves to be the driving force.

Parallel to these events, the Arctic Monitoring and Assessment Programme (AMAP) under the Arctic Council steadily increased the focus on Arctic climate change, publishing the Arctic Climate Impact Assessment (ACIA, 2005) together with the sister organization the

Conservation of Arctic Flora and Fauna (CAFF) and the non-governmental International Arctic Science Committee (IASC).

At the Arctic Council meeting in Reykjavik, Iceland in November 2004, the Ministers addressed the matter of Arctic climate change and variability by endorsing the ACIA policy recommendations for mitigation, adaptation, research, monitoring and outreach contained in the report of the Senior Arctic Officials to the Ministers.

The report of the Senior Arctic Officials specifically recommended to the Ministers that the member states would:

- *Encourage relevant national and international research bodies and sponsors to take into account the ACIA science recommendations in the planning, development and implementation of their programmes.*
- *Seek to expand and link circumpolar research and monitoring networks [...]*
- *Seek to ensure that relevant data from research, observation, monitoring and modelling activities are made available to local, national and international research and monitoring programmes.*

*(ACIA Policy Document, 2004)*

In 2007, the then Danish Minister of the Environment and Climate, Connie Hedegaard, took an important step towards implementing the recommendations endorsed in the ACIA Policy Document by initiating the Programme for Monitoring of the Greenland Ice Sheet (PROMICE).

PROMICE was envisioned as a Danish contribution to the Arctic Monitoring and Assessment Programme under the Arctic Council in response to the recommendations of the ACIA Policy Document and the later ACIA follow-up recommendations by the AMAP Expert Group on Climate and UV.

PROMICE has now been established as an on-going effort to assess changes in the mass budget of the Greenland Ice Sheet and is operated by the Geological Survey of Denmark and Greenland (GEUS) in collaboration with the National Space Institute (DTU Space) and the Greenland Survey (Asiaq).

Specifically, PROMICE aims to estimate the mass loss derived from three fundamentally different sources:

- Surface meltwater runoff from the ice sheet margin
- Iceberg discharge and submarine melt from ice sheet outlet glaciers
- Mass loss of individual glaciers and ice caps surrounding the ice sheet

The first is accomplished through a combination of observations from a network of automated climate stations on the ice sheet surface and numerical modelling of the melt processes.

The second is obtained by establishing a so-called 'flux gate' along the entire ice sheet margin and then keeping track of the ice passing through this gate. The flux gate is estab-

lished from airborne surveys of ice sheet elevation and thickness, which are repeated as the elevation might change. The volume of the ice passing through the gate is derived from maps of the surface velocity of the ice sheet, produced from satellite radar images with *in situ* GPS data from selected outlet glaciers providing the temporal variability.

The third is investigated through regular mapping of area and elevation, combined with mass balance modelling designed for disperse ice masses – a daunting task considering the approx. 20,000 individual glaciers and ice caps in Greenland. Mapping is carried out using recent, primarily optical, satellite imagery as well as aerial orthophotos. Comparison of maps from different years allows an estimate of the mass loss over time.

Apart from these primary goals, PROMICE is committed to maintain an accessible, safe and thoroughly documented database for storing and delivering the data. This is one particular aspect in which a monitoring programme like PROMICE differs significantly from regular research projects. Building and running such a database requires an existing framework, which GEUS can deliver through its Geological Data Centre as it is already the national database for a range of geological, geophysical and hydrological data.

Additionally, PROMICE is dedicated to outreach, disseminating knowledge and inspiration to the public at all levels right from primary school pupils to politicians, inquisitive journalists and fellow scientists. This dedication reaches beyond the programme itself, as the PROMICE team has successfully pursued and attracted nearly 1 mio. DKK in additional funding specifically for outreach projects, with a focus on e-learning for school children.

This report documents the initialization phase of PROMICE over the years 2007-2010. It thus describes the beginning of the road from a vision towards a useful tool for policy-making and science. As is always the case with monitoring programmes, the real value of PROMICE will manifest itself in the long run. The acquisition and storage of data, however essential these may be, is never central to regular research projects. On the other hand, as is evident from the opening quotes to this introduction, research into a system as complex as the interaction between climate and ice sheet without a substantial body of observational data is inherently at risk of not catching the physical mechanisms at work.

The foremost achievement of PROMICE is thus to gather crucial data that may be utilized in the work of the entire global research community. The secondary obligation is to provide a scientifically sound estimate on the mass loss of the Greenland Ice Sheet, based on observational evidence and modelling forced by observations. In doing so, we build and maintain important national scientific expertise on a subject of considerable interest to a low-lying country as Denmark, namely the ice sheet contribution to global sea level rise.

The implications are global though, and with an increasing awareness of the connection between climate change and security, PROMICE will strengthen our ability to identify and mitigate future potential conflicts. Recently, some focus has been given on the expected sea level rise by the year 2100. However, sea level change from melting land ice masses and thermal expansion of ocean water is *not* going to stop by 2100, but will most likely continue for centuries on. This raises issues for the survival of entire countries, such as Bangladesh or the Maldives and lends little confidence in the long term future of coastal

cities like Shanghai, Miami or Copenhagen. More than 10% of the Earth's population is estimated to live in the low elevation coastal zone defined as land below 10 metres elevation and within 100 km of the coast – a population likely to be vulnerable to a direct and significant impact from a sea level rise of a few metres (McGranahan et al., 2007).

Greenhouse gas levels in the atmosphere are already very high compared to the last million years and, given current policies, we are not likely to reduce emissions significantly in the near future. PROMICE will help us understand the implications of this and what might become the future we will have to adapt to. As a country, and indeed as a global society, we need to make difficult decisions. The mission of PROMICE is to make sure that those be educated decisions.

The Programme for Monitoring of the Greenland Ice Sheet is funded by the Danish Cooperation for Environment in the Arctic (DANCEA) and the Geological Survey of Denmark and Greenland (GEUS). The DANCEA funds made available for PROMICE are administered by the Danish Energy Agency under the Ministry of Climate and Energy.

# Automatic weather stations

## Purchase and calibration of instruments

One of the first tasks in PROMICE was to ensure the establishment of a network of automatic stations, measuring weather and ice-sheet surface mass balance. The glaciology group at GEUS already had a long experience in building and maintaining such stations, but the whole production line and maintenance plan was revised to facilitate the larger scale of the new monitoring programme. At GEUS, a technician was allocated a full-time position to form the backbone of this part of PROMICE. Thus we now have a flowing work plan for purchase of parts and instruments, modification of instruments, assembly of stations, testing of modified instruments, programming of data loggers, testing of complete stations set-ups and finally shipment to relevant ports or airports in Greenland. A list of suppliers complete with personal contacts is part of the common project space. During the first years of PROMICE a MS Access database (GlacioBase) was used to keep track of all instruments and meta-data, but this task is currently performed by our new central PROMICE database (see Section on the PROMICE database).

Each sensor on the PROMICE stations either outputs useable physical quantities, or is provided with calibration coefficients by the manufacturer. The only sensor we determine an extra set of calibration coefficients for before placing it in the field, is for the pressure transducer assembly. This is because we use the transducer in different conditions than it was designed for (i.e. in an anti-freeze mixture in a hose drilled into ice, as opposed to in water) and because there are reports of pressure transducer output being subject to a substantial drift.

Recalibration of all sensors is performed upon return. Sensors that have been damaged in the field or are suspected to give unreliable results are shipped back to the manufacturer for repair and recalibration. The remainder of the sensors will be recalibrated by GEUS personnel. Whereas the air pressure, humidity, ablation / surface height, tilt, and orientation can be checked and/or recalibrated at GEUS, the radiation, wind, and temperature sensors require placement outdoors to capture the atmosphere's variability. We are developing a set-up at a test site of the Danish Meteorological Institute, at which we can install multiple identical sensors simultaneously to compare readings. Wind speed sensors (which will have the bearings in the propeller shaft replaced at GEUS) and temperature sensors will be compared to the high-quality DMI data and either considered functional or send to the manufacturer. The radiation sensors will also undergo intercomparison with DMI data, with the goal to produce new calibration coefficients. If the automatic measurement frequency of the test set-up is high enough (for instance measuring every five minutes), one week of testing will suffice.

Table 1 gives an overview of the sensors, with the intended frequency of recalibration. The recalibration frequency is strongly dependent on the frequency of the station visits. If a station cannot be visited due to financial, logistical, or other reasons in the year that one or more sensors need recalibration, the recalibration will be delayed until the next visit.

Measured parameter	Sensor	Calibration frequency	Place of calibration	Method
Radiation	Kipp & Zonen CNR4	Every 2 years	Denmark, outdoors	Determining new coefficients
Wind	Young	Every 2 years	Denmark, outdoors	Check of accuracy
Temperature	Rotronic MP100H	Every 3 years	Denmark, outdoors	Check of accuracy
Humidity	Rotronic Hy- groClip	Every year	GEUS	Digital recalibration
Ablation	Ørum & Jensen NT1400	When melted out (>2 years)	GEUS	Determining new coefficients
Surface height	Campbell SR50	Every 3 years	GEUS	Check of accuracy
Ice tempera- ture	GEUS	When melted out (>1 year)	GEUS	Check of accuracy
Tilt	HL-Planar NS25/E2	Every 3 years	GEUS	Determining new coefficients
Orientation	In development	Every 3 years	GEUS	Check of accuracy
Air pressure	Campbell CS100	Every 3 years	GEUS	Check of accuracy

**Table 1.** Calibration plan for the sensors mounted on the stations.

## Assembling and testing automatic weather stations

After the equipment needed to build a weather station has arrived, we start the construction process. First step is to produce a set of steel wiring for the aluminum tripod. The tripod with all components (wires, shackles, kee clamps, wire tightener, etc.) is then constructed in the GEUS courtyard for testing purposes.



**Figure 1.** *Wiring of instruments, power and data transmission in the GEUS Glaciology Workshop.*

The sensors, battery enclosure, solar panel, Iridium antenna, and logger enclosure are wired up in the technician's office (see Figure 1). It takes a few days to wire up all equipment for one AWS. Most time-consuming to construct is the logger enclosure (see Figure 2). Also a considerable amount of time needs to be spent on the Rotronics assembly, which holds the temperature and relative humidity sensors, the thermistor string, and the pressure transducer assembly. The thermistor string is equipment that needs to be made to our exact specifications and up to this moment cannot be ordered from elsewhere. The thermistor string is thus custom-built from raw materials at GEUS. For the details of its construction, see Table 2. The construction of the pressure transducer assembly involves inserting the pressure transducer and wire in the hose, sealing it at the bottom with a weight, attaching a T-piece at the top end, connecting a plug and overflow bladder, and filling the system with an antifreeze mixture. Hereafter, the pressure transducer output is calibrated as mentioned in the previous section.



**Figure 2.** A look inside a data logger enclosure. Some instruments, such as the GPS and the barometer are actually inside the enclosure. The white bags contain dessicant to remove humidity inside the box, which could otherwise cause problems with the electronics.

1. Cut 10-string cable in 15 meter pieces.
2. Make 7-8 cm incisions where thermistors will be placed (8 in total, at 1, 2, 3, 4, 5, 6, 7 and 10 m depth), the 'lowest' at 10-20 cm from the end.
3. Cut the appropriate colored wire about halfway in each incision of the cable (orange, black, blue, yellow, green, brown, pink, violet). Cut away 'lower' part of the wire. The grey wire is not used, white is ground.
4. Remove 5-7 mm of coating from the end of the colored wires.
5. Remove about 1 cm of coating from the (uncut) white wire in every incision.
6. Place heat-shrinking tube around the loose end of a colored wire - this will prevent the two ends of the thermistor from touching. Don't shrink yet.
7. Twist one end of a thermistor around the bare end of a colored wire and solder it stuck.
8. Slide the heat-shrinking tube over the bare metal of the wire and thermistor and apply heat to fix it. Don't put too much heat on the thermistor itself!
9. Twist the other end of the thermistor around the uncoated part of the white wire and solder it to it.
10. Use some normal tape to prevent the thermistor from sticking out of the cable too much and getting damaged.
11. Repeat steps 6 to 10 for all incisions.
12. Make a mark for instance 20 cm next to each thermistor to be able to know their exact location after covering them up.
13. Cut heat-shrinking tube, diameter approx. 1 cm, in 15 cm pieces, one to cover every incision.
14. Slide these over the cable and fix partly directly over every incision by applying heat to one end. Shrink 2-3 cm. Be careful not to apply heat too long; this could damage the coating of the cable.
15. Prepare the glue. Don't touch, use gloves.
16. Fill the heat-shrinking tube with glue to 2-3 cm from the top using for instance a big syringe. Make sure no air is left inside.
17. Shrink the other end of the heat-shrinking tube. Glue might flow out and things will get messy.
18. Repeat steps 16 and 17 for the entire string, or do several thermistors simultaneously. You have 30-45 minutes before glue becomes inconveniently thick.
19. Leave thermistor string to dry for at least one night.
20. Determine the positions of the thermistors using the markings that you made.
21. Use these to determine where to place the piece of tape identifying the initial ice/snow surface during installation in the field (i.e. 1 meter above the first thermistor).
22. Put a 9-pole plug (preferably filled with silicone gel) on the top-end of the cable. Pin 1 = orange, 2 = black, ..., 8 = violet, 9 = white. No grey.
23. Place a piece of tape with the serial number of the thermistor string near the plug.
24. Close the bottom of the string using a heat-shrinking cap.
25. Attach ~4 cm cylindrical metal weight to the bottom of the string by filling it with silicone gel and pushing in the cable end. Let dry. Weight doesn't need to be too heavy.

**Table 2.** *Details of the thermistor string production.*

Before shipment, all sensors and other equipment for a station are mounted on a test tripod on the GEUS roof (see Figure 3). The new station is left running for a few days. If all systems are functional, the station is taken down and put in boxes for shipment to Greenland.



**Figure 3.** *Test tripod on the roof of GEUS.*

## **Development of the ablation assembly**

The GEUS ablation assembly is a 25 m long liquid-filled hose with a pressure transducer at the end/bottom. The sensor cable runs through the hose until it exits through a water-tight connection and is connected to the data logger of the automatic weather station. A liquid-filled bladder of a few litres at the beginning/top of the hose makes sure that volume changes in the liquid or the hose itself, by solar heating for instance, does not lead to an unrealistic increase in pressure in the assembly (see Figure 4). The hose is drilled into the ice up to 20 m depth. The pressure signal recorded by the transducer in the ice is that of the vertical column of liquid over the sensor. This signal can be translated into depth knowing the density of the liquid in the hose. As, over the years, the ablation assembly melts out of the ice (in the ablation zone), an increasingly large part of the hose will be found on the ice surface, and the vertical column of liquid in the hose will get smaller. This reduction in pressure gives us the amount of ice that has melted away over the period.

By measuring at (sub-)daily timescales this assembly is well-suited to monitor ice ablation in remote regions, with clear advantages over other well-established methods of measuring ice ablation in the field. For instance, stake readings provide accurate information on surface height change, but form a low-frequency record as readings can

only be done when the stakes are visited. Sonic ranger observations do give a continuous record of surface height, but the quality of the readings from these sensors reduces in time as they degrade due to continuous cycles of moisture freezing on and melting off them. A larger problem is that sonic rangers need to be mounted on stake assemblies drilled into the ice. After a single year of melt these stake assemblies can be melted out as much as six meters, often causing them to collapse during strong wind events. In theory, the pressure transducer ablation assembly can measure at high frequency, and keep on doing so until it has melted out of the ice – which can be several years, depending on drill depth and local ablation rate.

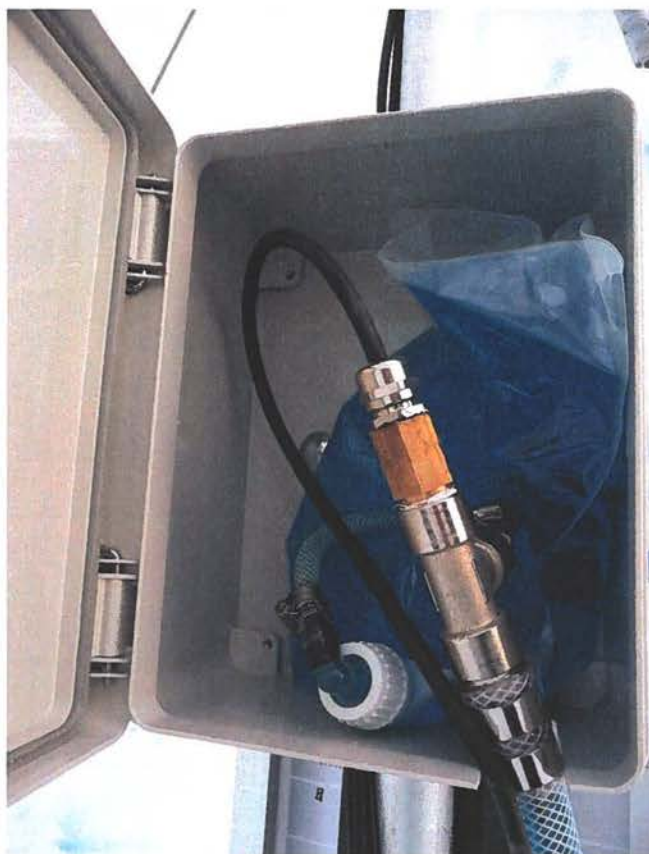


**Figure 4.** *The liquid-filled bladder at the top of the hose is housed in its enclosure to protect the system from the harsh climate.*

The first deployment of a pressure transducer assemblies aimed at measuring ice ablation, was in 2001 and 2002 on the Qassimiut lobe, in south Greenland. This region is characterized by extreme surface melt values in respect to most other locations on the Greenland ice sheet. Figure 5 shows the ablation record as obtained by pressure transducers between 2001 and 2010. Negative values indicate the amount of glacier ice that has ablated within a year. Positive values indicate the presence of a snow layer that has accumulated over the previous winter. Yearly net ablation values commonly range from 5 to 6 m of ice. In the record-setting warm year of 2010, however, about 9 m of ice ablated, which is also a new record for the Greenland Ice Sheet.

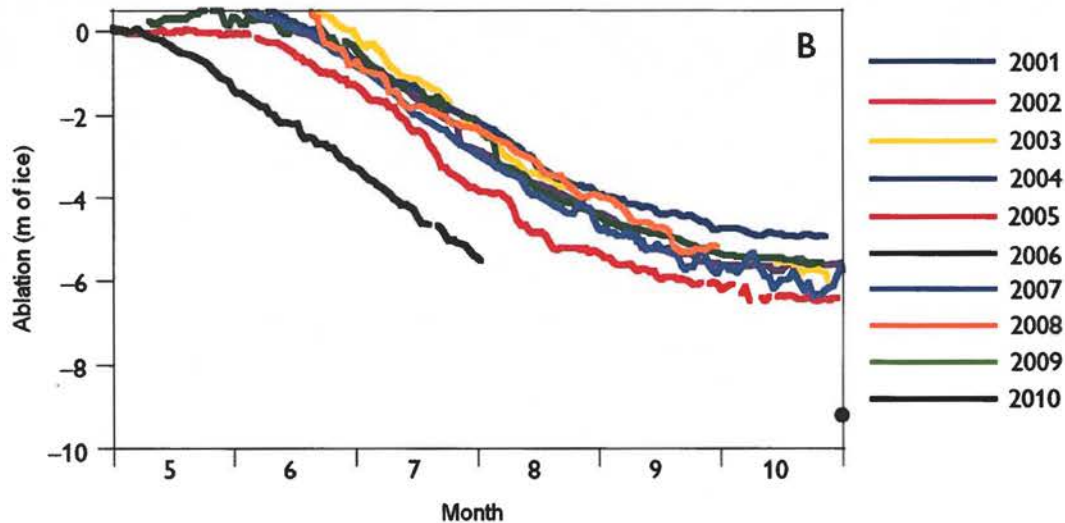


**Figure 5.** Melt records obtained with the pressure-transducer system on the ice sheet margin by Sermilik Bræ, near Qassimiut in South Greenland. Part of the 2010 melt season record was lost due to a data logger malfunction. The black dot gives the end-of-year ablation value for 2010.

In the past decade many more pressure transducers were installed on the Greenland ice sheet, initially for the pre-PROMICE project IceMon: three in the Nuuk region in 2003, two in the Tasiilaq region in 2004, and one in the Melville Bay region in northwest Greenland in 2004. Since then all PROMICE station were equipped with pressure transducer assemblies as well. Even though the first IceMon results were promising and showed that the idea had potential as seen in Figure 5, a few issues had to be dealt with in the development of the assembly. Here we will list the issues and changes that have been implemented over the past years.

#### Pre-PROMICE improvements

- Originally, the liquid used in the assembly was pure alcohol. Besides the problems this created with the customs when shipping to Greenland, there were occasions that upon return to the automatic weather stations, the alcohol had largely escaped the assembly due to reasons unknown. The alcohol was replaced by a 50/50 anti-freeze and water mixture, which can be bought anywhere and shipped without problems.
- Another improvement concerned the bladder, which used to be laying on the surface, allowing it to move around and be covered by snow in winter. The bladder was tied to one of the legs of the tripod of the automatic weather station to keep it in place, and protect it from the elements to a certain extent.
- Finally, the diameter of the hose used in the assembly was increased from roughly 1 cm to 2 cm to keep the hose from being pressed closed by the pressure of the ice.

## PROMICE improvements

- During PROMICE, we made the pressure transducer system shorter, for easier shipment, easier handling (less space and weight in the helicopter), and to prevent an assembly to remain in the ice for more than a few years (which would make it impossible to recalibrate them in accordance to the calibration plan). Previously, hoses were about 50 m in length. The current hoses are 25 m long, and are drilled roughly 20 m into the ice, which should be sufficient to monitor ice ablation for at least four years.
- The previous pressure transducers required an open connection to the atmosphere, to be able to measure the pressure of the vertical liquid column in respect to the local air pressure. This required a second thin tube to run from the sensor to the surface. To avoid closure of this delicate second tube, and to simplify the assembly altogether, we started using absolute pressure transducer, which do not require an open-air connection.
- Possibly the most important change is that the bladder of the assembly is no longer tied to one of the legs of the tripod, but is placed in an enclosure on the main mast. By keeping the bladder in an enclosure, it is much better protected from the elements and leaks should occur less often. By having the bladder on the main mast instead of a leg of the tripod, the unavoidable tilt of an automatic weather station in the ablation zone will result in less of a vertical change in position of the bladder, thus increasing or decreasing the length of the vertical liquid column.

The fact that PROMICE automatic weather stations are equipped with both a pressure transducer and two sonic rangers, allows us to validate the output of the former sensor. Current results show that some PROMICE pressure transducers show a fairly large variability, which is due to atmospheric pressure variability. We developed a method to filter out the atmospheric pressure signal, resulting in reliable ablation measurement. Overall we have improved the system considerably since the early test in 2001. The data of the current stations will help us to assess any issues with the pressure transducer system and improve the system further.

## Development of data transmission by satellite

Telemetry from the AWS's in the field to GEUS answers four major requirements of the PROMICE monitoring programme:

1. Reliably provide early observational data for science use
2. Secure the availability of field data even in case the station disappears
3. Assist in maintaining the observation network operational while minimizing the frequency of expensive site revisits

#### 4. Satisfy requirements 1 and 2 at an affordable cost

Ideally, one single communication solution should suit all of the planned sites, to allow a standardized design of the stations.

Ground-based radio-modem transmission has been ruled out based on cost and technical issues, since the remote location of most sites would require either intermediate radio repeaters (involving expensive field maintenance) or powerful transmitters consuming more supply power than available. This leaves only satellite-based telemetry as an option, and previous experience both within and outside GEUS support this choice.

During the late 1990's and early 2000's several commercial operators of satellite telecommunication services faced serious financial difficulties or even faced bankruptcy. Given the considerable investment in dedicated equipment and design effort to integrate a specific telemetry solution into the AWS design, the outlook for future availability of the service has been taken into account.

Several satellite systems are in use within the glaciological community for transmitting ground observations from remote locations. The AWS's of the Greenland Climate Network (GC-Net) operated by the University of Colorado at Boulder use the GOES Data Collection System (DCS) south of 72 N and ARGOS DCS north of 72 N. The ARGOS DCS system is also used by AWS's operated by the Institute for Marine and Atmospheric Research, Utrecht University (IMAU) both in Greenland and Antarctica, as well as by several other Institutions. More recently, applications based on the Iridium satellite constellation are also being introduced. The existing GEUS stations have been using the Inmarsat system of geostationary satellites, and further details about its performance, as well as the rationale for switching to a better option, are discussed below.

The GOES DCS is a relay system where synchronized AWS's on the ground transmit to one of the two geostationary GOES satellites within preassigned wavelength and time slots. The satellites retransmit the message to a ground station but the one-way nature of the communication doesn't provide any acknowledgment of successful transmission. The GOES DCS is technically unsuitable for PROMICE because the coverage is limited to latitudes south of 72 N. In addition to this, achieving high reliability would be difficult due to the lack of acknowledgment of successful transmission and to the requirement of maintaining a comparatively tight synchronization to transmit during the predefined time slot allocated to each AWS. Furthermore, direct access to the system is only available to U.S. federal, state, and local government agencies, and a U.S. government sponsor is otherwise required.

The Argos DCS is another one-way data collection relay system that adds the benefits of providing global coverage and platform location. The AWS's on the ground transmit to the Argos instrument aboard the NOAA Polar-orbiting Operational Environmental Satellites (POES), but no acknowledgment of successful transmission is available in the original Argos system (it is currently being implemented in Argos-3 instruments). The data rate is still limited, and new terminal devices able to implement the full Argos-3 have only started being introduced in late 2007, therefore Argos has not been selected for use in the PROMICE AWS.

The existing GEUS pre-PROMICE AWS design used a Thrane & Thrane A/S device to transmit data through the Inmarsat satellite network. Due to the geostationary orbit of the Inmarsat satellites, their coverage is generally specified as limited to 82 N, and local topography and environmental conditions may make service availability marginal at high latitudes (see Figure 6). This setup suffered from some shortcomings:

- Marginal radio performance due to the low elevation of the geostationary satellite over the horizon
- Unsuitable for the northernmost planned AWS sites
- Low reliability with several lost transmissions
- No wintertime transmission for power consumption considerations

Because of these limitations, it was decided to switch for a better suited satellite telemetry system not based on geostationary satellites.

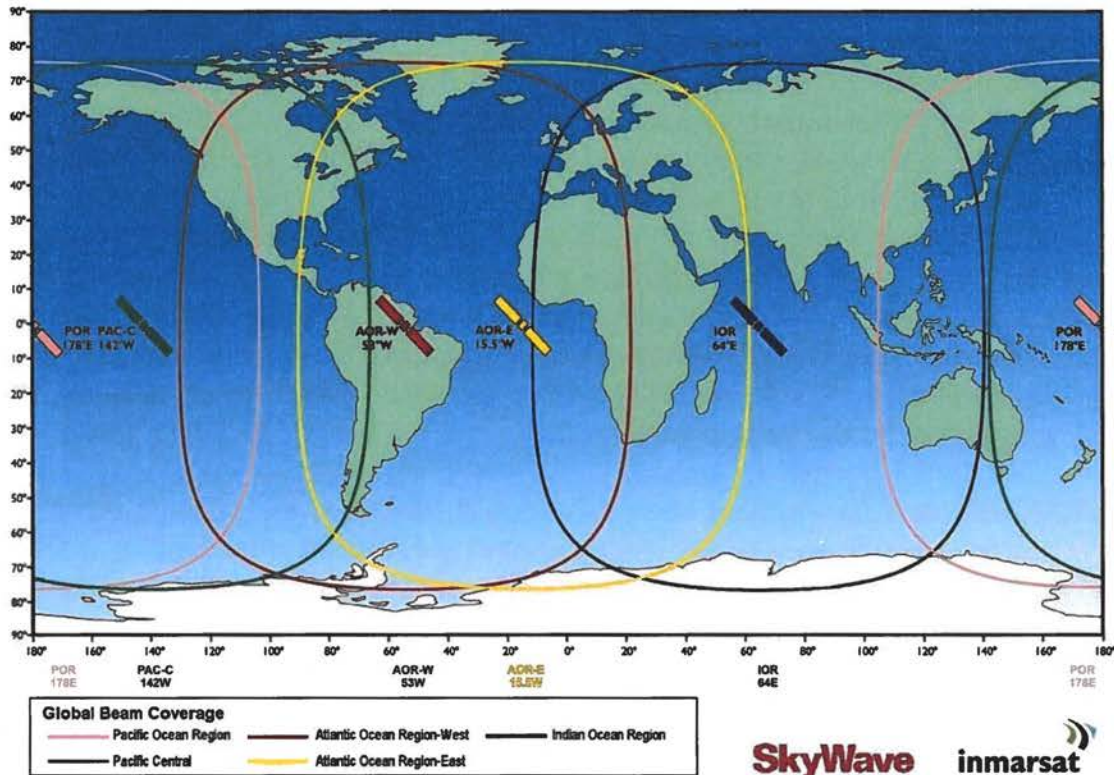


**Figure 6.** Radio footprint of the Inmarsat geostationary satellites used by GEUS' existing pre-PROMICE AWS's. The coverage at high latitudes is marginal.

Iridium, GlobalStar and ORBCOMM are the three major operators but only Iridium satisfies all PROMICE requirements, in particular concerning to good coverage at high latitudes. Due to their orbital configurations both and provide limited (GlobalStar) or no coverage (ORBCOMM) (Figure 7). The Iridium satellite constellation is based on 66 active satellites in low Earth orbit (LEO) at a height of approximately 781 km and inclination of 86.4°, with several in-orbit spares. Coverage of polar regions is therefore optimal (Figure 8), and data transmission service and equipment are readily available commercially. The initial financial difficulties experienced by the Iridium commercial operator have been overcome and the

outlook for continued reliable service has been considered good, based on the reported growing number of subscribers and extensive use by the U.S. Department of Defence. Iridium has therefore been chosen as the satellite telemetry system used by PROMICE AWS's.

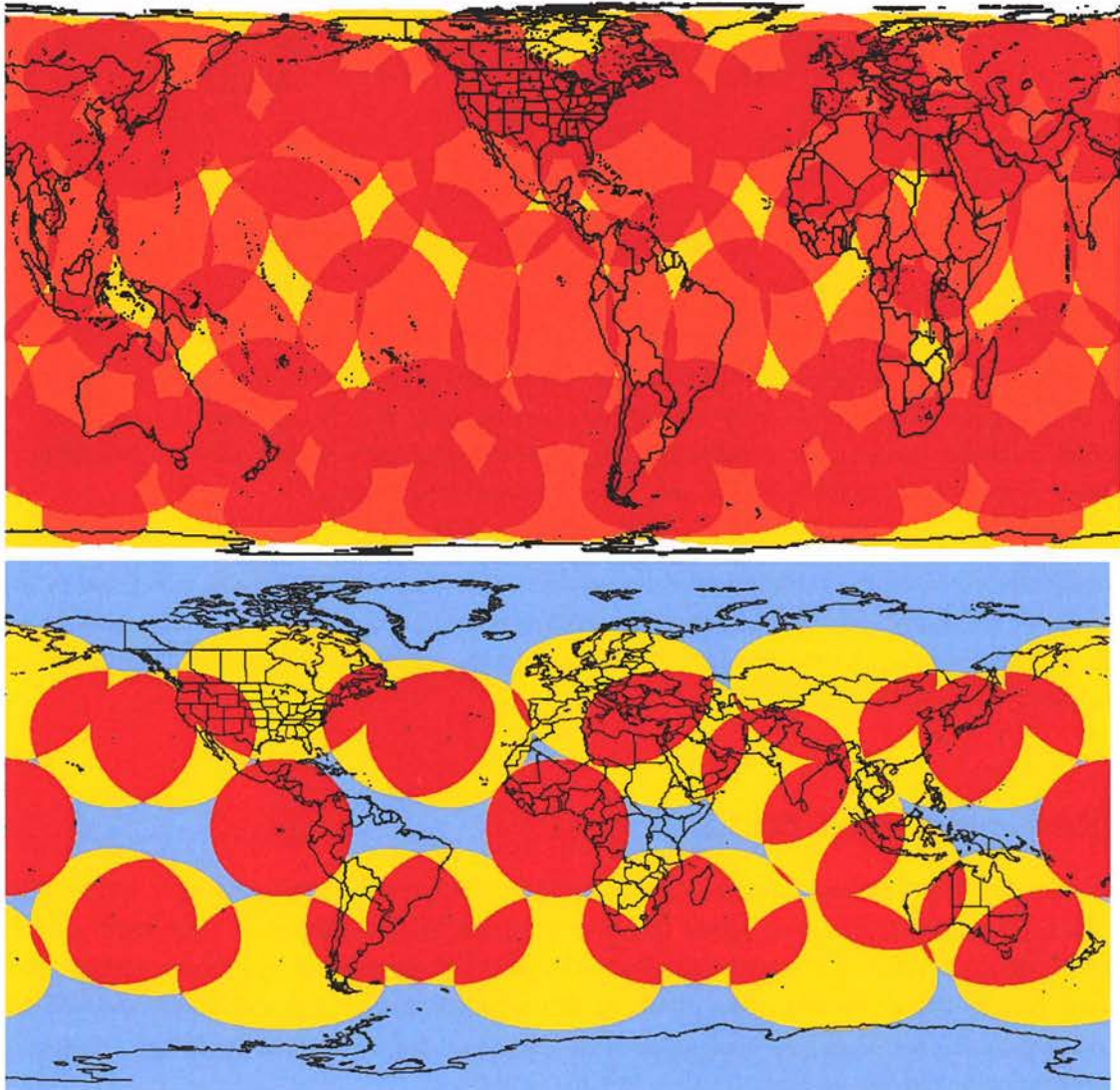


**Figure 7.** Snapshot radio footprint of the GlobalStar (above) and ORBCOMM (below) satellite constellations. Since the satellites are in LEO polar orbits, the footprint of each satellite changes rapidly over time, however the system coverage remains comparable and limited (GlobalStar) or absent (ORBCOMM) over polar regions (yellow: one satellite in view; darker shades of orange and red: two or more satellites in view).



**Figure 8.** A snapshot radio footprint of the Iridium satellite constellation. Since the satellites are in LEO polar orbits, the footprint of each satellites changes rapidly over time, however the system coverage remains comparable and very dense over polar regions (yellow: one satellite in view; orange: two satellites in view, red: 3 or more satellites in view).

A particularly interesting operational mode called SBD (short burst of data) is offered at an affordable price, and specialized data terminals are commercially available. The cost analysis including various billing options is described in the following section based on rates in USD from early 2008.

## Data transmission cost analysis

The cost of Iridium airtime has been determined in relation to the fees levied in early 2008 by NAL Research Corp. Two types of service contracts are offered: a “standard” and a “fixed” rate contract. For the anticipated volume of traffic generated by this application, the “fixed” rate is the cheapest option both at the wintertime and summertime transmission rates (Figure 9). A check has been done with the actual costs invoiced by NAL for one entire month showing the estimates below to be accurate.

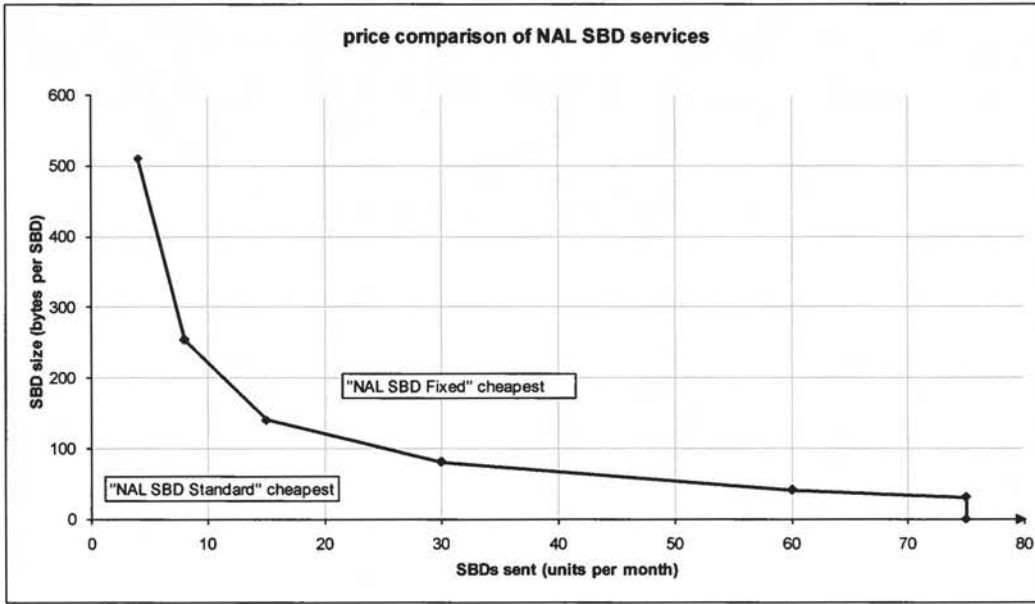


**Figure 9.** Plot comparing the "fixed rate" and the "standard rate" fees offered by NAL Research Corp. for Iridium SBD airtime.

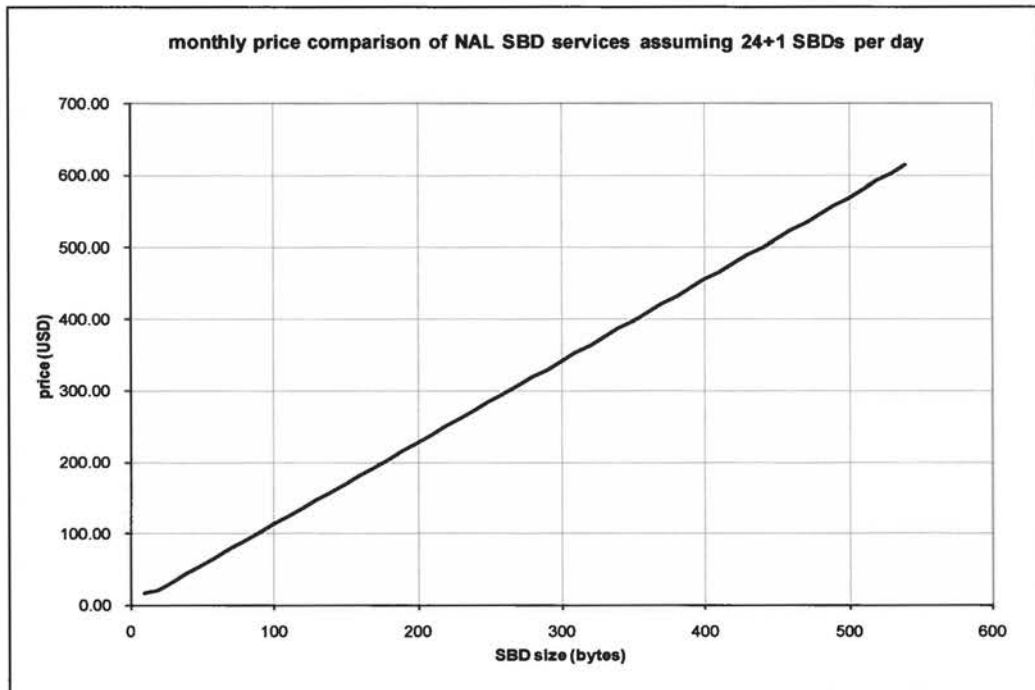


**Figure 10.** Monthly price of SBD airtime at summertime transmission rates.



**Figure 11.** Monthly price of SBD airtime at wintertime transmission rates.

The summertime estimated monthly cost of Iridium SBD airtime, based on a volume of traffic of 760 SBD messages per month (also including the diagnostic messages) and an average size of 300 bytes per SBD message corresponds to about 340 USD (Figure 10). The entire April to October season will cost 2380 USD. The wintertime estimated monthly cost of Iridium SBD airtime, based on a volume of traffic of 275 SBD messages per month (also including the diagnostic messages) and an average size of 300 bytes per SBD message size corresponds to about 120 USD (Figure 11). The entire November to March season will therefore cost approximately 600 USD.

The cost of Iridium SBD airtime for an entire year will therefore amount to about 3000 USD, which fits within the anticipated budget. This expense could be significantly reduced by modifying the program so that it encodes the data in a binary format before transmission.

## Hardware and software implementation

The Iridium SBD transceiver model 9601-DG manufactured by NAL Research Corporation has been selected as it offers two-ways SBD communication and integrated GPS positioning in a rugged device specified for operations within the temperature range -30 to 60 °C (storage -40 to +85 °C) and certified to military standards for thermal and mechanical shocks, humidity and vibrations. The unit requires sufficiently low power that transmissions can be extended to cover the entire winter season. This is a particularly important advantage over the previous system because several stations in the past operated and transmitted properly until transmissions were suspended for the winter and then never re-

sumed transmitting in the spring, thus providing no clue about what kind of failure might have occurred and what field maintenance would have been required.

The required code was integrated in the new datalogger program developed for the Campbell Scientific CR1000 dataloggers included in the new AWS design.

Power supply and data connection to the NAL 9601-DG is through a NAL SYN-DC-936 DC-DC power converter efficiently lowering the 12 V battery supply to the required 5 V. The datalogger controls the 12V supply to the NAL SYN-DC-936 through a solid state relays, only activating the supply at times scheduled to acquire reliable GPS fixes or to transmit data messages. The datalogger communicates to the NAL 9601-DG over an RS-232 serial link passing through the NAL SYN-DC-936, and every unit requires that the male 9 pins D-type connector supplied by NAL be replaced with a female 9 pins D-type connector matching the connector in the CR1000 datalogger. It is also required to rewire the connector pins because the transceiver expects to be attached to an RS-232 DTE (data terminal equipment) device but the CR1000 connector is wired as a DCE (data communication equipment) device. The transceiver is housed within the logger enclosure and connection to the antenna mounted on top of the mast is through an RG58 coaxial cable.

Transmission is currently encoded as printable ASCII and Figure 12 shows an example message as received from a PROMICE AWS in the field. As a future improvement it is being considered to switch from ASCII to binary encoding, which would reduce the amount of bytes transmitted by about 50%, with a corresponding cost reduction. The transmitted data messages are automatically sent to GEUS as email attachments.

```
2008-09-06
01:00:00,360060,912,1.93,41.56,99.4,1.581,264.1,10.13,0.221,
-0.331,0.433,-4.745,1.712,2.858,0.826,13.09,-0.528,-1.726,-2.751,-
3.59,
-4.199,-4.584,-4.725,-4.525,-
0.37,2.195,010014.60,6705.83936,04955.91265,
671.4,0.94,123.3,12.81,!S,!M
```

**Figure 12.** An example of a message from the PROMICE AWS at 300034012250840.

The logger program implements several configurable functionalities aimed at increasing the reliability of the telemetry and at the same time reducing power consumption. The program can switch on the NAL 9601-DG at predefined intervals independently either for obtaining a GPS fix, for transmitting tasks or for both tasks at the same time, in every case supplying power only for the shortest time needed. This is important because the GPS needs some time to produce a reliable fix, but this is not necessary at times when only transmission has to be performed. The logger program also uses the available power management commands to selectively switch on and off the internal components of the NAL 9601-DG (i.e. GPS module, control interface, and RF section).

When transmission is to be performed, the logger uploads the message to the NAL 9601-DG, activates the RF section and waits for confirmation that an Iridium satellite is in view

before trying to transmit the message. If, for any reason, no satellite is found within a short predefined timeout, the logger switches off the transceiver and queues the message that failed to be transmitted in a first-in first-out queue implemented in the logger program. This is necessary in spite of the good Iridium coverage of the polar region to prevent a faulty transceiver, coaxial cable or antenna from wasting battery power by waiting too long or by transmitting "in the blind". If, as normally is the case, a satellite is detected and signal strength is good, transmission is attempted. In case of transmission failure, as indicated by the return codes issued by the NAL 9601-DG, the logger will check that the satellite is still in view and then try again to transmit the message until transmission is successful or until the predefined timeout is reached, after which the transceiver is powered down. In any case, all messages that could not be sent will be queued in the FIFO. The queued messages will then be sent at the next scheduled transmission, if possible, or kept in the queue for further attempts until they are transmitted successfully or the FIFO is full, after which the oldest unsent messages will be dropped. This system allowed obtaining 100% transmission reliability in the AWS's deployed to date.

Both GPS and transmission intervals can be configured in the logger program at different rates for summer and winter, in order to save costs and battery power during wintertime. As a further safety, the datalogger monitors the battery voltage and stops using the GPS and Iridium transceiver if the battery voltage drops below a predefined low-battery threshold. A configurable hysteresis prevents instability and erratic behavior by resuming full operation only after the battery has been charged by the solar panels to a voltage higher than low-battery threshold. This system makes much better use of the available batteries by allowing to wire them as one single large battery array in place of the commonly adopted scheme of wiring two separate arrays dedicated one to the datalogger and the other to the satellite transmission.

# Data

## Database development

For a long term monitoring project such as PROMICE it is important that the acquired data is stored in a systematic way. For that purpose the PROMICE Automatic Weather Station database has been developed to keep track of all data acquired in the PROMICE project, including specifications on the instruments the data was acquired with and what processing has been done to it.

The PROMICE automatic weather station data consists of measurements from a number of instruments. The measurements are stored locally in a data logger and emailed to GEUS. Therefore two sets are produced in most cases. The transmitted data received at GEUS at near real time and the collected data stored in the data logger which is retrieved at station visits. Both data sets are stored in the data base. All meta data information on the station, instruments (type, serial number, accuracy, calibration, etc.) and conversion/correction factors are also stored. The information is updated as instruments are replaced/updated/calibrated or conversion factors change otherwise.

The database is being developed by the GEUS database group in close collaboration with the glaciology group and is stored in the GEUS data system.

Initial planning of the PROMICE database was carried out during 2007/08. The database including also a web interface was developed and deployed in 2009. Further development of the database, web interface and addition of the instrument inventory as part of the database was done in 2010. Adjustment, refinement and maintenance of the database is anticipated in the coming years.

The PROMICE database has been developed as a separate entity of a larger ORACLE database which is maintained at GEUS. The database is stored in the GEUS data system which has been equipped with the presently required storage space and provides the possibility of expansions when necessary. Daily backups are run on the GEUS system.

The GEUS database system is a complicated system containing several types of data. To ease the use and maintenance, interfaces to the PROMICE database have been developed. This has been done by the database group with input from the glaciology group.

The different types of data in the database need to be quality assured. It is particularly important for the automatically collected station data to have standard quality assurance procedures. Therefore quality control is an integrated part of the database and partly automatic. Consultations have been made with ASIAQ and DMI to learn from their experiences with weather station databases and quality control systems before designing the PROMICE database.

Data from complimentary stations funded by other sources such as from the projects FreshLink, SEDIMICE, Glacio-Basis, Greenland Analogue Project and others have been included in the database for the benefit of the PROMICE programme.

There are three types of users of the PROMICE data: the GEUS glaciology group, the scientific community and the general public. Furthermore it is a condition that data from the PROMICE project should be made publicly available. Therefore a website has also been developed where data from the database can be displayed in real-time and freely downloaded.

The database effort has been concentrated on data from the automatic weather stations. However other PROMICE data such as airborne altimetry data, radar surface velocity data and GLIMS glacier map data are also stored securely in the GEUS system and will be made available to the public through the database website.

PROMICE database and PROMICE data download website are described in more detail below.

## **PROMICE database**

### **Safe storage of PROMICE data**

The observations and measurements collected from automatic weather stations within the PROMICE program are all stored in the data banks of the Geological Survey of Denmark and Greenland, GEUS. GEUS is a *Research and Advisory Institute in the Ministry of Climate and Energy* in the Kingdom of Denmark, and GEUS manages the national storage of geological data and some environmental data, as well as data from external partners. PROMICE data are stored in a separate database schema as part of a larger Oracle Database maintained by GEUS.

The PROMICE database complies with common principles for relational databases, and the consistency and integrity of the data is ensured via database features, rather than by external computer programs

### **PROMICE database schema**

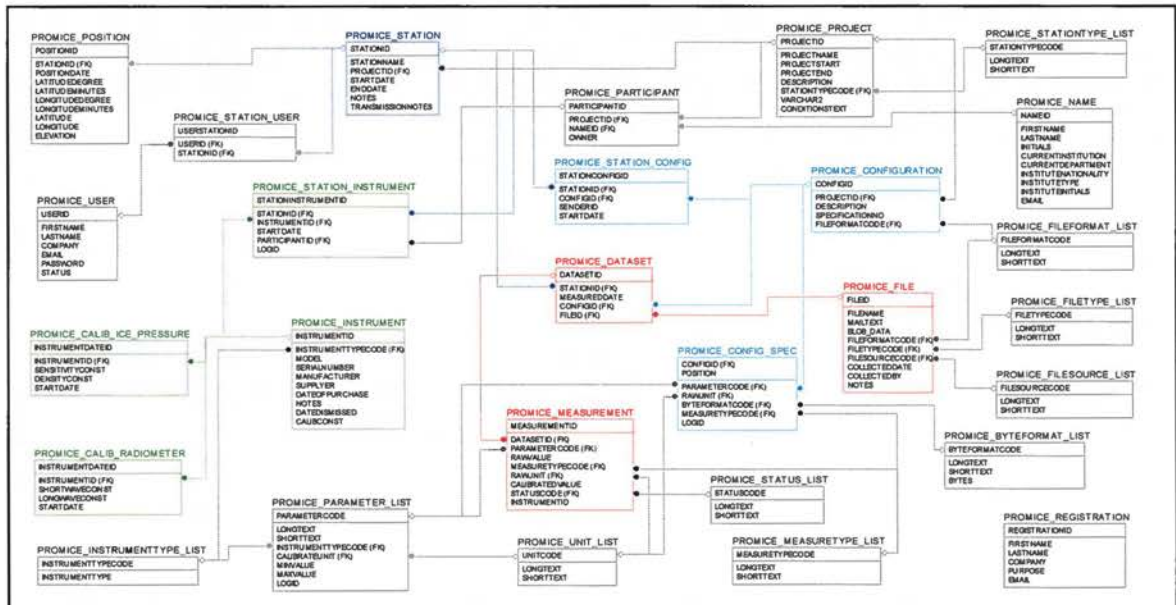


**Figure 13.** Diagram showing the PROMICE database

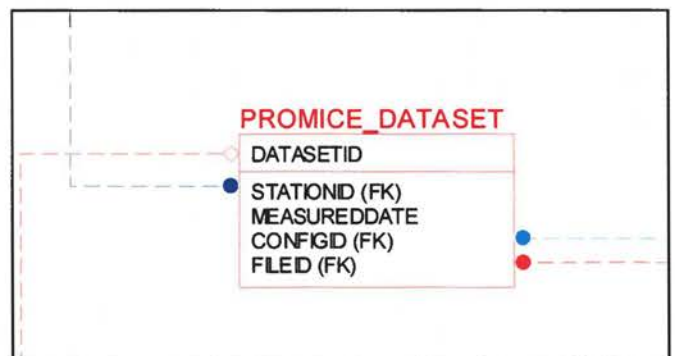
This diagram shows the entity – relation diagram of the PROMICE database.

Each box represents a table in the database, and the dotted lines shows relations between tables. The more important tables are colored, and described in details below. Some attributes, like insert date, common to all tables, have been omitted in this diagram for clarity.

Below is shown a close up of the table PROMICE\_DATASET from the database schema.

Here follows a short explanation of the information that may be obtained from this kind of diagram.

- The name of the table is written above the box.
- The upper part of the box is the unique key, *Datasetid* in this case.
- The lower part of the box shows the other attributes of the table.
- The red hollow diamond and line leaving from the unique key shows that another table refers to this table.
- The 3 filled dots show that this table refers to 3 other tables.



### Storage of observations

At the center of the database are the 3 tables:

- PROMICE\_MEASUREMENT
- PROMICE\_DATASET
- PROMICE\_FILE

These 3 tables are shown in red in the diagram, and they store all observations and measurements from the automatic weather stations.

### PROMICE\_DATASET

This table holds information common to a dataset.

A dataset in this context is a set of observations with a common timestamp acquired from a specific automatic weather station. Datasets can have from 10 to 40 observed values depending on how the automatic weather station is set up. Typically, a dataset is a set of observations that have come to the database via satellite in one attached file from an automatic weather station. A dataset may also be a single line in a CSV - file from a data logger at a station being visited.

Each row in this table stores information about a dataset, identified by a datasetid and has references to 3 other tables, in this case:

- PROMICE\_STATION, which tells where, or rather at which automatic weather station this set of observations were made.
- PROMICE\_CONFIGURATION which tells how the data logger at the automatic weather station has ordered the observed values in the dataset. A dataset is just a row of values, and the database interprets each value according to its position in the dataset.
- PROMICE\_FILE which tells where the original file containing the observations, are stored.

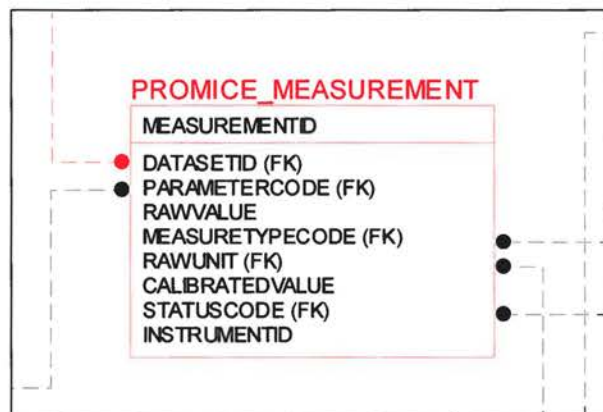
Finally, the timestamp of the dataset is also stored here.

### PROMICE\_MEASUREMENT

This is the table where the actual measurements are kept. In the time of this writing, May 2011, the PROMICE database holds about 3.5 million observations.

Each row in this table stores a single observed value in *Rawvalue*, along with references to 5 other tables:

- PROMICE\_DATASET, with information on the timestamp and the station where the observation was made.
- PROMICE\_PARAMETER\_LIST, which tells the kind of observation, for example if this row is an observation of *air pressure*, of *incoming low frequency radiation* or whatever.
- PROMICE\_UNIT\_LIST, which tells the unit of the observation such as *m/s*, *W/m<sup>3</sup>* and so on.
- PROMICE\_MEASURETYPE\_LIST, which just tells, if the observation is an *instantaneous* or *averaged* value.
- PROMICE\_STATUS\_LIST, which tells if this particular measurement is qualified and found to be *valid* or if it is regarded to be an outlier, *invalid* for some reason.



Each row also may hold 2 calculated values that are carried out automatically when a dataset is stored:

1. *Instrumentid* which identifies the instrument by which this observation was made. This is merely a look up in the table PROMICE\_STATION\_INSTRUMENT, a table where specific instruments are assigned to specific weather stations.
2. *Calibratedvalue* is calculated from the *Rawvalue* and perhaps some other values within the same dataset.

Presently calculations are carried out for the observations of humidity, radiation, snow height, tilt and ice pressure. Thus valid observations become measurements.

For example, the snow height observed by a sonar ranger is calculated as:

$$\text{Calibratedvalue} = \text{Rawvalue} * \sqrt{\frac{T}{273,15}}$$

Where T is the absolute temperature measurement from the dataset.

```

FUNCTION PROMICE_CALC_SONAR_RANGER
(InRawVal IN NUMBER, InPt100Temp IN NUMBER) RETURN NUMBER AS
-- Calibrate observed value according to temperature
CalibVal NUMBER := 0;

BEGIN
  CalibVal := ROUND(InRawVal * POWER(InPt100Temp/273.15,0.5), 2);
  Return CalibVal;
END PROMICE_CALC_SONAR_RANGER;

```

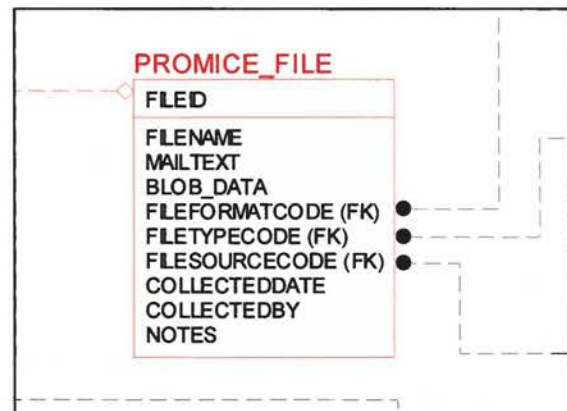
### PROMICE\_FILE

This table stores the original files as they were obtained from the data logger at the automatic weather station.

This information is somewhat redundant of course, but it is kept for safety. If needed, the tables PROMICE\_DATASET and PROMICE\_MEASUREMENT could be repaired from the content in PROMICE\_FILE. Each row in PROMICE\_FILE stores a file, identified with a *Fileid*. The file content is stored in *Blob\_data*. A file with data sent by satellite contains one dataset per file, most often in binary form. Files that have been collected by visit to an automatic weather station are always in ASCII and may contain several hundreds of thousands of dataset, one dataset per line, and the values on each line are comma separated. Both kinds of files are stored in *Blob\_data*.

PROMICE\_FILE references 3 simple code lists:

- PROMICE\_FILEFORMAT\_LIST tells if the file is in binary or text format.
- PROMICE\_FILETYPE\_LIST is actually redundant, but what meant to tell the kind of file, such as *Default attached file from Iridium Network*.
- PROMICE\_FILESOURCE\_LIST tells whether the file is received by mail or collected from the data logger at a weather station.



Each file is stored with a unique file-name, such as *TAS\_L 2008-2009*, so that humans can search the table.

Additional information may be stored in *Mailtext*, *Collecteddate*, *Collectedby* and *Notes*.

### Keeping Track of the Setup of Automatic Weather Stations

Four Tables are storing information about the automatic weather stations and how each automatic weather station is set up to measure.

- PROMICE\_STATION
- PROMICE\_CONFIGURATION
- PROMICE\_STATION\_CONFIG
- PROMICE\_CONFIG\_SPEC

The first one is shown in dark blue and the other three are all shown in light blue in the diagram.

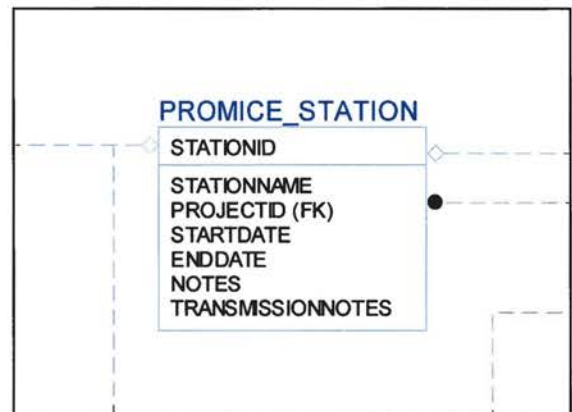
When the observations are read into the table PROMICE\_MEASUREMENT, a dataset is simply a row of values, and the dataset should be interpreted according to the actual weather station setup, which is stored in these tables.

#### PROMICE\_STATION

This table stores details of the automatic weather stations. Each row in this table stores information about one station, identified by its *Stationid*. It also must have a unique *Stationname*, readable for humans. This table is a basic table in the PROMICE database, five other tables relates to this table.

It references 1 table:

- PROMICE\_PROJECT\_LIST, telling what project the station belongs to. This is because the database stores measurements from several affiliated projects.



A station's *Startdate* is the day, when it was established at its site on a glacier, and once it is taken down, the *Enddate* can be stored too. It is also possible to store *Notes* for maintenance, and *Transmissionnotes*, for example if a station has not been working properly for a period.

#### PROMICE\_CONFIGURATION

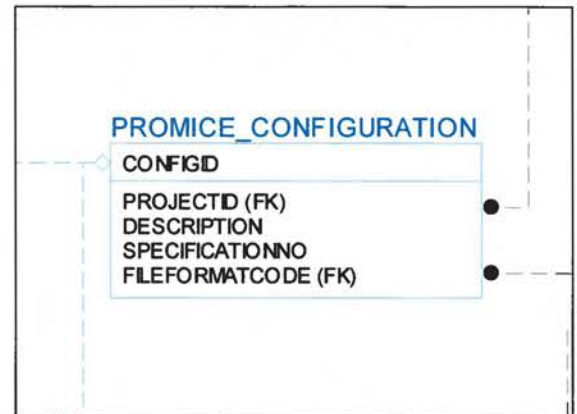
This table stores a list of different setups, each row in the table is another setup and there are about 20 different setups by May 2011.

The setups are called configurations and they are identified by a *Configid* for computers, but they must also have a unique *Description* for humans.

Also, the binary configurations have a *Specificationno*, a number written in the binary datasets by which they identify themselves.

It references 2 tables:

- PROMICE\_PROJEC, telling which project the setup belongs to.
- PROMICE\_FILEFORMAT\_LIST, telling whether this setup is for data in binary or text format.

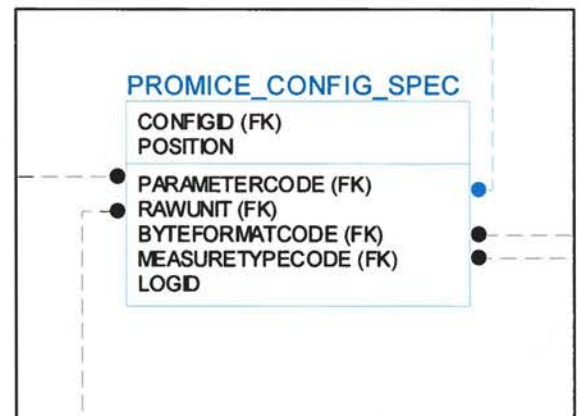


### PROMICE\_CONFIG\_SPEC

This is the table where each configuration is actually specified. Each row pairs a value position in a specific configuration to an observed parameter. For example a row in this table might say: *In the "PROMICE 2009 hourly summer message, binary" configuration, value number 4 represents observed humidity.*

It references 4 other tables:

- PROMICE\_PARAMETER\_LIST, telling what parameter is observed.
- PROMICE\_UNIT\_LIST is telling the unit of measurement. This parameter is not actually used.
- PROMICE\_BYTEFORMAT\_LIST is used for binary configurations only. It says if the value is 2 or 4 bytes.
- PROMICE\_MEASURETYPE\_CODE tells whether the observed value is instantaneous or averaged.



Also, a *Logid* is used to differentiate between multiple occurrences of a parameter in one dataset. For example there may be 2 sonar rangers on a weather station, one measuring snow height at the station and another measuring snow height when fixed to a stake. They will have *Logid* 0 and 1 respectively.

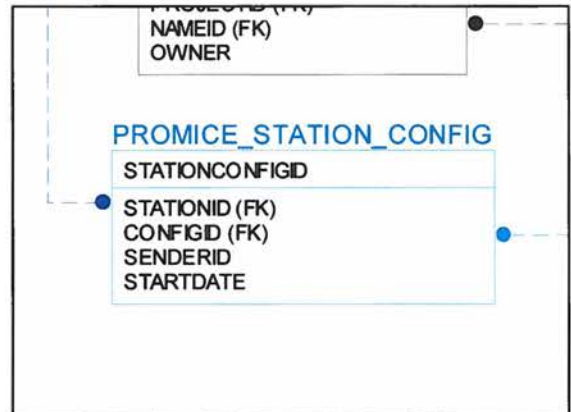
### PROMICE\_STATION\_CONFIG

This table stores information about which configurations are used by a specific automatic weather station, and also about the senderid of the Iridium satellite sender.

It references 2 other tables:

- PROMICE\_STATION, the ID of the station
- PROMICE\_CONFIGURATION, the ID of the configuration.

When receiving mails from the automatic weather stations, this senderid, together with the date the mail was sent, is used to look up, from which station the mail was sent.



### Instrument Inventory

Four tables are used for keeping track of instruments:

- PROMICE\_INSTRUMENT
- PROMICE\_STATION\_INSTRUMENT
- PROMICE\_CALIB\_ICE\_PRESSURE
- PROMICE\_CALIB\_RADIOMETER

They are all shown in green in the diagram.

One benefit of having the instruments in the PROMICE database is the practical that it allows the technicians to keep track of where the instruments have been deployed. More important, knowing the instrumentation at a specific weather station at any given time, each observation can be linked to a specific instrument.

### PROMICE\_INSTRUMENT

This table has one row for each instrument, and has a reference to:

- PROMICE\_INSTRUMENTTYPE\_LIST which tells the type of the instrument. For example *Inclinometer* or *Barometric Pressure Sensor*. Also other instruments than sensors are stored here, for example *Solar Panel* or *Iridium Antenna*.



Other attributes stored for each instrument are *Model*, *Serialnumber*, *Manufacturer*, *Supplier* and (maintenance) *Notes*. Also each instrument stores the date when it was purchased as *Purchaseddate* and the date if it is dismissed if it is lost or worn out as *Dismisseddate*.

The table PROMICE\_STATION\_INSTRUMENT has a row for each time an instrument is assigned to a station. It references 3 other tables:

- PROMICE\_STATION, telling which station the instrument is assigned to.
- PROMICE\_INSTRUMENT, telling which instrument is assigned.
- PROMICE\_PARTICIPANT, optionally telling who visited the station and mounted the instrument.



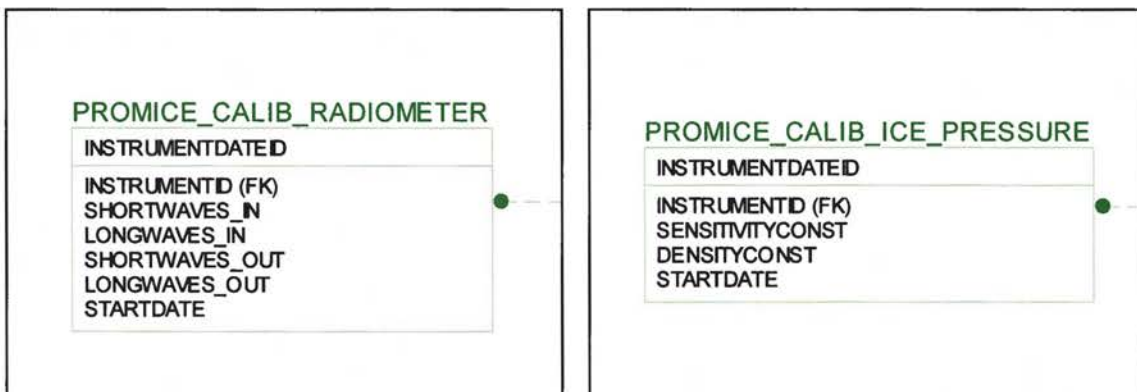
The date *Startdate* is the date, when the instrument is mounted to the weather station. It is generally assumed that there is only one instrument of a kind at a station; therefore no end date is needed. Should there be two or more instruments of the same kind at one station, they will differ by their *Logid*. If an instrument is dismantled from the weather station, but left at the station because, for example, it is frozen into the ice, it should be noted in the *Notes* in PROMICE\_INSTRUMENT, so that it is not expected to be re-used at another station before it becomes available.

#### PROMICE\_CALIB\_RADIOMETER and PROMICE\_CALIB\_ICE\_PRESSURE

These tables store sensitivities specific to an instrument, which may even change over time.

Each row stores information of one calibration of an individual instrument. It has a reference to:

- PROMICE\_INSTRUMENT, to tell what specific instrument was calibrated.



PROMICE\_CALIB\_RADIOMETER stores 4 measured sensitivities for radiometers:

*Shortwaves\_in* is the instruments sensitivity for incoming short wave radiation.

*Longwaves\_in* is the instruments sensitivity for incoming long wave radiation.

*Shortwaves\_out* is the instruments sensitivity for outgoing short wave radiation.

*Longwaves\_out* is the instruments sensitivity for outgoing long wave radiation.

PROMICE\_CALIB\_ICE\_PRESSURE stores values for the assembly for measuring ice heights:

*Sensitivityconst* is the sensitivity of the barometric pressure transducer, while

*Densityconst* is the density of the fluid in the hose attached to the pressure transducer.

The date *Startdate* is the day of calibration for the instruments. For each instrument several calibrations may be stored, and the automatic procedure will use the latest sensitivity values for the specific instruments, when calculating *Calibratedvalue* in PROMICE\_MEASUREMENT.

### How the data is read into the database

The automatic weather stations are sending **averaged** preliminary data via satellite to an Outlook mailbox. A small java program is scheduled to read mails from PROMICE's mailbox into the database several times a day. In short, this program will find the latest mail in the mailbox that is not yet in the database, and from there, for each mail, it will:

- Get the subject and the date of the mail, and parse the sender ID from the mail subject.
- With this information, sender ID and date, query from the database: *From which weather station did the mail arrive?* And also query the format of the attached file containing the observations: *Are the observations sent in binary or ASCII format?*
- Store the attached file in PROMICE\_FILE.
- With the attached file and knowledge of the file format, query the configuration: *Which observations, and in what order can be found in the attached file?*
- Now, when the configuration is known, the attached file is opened and the timestamp is read, so that a dataset can be stored in the table PROMICE\_DATASET, and a datasetid can be obtained.
- Then the rest of the attached file is parsed, and the individual observations are stored in the table PROMICE\_MEASUREMENT, in accordance with the configuration.
- If everything goes well, the data is persisted into the database. Some database procedures are called, to make the extra calculations for *CalculatedValue* in the table PROMICE\_MEASUREMENT.

Most of the observations in the PROMICE database so far, are preliminary data. In the near future the glaciologists will be reading in the full data files, containing all the instantaneous observations, which are obtained directly from the data loggers at the weather stations. They will use another small java program with a simple interface:

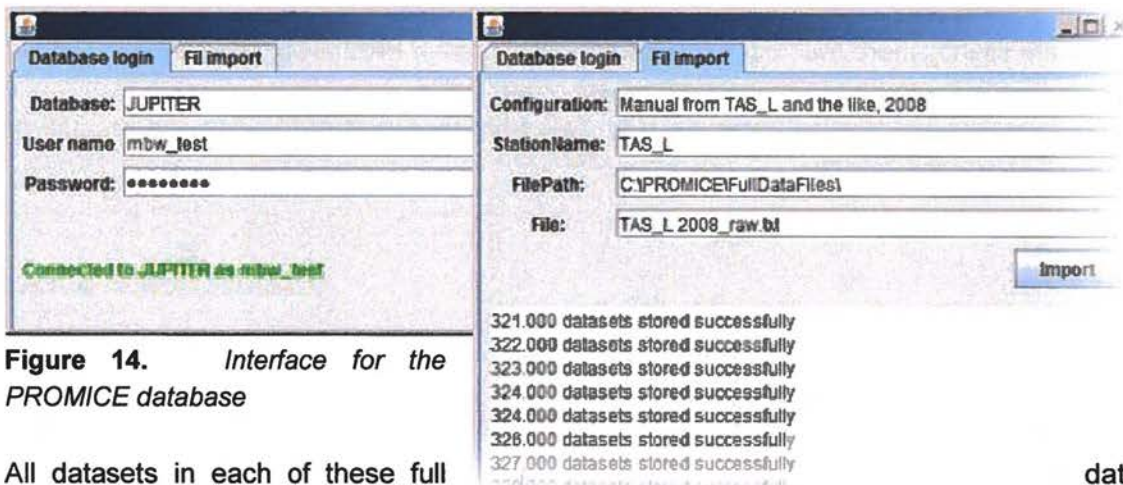
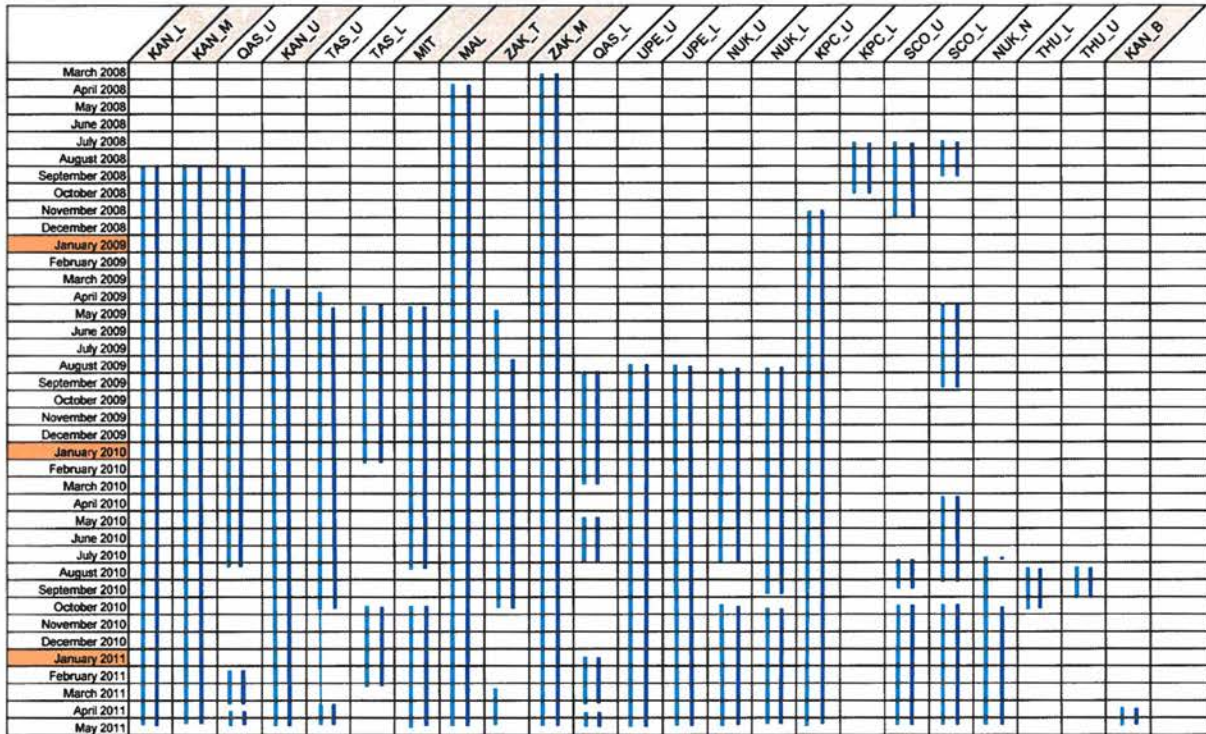


Figure 14. Interface for the PROMICE database

All datasets in each of these full data files share the same configuration, and in this case the program will get its information on the origin of the data and the configuration / order of measurements directly from the glaciologist, who uses the program.

Mails and data in PROMICE database, from weather stations belonging to PROMICE and to affiliated projects



**Table 3.** Overview of the collected data

This figure gives an overview of the data that has arrived to the 'Ice' mailbox, (light blue), and the data that have been stored in the database (dark blue). By May 2011 the database contains more than

- 162.000 records in PROMICE\_FILE
- 160.000 records in PROMICE\_DATASET
- 3.753.000 records in PROMICE\_MEASUREMENT

There are slightly more records in PROMICE\_FILE than in PROMICE\_DATASET, because diagnostic message files from the stations are stored here.

Once the glaciologists read in the full data files from the weather stations, the amount of data will grow considerably.

### Maintenance of the database

Since the PROMICE database is also used as an inventory of valuable sensors and other weather station equipment, a web based interface to the database has been established. This interface makes it safe for technicians to insert, update and delete rows in the tables concerned with the Instruments (basically the tables shown in green in database diagram). With this interface to the database, technicians may log in and:

- Add new Instruments to the PROMICE database
- Store calibration constants for radiometers
- Store calibration constants for pressure transducers
- Assign Instruments to weather stations

Figure 15 shows how a specific instrument is assigned to a weather station:

The screenshot shows a web-based interface for the PROMICE database. The title bar reads 'Promice Database Maintenance: Instruments Stations Instrument Assignments Ice Pressure Calibrations Radiometer Calibrations Users Projects Registrations'. The main content area is titled 'New Assignment of Instrument to Station' and contains several form sections:

- Station \***: A table with columns 'Stationname' and 'Station Notes'. The 'Stationname' field contains 'KPC\_L' and 'Station Notes' contains '17-07-2008 DVA, FMN: Station established'. Below the table is a 'Change Station' button.
- Instrument \***: A table with columns 'Type', 'Manufacturer', 'Model', 'Serial#', and 'Instrument Notes'. The 'Type' field contains 'Humidity+Temp', 'Manufacturer' contains 'Rotronic', 'Model' contains 'HygroClipS3', and 'Serial#' contains '55025178'. Below the table is a 'Change Instrument' button.
- Log Id \***: A text input field containing the value '0'.
- Participant**: A table with columns 'Initials' and 'Project'. The 'Initials' field contains 'DVA' and 'Project' contains 'PROMICE'. Below the table is a 'Change Participant' button.
- Active from \***: A date input field containing '17 Jul 2008'.

A legend at the bottom left indicates that asterisks (\*) denote required fields.

Figure 15. Interface of the database, showing a specific instrument

Figure 16 shows the history of a specific instrument can be obtained:

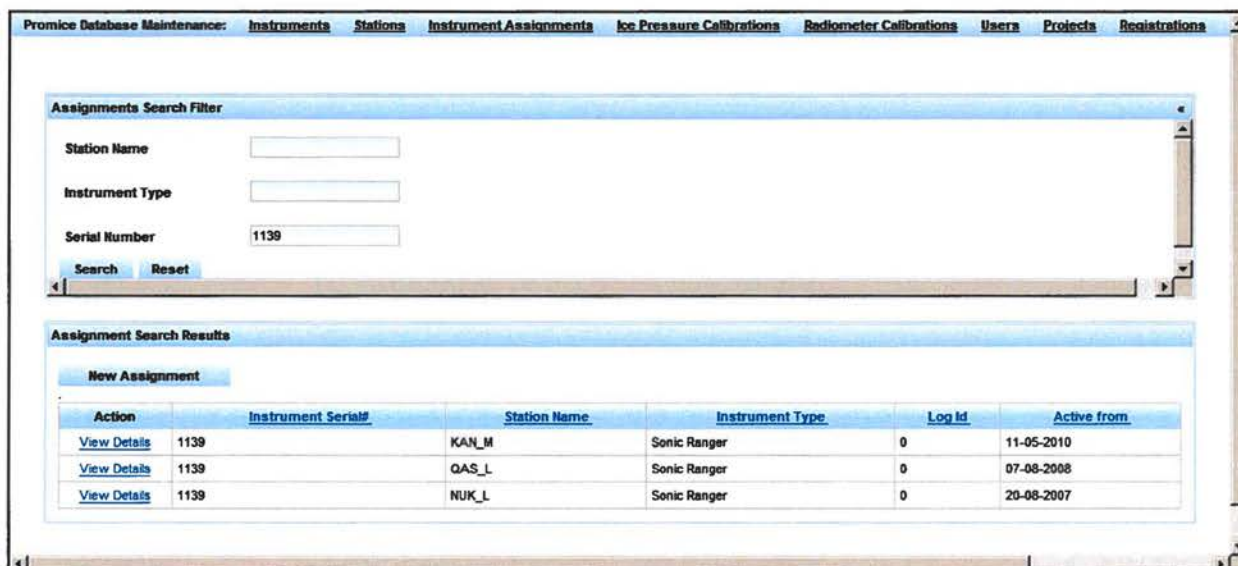


**Figure 16.** Interface of the database showing the history of an instrument

A list of all the parameters that are measured by the automatic weather stations can be found at <http://jupiter.geus.dk/promiceWWW/PromiceParameterListList.seam>

#### Data download website

In order to make data from the PROMICE project publicly available a website interfacing the database has been made. The website is accessible through <http://jupiter.geus.dk/promiceWWW/home.seam> or via a link on [www.promice.org](http://www.promice.org).

The website offers the data that was transmitted by all PROMICE weather stations, and the opportunity to see the latest transmissions from the ice sheet. The PROMICE data are free to download for everyone; all that needs to be done is to complete a short registration form.

It is possible either to browse the real-time data directly on the screen as shown in (figure 18) or download the quality controlled data sets. The data can be accessed both from a list of stations (figure 19) or a map showing the station locations (figure 20).

Before downloading PROMICE data a form with contact information and purpose of use needs to be filled in. The information is stored in the PROMICE data base with the purpose of assessing the use of the PROMICE programme data.

Complimentary weather station data from other GEUS projects dealing with Greenland glaciology such as FreshLink, SEDIMICE, Glacio-Basis, and Greenland Analogue Project are included in the PROMICE data base, and may in some cases be available for download on request. This part of the data base requires login information which can be requested on the download pages.

**PROMICE**  
Programme for Monitoring of the Greenland Ice Sheet

Home Weather Station Map Weather Station List Weather Station Parameters Download Data

**Welcome to the automatic weather station download site**

Currently GEUS operates 24 automatic weather stations on Greenland. The stations measure air temperature, relative humidity, wind speed and direction, atmospheric pressure, incoming and outgoing short- and longwave radiation, ice temperature, surface velocity, snow depth and ice motion. Our stations measure every 10 minutes. Hourly-average values are transmitted in real time (day or week 100-300) and daily averages in winter.

There are 14 automatic weather stations around the margin of the Greenland ice sheet with PROMICE. We offer the data that was transmitted by all PROMICE weather stations, and the opportunity to use the latest transmission from the ice sheet. The data are free to download for everyone, all that needs to be done is to complete a short registration form. For more information on PROMICE see [green.geus.dk](#)

Weather station data from other GEUS projects dealing with Greenland (glaciology) are included in the PROMICE data base, and may in some cases be available for download on request. This part of the data base requires high resolution which you can request on the download pages.

Projects affiliated with PROMICE are:

- [The Greenland Aerial Ice Project](#) (Kangerlussuaq region)
- [Umanuq](#) (Aasiaat region)
- [Preston](#) (Narsarsuaq region)
- [Tasiliuq](#) (Tasiliuq region)

If you have any questions concerning the data or weather stations, do not hesitate to contact [John van den Broek](#) or [Thomas Gammal](#). For general enquiries about PROMICE, contact [Andreas P. Abrahamsen](#), Head of Programme.

© GEUS Øster Voldgade 10, 1320 Copenhagen K, Denmark. Phone: +45 3214 2000 E-mail: [info@geus.dk](mailto:info@geus.dk)

Figure 17. Main page of the PROMICE automatic weather station download site.

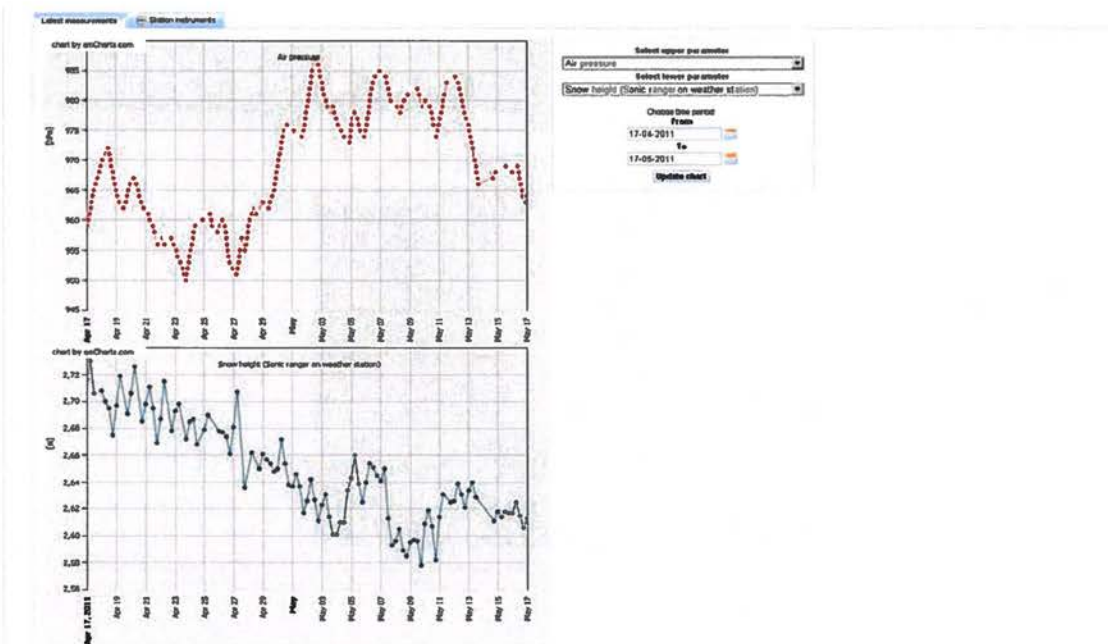


Figure 18. Example of real-time plots of automatic weather station data

**PROMICE**  
Programme for Monitoring of the Greenland Ice Sheet

Home Weather Stations Map Weather Station List Weather Station Parameters Download Data

Automatic Weather Station List - Positions of Start Date

The Automatic Weather Stations are mostly part of the PROMICE project. PROMICE weather station data are available for everyone. However, the site map shows results from other projects. Data from stations other than PROMICE may be available for download under certain conditions. Please refer to the Project and Data/IDV links to see remarks.

Measurements	Reference	Project	Start Date	End Date	Latitude	Longitude	Direction
<a href="#">View Measurements</a>	KAN_B	QAP-FRASP	Apr 13, 2011				
<a href="#">View Measurements</a>	KAN_L	QAP-FRASP	Sep 1, 2008		67.687	-45.823	600
<a href="#">View Measurements</a>	KAN_M	QAP-FRASP	Sep 2, 2008		67.666	-46.816	1270
<a href="#">View Measurements</a>	KAN_U	QAP-FRASP	Apr 4, 2009		67.620	-47.017	1650
<a href="#">View Measurements</a>	KPC_L	PROMICE	Jul 12, 2009		70.911	-26.000	300
<a href="#">View Measurements</a>	KPC_U	PROMICE	Jul 17, 2009		78.826	-25.170	870
<a href="#">View Measurements</a>	MT	SESMICE	Mar 3, 2009		65.693	-37.829	460
<a href="#">View Measurements</a>	MUK_L	PROMICE	Aug 20, 2007		64.402	-45.529	500
<a href="#">View Measurements</a>	MUK_M	PROMICE	Jul 25, 2010		64.396	-46.119	920
<a href="#">View Measurements</a>	MUK_U	PROMICE	Aug 20, 2007		64.459	-43.266	1140
<a href="#">View Measurements</a>	QAS_L	PROMICE	Aug 24, 2009		61.021	-46.848	510
<a href="#">View Measurements</a>	QAS_U	PROMICE	Aug 7, 2008		61.178	-46.817	600
<a href="#">View Measurements</a>	SCO_L	PROMICE	Jul 21, 2008		72.229	-26.816	470
<a href="#">View Measurements</a>	SCO_U	PROMICE	Jul 21, 2008		72.284	-27.264	1000
<a href="#">View Measurements</a>	TAS_L	PROMICE	Aug 23, 2007		65.641	-30.899	270
<a href="#">View Measurements</a>	TAS_U	PROMICE	Aug 15, 2007		65.701	-30.855	600
<a href="#">View Measurements</a>	THU_L	PROMICE	Aug 9, 2010		76.400	-47.736	570
<a href="#">View Measurements</a>	THU_U	PROMICE	Aug 9, 2010		76.420	-47.056	770
<a href="#">View Measurements</a>	URF_L	PROMICE	Aug 17, 2009		72.892	-44.295	230
<a href="#">View Measurements</a>	URF_U	PROMICE	Aug 17, 2009		72.891	-53.535	880
<a href="#">View Measurements</a>	ZAK_M	CloudBase	Mar 29, 2008		74.626	-20.824	800
<a href="#">View Measurements</a>	ZAK_S	CloudBase	Mar 25, 2008				
<a href="#">View Measurements</a>	ZAK_I	CloudBase	May 5, 2009		74.620	-21.820	0

© GEUS Øster Voldgade 10, 1350 Copenhagen K, Denmark. Phone +45 3014 2000 E-mail [info@geus.dk](mailto:info@geus.dk)

Figure 19. Automatic weather station list



Figure 20. Automatic weather station map

## Data treatment and success rate

### Station description

We currently maintain a network of 14 identical automatic weather stations (AWSs) within PROMICE. For various reasons the AWSs and their logger programs underwent a few changes since the start of the programme in 2007. The text in this chapter deals with the latest assemblies of hardware and software versions: the PROMICE 2008/2009 station design, and the 2009 logger program.

The PROMICE AWSs are equipped with:

- a CR1000 data logger and AM 16-32A Multiplexer
- a NAL 9601-D Iridium transmission system with GPS antenna
- a Campbell CS100 barometric pressure sensor
- a ventilated Rotronics radiation shield holding a MP100 temperature probe and a HygroClip temperature & relative humidity sensor
- a Young 05103 wind monitor
- a Kipp & Zonen CNR1 net radiometer
- two Campbell SR50 sonic rangefinders (one on the AWS, one on stakes)
- one GEUS-made ablation assembly using a NT1400 pressure transducer
- a GEUS-made thermistor string with eight PT100 thermistors
- a NS25-E2 tilt sensor
- a BP Solar 10-Watt solar panel
- four Panasonic 28 Ah sealed lead-acid batteries

### AWS output

#### *Measurement and transmission frequencies*

The PROMICE AWSs measure and store data every ten minutes. The only exception to this are the wind speed observations, which give the mean wind speed since the last measurement cycle, and the GPS measurements, which follow the transmission schedule. In winter (days of year 300 to 100), values of measured quantities are transmitted just once a day – to limit power consumption when solar power is not available – at midnight. In summer (days of year 100 to 300), values are transmitted on the hour, every hour. The transmissions consist of average values (daily or hourly) of the more variable quantities, such as temperature and radiation. Instantaneous values of less variable quantities, such as surface height and station tilt, are appended once every six hours in summer, and every day (thus for all transmissions) in winter.

#### *Column assignment of raw data files*

#### Locally stored logger data

- 1- Date and time (UTC)
- 2- Record number
- 3- Minutes in year
- 4- Air pressure (hPa)
- 5- Air temperature by PT100 (°C)
- 6- Air temperature by HygroClip (°C)
- 7- Relative humidity (% with respect to water, not ice)
- 8- Wind speed (m/s)
- 9- Wind direction (° relative to north at installation)
- 10- Wind direction standard deviation
- 11- Incoming shortwave radiation (~V)
- 12- Outgoing shortwave radiation (~V)
- 13- Incoming longwave radiation (~V)
- 14- Outgoing longwave radiation (~V)
- 15- CNR1 casing temperature (°C)
- 16- Snow height by SR50 on AWS (m)
- 17- Snow height SR50 measurement quality
- 18- Surface height by SR50 on stakes (m)
- 19- Surface height SR50 measurement quality
- 20- Ice height by NT1400 (~V)
- 21-28- Ice temperature 1-8, roughly 1, 2, 3, 4, 5, 6, 7, 10 m depth at installation (°C)
- 29- Station tilt in X-direction = east-west direction at installation (~V)
- 30- Station tilt in Y-direction = north-south direction at installation (~V)
- 31- GPS time
- 32- Latitude (ddmm.mmmmm)
- 33- Longitude (ddmm.mmmmm)
- 34- Elevation (m)
- 35- Geoidal height (m)
- 36- Unit
- 37- GPS quality
- 38- Number of GPS satellites
- 39- Horizontal dilution of precision
- 40- Temperature in logger enclosure (°C)
- 41- Current drawn by ventilator in Rotronics assembly (mA)
- 42- Voltage of batteries before measurements (V)
- 43- Voltage of batteries after measurements (V)

#### Transmitted data

- 1- Date and time (UTC)
- 2- Air pressure (hPa) - *average*
- 3- Air temperature by PT100 (°C) - *average*
- 4- Air temperature by HygroClip (°C) - *average*
- 5- Relative humidity (~% with respect to water, not ice) - *average*
- 6- Wind speed (m/s) - *average*
- 7- Wind direction (° relative to north at installation) - *average*

- 8- Wind direction standard deviation - *average*
- 9- Incoming shortwave radiation (~V) - *average*
- 10- Outgoing shortwave radiation (~V) - *average*
- 11- Incoming longwave radiation (~V) - *average*
- 12- Outgoing longwave radiation (~V) - *average*
- 13- CNR1 casing temperature (°C) - *average*

- 
- 14- Snow height by SR50 on AWS (~m) - *instantaneous*
  - 15- Surface height by SR50 on stakes (~m) - *instantaneous*
  - 16- Ice height by NT1400 (~V) - *instantaneous*
  - 17-24- Ice temperature 1-8, roughly 1, 2, 3, 4, 5, 6, 7, 10 m depth at installation (°C) - *instantaneous*
  - 25- Station tilt in X-direction, east-west direction at installation (~V) - *instantaneous*
  - 26- Station tilt in Y-direction, north-south direction at installation (~V) - *instantaneous*
  - 27- GPS time- *instantaneous*
  - 28- Latitude (ddmm.mmmmm) - *instantaneous*
  - 29- Longitude (ddmm.mmmmm) - *instantaneous*
  - 30- Elevation (m) - *instantaneous*
  - 31- Horizontal dilution of precision - *instantaneous*
  - 32- Current drawn by ventilator in Rotronics assembly (mA) - *instantaneous*
  - 33- Voltage of batteries (V) - *instantaneous*

- 
- 34- Air pressure (hPa) - *instantaneous*
  - 35- Air temperature by PT100 (°C) - *instantaneous*
  - 36- Relative humidity (~% with respect to water, not ice) - *instantaneous*
  - 37- Wind speed (m/s) - *instantaneous*
  - 38- Wind direction (° relative to north at installation) - *instantaneous*
  - 39- Wind direction standard deviation – *instantaneous*

### **Calculation of physical quantities**

All raw measured variables are outputted in useable physical units, with the exception of the following.

#### *Shortwave and longwave radiation*

The PROMICE logger program multiplies all four radiation readings (shortwave in&out (SR), longwave in&out (LR); output in mV) by a factor 100 to better resemble flux values (W/m<sup>2</sup>). In the processing stage the output is recalculated into μV units, and divided by the calibration coefficient C (in μV/(W/m<sup>2</sup>)) as provided by the sensor's manufacturer. Incoming and outgoing longwave radiation also needs an adjustment for sensor casing temperature. Recalculation:

$$SR = SR * 10 / C_{SR}$$

$$LR = LR * 10 / C_{LR} + 5.6704e^{-8} (T_{CNR1})^4$$

where sensor casing temperature  $T_{CNR1}$  is in Kelvin ( $=T_{CNR1}(°C)+273.15$ ).

### Ice height

The pressure transducer is drilled into the ice a few meters to a few tens of meters, enclosed in a closed system of a liquid that is non-freezable at common Greenlandic temperatures (pure antifreeze or an antifreeze & water mixture). As surface ice melts, the station will lower with it, and the pressure of the vertical liquid column on the pressure transducer will decrease. Wintertime accumulation cannot be recorded by pressure transducer. A wintertime increase in pressure transducer output indicates a higher pressure on the hose lying on the surface caused by a snow pack. This signal cannot be translated in accumulated mass and should be disregarded.

In processing the data, the voltage output is recalculated into a vertical liquid column over the sensor. This is done by multiplying the output value by a constant coefficient ( $C_{pt}$ ) as determined from a four-point calibration performed by the manufacturer, and adjust for density of the liquid:

$$H_{pt} = H_{pt} * C_{pt} * \rho_w / \rho_m$$

where  $\rho_w$  is the density of water at room temperature (998 kg/m<sup>3</sup>) and  $\rho_m$  is the density of the liquid/mixture in the pressure transducer system at the approximate ice temperature (see Table 4):

- 100% ethylene glycol = ~1150 kg/m<sup>3</sup> around 0 °C
- 50/50 ethylene glycol & water mixture = ~1090 kg/m<sup>3</sup> around 0 °C

For more accurate determination, GEUS calibrations and exact values for  $\rho_m$  as determined at GEUS can be found in the AWS metadata.

Specific Gravity from www.engineeringtoolbox.com							
Temperature (°C)	Ethylene Glycol Solution (% by volume)						
	25	30	40	50	60	65	100
-40	frozen	frozen	frozen	frozen	1.12	1.13	frozen
-17.8	frozen	frozen	1.08	1.10	1.11	1.12	1.16
4.4	1.048	1.057	1.07	1.088	1.1	1.11	1.145
26.7	1.04	1.048	1.06	1.077	1.09	1.095	1.13
48.9	1.03	1.038	1.05	1.064	1.077	1.082	1.115

**Table 4.** Density of the liquid/mixture used for the pressure transducer at approximate temperatures.

### Tilt

Tilt readings in V are multiplied by a factor 10 in the logger to better resemble tilt values in degrees. In the recalculation we remove this factor (Tilt=Tilt/10) and use the following polynomial to obtain tilt in degrees in both 'X' and 'Y' direction:

$$\text{Tilt}(\text{°}) = [\text{sign of Tilt}] * (-0.49 \text{ abs}(\text{Tilt})^4 + 3.6 \text{ abs}(\text{Tilt})^3 - 10.4 \text{ abs}(\text{Tilt})^2 + 21.1 \text{ abs}(\text{Tilt}))$$

Note that we strive to place the tilt sensor so that its output resembles mast and radiation sensor tilt within 0.5°, but differences up to a few degrees may occur - chiefly in the X direction (east-west) due to the method of attaching the sensor to the boom.

## Corrections

### *Air temperature by HygroClip*

Due to an error by our supplier some of the HygroClips deployed in Greenland measure in a different voltage range than others. For this reason *some* HygroClips have an offset of 40 °C. Correction:  $T = T - 40$ .

You may notice that the temperatures as measured by PT100 and HygroClip can differ more than one degree, which cannot be explained by sensor inaccuracies as stated in the manuals. We recommend you use the more accurate PT100 readings.

### *Relative humidity*

Relative humidity is measured with respect to water, i.e. it needs correction at sub-freezing temperatures.

Recalculation:

$RH = RH * e_w / e_i$  for  $T < 0$  °C.

Saturation vapour pressure over water  $e_w$  (Goff & Gratch):

$$\log_{10} e_w = -7.90298 (373.16/T-1) + 5.02808 \log_{10}(373.16/T) \\ - 1.3816 \cdot 10^{-7} (10^{11.344 (1-T/373.16)} - 1) + 8.1328 \cdot 10^{-3} (10^{-3.49149 (373.16/T-1)} - 1) \\ + \log_{10}(1013.246)$$

Saturation vapour over ice  $e_i$  (Goff & Gratch):

$$\log_{10} e_i = -9.09718 (273.16/T - 1) - 3.56654 \log_{10}(273.16/T) \\ + 0.876793 (1 - T/273.16) + \log_{10}(6.1071)$$

with T in Kelvin (= T(°C)+273.15) and  $e_w$  and  $e_i$  in hPa. We use PT100 temperatures for calculation.

After this the values may need a small offset correction based on calibration of the sensor upon return from the field.

### *Wind direction*

When metadata indicate that the wind sensor / AWS is not north-south aligned, a (possibly time-dependent) offset value is added / subtracted. Correction:  $WD = WD +/- \text{offset}$ . We are working on a solution with a compass to keep track of station orientation.

### *Shortwave radiation*

Shortwave radiation measurements are highly sensitive to the tilt of the radiation sensor, which is the main reason why PROMICE AWSs are equipped with a tilt sensor. Since the incoming shortwave radiation correction is complicated and relies on a number of assumptions, we leave the correction of the data to the user. For assistance in performing this correction, or to obtain IDL code to do it for you, data users can contact Dirk van As (GEUS).

### *Snow and surface height by sonic ranger*

Sonic ranger observations are sensitive to air temperature since the speed of sound depends on the density of the medium that it travels through. The distance H as measured by both sonic rangers is corrected as follows:

$$H = H * (T/273.15)^{0.5}$$

with T in Kelvin (= T(°C)+273.15). We use PT100 temperatures for calculation.

#### *Ice temperatures*

Note: As with all observations, the vertical position relative to the surface of the measured ice temperatures changes depending of the time of year, though most sensors have a fixed height after the wintertime accumulation has melted away. Keep in mind that, depending on the net mass balance at the AWS site, the thermistor string will melt out in two or more years.

#### **Data overview**

Since the start of PROMICE in 2007 a wealth of data from the AWSs on the ice sheet was gathered. For instance, Table 5 gives the overview of the temperature data coverage from the PROMICE automatic weather station. We have 77% coverage of useable data up to January 2011, either collected in the field or successfully transmitted since the last station visit. Including the data that has not been transmitted, but is stored in the data loggers awaiting the next station visit, the success rate could reach 86%. These 9% are from stations that did not transmit part of the recorded data since the last station visit, which is related to a threshold we built into the station's logger program: if battery power drops below a certain value the station will continue to operate, but without power-consuming functions such as transmission.

Data gaps have occurred due to malfunctioning Campbell Scientific data loggers. for instance, one station (NUK\_U) was equipped with a troubled older type CR10X logger which stopped operation in December 2007 and again in 2008. All of these older data logger types have been replaced by the new CR1000 loggers since. But our largest problem to date occurred after the station visits in 2010, during which we uploaded the latest version of the Campbell Scientific operating system (OS18). This operating system contains a bug that caused all visited stations to get stuck during a measurement cycle, halting all functions and draining the batteries. The bug was triggered when a certain measurement value occurred, one that we could not come across during testing in Denmark. We revisited all affected weather stations as soon as we could, and uploaded a previously well-tested operating system.

In other instances data quality was reduced by a station either being blown over by extreme winds, or having fallen into a crevasse. Problems related to power supply and malfunctioning equipment can be overcome and will become less likely to occur the more we learn from past experiences. But problems due to crevassed terrain and wind damage will be a recurring theme for automatic weather stations in the ablation zone of the Greenland ice sheet. We will not consider replacing the weather stations in the harshest locations to areas that are more forgiving, since we do need measurements in all sectors of the ice sheet, not just the ones where operating a weather station is relatively easy.

Year	Month	KPC_L	KPC_U	SCO_L	SCO_U	TAS_L	TAS_U	QAS_L	QAS_U	NUK_L	NUK_U	UPE_L	UPE_U	THU_L	THU_U
2007	8					3.63	3.53	5.64		5.27	2.45				
2007	9					1.52	1.98	2.76		0.91	-3.00				
2007	10					-1.62		0.41		-3.31	-7.63				
2007	11					-3.88		-2.68		-6.09	-9.67				
2007	12					-6.22		-9.52		-12.99	-16.38				
2008	1					-8.89		-11.44		-15.64					
2008	2					-11.57		-11.14		-15.41					
2008	3					-7.81	-11.17	-6.18		-9.95					
2008	4					-2.62	-3.95	1.05		-0.82					
2008	5					0.31	-0.44	3.48		3.18					
2008	6					3.83	3.03	3.95		5.03					
2008	7	5.13	1.19	4.43	3.04	4.41	3.49	4.13		5.88					
2008	8	1.90	-1.61	3.06	1.60	4.08	3.14	4.36	0.98	4.12	0.54				
2008	9	-5.72	-9.53	-1.86	-4.55	2.16	0.51	2.29	-2.46	0.62	-3.12				
2008	10	-15.71	-22.22	-11.08	-14.66	-3.16	-5.52	-1.22	-7.39	-3.92	-7.88				
2008	11		-26.49	-16.90	-19.83	-6.28	-6.86	-2.46	-7.92	-4.35	-7.95				
2008	12		-26.92	-14.21	-16.47	-5.68	-7.41	-8.07	-14.75	-11.10	-13.13				
2009	1		-27.88	-14.51	-17.34	-5.00	-5.99	-5.77	-13.30	-7.92					
2009	2		-30.55	-20.55	-21.55	-4.57	-5.52	-4.11	-11.96	-7.86					
2009	3		-31.09	-19.06	-21.28	-4.52		-7.45	-14.88	-13.09					
2009	4		-26.06	-15.43	-16.57	-2.61		-1.11	-5.33	-4.18					
2009	5		-9.47	-1.69	-3.61	0.43	-0.71	0.32	-1.40	-1.48					
2009	6		-4.66	1.54	1.04	1.67	1.31	3.79	0.36	4.17					
2009	7		0.94	3.82	3.29	3.39	2.86	4.64	1.72	5.55					
2009	8		-2.38	2.28	0.67	2.30	2.00	4.30	1.20	4.97	1.24	3.66	-0.48		
2009	9		-12.27	-5.08	-8.05	-0.33	-1.59	1.15	-3.15	-0.43	-4.32	-1.87	-7.90		
2009	10		-20.52	-13.73	-15.54	-4.17	-6.07	-1.47	-7.72	-4.70	-9.51	-8.40	-13.54		
2009	11		-26.64	-15.79	-15.58	-5.76	-7.69	-6.53	-12.40	-11.00	-13.63	-14.91	-20.33		
2009	12		-23.34	-13.29		-5.28	-6.94	-3.91	-9.70	-5.31	-9.00	-9.28	-14.04		
2010	1		-29.76	-13.80		-2.97	-4.36	-2.72	-8.02	-5.86	-8.09	-16.36	-19.35		
2010	2		-27.07	-18.35		-7.57	-9.53	-1.72	-8.84	-3.82	-8.19	-11.44	-14.64		
2010	3		-30.10	-19.93		-7.24	-8.84	-3.67	-9.96	-6.96	-10.41	-15.62	-16.38		
2010	4		-19.88	-10.32		-4.38	-6.86	-0.37	-5.36	-2.71	-6.79	-10.26	-12.66		
2010	5		-10.08	-2.60				0.32	4.25	0.59	4.13	0.89	-0.53	-3.13	
2010	6		-1.88	2.21				2.81	4.09	1.20	4.31	1.78	4.23	1.85	
2010	7		0.85	4.24	3.68			2.88	4.37	1.78	5.15	2.45	5.07	2.08	
2010	8		-2.98	2.86	1.47	2.81	3.03		2.90	5.78		5.11	2.26	2.97	2.17
2010	9		-13.22	3.18	-0.98	2.47	2.14			3.83		0.58	-3.41	-3.03	1.32
2010	10		-20.08	-12.44	-16.24	-3.47	-2.42			-0.98	-2.97	-3.48	-8.38		
2010	11		-24.44	-15.45	-16.91	-5.97	-6.16	0.31		-2.49	-5.85	-4.38	-9.60		
2010	12		-23.70	-13.22	-16.23	-4.07	-7.68	1.92		-3.05	-5.91	-7.78	-12.62		
2011	1		-27.55	-16.10	-18.64	-8.00	-11.16	-8.49		-9.02	-11.69	-9.46	-16.11		

**Table 5.** Data coverage chart for each PROMICE automatic weather station. Yellow indicates that data have been collected in the field. Red: no data collected in the field yet; values (if available) were transmitted through satellite link. Blue: data record is complete, but reduced accuracy because station had been blown over or slid into a crevasse. White gaps: no data due to data logger malfunction.

**Direct data delivery to WMO network**

PROMICE delivers real-time data to the global observational network of the World Meteorological Organisation (WMO). These data are used for improved performance of atmospheric circulation models in an area of the globe where observations to feed models are sparse.

As mentioned in section X, appended to transmissions of hourly or daily averages of meteorological variables measured by the PROMICE stations, are instantaneous values for air pressure, air temperature, relative humidity, wind speed and wind direction (every 6 hours in summer and 24 hours in winter). We forward the email messages containing these instantaneous values to the Danish Meteorological Institute, which has a line of communication with WMO.

## Fieldwork

### Placing transects of automatic weather stations on the ice sheet

There are currently seven PROMICE automatic weather station transects in Greenland, i.e. the network is complete. Each transect consist of two AWSs; one near the equilibrium line where yearly accumulation and ablation are balanced, and one at low elevation well into the ablation zone. (NB: The TAS-transect in the southeast / Tasiilaq region is the exception, where both stations are positioned at a fairly low elevation for reasons of accessibility). A map of the currently active automatic weather stations (and a few prior stations) placed on ice in Greenland is shown in Figure 21.

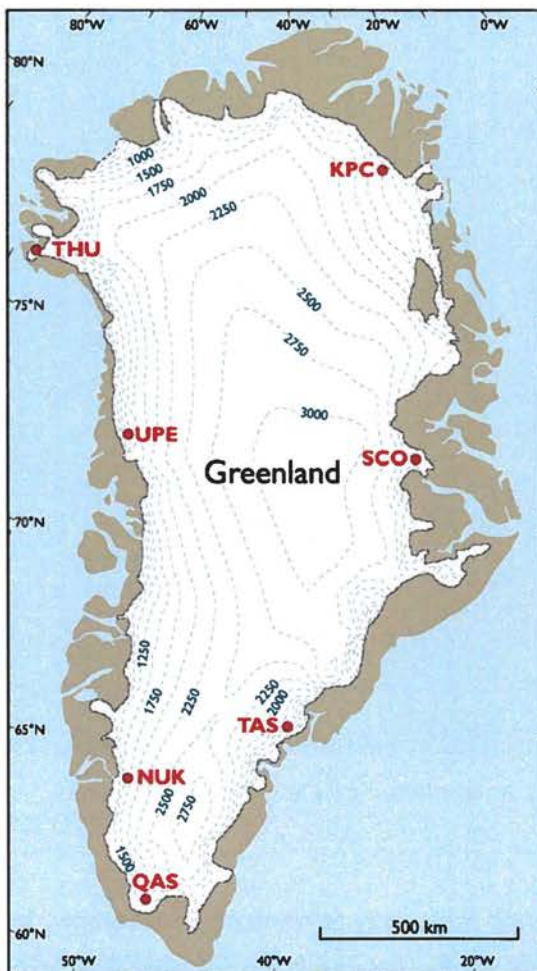


**Figure 21.** Map of PROMICE automatic weather stations in Greenland. Other weather stations (the American GC-Net, the Dutch K-transect and nine GEUS stations from other projects) are not shown.

The initial construction of all AWS transects was done by helicopter. This means of transportation allows us to bring more weight to the ice than the alternatives offer, albeit at much higher cost. Unless the situation requires a different approach, we start constructing the upper AWS, as the weather is often less predictable the higher you travel onto the ice sheet. Placement of a single AWS takes about three hours depending on the level of preparation done before going to the ice. A way to shorten the stay on the ice is to construct the entire aluminium tripod prior to the helicopter charter, which involves attaching wires, shackles, kee clamps, feet, etc., and folding it to be able to fit it into the helicopter. Also, the boom holding most of the sensors can be prepared off the ice provided the sensors on the boom will be wrapped before shipment to avoid damage.

A major advantage in this is that the sensors need to be aligned precisely, for which you need to take time and which is easier in a warm environment.

The placement of an AWS starts with unfolding the tripod, tightening the steel wires, and laying it on its side using a custom-made rest (see Figure 22). The boom with sensors is is

mounted at the top of the mast, and below we mount the temperature and humidity assembly, the solar panel, the enclosure of the pressure transducer assembly, and the logger enclosure. All cables are plugged into the logger enclosure and tied to the mast. After putting the tripod on its feet, we carefully orientate the station so that the boom is exactly in north-south direction, with the radiation sensor directed towards the south, and the wind speed sensor towards the north. Also, the solar panel is mounted facing south – so that at the end of the dark winter during which the station has been using up part of its power reserve, the batteries can be recharged as soon as the sun rises over the horizon for the first time in the year. After orientating the station, the heavy battery box is hung underneath the tripod with a set of wires, and the station is powered up. The weight of the battery box (about 48 kg), and its low position keeps the station upright during strong winds.



**Figure 22.** *Mounting of instruments and boom on a station tripod on the ice sheet. Note the practical, adjustable custom-made rest.*

Three sensors are not (fully) mounted on the AWS: the pressure transducer assembly, the thermistor string, and the second of the sonic rangers. The holes for the pressure transducer and thermistor string are drilled into the ice using either a mechanical Kovacs drill (faster and lighter), or a steam drill (more reliable). The second sonic ranger is mounted on a stake assembly consisting of three interconnected stakes, which is also drilled into the ice. All drill holes combined add up to a length of over 50 meters.



**Figure 23.** *Drilling with the Kovacs mechanical drill. Note the practical one metre auger pieces.*

With all sensors mounted and the system powered up, the station is operational. We test the AWS by connecting a laptop to the logger. With this we read out the current values that the sensors measure, including for instance GPS position and the current of the fan ventilating the temperature and humidity assembly. If a value is out of its normal range, we look into the problem.

Finally, we fill in a check list, which gives us crucial information on position, initial station tilt, length of the stakes at installation, anything out of the ordinary, anything we may have forgotten, etc. After this, we pack everything in the helicopter and clean up behind us before we move to the second location to place the other AWS.

## **Performing maintenance on transects of automatic weather stations**

Visiting an existing (transect of) automatic weather station(s) is commonly done by helicopter – as is the initial installation. However, three transects have been placed in regions where we can get to over land. For the stations in the northeast (the KPC transect in Figure X) the use of snow mobiles allows us to visit the stations from Station Nord in spring. For the stations in the southeast (the TAS transect in Figure 14) we have connections with the inhabitants of Tasiilaq and surroundings, who assist us in travelling to the stations by dog sled (see Figure X).



**Figure 24.** *Visiting the station transect near Tasiilaq in Southeast Greenland by dog sleds.*

There are several levels of thoroughness in performing automatic weather station maintenance. The lowest level for a station visit occurs when someone unfamiliar with the system is visiting a station. We ask this person to either download the data or replace the memory card in the logger enclosure so we obtain the full data record. In addition, the person is asked to fill in a checklist and make photos so we learn of the current status of the station.

The next level of thoroughness is when GEUS personnel familiar with the station design visit a station. For a station that is fully functional, standing upright and orientated correctly, we perform the actions as described above, and replace the hygrocip (humidity and temperature) and the membranes in the sonic rangers. If needed, we upload a new program into the logger. A station visit of this type takes about an hour. It takes 30-45 minutes to download one year worth of data onto a laptop. Depending on the ablation rate at the station we may have to drill new holes for the stake assembly and/or thermistor string and/or pressure transducer, which will add to the time spent at the station considerably.

If more sensors need to be replaced since they require recalibration or are malfunctioning, maintenance will take up more time (at least three hours, but up to six hours if there is damage to the station). Problems can range from sensors being destroyed by strong winds, to having melt water in the system, to finding bent tripod legs, or stations toppled by extreme winds or crevasses (see Figure 25). If a station is visited in spring (See Figure 26), a snow layer of up to two meters will complicate work on the station – digging through such a layer of snow will take hours alone. For a particular visit at the lower TAS station in spring

2009, removing the snow from the (toppled) station took six hours with six men working in shifts of three.

In our experience, replacing an old station by a completely new one often takes less time than doing a considerable amount of maintenance work on a station, i.e. replacing parts and sensors. This has to do with the fact that building and taking down stations are straight-forward activities, while doing repairs on a station could involve all sorts of surprises.



**Figure 25.** *Salvaging instruments from a station fallen into a crevasse on the Qassimiut lobe in South Greenland.*



**Figure 26.** Station QAS\_U in South Greenland in springtime covered in snow.

## Development of a new calving model for numerical ice flow modelling

### Introduction

Calving of icebergs accounts for perhaps as much as half the ice transferred from the Greenland Ice Sheet into the surrounding ocean, and virtually all of the ice loss from the Antarctic Ice Sheet. Recent observations have shown that changes in calving rate can greatly reduce the extent of floating ice shelves and ice tongues, potentially resulting in increased discharge from the interior [Joughin et al, 2004; Rignot et al., 2004]. While the break-up of floating ice tongues has no direct effect on global sea level, the resulting speed up of grounded ice can have dire consequences for global sea level. Indeed, a wide range of observations applying to both current ice masses and paleo ice sheets, point to iceberg calving as a major factor in rapid ice-sheet changes [Van der Veen, 2002]. It is, therefore, important to formulate a calving model that can be readily incorporated into time-evolving numerical ice-flow models.

We have formulated a calving model that can be readily incorporated into time-evolving numerical ice-flow models. This new calving criterion is based on a physical model of calving processes.

Our model is based on downward penetration of water-filled surface crevasses and upward propagation of basal crevasses. A calving event occurs when the depth of the surface crevasse (which increases as melting progresses through the summer) reaches the height of the basal crevasse (Figure 27).



**Figure 27.** Diagram showing the calving mechanism

#### **Ice flow model**

The calving model has been implemented into a numerical ice flow model that calculates the flow and evolution of the geometry, which is based on the model used in *Nick et al.* [2009]. Figure (28) illustrates the geometry of the model extended from the ice divide to the calving front.

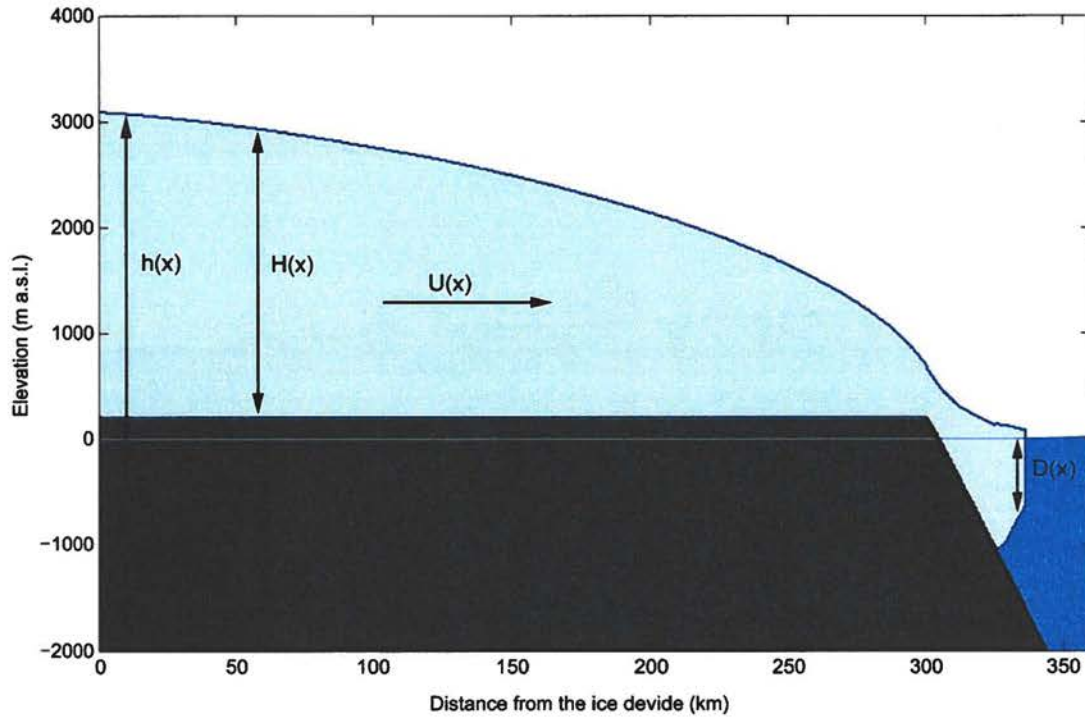


**Figure 28.** *Geometry of the model.*

### Continuity and force balance

Considering a flowband of width  $W$  and thickness  $H$ , conservation of mass is expressed by the depth-integrated continuity equation [Van der Veen, 1999; Oerlemans, 2001]. Vertically-integrated model includes (Longitudinal, lateral, basal stresses)

$$\frac{\partial H}{\partial t} = -\frac{1}{W} \frac{\partial q}{\partial x} + a \quad (1)$$

where  $t$  is time,  $x$  is the distance along the central flowline,  $a$  is the surface mass balance. Neglecting the effect of sloping sidewalls, the horizontal ice flux through a cross section of the flowband is given by  $q=HWU$ , with  $U$  the vertically-averaged horizontal ice velocity.

Conservation of momentum requires [Vieli and Payne, 2005]

$$2 \frac{\partial}{\partial x} \left[ H \nu \frac{\partial U}{\partial x} \right] - \mu A_s \left( \left( H - \frac{\rho_i}{\rho_p} D \right) U \right)^{\frac{1}{n}} - \frac{2HB}{W} \left( \frac{5U}{W} \right)^{\frac{1}{n}} = \rho_i g H \frac{\partial h}{\partial x} \quad (2)$$

$A_s$  and  $\mu$  are the sliding and friction parameter.  $\nu$  is the strain-rate dependent effective viscosity.

### Boundary Conditions

The upglacier boundary ( $x = 0$ ) corresponds to the ice divide where the surface slope and horizontal velocity are set to zero. At the calving front, the longitudinal stress is balanced by

the difference between hydrostatic pressure of the ice and water, giving for the stretching rate at the terminus

$$\frac{\partial U}{\partial x} = \left[ \frac{\rho_i g}{4B} \left( H - \frac{\rho_p}{\rho_i} \left( \frac{D^2}{H} \right) - \frac{\sigma_B}{\rho_i g} \right) \right]^n \quad (3)$$

$\sigma_B$  is the back pressure from sea ice or sikkusak.  $\rho_p$  is the density of sea or lake water.

The second boundary condition at the terminus is the calving criterion. Using the new calving model, the glacier terminus calves off when the sum of the basal and surface crevasse depths reaches the glacier thickness. This calving criterion allows formation of an ice shelf or a floating tongue when this sum is smaller than the flotation thickness. The transition between grounded ice and shelf is achieved through setting basal resistance to zero; that is, the friction parameter,  $\mu$ , in Equation (2) is set to zero when the ice thickness becomes less than the flotation thickness.

## Results

Our numerical ice sheet model is able to reproduce observed seasonal changes of Greenland outlet glaciers, such as fluctuations in flow speed and terminus positions. We have applied the model to Helheim Glacier on the east coast. The model is capable of reproducing the recent rapid changes of Helheim Glacier (See Figure 29).

Our model suggests that rapid retreat of the calving front is highly affected by the amplified calving rate due to increasing water level in surface crevasses during warmer summers. Our results show little response to seasonally enhanced basal lubrication from surface melt.

This modelling study provides insights into the role of surface and basal hydrology to ice sheet dynamics and on how to incorporate calving in ice sheet models and therefore advances our ability to predict future ice sheet change. Perhaps the most important finding here is that the physically-based calving model directly linked to climate, reproduces seasonal retreat and advance of the glacier terminus.

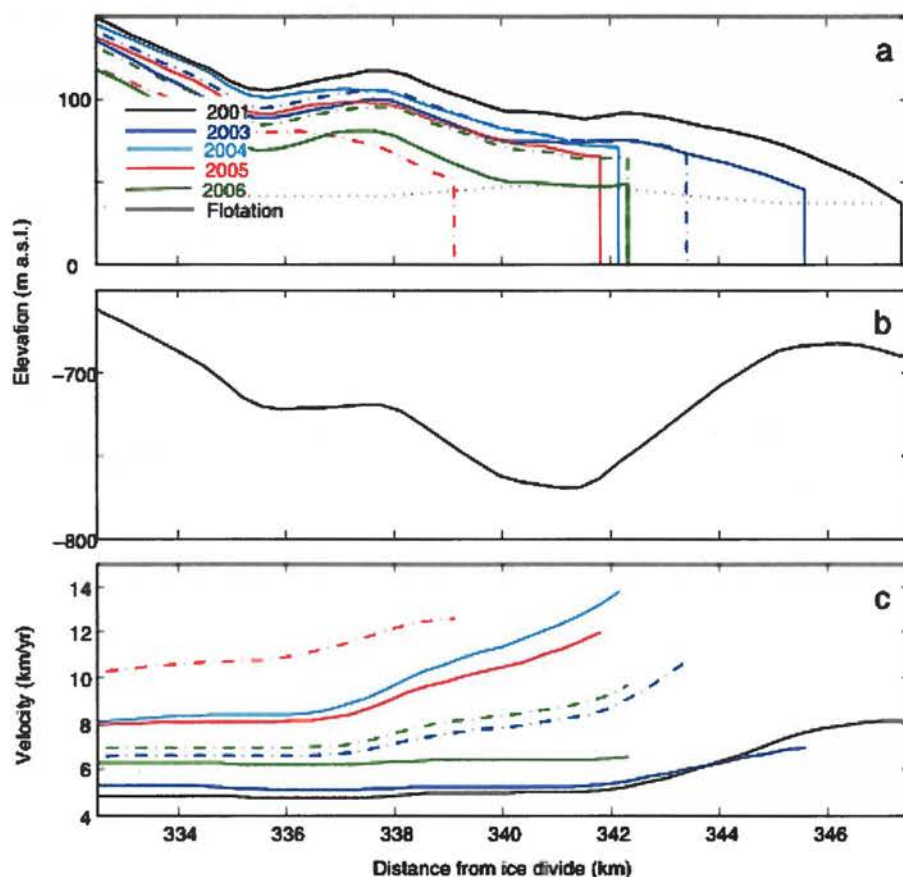


**Figure 29.** Surface (a) and velocity profiles (c) along the flow line near the ice front in the water level experiment. The solid lines correspond to the beginning of the summer season, while the dashed-dotted lines correspond to the end of summer for different years. The dotted line in (a) shows the flotation height, above which the glacier is grounded. (b) The glacier bed topography based on the data from the University of Kansas.

In conclusion, while there are refinements that can be made to better quantify climate forcing on outlet glaciers, our model experiments are robust as to outlet glacier response to these external forcings.

## Improvement of a new air temperature parameterization

This section describes the new and improved near-surface air temperature and its standard deviation parameterizations for Greenland with the use of new observations from automatic weather stations (AWSs) located on land, in the ablation (Abl.) zone and up to the dry snow in the accumulation (Acc.) zone on the ice sheet. The parameterizations are tested by comparing melt area observations from satellite algorithms with the calculated melt area from a PDD model. A comparison with a previous study by Ritz and others (1997) is also carried out to test if the new parameterization improves the calculated melt area extent.

The primary motivation for developing a temperature parameterization is to use it with a PDD model to calculate spatial and temporal variability of the surface mass balance in numerical ice-sheet models without a full coupling between atmosphere and ice sheet, which takes a longer time to integrate numerically. Regional climate models would be more suitable to couple to an ice-sheet model in order to model the behaviour of the climate system on short timescales. Unfortunately, models of this type (Box and others, 2006; Fettweis, 2007) cannot be applied in studies of the evolution of the Greenland ice sheet (GrIS) through ice ages with a sufficiently high spatial and temporal resolution, due to poorly constrained input parameters, such as radiative fluxes and wind speed. This makes the combination of a temperature and standard deviation parameterizations and a PDD model currently the best option for studies of the long-term evolution of ice sheets.

### **Temperature observations**

Temperature observations from the GC-Net (Steffen and others, 1996; Steffen and Box, 2001), the Geological Survey of Denmark and Greenland (GEUS) (Ahlstrøm and others, 2008) and the K-transect (Van de Wal and others, 2005) (Table 6), are used in order to calculate a mean monthly near-surface air temperature for the locations shown in Figure 30.

A monthly mean near-surface air temperature is calculated from hourly observations for each station. The annual mean and the July mean temperatures are calculated for each station using all available mean values for the whole period (1996-2006,

Station Name	Location (latitude and longitude)	Data Period (year, month, day)	Altitude (m.a.s.l)
Data from GEUS			
Sermilik1	61°01.525' N, 046°52.270' W	2001-5-16 to 2002-5-16	350
Sermilik1.2	61°01.525' N, 046°52.270' W	2004-4-16 to 2006-4-25*	350
Tasiilaq2	65°37.200' N, 038°53.522' W	2004-4-1 to 2004-5-29	300
Nuuk2	64°44.174' N, 049°29.555' W	2003-6-1 to 2006-6-1	900
Cryo	75°14.153' N, 057°44.837' W	2004-5-7 to 2006-8-17	200
ImersuaqA	66°17.838' N, 049°44.782' W	1999-6-16 to 2001-3-18	886
Data from GC-NET (CIRES)			
Swiss Camp	69°34.050' N, 049°19.283' W	1995-9-1 to 2006-5-9	1169
Craw. Pt.1	69°52.783' N, 046°59.200' W	1995-9-1 to 2006-5-4	2022
NASA-U	73°50.517' N, 049°29.900' W	1995-9-1 to 2006-4-26	2369
Humboldt	78°31.600' N, 056°49.833' W	1995-9-1 to 2005-4-28	1995
Summit	72°34.783' N, 038°30.300' W	1996-5-14 to 2006-5-2	3208
Tunu-N	78°00.983' N, 033°59.000' W	1996-5-17 to 2005-1-1	2052
DYE-2	66°28.800' N, 046°16.733' W	1996-5-25 to 2006-5-7	2165
JAR1	69°29.850' N, 049°41.267' W	1996-6-20 to 2006-5-10	952
Saddle	65°59.967' N, 044°30.050' W	1997-4-20 to 2006-5-7	2456
South Dome	63°08.933' N, 044°49.033' W	1996-4-23 to 2006-1-1	2901
NASA-E	75°00.033' N, 029°59.833' W	1997-5-3 to 2006-5-3	2614
Craw. Pt.2	69°54.800' N, 046°51.283' W	1997-5-11 to 2001-5-30	1990
NGRIP	75°05.983' N, 042°19.950' W	1997-7-9 to 2005-1-1	2950
NASA-SE	66°28.750' N, 042°29.933' W	1998-4-24 to 2005-5-26	2393
KAR	69°41.967' N, 033°00.350' W	1999-5-17 to 2001-6-7	2579
JAR2	69°25.150' N, 050°03.917' W	1999-6-2 to 2006-5-7	542
JAR3	69°23.667' N, 050°18.600' W	2001-1-1 to 2004-5-27	283
Peterm. ELA	80°05.033' N, 058°04.033' W	2003-5-25 to 2006-4-28	965
Data from the K-transect (IMAU)			
s5	67°03.084' N, 048°14.463' W	2003-8-27 to 2007-8-27	510
s6	67°04.666' N, 049°23.338' W	2003-9-1 to 2007-8-31	1020
s9	67°05.992' N, 050°07.322' W	2003-9-1 to 2007-8-31	1520

\*No data in the winter of 2004/2005

Table ). The mean values show a strong seasonal variation with the lowest temperatures during winter and the highest during summer. The observations show that the slope lapse rate exhibits a strong seasonal variation with a minimum in July and a maximum in February. The temporal coverage is in general sparse, but the above mentioned initiatives, are all the in situ data that are available.

Station Name	Location (latitude and longitude)	Data Period (year, month, day)	Altitude (m.a.s.l)
Data from GEUS			
Sermilik1	61°01.525' N, 046°52.270' W	2001-5-16 to 2002-5-16	350
Sermilik1.2	61°01.525' N, 046°52.270' W	2004-4-16 to 2006-4-25*	350
Tasiilaq2	65°37.200' N, 038°53.522' W	2004-4-1 to 2004-5-29	300
Nuuk2	64°44.174' N, 049°29.555' W	2003-6-1 to 2006-6-1	900
Cryo	75°14.153' N, 057°44.837' W	2004-5-7 to 2006-8-17	200
ImersuaqA	66°17.838' N, 049°44.782' W	1999-6-16 to 2001-3-18	886
Data from GC-NET (CIRES)			
Swiss Camp	69°34.050' N, 049°19.283' W	1995-9-1 to 2006-5-9	1169
Craw. Pt.1	69°52.783' N, 046°59.200' W	1995-9-1 to 2006-5-4	2022
NASA-U	73°50.517' N, 049°29.900' W	1995-9-1 to 2006-4-26	2369
Humboldt	78°31.600' N, 056°49.833' W	1995-9-1 to 2005-4-28	1995
Summit	72°34.783' N, 038°30.300' W	1996-5-14 to 2006-5-2	3208
Tunu-N	78°00.983' N, 033°59.000' W	1996-5-17 to 2005-1-1	2052
DYE-2	66°28.800' N, 046°16.733' W	1996-5-25 to 2006-5-7	2165
JAR1	69°29.850' N, 049°41.267' W	1996-6-20 to 2006-5-10	952
Saddle	65°59.967' N, 044°30.050' W	1997-4-20 to 2006-5-7	2456
South Dome	63°08.933' N, 044°49.033' W	1996-4-23 to 2006-1-1	2901
NASA-E	75°00.033' N, 029°59.833' W	1997-5-3 to 2006-5-3	2614
Craw. Pt.2	69°54.800' N, 046°51.283' W	1997-5-11 to 2001-5-30	1990
NGRIP	75°05.983' N, 042°19.950' W	1997-7-9 to 2005-1-1	2950
NASA-SE	66°28.750' N, 042°29.933' W	1998-4-24 to 2005-5-26	2393
KAR	69°41.967' N, 033°00.350' W	1999-5-17 to 2001-6-7	2579
JAR2	69°25.150' N, 050°03.917' W	1999-6-2 to 2006-5-7	542
JAR3	69°23.667' N, 050°18.600' W	2001-1-1 to 2004-5-27	283
Peterm. ELA	80°05.033' N, 058°04.033' W	2003-5-25 to 2006-4-28	965
Data from the K-transect (IMAU)			
s5	67°03.084' N, 048°14.463' W	2003-8-27 to 2007-8-27	510
s6	67°04.666' N, 049°23.338' W	2003-9-1 to 2007-8-31	1020
s9	67°05.992' N, 050°07.322' W	2003-9-1 to 2007-8-31	1520

\*No data in the winter of 2004/2005

**Table 6.** Details of the automatic weather stations placed on the ice sheet.

### Temperature standard deviation

The standard deviation is the measure of the variability in a series of observations. Mean values of the temperatures together with the standard deviation were calculated from hourly measurements. The standard deviations show a distinct annual cycle with the largest values during winter and the smallest during summer. Smaller values during summer can be explained by the limiting of temperature over a melting snow and ice surface. When the surface temperature reaches the melting point, energy that could potentially raise the near-surface air temperature is used for melting. In the winter no melting occurs and the temperature variations are not limited by the melting point temperature. The temperature variation comes mainly from the diurnal cycle and from low pressure system (Lefebvre and others, 2002). The standard deviations of the mean monthly values are important because they indicate whether the temperature has been above freezing during a month even though the mean monthly value is below. The calculated standard deviation from the mean monthly

temperatures has a strong elevation dependence, which is a dominant parameter for changes seen in the station data.

### Slope lapse rates

Vertical temperature gradients are much larger than the horizontal ones. The common practice when extrapolating temperature fields to higher or lower elevations is to assume a constant atmospheric lapse rate (Ohmura, 1987; Reeh, 1991; Ritz and others, 1997). The choice is based on the average observed lapse rate in the free atmosphere and represents a typical moist adiabatic lapse rate. Despite their broad application it is not clear that free-air lapse rates offer an appropriate estimate of slope lapse rates, as atmospheric boundary layer processes are left out of the equation. The slope lapse rate is the difference between near-surface air temperature at two locations divided by the difference in elevation (Pepin and Losleben, 2002; Marshall and others, 2007).

Mean monthly slope lapse rates and standard deviation (°C/km)	
Jan	-7.9 (±4.6)
Feb	-8.9 (±3.5)
Mar	-7.9 (±2.8)
Apr	-7.3 (±2.3)
May	-5.9 (±2.7)
Jun	-4.7 (±0.6)
Jul	-4.6 (±0.6)
Aug	-5.7 (±0.8)
Sep	-6.9 (±2.2)
Oct	-7.3 (±3.1)
Nov	-6.5 (±3.5)
Dec	-7.6 (±3.7)
Mean	-6.8 (±2.5)

**Table 7.** Mean monthly slope lapse rates and their standard deviation from the seven transects (see figure 30).

Mean monthly slope lapse rates (Table 7) are calculated between stations along seven different transects around Greenland in order to determine the altitudinal variability. The transects are established between low-lying stations located in the ablation zone and stations in the accumulation zone on the GrIS (30). The results show considerable variability with a distinct seasonal cycle. The largest slope lapse rates are seen in the winter and the smallest are observed in the summer. The standard deviation of the slope lapse rate also shows larger values in the winter (Table 7). The maximum monthly slope lapse rate of  $-8.9\text{ }^{\circ}\text{C km}^{-1}$  occurred in February, and the minimum ( $-4.6\text{ }^{\circ}\text{C km}^{-1}$ ) occurred in July. The relatively cold and variable winter temperatures in the interior of the GrIS result in large slope lapse rates and large standard deviations and vice versa for the summer (Table 7). More importantly, in the summertime, the near-surface air temperature in the interior can rise further than at the margin, since temperatures are low enough not to be limited by the ice

surface reaching the melting point. The highest standard deviation values of the ablation season ( $2.2\text{-}2.7\text{ }^{\circ}\text{C km}^{-1}$ ) are found in May, June and September. The lowest values ( $< 0.8\text{ }^{\circ}\text{C km}^{-1}$ ) occur in June, July and August.

The proximity of land to AWSs at low elevations complicates the slope lapse rates. Whereas, over ice there is an often present shallow near-surface inversion layer, where on land conditions vary between convective and stable (Grotjahn, 1993). The observed slope lapse rate could also be influenced by the presence of water, such as the frequent oceanic inversion layers under conditions of low clouds or fog (approximately 400-500 meters deep) (Box and Cohen, 2006). This coastal inversion layer will only affect a few AWS sites on GrIS.

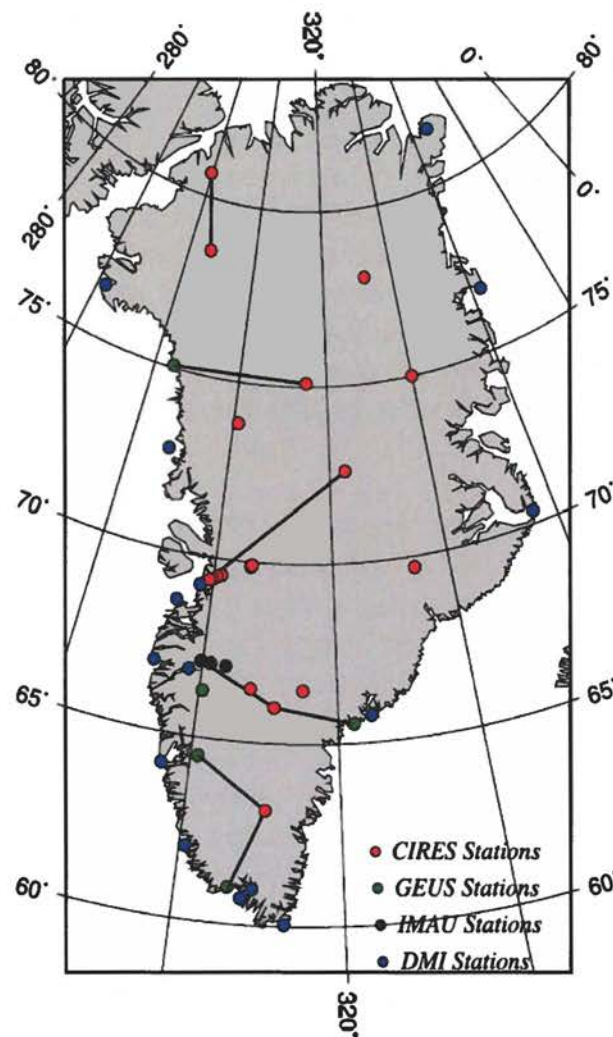


**Figure 30.** The locations of the automatic weather stations on the ice and land used in this study. Black lines indicate seven transects used for slope lapse rate calculations.

### Near-surface air temperature and its standard deviation parameterizations

The near-surface air temperature is one of the boundary conditions of the ice sheet model and it is considered to be a relatively straightforward meteorological variable to extrapolate or interpolate on climatic time scales. Temperature fields are in general continuous and

horizontal temperature gradients are typically low for long-term climatology, in which the effects of weather systems and fronts average out (Ohmura, 1987; Grotjahn, 1993). Vertical temperature gradients are much larger, and the common practice when extrapolating temperature fields to higher or lower elevations is to assume a constant atmospheric lapse rate (Ohmura, 1987; Reeh, 1991; Ritz and others, 1997). The choice is based on the average observed moist adiabatic lapse rate in the free atmosphere. Despite their broad application it is not clear that free-air lapse rates offer an appropriate estimate of slope lapse rates, which is the difference between near-surface air temperature at two locations divided by the difference in elevation (Pepin and Losleben, 2002; Marshall and others, 2007).

Observations from the Greenland Climate Network (GC-Net) (Steffen and others, 1996; Steffen and Box, 2001), the Geological Survey of Denmark and Greenland (GEUS) (Ahstrøm and others, 2008) and the K-transect (Van de Wal and others, 2005), and the automatic weather stations (AWS) from the Danish Meteorological Institute (DMI) (see [www.dmi.dk](http://www.dmi.dk) for further information), are used in order to determine a new present day near-surface air temperature parameterization for the GrIS (Figure 30). This study uses observations from locations on land, in the ablation zone and in the accumulation zone of the GrIS. A mean monthly temperature is calculated from hourly observations each month in a given year for each station. Subsequently, the annual mean and the July mean temperatures are calculated for each station using all available mean values for the whole period (1996-2006). The reason for including the July mean temperature is, because the observations show that the slope lapse rate (Table 7) exhibits a strong seasonal variation with a minimum in July. This variation needs to be taken into account in order to produce a realistic temperature field.

Most ice-sheet models use a positive degree-day (PDD) method to calculate the surface mass balance (Fausto and others, 2009a). Modelling the surface mass balance of the Greenland Ice Sheet (GrIS) in large-scale ice sheet models using temperature parameterizations in relation with the PDD-approach is highly sensitive to a parameter: the temperature standard deviation (Braithwaite, 1984; Reeh, 1991). The PDD method is a statistical approach that relates the totals of positive near-surface air temperatures to the amount of snow or ice that melts. The standard deviation of the near-surface air temperature ( $\sigma_{pdd}$ ) important for PDD-modelling because it indicate whether the temperature has been above freezing during a month even though the mean monthly near-surface air temperature value is below. Fausto and others (2009) demonstrated that a uniform increase of  $\sigma_{pdd}$  from 2.5 to 4.5 °C results in a 33% increase in the modelled melt area over Greenland, so it is important to constrain the  $\sigma_{pdd}$  value with observations. In large-scale ice sheet models of Greenland, it is common that  $\sigma_{pdd}$  is assigned a single value, which typically span the interval 4.5-5.5 °C (Reeh, 1991; Ritz and others, 1997; Tarasov and Peltier, 1999; Greve, 2005). The value of  $\sigma_{pdd}$  is often used as a tuning parameter, instead of using the temperature standard deviations observed at the automatic weather stations (AWSs) on the ice sheet. To add to the temperature parameterization presented by Fausto and others (2009), it is proposed to construct a similar distributed parameterization for temperature standard deviation using the same dataset.

Commonly, large-scale ice sheet models over Greenland calculate the amount of melt using the PDD method by assuming an annual sinusoidal evolution of the near-surface air

temperature (e.g. (Greve, 2005)). The number of PDDs from the normal probability distribution around the monthly mean temperatures during the years, following Reeh (1991), is given as:

$$PDD = \frac{1}{\sigma_{pdd}\sqrt{2\pi}} \int_0^A dt \int_0^{\infty} dTT \exp\left(-\frac{(T - T_{anc}(t))^2}{2\sigma_{pdd}^2}\right) \quad (4)$$

where  $t$  is the time,  $T$  (°C) is the near-surface air temperature (2m),  $T_{anc}$  (°C) is the annual near-surface temperature cycle and  $\sigma_{pdd}$  is the standard deviation of the near-surface air temperature.  $T_{anc}$  is assumed to vary sinusoidally over time,

$$T_{anc}(t) = T_{ma} + (T_{mj} - T_{ma}) \cos\left(\frac{2\pi t}{A}\right) \quad (5)$$

where  $A$  is one year.  $T_{mj}$  and  $T_{ma}$  are the mean July and mean annual near-surface air temperatures.  $\sigma_{pdd}$  is also assumed to vary sinusoidally over time,

$$\sigma_{pdd}(t) = \sigma_a + (\sigma_{j, jja} - \sigma_a) \cos\left(\frac{2\pi t}{A}\right) \quad (6)$$

where  $A$  is one year.  $\sigma_j$ ,  $\sigma_{jja}$  and  $\sigma_a$  are the mean July, mean summer (June, July and August) and mean annual standard deviation of the near-surface air temperatures.

Based on Reeh (1991) and following the study of Fausto and others (2009) the annual mean ( $T_{ma}$ ) and July mean ( $T_{mj}$ ) temperatures are parameterized as a function of altitude ( $z_s$ ), latitude ( $\varphi$ ) and longitude ( $\lambda$ ):

$$T_{ma,mj} = d_{ma,mj} + \gamma_{ma,mj} z_s + c_{ma,mj} \varphi + \kappa_{ma,mj} \lambda \quad (7)$$

where  $\gamma_{ma}$  is the annual mean slope lapse rate,  $\gamma_{mj}$  is the July mean slope lapse rate,  $c_{ma}$  and  $c_{mj}$  are coefficients determining the dependence on latitude,  $\kappa_{ma}$  and  $\kappa_{mj}$  determine the dependence on longitude, and  $d_{ma}$  and  $d_{mj}$  are constants. The values of the coefficients are given in Table 11. The coefficients were optimized by fitting the two parameterization functions to the observed mean temperature values (Table 10), using the least-squares method. The longitudinal dependence is new compared to the study of Ritz and others (1997) and is introduced in order to include the observation that temperatures are generally slightly colder in East Greenland than West Greenland for similar altitudes and latitudes. Mean monthly slope lapse rates (Table 7) are calculated between stations along seven different transects around Greenland in order to determine the variability of  $\gamma_{ma}$  and  $\gamma_{mj}$  used in the temperature parameterization. The transects are established between lowlying stations located in the ablation zone and stations in the accumulation zone on the GrIS (Figure 30).

The standard deviation of the near-surface air temperature over the GrIS is parameterized using data from AWSs located on the ice sheet. The parameterizations are expressed in terms of mean annual, mean summer and mean July temperature standard deviations. Mean monthly values are calculated from hourly temperature observations for each month

in a given year for the Greenland AWSs (for details see Fausto and others (2009a)). The associated standard deviations around the monthly means were calculated and a least-square fit was applied to the observed  $\sigma_{pdd}$  values, assuming a linear dependence on altitude ( $z_s$ ), latitude ( $\phi$ ) and longitude ( $\lambda$ ):

$$\sigma_{pdd} = D_{a,j,jja} + \Gamma_{a,j,jja}z_s + C_{a,j,jja}\phi + K_{a,j,jja}\lambda \quad (8)$$

where  $\sigma_{pdd}$  is the standard deviation parameterization. The values of the coefficients are given in Table 8.

Best Annual ( $\sigma_a^m$ ) fit					
	$D_a$ (°C)	$\Gamma_a$ (°C/km)	$C_a$ (°C/°N)	$K_a$ (°C/°W)	RMSD
This study with $K_a$	0.81	1.031	0.0626	-0.0159	0.56
This study without $K_a$	0.324	1.104	0.0573	0	0.57
This study without $K_a$ and $C_a$	4.22	1.171	0	0	0.63
Best July ( $\sigma_j^m$ ) fit					
	$D_j$ (°C)	$\Gamma_j$ (°C/km)	$C_j$ (°C/°N)	$K_j$ (°C/°W)	RMSD
This study with $K_j$	2.61	1.200	-0.0136	-0.0129	0.55
This study without $K_j$	2.22	1.259	-0.0178	0	0.55
This study without $K_j$ and $C_j$	1.00	1.239	0	0	0.56
Best Summer ( $\sigma_{jja}^m$ ) fit					
	$D_{jja}$ (°C)	$\Gamma_{jja}$ (°C/km)	$C_{jja}$ (°C/°N)	$K_{jja}$ (°C/°W)	RMSD
This study with $K_{jja}$	0.049	1.0797	0.0437	-0.0284	0.57
This study without $K_{jja}$	-0.785	1.2099	0.0338	0	0.59
This study without $K_{jja}$ and $C_{jja}$	1.574	1.2224	0	0	0.61

**Table 8.** Coefficients for Equation (8) and their root mean square difference (RMSD) relative to the observed standard deviation.

Nr.	Station	Location	Elev.	$\sigma_a^m$	$\sigma_a$	diff.	$\sigma_j^m$	$\sigma_j$	diff.	$\sigma_{jja}^m$	$\sigma_{jja}$	diff.
1	Swiss Camp	Abl.	1169	5.6	5.9	-0.3	2.5	2.2	0.3	2.9	2.5	0.4
2	Craw. Pt.1	Acc.	2022	6.5	6.8	-0.3	3.5	4.2	-0.7	3.9	4.3	-0.4
3	NASA-U	Acc.	2369	7.1	7.5	-0.4	3.9	4.3	-0.4	4.4	4.7	-0.3
4	Humboldt	Acc.	1995	7.0	6.8	0.2	3.5	3.7	-0.2	4.0	4.4	-0.4
5	Summit	Acc.	3208	8.0	8.6	-0.6	5.0	4.6	0.4	5.6	5.8	-0.2
6	Tunu-N	Acc.	2052	7.4	7.1	0.3	3.6	3.7	-0.1	4.7	4.6	0.1
7	DYE-2	Acc.	2165	6.4	7.0	-0.6	3.7	3.8	-0.1	3.9	4.3	-0.4
8	JAR1	Abl.	952	5.4	5.3	0.1	2.2	1.8	0.4	2.7	2.2	0.5
9	Saddle	Acc.	2456	6.7	6.9	-0.2	4.0	4.0	0.0	4.3	4.4	-0.1
10	South Dome	Acc.	2901	6.9	6.0	0.9	4.5	4.0	0.5	4.6	4.2	0.4
11	NASA-E	Acc.	2614	7.7	7.1	0.6	4.3	3.8	0.5	5.3	4.8	0.5
12	Craw. Pt.2	Acc.	1990	6.5	6.5	0.0	3.5	4.0	-0.5	3.9	4.3	-0.4
13	NGRIP	Acc.	2950	7.9	8.9	-1.0	4.7	4.9	-0.2	5.3	5.6	-0.3
14	NASA-SE	Acc.	2393	6.7	6.9	-0.2	4.0	4.3	-0.3	4.3	4.8	-0.5
15	KAR	Acc.	2579	7.2	6.4	0.8	4.2	4.9	-0.7	4.9	5.1	-0.2
16	JAR2	Abl.	542	5.0	4.8	0.2	1.8	1.4	0.4	2.6	1.7	0.9
17	JAR3	Abl.	283	5.3	4.6	0.7	2.1	1.6	0.5	2.2	1.9	0.3
18	Peterm. GL	Abl.	37	5.3	5.9	-0.6	1.1	1.3	-0.2	2.8	1.9	0.9
19	Peterm. ELA	Abl.	965	4.2	5.0	-0.8	1.5	3.2	-1.7	3.7	2.9	0.8
20	Sermilik1	Abl.	350	4.6	5.8	-1.2	1.5	1.4	0.1	3.7	1.7	-2.0
21	Tasilaq2	Abl.	300	5.0	4.1	0.9	2.2	1.6	0.6	2.1	2.5	-0.4
22	Nuuk2	Abl.	900	5.1	4.5	0.6	2.2	1.7	0.5	2.4	2.0	0.4
23	Imersuaq A	Abl.	886	5.0	4.2	0.8	1.3	1.8	-0.5	2.5	1.9	0.6
24	Cryo	Abl.	200	4.8	4.8	0.0	1.7	1.7	0.0	1.9	2.2	-0.3
25	s5	Abl.	510	5.3	5.5	-0.2	2.3	1.6	0.7	2.1	1.8	0.3
26	s6	Abl.	1020	5.8	6.0	-0.2	2.9	2.4	0.5	2.7	1.7	1.0
27	s9	Abl.	1520	6.1	5.9	0.2	2.2	2.1	0.1	3.2	2.5	0.7

**Table 9.** A comparison between the modelled ( $\sigma_{a,jjja}^m$ ) standard deviation distribution and observed data ( $\sigma_{a,jjja}$ ) from the stations.  $\sigma_a$ ,  $\sigma_j$ ,  $\sigma_{jja}$  are the mean annual, July and summer (June, July, August) standard deviation, respectively. The difference (diff.) is calculated between the modelled and observed data. Acc. and Abl. denotes stations located in the accumulation zone or in the ablation zone. The elevations (Elev.) of the stations are in meters above sea-level.

### Results from including GEUS data

The inclusion of data from the GEUS stations provides a much clearer picture of the slope lapse rates (Table 7). The results from the transects show a great deal of variability, with a distinct seasonal cycle that has a double peak in winter. The largest slope lapse rates are seen in winter and the smallest in summer. The standard deviation of the slope lapse rate is also calculated, with the highest values in the winter and the smallest in the summer (Table 7). The maximum monthly slope lapse rate of  $-8.9 \text{ }^\circ\text{Ckm}^{-1}$  occurred in February, and the minimum ( $-4.6 \text{ }^\circ\text{Ckm}^{-1}$ ) occurred in July. The relatively cold and variable winter temperatures in the interior of the GrIS result in steep slope lapse rates and high standard deviations in contrast to the summer (Table 7). In the summer, the near-surface air temperature can rise further in the interior than at the margin, since temperatures are low enough not to be limited by the ice surface reaching the melting point.

The values of the coefficients found for Equation (8) are given in Table 8. Table 9 presents the modelled and observed values of the mean annual, mean July and mean summer near-surface air temperature standard deviation together with their differences for the 27 AWSs on the GrIS used in this study. The standard deviations show an annual cycle with the

smallest values during summer and the largest during winter. Smaller values during summer can be explained by a limiting influence of the surface temperature over a melting snow and ice surface. When the surface temperature reaches the melting point, energy that could potentially raise the near-surface air temperature is used for melting. In the winter no melting occurs and the temperature variations are not limited by the surface temperature. The highest standard deviation values of the ablation season (3.0–6.0 °C) are found in May, June and September. The lowest values (<2.0 °C) occur in July and August. Furthermore, the standard deviation has a clear altitudinal dependence with minor influences by the latitude and longitude as indicated by the coefficients and their root mean square difference (RMSD) in Table 3. Both tables show that the smallest standard deviations are found at low elevation ( $\sigma_{pdd} < 2$  °C). The highest standard deviations are found at high surface elevation ( $\sigma_{pdd} \sim 7$  °C) (Tables 7 and 8).

The optimized values for  $\gamma_{ma}$  in Equation (7) (Table 11) is well within the standard deviation of the observed values. The discrepancy between  $\gamma_{mj}$  and the observations may be related to the fact that the observed slope lapse rates in Table 9 were calculated without using data from the land stations, while all the available data to determine the coefficients for Equation (7) were used.

	Station	Location	$T_a$ mod.	$T_a$ obs.	diff.	$T_j$ mod.	$T_j$ obs.	diff.
1	Swiss Camp	Abl.	-12.25	-11.15	-1.10	-0.01	0.06	0.07
2	Craw. Pt.1	Acc.	-18.01	-16.85	-1.16	-4.82	-5.18	0.36
3	NASA-U	Acc.	-22.88	-22.56	-0.32	-7.19	-7.13	-0.06
4	Humboldt	Acc.	-23.39	-25.51	2.12	-5.51	-5.89	0.38
5	Summit	Acc.	-28.00	-27.54	-0.46	-12.14	-12.39	0.25
6	Tunu-N	Acc.	-24.92	-26.17	1.25	-6.97	-7.52	0.55
7	DYE-2	Acc.	-16.51	-17.84	1.32	-5.09	-4.01	-1.08
8	JAR1	Abl.	-10.80	-10.10	-0.70	1.19	1.08	0.11
9	Saddle	Acc.	-18.12	-19.41	1.29	-6.69	-6.39	-0.30
10	South Dome	Acc.	-18.86	-19.04	0.18	-8.64	-7.66	-0.98
11	NASA-E	Acc.	-26.57	-27.31	0.74	-9.76	-10.30	0.54
12	Craw. Pt.2	Acc.	-17.84	-17.12	-0.72	-4.66	-4.72	0.06
13	NGRIP	Acc.	-27.93	-27.62	-0.31	-10.93	-10.47	-0.46
14	NASA-SE	Acc.	-18.21	-19.66	1.45	-6.53	-6.94	0.41
15	KAR	Acc.	-22.33	-21.03	-1.30	-8.56	-9.05	0.49
16	JAR2	Abl.	-8.13	-6.95	-1.18	3.45	2.80	0.65
17	JAR3	Abl.	-10.22	-6.31	-3.91	1.65	2.56	-0.91
18	Peterm. ELA	Abl.	-18.21	-17.17	-1.04	-0.08	2.39	-2.47
19	Sermilik1	Abl.	-1.00	-1.10	0.10	5.68	4.72	0.96
20	Tasiilaq2	Abl.	-4.58	-4.01	-0.57	4.78	3.74	1.04
21	Nuuk2	Abl.	-6.90	-5.33	-1.57	2.26	2.74	-0.48
22	Imersuaq A	Abl.	-8.08	-9.51	1.43	2.06	2.92	-0.86
23	Cryo	Abl.	-9.52	-6.32	-3.20	4.83	4.29	0.54
24	s5	Abl.	-6.26	-5.40	-0.86	4.00	4.01	-0.01
25	s6	Abl.	-9.51	-9.68	0.17	1.19	0.88	0.31
26	s9	Abl.	-12.72	-12.40	-0.32	-1.58	-0.75	-0.83
27	Station Nord	Land	-15.94	-16.90	0.96	2.47	3.40	-0.93
28	Danmarkshavn	Land	-12.17	-12.30	0.13	3.48	3.70	-0.22
29	Ittoqqortoormiit	Land	-7.69	-7.50	-0.19	4.37	3.30	1.07
30	Tasiilaq	Land	-3.01	-1.70	-1.31	6.09	6.03	0.06
31	Prins Chr. Sund	Land	1.10	0.70	0.40	7.11	4.50	2.61
32	Qaqortoq	Land	1.05	0.60	0.45	7.37	7.20	0.17
33	Narsarsuaq	Land	0.87	0.90	-0.04	7.34	10.30	-2.96
34	Paamiut	Land	0.49	-0.80	1.29	7.46	5.60	1.86
35	Nuuk	Land	-1.32	-1.40	0.08	6.89	6.50	0.39
36	Kangerlussuaq	Land	-3.16	-5.70	2.54	6.55	10.70	-4.15
37	Sisimuit	Land	-2.73	-3.90	1.17	6.93	6.30	0.63
38	Aasiaat	Land	-4.57	-4.90	0.33	6.17	5.70	0.47
39	Ilulissat	Land	-4.76	-5.00	0.24	6.26	7.50	-1.24
40	Upernavik	Land	-7.12	-7.20	0.08	5.85	5.20	-0.65
41	Pituffik	Land	-8.58	-11.10	2.52	6.23	4.50	1.73

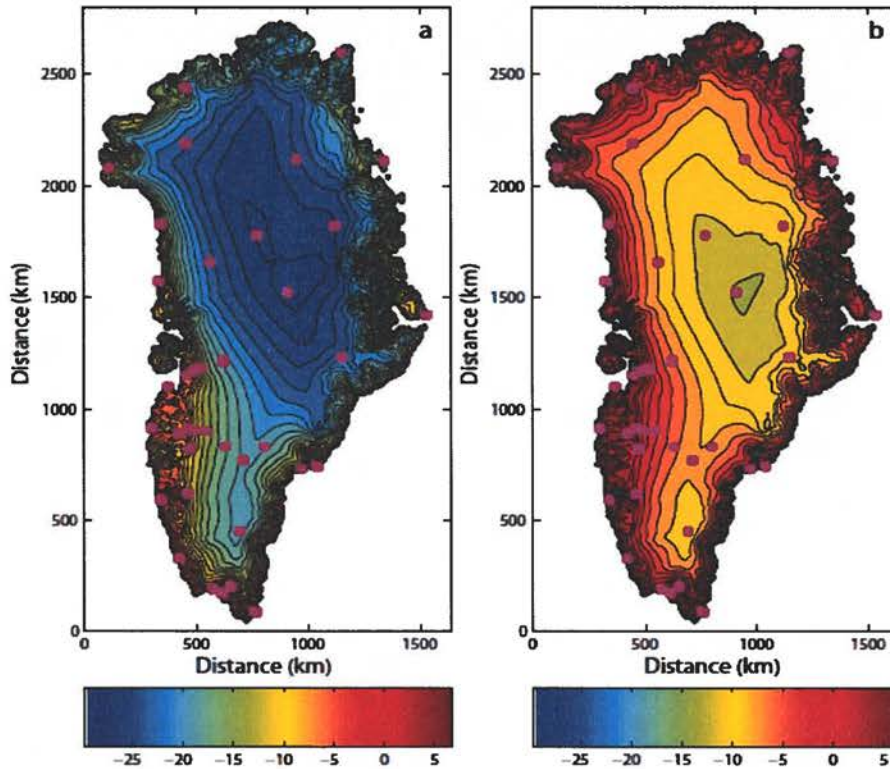
**Table 10.** A comparison between the modelled (mod.) temperature distribution and observed

data (obs.) from the stations.  $T_a$  is the annual mean temperature and  $T_j$  is the mean July temperature. The difference (diff.) is calculated between the modelled and observed data. Acc., Abl. and Land denote stations located in the accumulation zone, in the ablation zone or on land, respectively.

	$d_{ma,j}$ °C	$\gamma_{ma,j}$ °C km <sup>-1</sup>	$c_{ma,j}$ °C °N <sup>-1</sup>	$\kappa_{ma,j}$ °C °W <sup>-1</sup>	rmsd
<b>Best annual fit</b>					
This study with $\kappa_{ma}$	41.83	-6.309	-0.7189	0.0672	1.31
This study without $\kappa_{ma}$	46.01	-6.380	-0.7340	0	1.48
This study without land stations	40.96	-6.988	-0.6901	0.0742	1.29
Ritz and others (1997)	49.13	-7.992	-0.7576	0	2.27
<b>Best July fit</b>					
This study with $\kappa_{mj}$	14.70	-5.426	-0.1585	0.0518	1.24
This study without $\kappa_{mj}$	17.86	-5.494	-0.1681	0	1.35
This study without land stations	13.46	-5.172	-0.1809	0.1049	0.83
Ritz and others (1997)	30.38	-6.277	-0.3262	0	2.02

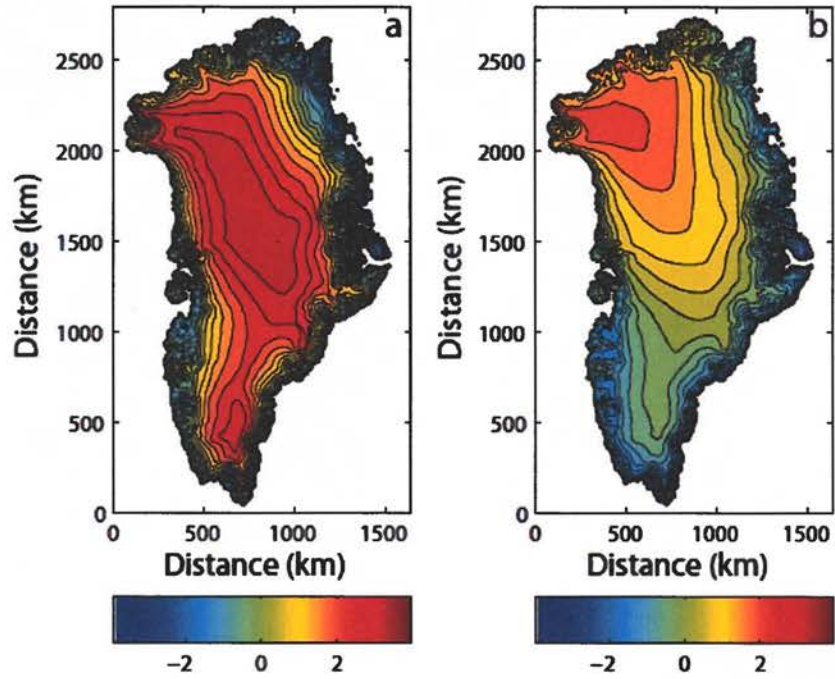
**Table 11.** Coefficients for Equation (7) and their root-mean-square difference (rmsd) in relation to the observed temperatures.

Figure 31 gives a visual presentation of the near-surface air temperature fields computed from the new parameterization. It is clear that the altitudinal component dominates the temperature field. The figure shows that the effect of the latitudinal component changes with time of year due to the abundance of solar radiation in summer, or lack of it in winter. The effect of the longitudinal dependence can be examined by comparing the difference maps of Figure 32a and b (including longitudinal dependence) with those of Figure 33a and b (excluding longitudinal dependence). For example, the effect can be seen in the northwestern part of Greenland, where the temperatures in Figure 32a and b show higher positive differences than in Figure 33a and b. The new temperature parameterization, in general, also yields higher temperatures over the ice sheet for the annual case, whereas the July temperature only yields higher temperatures over the north and northwestern part of the ice sheet, due to a small latitudinal dependence combined with the longitudinal component.



**Figure 31.** Parameterized (a) mean annual and (b) mean July temperatures. Dots show the locations of the AWS.

Similar higher temperatures also exist when not taking the longitudinal component into account, but with less difference in the northwestern part of Greenland. Figure 34a and b show the difference between the new temperature parameterization with and without data from the land stations. Without the land-station data the northeastern part of Greenland appears too cold compared with observations, due to a stronger longitudinal dependence, especially in the July temperature (Table 11). This is likely to be because of the sparse station data available in the north; land stations are therefore needed to predict the temperature more accurately.



**Figure 32.** The difference between the temperature parameterization for this study with a longitudinal dependence and that of Ritz and others (1997): (a) for the annual temperature and (b) for the July temperature.

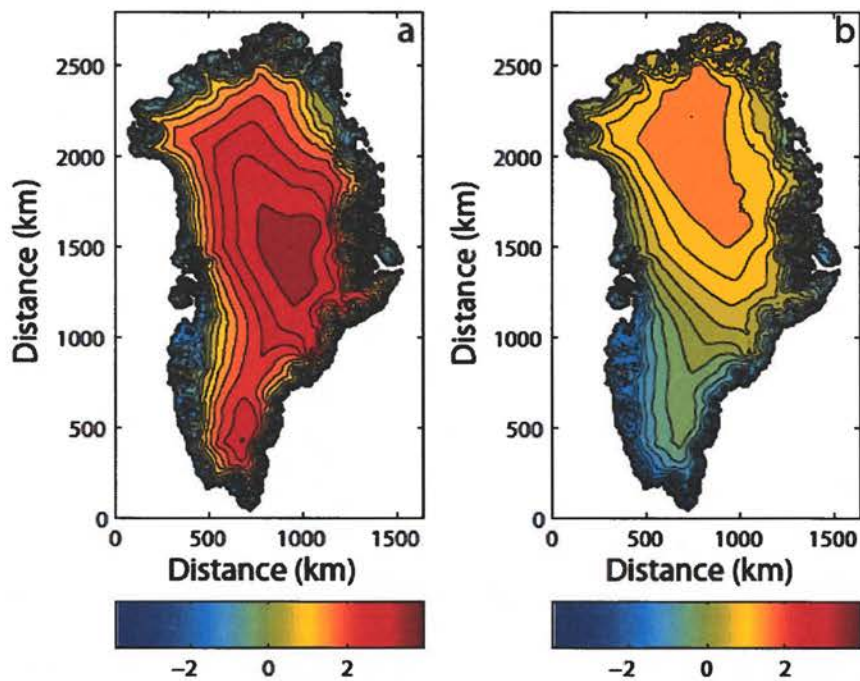


**Figure 33.** Same as Figure 3 but without a longitudinal dependence.

Figure 35 shows the temperature difference between the observed values from the AWS and the temperature parameterizations of this study and those of Ritz and others (1997). The differences in temperature between the parameterization of this study and the observations are also given in Table 10. Comparing the new parameterization with Ritz and others (1997), both the annual and July temperature of the new parameterization show a better

performance at 37 station sites out of 41, in relation to observations, corresponding to over 90%. The parameterizations by Ritz and others (1997) have a general overestimation at low elevations and a general underestimation at high elevations.

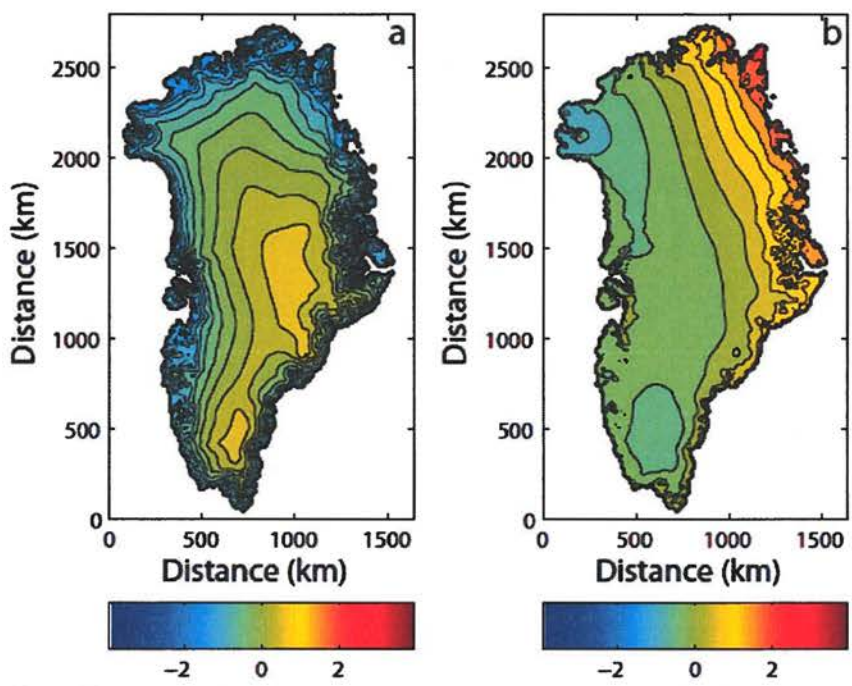


**Figure 34.** The difference between the temperature parameterization for this study with and without land stations: (a) for the annual temperature and (b) for the July temperature.

The root-mean-square difference (rmsd) on the residuals from the temperature parameterization is given in Table 11. The values of the rmsd indicate a slight improvement when longitudinal dependence is included in the temperature parameterization.

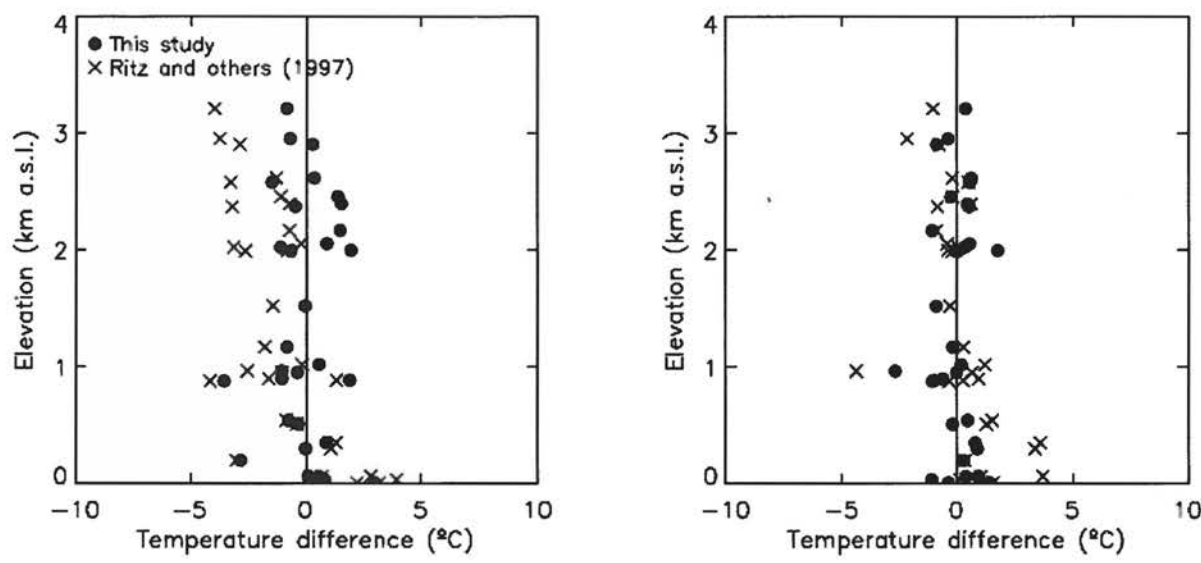


**Figure 35.** The temperature difference between the observed values from the AWS and the temperature parameterizations of this study and that of Ritz and others (1997). (a) The annual temperature and (b) the July temperature.

Figure 36 shows, as an example, the observed summer (June, July and August) standard deviation from the AWSs and the difference between the standard-deviation parameterization and the observed values relative to elevation (also listed in Table 9). The standard deviation has a strong dependence on altitude. The stations at lower altitudes show a larger scatter in their calculated values than the stations located at higher elevations. This is due to the higher exposure of low-elevation AWSs to atmospheric variability over land and ocean. This is illustrated at Sermilik1, the southernmost and most exposed of the AWSs on the GrIS. Here, the observed standard deviation is relatively large, causing the largest mismatch in our fitting procedure. Overall, the parameterization approximates the standard deviation within 1°C, and has increasing accuracy with elevation, which benefits the surface mass balance modelling as changes in this concern the whole modelled ice sheet mass balance.

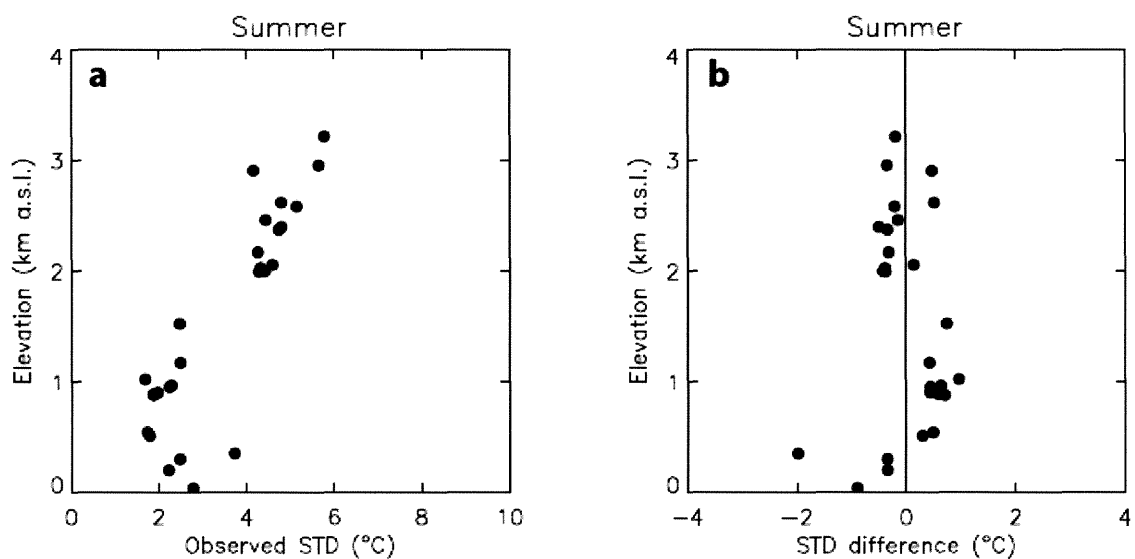


**Figure 36.** (a) Standard deviation calculated from hourly temperature observations relative to elevation. (b) Difference between the standard-deviation parameterization and the observed values from the AWS relative to elevation.

The annual melt extent was calculated with the PDD model using both the new parameterization and the temperature parameterization by Ritz and others (1997) for a spatial resolution of 10 km. The cut-off value for the Gaussian distribution in the degree-day integral (Equation (4)) is set to 1mm of melt, which implies that melt rates  $<1 \text{ mm a}^{-1}$  will be regarded as dry snow. The melt area extent for the parameterization by Ritz and others (1997) is  $13.1 \times 10^5 \text{ km}^2$  (Figure 36b). The melt area extent from the new parameterization is  $6.6 \times 10^5 \text{ km}^2$  (Figure 37a). The modelled melt area extent is then compared to a satellite-derived melt area extent. The satellite-derived melt area extent has a mean value of  $4.6 \times 10^5 \text{ km}^2$  calculated over a 6 year period (2000–05) based on a moderate-resolution imaging spectroradiometer (MODIS) algorithm (Fausto and others, 2007). A mean value of  $\sim 4.6 \times 10^5 \text{ km}^2$  for a period (1979–2002) of 24 years by Steffen and others (2004) and  $\sim 5.2 \times 10^5 \text{ km}^2$  for a period (1979–2005) of 27 years by Fettweis and others (2007) is calculated using passive- and active-microwave data. Wang and others (2007) derive a melt area extent using the SeaWinds scatterometer on QuikSCAT, which is an active-microwave radar (Ku-

band sensor). The QuikSCAT melt area extent has a mean value of 58% for the ice-sheet area of Greenland during the period 2000–04, corresponding roughly to a melt area extent of  $7.1 \times 10^5 \text{ km}^2$ . The largest difference in melt area extent between the modelled area and the satellite-derived area is ~18% for Fausto and others (2007), and the smallest difference is 4% for Wang and others (2007). The four satellite-derived melt area extents agree reasonably well with the PDD model using the new parameterization, which gives confidence in its applicability.

## Discussion

Model parameterizations of this type have been applied often to the existing ice sheets of Greenland and Antarctica, and to those which covered the continents of the Northern Hemisphere during the Quaternary ice ages (Huybrechts and deWolde, 1999; Tarasov and Peltier, 1999; Greve, 2005). For example, Greve (2005) uses a glacial index, which is based on the results from ice-core data, to derive a time-dependent temperature forcing. A temperature distribution is then interpolated linearly between the present and the Last Glacial Maximum (LGM) values from a general circulation model. The glacial index scales the Greenland Icecore Project (GRIP) record to represent glacial and present conditions. The simulated anomaly from the glacial index is added to the near-surface air-temperature field over the whole region. The index is a useful tool, but it implies that the temperature distribution of Greenland can be interpolated between two climate extremes and that the climatic perturbation is the same for the whole ice sheet, which will not be the case. The parameterizations were primarily based on data from AWSs located on ice and a few AWSs on land. This may give a clearer picture of the evolution of the temperature field, due to different climatic and environmental conditions, and parameters that influence the temperature. However, the land-station data are needed to calculate the temperature parameterization, as without it the optimized coefficients would yield unrealistic temperatures, especially in the northeast.

The transition from land to ice further complicates the temperature distribution. Land and ice interact differently with the atmosphere. Over ice there is an ever-present shallow near-surface inversion layer, but land conditions will vary between convective and stable conditions (Grotjahn, 1993). The observed slope lapse rate could be biased by frequent inversion layers that dominate the coastal climate under conditions of low clouds or sea fog coming from the ocean (~400–500ma.s.l.; Box and Cohen, 2006). Reeh (1991) includes a simple way to account for the coastal inversion layer in his parameterization to get a better fit to observations. It was necessary to include an inversion layer, because he used over 30 land stations and only 5 stations on the ice sheet, to parameterize his temperature field. The coastal inversion layer is not accounted for in this study because the majority of the stations used for the parameterization are located on the ice sheet. However, this could be a reason for the small discrepancy in the optimized coefficients in Equation (4) compared to the observations in Table 11.

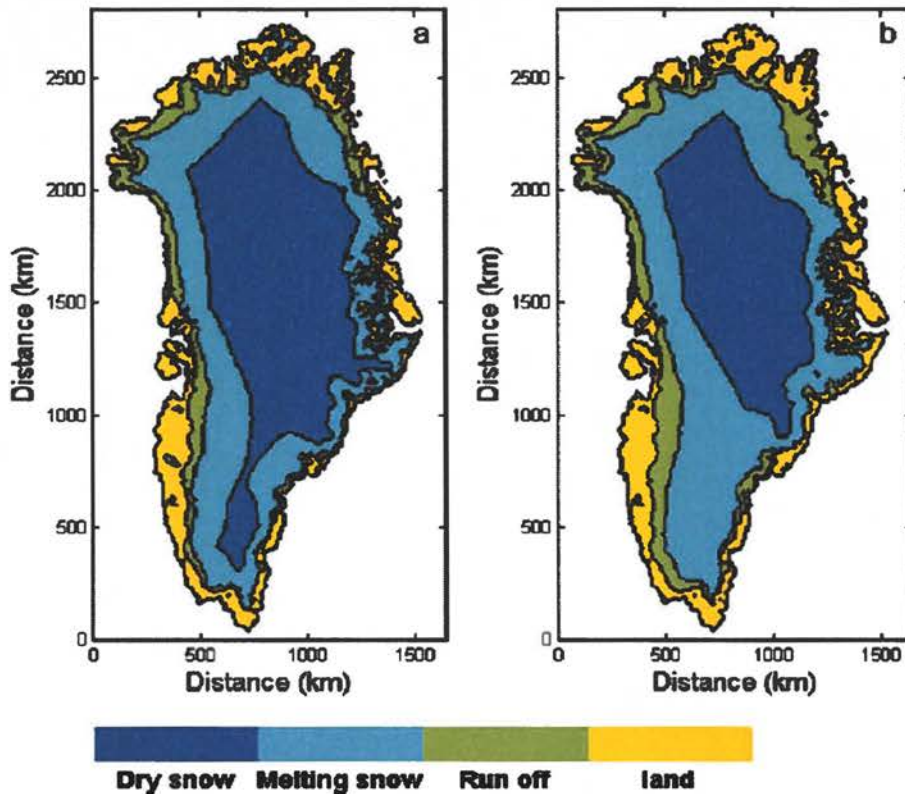


**Figure 37.** (a) the annual melt area extent for this study. (b) The annual melt area extent for Ritz and others (1997).

The new temperature parameterization may not fully represent a climatological mean, as only limited data are available, obtained over different periods and sometimes for only a few months. This may therefore be responsible for a bias in the modelled temperature distribution. A proper validation of the parameterization is very difficult because all trustworthy observational data are used for optimizing the coefficients in Table 11. It could be argued that some of the station data should be used for validation. However, the scarcity of near-surface air-temperature observations and their uneven spatial and temporal distribution means that omitting any part of the dataset would cause a substantial change in the resulting optimized coefficients of Table 11.

The parameterization of the near-surface air temperature standard deviation is deduced from observations, so it closely reflects the variability of the near-surface air temperature. The new standard-deviation parameterization may not in full correspond to a climatological mean, due to the limited dataset available. The data, obtained over different periods and sometimes for only a few months, could introduce a bias in the modelled standard deviation distribution. It is considered that the standard deviation parameterization is a fair approximation for the period with good AWS coverage (1996–2006) (Fausto and others, 2009a). The parameterization is difficult to validate further in regions where no in situ data is available. The new standard-deviation parameterization is also tested, and the performance in the SMB calculation indicates an improvement compared to the constant value used by Greve (2005) (Fausto and others, 2009b).

To investigate inter-annual variability and the effect of varying spatial data coverage, the

optimized coefficients in Equation (7) is calculated for each year in the data period (1996–2006; Table 12). The difference is quite high in some of the years when compared to the coefficients in Table 11, and the largest difference is seen in 1996 where the longitudinal dependence is negative, compared to the other years, for the July fit. However, all parameters obtained in this study (Table 11) fall within the standard deviations in Table 12. This gives us confidence that our parameters are representative of present-day conditions over the GrIS.

Year	$d_{ma,j}$ °C	$\gamma_{ma,j}$ °C km <sup>-1</sup>	$c_{ma,j}$ °C °N <sup>-1</sup>	$\kappa_{ma,j}$ °C °W <sup>-1</sup>	rmsd	Number of stations used
<b>Annual fit</b>						
1996	50.73	-4.343	-0.8178	0.0048	1.32	20
1997	46.49	-5.681	-0.7749	0.0349	1.53	25
1998	50.70	-5.439	-0.8352	0.0306	1.29	26
1999	46.79	-6.106	-0.7770	0.0427	2.07	32
2000	45.64	-6.488	-0.7671	0.0469	0.99	31
2001	45.96	-6.522	-0.7750	0.0613	1.74	33
2002	43.71	-6.428	-0.7395	0.0487	1.20	30
2003	31.40	-5.963	-0.6006	0.1269	2.61	32
2004	40.15	-6.698	-0.7005	0.0821	2.03	34
2005	33.78	-6.018	-0.6292	0.1111	2.01	33
2006	45.70	-6.109	-0.7632	0.0366	0.78	19
Mean	43.73	-5.981	-0.7436	0.0570	1.60	—
Std dev.	(±6.25)	(±0.661)	(±0.0730)	(±0.0363)	—	—
<b>July fit</b>						
1996	24.88	-5.777	-0.2697	-0.0087	2.34	20
1997	21.40	-6.156	-0.2406	0.0309	1.59	25
1998	14.77	-5.364	-0.1526	0.0434	1.33	26
1999	19.45	-5.402	-0.2194	0.0446	1.38	32
2000	21.48	-5.600	-0.2441	0.0321	1.42	31
2001	19.50	-5.586	-0.2185	0.0340	1.47	33
2002	12.81	-4.894	-0.1204	0.0362	1.52	30
2003	13.77	-5.894	-0.1435	0.0558	1.37	32
2004	16.43	-5.270	-0.1759	0.0380	1.32	34
2005	13.93	-4.710	-0.1433	0.0484	1.21	33
2006	16.63	-5.162	-0.1749	0.0345	1.54	19
Mean	17.73	-5.438	-0.1912	0.0354	1.50	—
Std dev.	(±3.88)	(±0.427)	(±0.0495)	(±0.0164)	—	—

**Table 12.** Coefficients for Equations (7) and their rmsd in relation to the observed temperatures.

### Conclusions on the new temperature parameterization

A new temperature parameterization is used to estimate a melt area extent derived from a PDD approach. The temperature and its standard deviation parameterizations and the PDD model, which is based on physical and statistical considerations (Ohmura, 2001), allow a fast integration speed in numerical schemes. The inclusion of new observational data and a longitudinal dependence in the parameterizations gives more accurate sensitivity values for elevation and latitude, and has produced a reliable near-surface air-temperature map. Acquisition of more temperature data and a longer time series is crucial to improve the parameterizations further; such an improvement closely follows the technical progress in such fields as ice-core drilling, remote sensing and the establishment of more AWS on the ice sheet. So far, the scarcity in the observational dataset precludes a proper validation of the parameterizations. More observational data will help improve this situation and are expected from the more than 30 AWS currently in operation on the GrIS.

## Development of a surface melt model

The PROMICE automatic weather stations measure ablation, which is the surface mass loss by melting and sublimation combined, in two ways: by pressure transducer and by sonic ranger (see the section on development of the ablation assembly). However, the main purpose of the AWS is to measure all meteorological variables that contribute to the surface energy budget. Through a modelling approach involving these variables we are able to quantify the contributions from different energy sources to the ablation, and thus help us to interpret the surface mass changes in terms of climatic forcings. For instance, higher melt rates could be the result of:

- larger atmospheric turbulent heat fluxes due to increased temperature or (katabatic) wind speed,
- a larger net longwave radiation budget due to higher atmospheric temperatures or cloud amounts,
- larger amounts of absorbed radiation at the snow/ice surface due to changes in albedo or a reduction in cloud cover,
- or an increase in the sub-surface heat flux due to a reduction in the build-up of cold content in the snow and ice in relation to high winter temperatures.

The melt model that was developed for PROMICE builds upon a surface energy balance method that has been successfully applied to many different ice bodies over the globe, including e.g. tropical glaciers (Mölg et al.) and blue ice areas in Antarctica (Bintanja). The method uses measurements of air temperature, humidity, wind speed, incoming and reflected shortwave (solar) radiation, down-welling longwave (terrestrial) radiation, and preferably air pressure to calculate all contributing energy fluxes to the surface energy budget: the sensible heat flux, the latent heat flux, the absorbed shortwave radiation, the net longwave radiation (absorbed minus emitted), and the sub-surface heat flux. If these energy fluxes cannot balance each other out, the remainder of the energy is spent on melt. On Greenland, this method has been applied to various regions, such as the northeast (Braithwaite), Helheim glacier in the southeast (Andersen et al.), Russell glacier in the southwest (Van den Broeke et al.), and Steenstrup glacier in the northwest (Van As).

We do not use our ablation measurement directly to draw major conclusions from; their main purpose is to validate our surface mass budget calculations. A second validation is performed making use of the measured up-welling longwave radiation, from which surface temperatures can be determined - one of the crucial model-generated variables.

On top of being able calculate and explain the surface mass budget at the AWS sites, the modelling approach enables us to do so for a larger region. Whereas ablation measurements cannot be extrapolated over a certain region as it is a non-linear product of the above-mentioned meteorological and radiative variables, the actual input variables can be extrapolated with confidence. With PROMICE AWS transects taking measurements at two or more elevations above sea level, our model can interpolate temperature, humidity, etc. to calculate ablation at different elevation intervals on sections of the Greenland Ice Sheet. However, the straightforward interpolation of input variables is not possible for the reflected shortwave radiation, since the ice sheet surface albedo is spatially highly variable. To over-

come this, we make use of satellite (MODIS) derived surface albedo, which we can validate and tune using our AWS-derived albedos.

The surface mass budget model or 'melt model' can only be applied to the region for which the AWS data can be extrapolated with confidence. At a few tens of kilometres distance from the AWSs the spatial correlation drops below the point of statistical significance, and it is no longer justified to calculate the mass budget. To provide an estimate of the surface mass budget for the entire Greenland Ice Sheet, we have to make use of regional climate model (RCM) calculations.

The Danish Meteorological Institute is currently running a regional climate model (HIR-HAM5) that is for example used to assess the impact of greenhouse gas emission scenarios. This model is being developed to also include surface mass balance of the Greenland Ice Sheet, enhancing the need for PROMICE data to establish valid parameterizations. The primary aim of PROMICE is, however, to capture present-day mass balance correctly. Fortunately, the prognostic regional climate model run by DMI (HIRLAM) is now also being modified to be able to deliver surface mass balance of the Greenland Ice Sheet, facilitated by the accessibility of near real-time automatic weather station data from PROMICE and the US programme, Greenland Climate Network (GC-Net). DMI is currently receiving the AWS data directly. Thus we expect that in the near future, it should be feasible to calculate near real-time mass balance of the Greenland Ice Sheet. The role of PROMICE is to ensure that such model estimates are firmly tied to, and indeed utilizing, the observed reality at the stations. This link is ensured by the established and on-going collaboration between DMI and GEUS on the subject. The unique combination of the station network and the regional climate modelling, strengthened by the strong research capabilities at GEUS and DMI on model parameterization development, puts Denmark at the forefront of climate change impact studies worldwide.

Naturally, PROMICE data is likewise available to other research groups outside Denmark working along the same lines, creating the globally open and competitive research environment that is most likely to produce new breakthroughs in this important subject. We have already established direct contact to several groups outside Denmark also working with regional climate models to calculate surface mass balance, in order to ensure that the data is utilized.

# Optical remote sensing and glacier mapping

## Background

A complete inventory of glaciers and ice caps (GIC) surrounding the Greenland ice sheet is needed to estimate the total mass of GIC, and to model their present and future contribution to global sea level rise. Currently, the WGI-XF (World Glacier Inventory – Extended Format), an inventory obtained by combining the WGI with other regional inventories (Cogley, 2009) is the most complete global source. It only accounts for 14,555 km<sup>2</sup> of GIC area, i.e. the extent covered by the Glacier Inventory of West Greenland (Weidick et al., 1992), and it was estimated that additional ca. 40,000 km<sup>2</sup> of not inventoried GIC area exist in Greenland (Cogley, 2009). Furthermore, the WGI-XF only contains tabulated glacier data without glacier outlines. The limited amount of glacier outlines and metadata from the database of the GLIMS Project (Global Land Ice Measurements from Space), essentially limited to the Geikie Plateau, are therefore not included in the WGI-XF. A widely cited review of previous GIC area provides a thorough discussion of the issues involved and suggests a likely range of 50 – 80 x 10<sup>3</sup> km<sup>2</sup>, with ca. 70 x 10<sup>3</sup> km<sup>2</sup> being a cautious minimum figure (Weidick and Morris, 1998). Estimates of the total area covered by GIC in Greenland currently used as starting point for state of the art modelling studies vary significantly among authors, ranging from lower estimates of 54 x 10<sup>3</sup> km<sup>2</sup> (Meier et al., 2007) and 54,400 ± 4400 km<sup>2</sup> (Radić and Hock, 2010) to higher estimates of 76,200 km<sup>2</sup> (Dyurgerov et al., 2005), with extremes of up to 150,000 km<sup>2</sup> (Oerlemans, 2001). Other studies deem the GIC in Greenland (and Antarctica) as important but explicitly exclude them from the analysis due to lack of data (Raper and Braithwaite, 2006).

## Glacier mapping overview

Glacier mapping and inventorying in PROMICE is aimed at filling the current gaps in the knowledge of GIC in Greenland by estimating their total area and by making available a complete glacier inventory of Greenland. The work started in 2008 using optical satellite remote sensing of Disko Island, Nuussuaq and Svartenhouk peninsulas (Citterio et al., 2009) to produce a local glacier inventory and change assessment, and it is now being extended to cover the entire of Greenland by following two independent approaches: 1) remote sensing and 2) GIS analysis of aerophotogrammetric maps.

### Glacier mapping by multispectral classification of Landsat imagery

The remote sensing work was carried out through the participation of PROMICE to the Users Group of GlobGlaciers, a project funded by ESA and led by the University of Zurich. GEUS being the Regional Center for Greenland within the GLIMS Project (Global Land Ice Measurements from Space), the contribution of PROMICE consisted in prioritizing the target subregions for GlobGlaciers products, in validating glacier outlines and metadata produced by GlobGlaciers, and in providing feedback on report deliverables documenting the methods and workflow employed, including challenges posed by ground conditions. In the first phase, the multispectral classification and vector mapping workflow (Fig. 38) was car-

ried out on three Landsat 7 ETM+ scenes at GEUS and in Zurich (Citterio et al., 2009). Glacier change since the little ice age was mapped, accounting for the impact of glacier surges (Fig. 39).

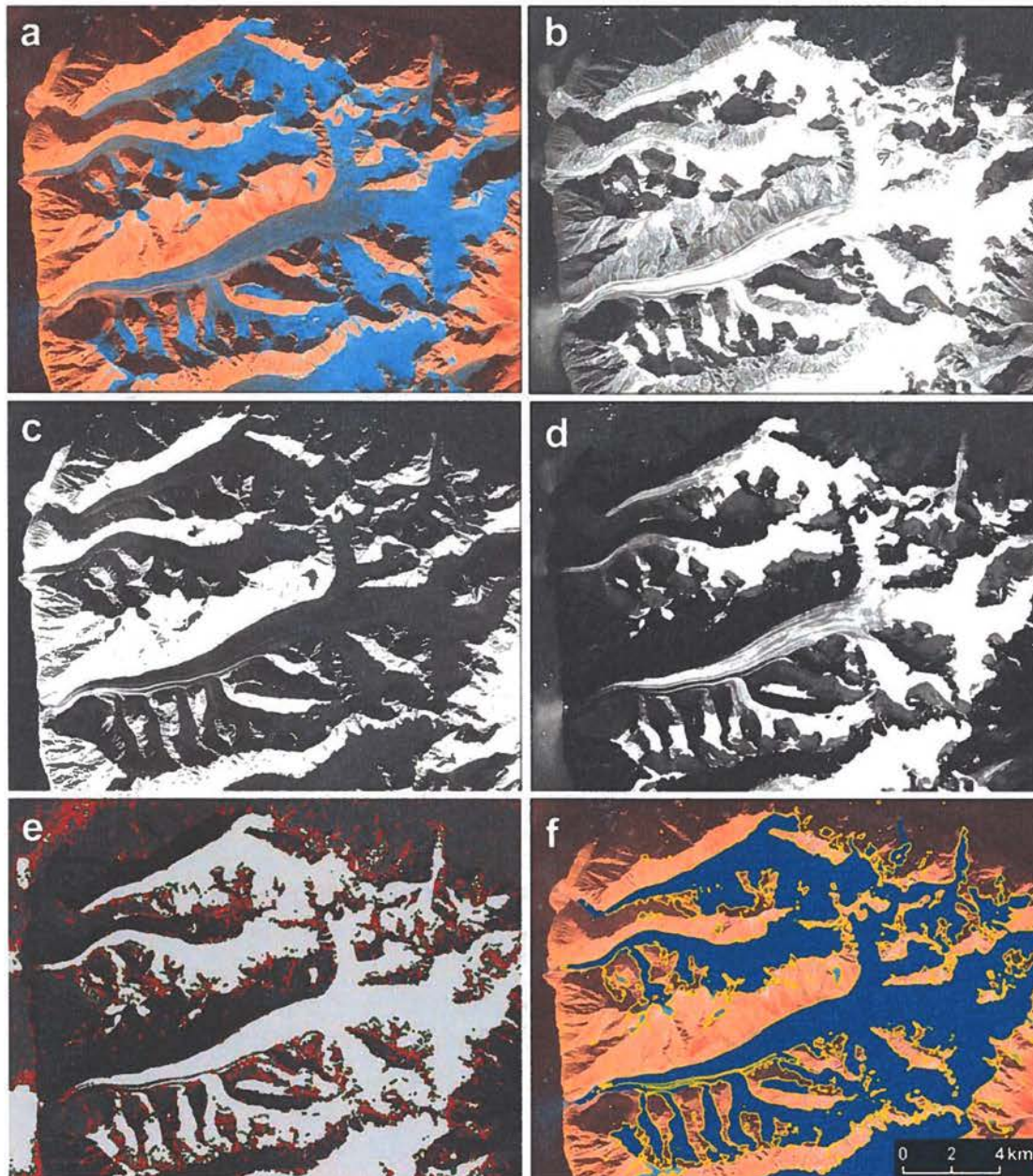


**Figure 38.** Overview of the steps involved in the band ratio method: (a) test region for Upernivik Island to the north of Nuussuaq peninsula using a false-colour composite with ETM+ bands 5, 4 and 3 as red, green and blue, respectively; (b) the region as seen with ETM+ band 3; (c) as (b) but with band 5; (d) the resulting band 3/5 ratio image; (e) resulting glacier map (grey) using a threshold of 2 (red pixels were deleted by the majority filter, blue pixels added); and (f) glacier outlines after raster–vector conversion (yellow) and manually corrected regions (blue). (Citterio et al., 2009)

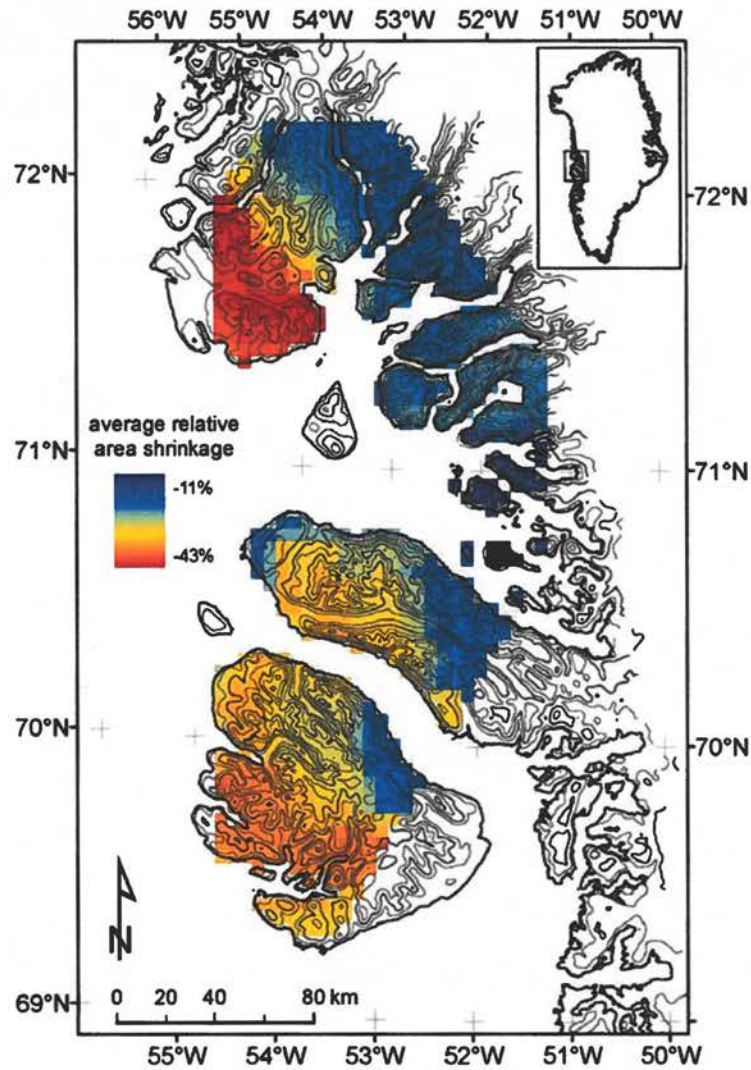


**Figure 39.** Spatial variability of the LIA to 2001 relative area change over the entire region computed as 50 km x 50 km average of glacier change. Yellow to red colours mark areas with larger change, blue areas smaller changes (Citterio et al., 2009).

In the follow-up to this study, the cooperation with GlobGlaciers resulted in the production of vector glacier outlines in West Greenland south of the area already mapped. Following final validation and reformatting, these vector GIS dataset will be contributed to the freely accessible GLIMS database (Raup et al., 2007) at the National Snow and Ice Data Center (NSIDC) at the University of Colorado Boulder, ensuring the widest dissemination and impact. The future roadmap for the remote sensing line of work includes continuing the production of glacier outline, mostly in Zurich where the full processing workflow is already implemented, to cover glaciers in most of East Greenland, again using Landsat 7 ETM+ scenes. Unfortunately, the availability of suitable imagery is constrained to latitudes south of about 80 N, making the full coverage of GIC in Greenland difficult and dependent on the use of lower resolution satellite sensors and a different processing. This is a serious shortcoming because a significant fraction of GIC area is located in North Greenland (ca.  $37.4 \times 10^3 \text{ km}^2$  according to our preliminary estimate described below). Furthermore, ground conditions are not favourable to medium resolution optical remote sensing (MODIS, MERIS)

because fields of semi-permanent snow patches can introduce large overestimations of glacierized area, as can be observed in Fig. 40.

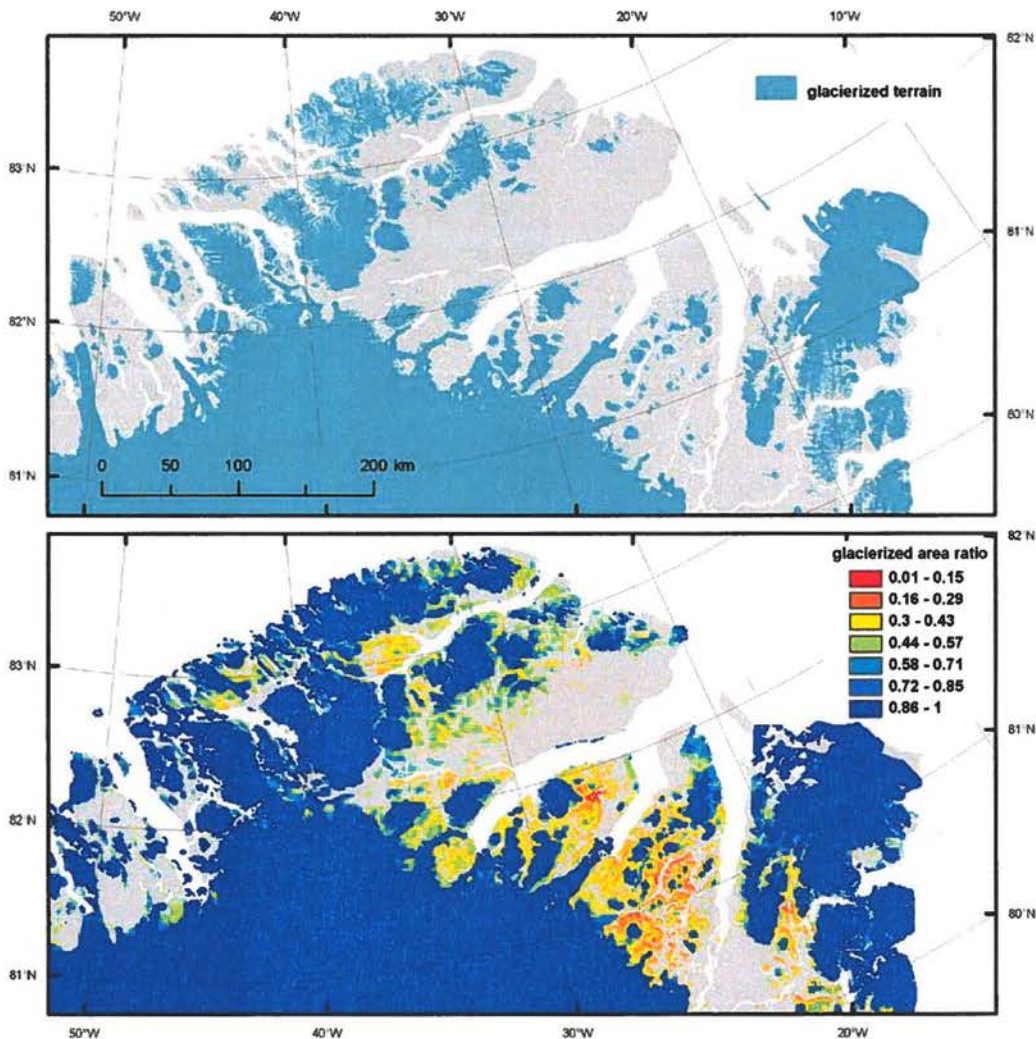


**Figure 40.** Several large ice caps exist in North Greenland above 80 N (top panel) where adequate Landsat coverage is not available. Coarser resolution sensors such as MODIS have been used to map the fraction of terrain covered by glaciers, but adverse weather and perennial snow patches create troubles (lower panel, unpublished grid by Jason Box, Ohio State University).

### Glacier mapping by GIS analysis of topographic datasets

The second line of work being pursued is based on GIS analysis of the aerophotogrammetric topographic maps available at GEUS through the GeoGreen geospatial database. These maps, produced over the years by KMS and GEUS, consist of a number of vector layers including land cover type (land, ice, sea, lake and glacial lake classes) elevation contour lines at 100 m equidistance over land and partly over the ice. This map series is produced in UTM projection referenced to the NAD83 datum. The vertical datum is mean sea level as determined at a number of sites by tide gauge measurements of variable duration carried out over the past decades. The map sheets were produced in the 1:250,000 and 1:100,000

scales based on the 1:150,000 vertical aerial photographs from the G150k campaign carried out between 1978 and 1987.

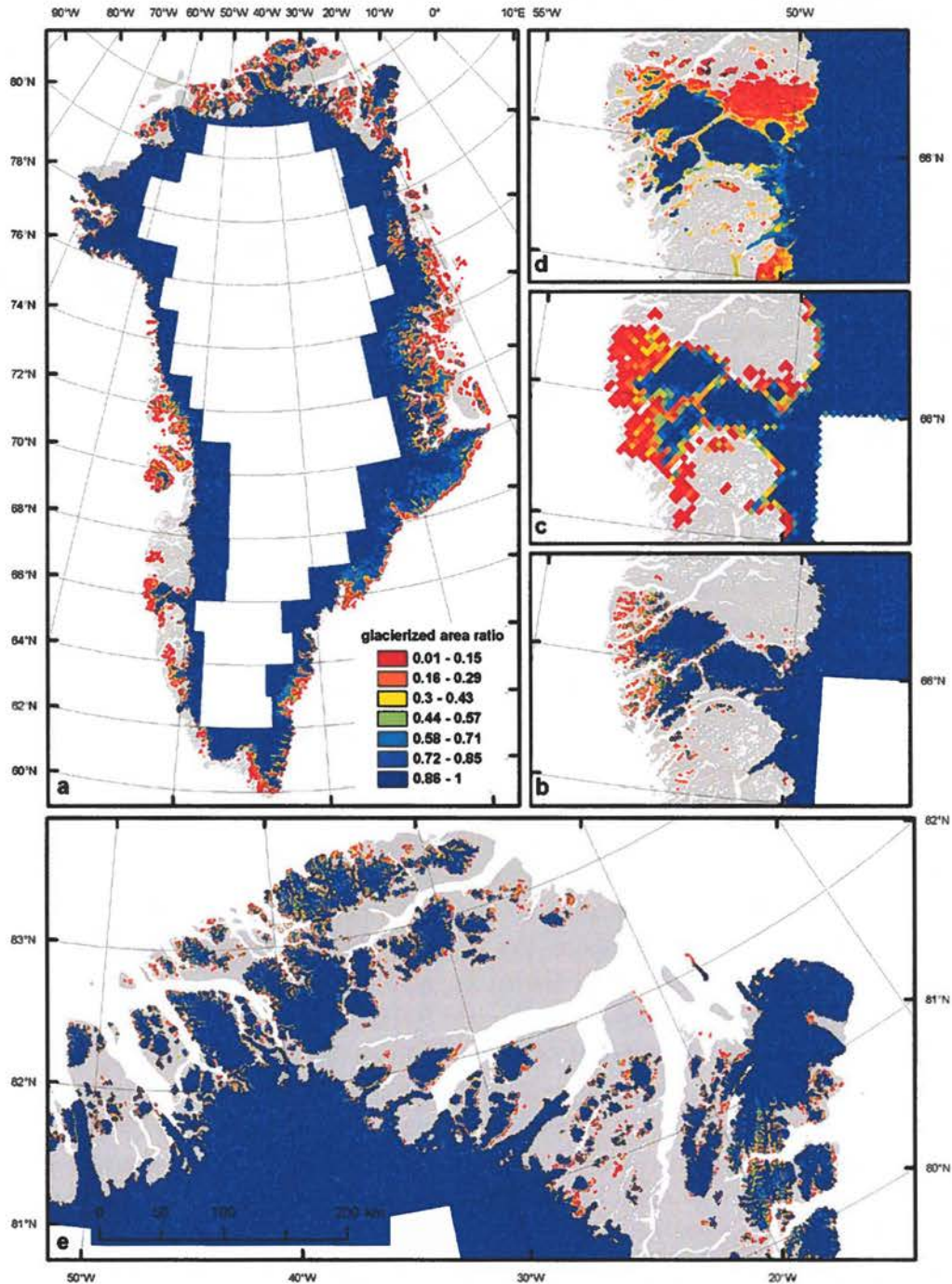


**Figure 41.** Grids of glacierized area ratios over Greenland produced from the GEUS topographic maps at 5 x 5 km cell size (a), details of the Sukkertoppen Ice Cap region in the 1 x 1 km cell size (b); 5 x 5 km cell size (c); and an unpublished grid derived from MODIS data by Jason Box, Ohio State University (d); detail of the 1 x 1 km cell size grid produced from the GEUS topographic maps same for the same sector of North Greenland shown in Figure 40

It is known that aerial photographs from older flights have been occasionally used to better resolve some minor cloud or snow covered areas, or other such difficulties in the 1978-1987 photographs. Unfortunately, systematic metadata recording which features or areas are based on older imagery is not attached to the maps, but this issue does not severely reduce the usefulness of these maps as only a very minor part of the mapped entities is affected. During 2010 a set of raster grids of the glacierized area coverage were produced with cell size of 1 x 1 and 5 x 5 km (Fig. 41).

These grids derive from a reprojection of the vector maps from the original UTM projection into the Lambert equal area projection, so that every cell in the raster covers exactly the same area regardless of its longitude and latitude. Batch processing of map tiles was needed because the size of the entire Greenland dataset hit hardware and software memory constraints and triggered a number of bugs in the ArcGIS 9.2 and 9.3 software used. The grid cell values in the resulting datasets represent the fraction of ice covered area within the cell and are useful as input data to models requiring proper representation of mixed surface cover types within individual grid cells. Furthermore, it allows a direct comparison with similar products derived from remote sensing, highlighting issues over wide areas in north Greenland where semi-permanent snow patches lead to significant overestimation of the actual glacierized area (Fig. 40). Gridded dataset can only provide the total glacierized area and they do not allow discriminating between ice sheet and GIC. Furthermore, they can't be used for area-volume scaling studies (Bahr et al., 1997), (Raper and Braithwaite, 2005), where the entire area of individual glaciers is required (Meier, 2005), (Raper, 2005). To overcome the first problem and allow measuring the area of GIC and the Greenland ice sheet separately, the vector polygons over all of Greenland are being inspected and edited manually to tag each individual polygon as belonging to the ice sheet or to GIC. This is a very labour intensive task and involves a degree of subjective interpretation to deal with those cases, quite frequent in East and North Greenland, where ice caps independent of the ice sheet are topologically connected with it from a purely geometric standpoint. As always with natural objects, the full spectrum of intermediate and ambiguous cases exists between clearly disconnected glaciological units and marginal areas sharing a significantly extended boundary with the ice sheet. We do not delve into these issues here, as they have been exhaustively discussed in the literature (Weidick and Morris, 1998), so we only describe the approach followed to maintain a full record of any subjective interpretation of ambiguous cases. During the manual inspection and editing of the maps each vector polygon classified as 'ice' in the original map has been flagged as either 'ice sheet', 'GIC' or 'edited GIC', with the last class containing all polygons resulting from manual splitting of an original 'ice sheet' polygon into a 'GIC' interpreted as being independent from the ice sheet from a glaciological point of view. In detail, the guideline followed was to split entities with no mass balance nor glacio-dynamic relation with the ice sheet, i.e. those neither feeding ice, being fed, or contributing flow units to any outlet glacier or marginal area of the ice sheet proper. This approach provides the added benefit of allowing comparison of our results with published estimates explicitly stating that a strict topologic rule was followed in partitioning ice masses between GIC and the ice sheet. Our preliminary results for the total GIC glacierized area is  $88.0 \times 10^3 \text{ km}^2$ , and of the ice sheet is  $1715.9 \times 10^3 \text{ km}^2$  (Fig. 42).

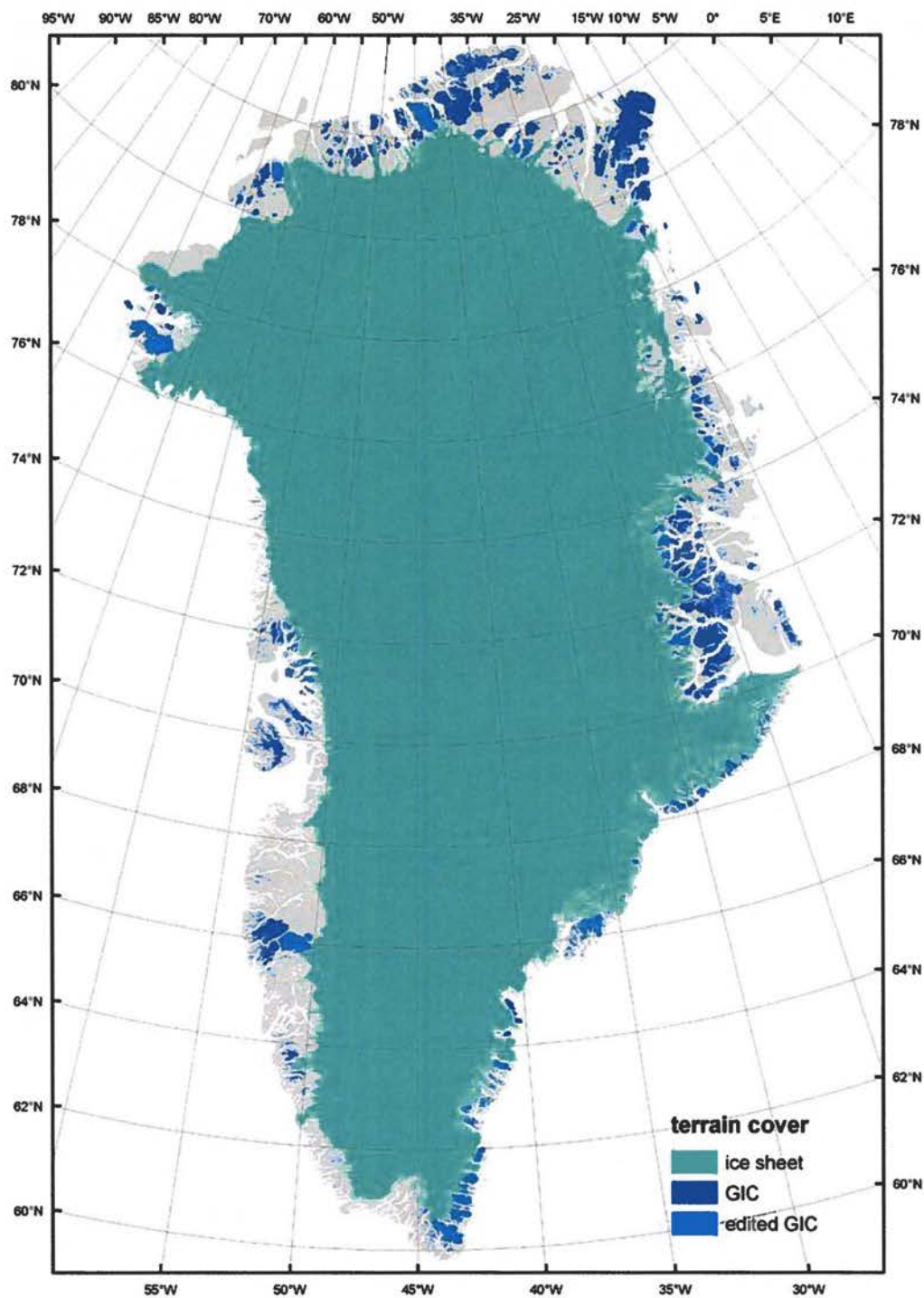


**Figure 42.** Map of glacierized terrain classified as 'ice sheet', 'GIC' and 'edited GIC'.

Large parts in central east Greenland have not yet been fully analyzed, due to the exceptional complexity of the topography. It is therefore expected that the preliminary GIC extent provided here is underestimated. When strictly considering only those ice masses topologically disconnected from the ice sheet in the original vector maps, a total of 67.2 x 103 km<sup>2</sup> is obtained. This is however rather meaningless from a glaciological standpoint, as it be-

comes obvious when considering that the 2058 km<sup>2</sup> Freuchen Land Ice Cap in North Greenland, among others, would disappear as a separate ice cap (Fig. 43).

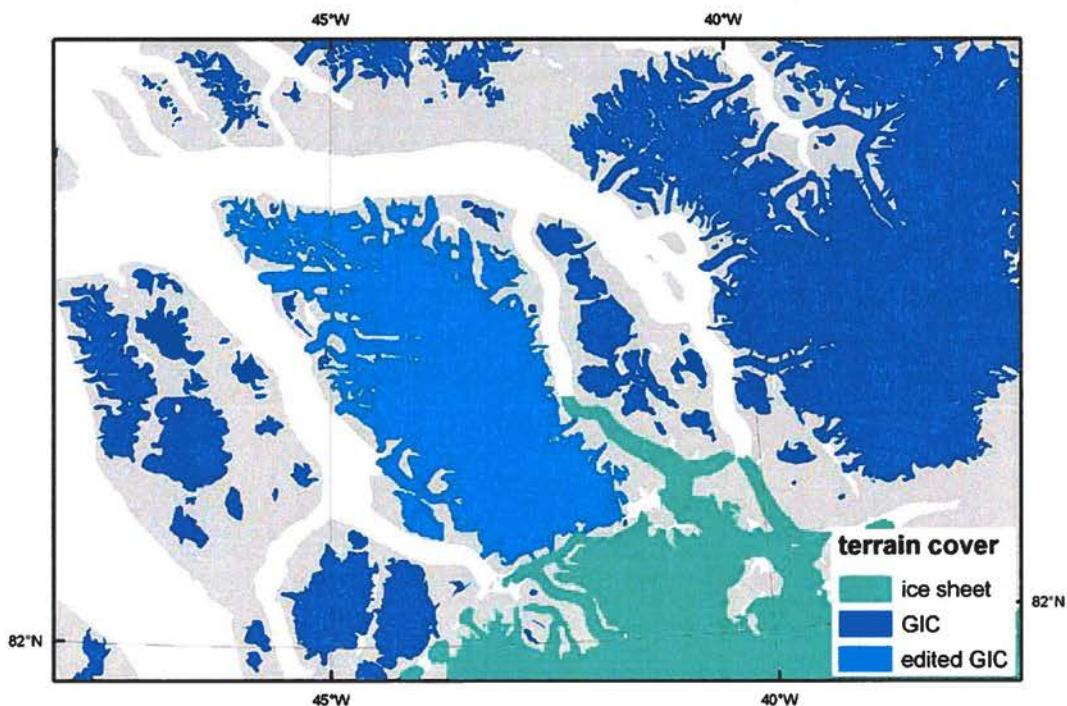


**Figure 43.** The 2058 km<sup>2</sup> Freuchen Land Ice Cap in North Greenland is a typical example of an independent ice mass touching the ice sheet and therefore at risk of not being counted without manual editing.

Our preliminary results are higher than most previous estimates, and we expect our final figures will be even higher. It is therefore interesting to note that we have been conservative in not including some major ice masses like Julianehåb Ice Cap in South Greenland that have been classified as independent units in previous, widely cited literature (Weidick and Morris, 1998).

#### **Remote sensing of glacier dammed lakes emptying events**

Alongside the main task of glacier mapping and inventorying, the history of repeated filling and emptying events of the glacier dammed lake Isvand on the western flank of Kangiata Nunaata Sermia outlet of the ice sheet in West Greenland has been reconstructed using ASTER and Landsat visible and thermal infrared imagery up to the most recent, and likely permanent emptying occurred in 2009 (Fig. 44) (Weidick and Citterio, 2011). An exceptionally long record of documentary information on the lake and the glacier are available for this site, which allowed reconstructing the fluctuations of the glacier and the discharge routes of the lake over about 250 years.

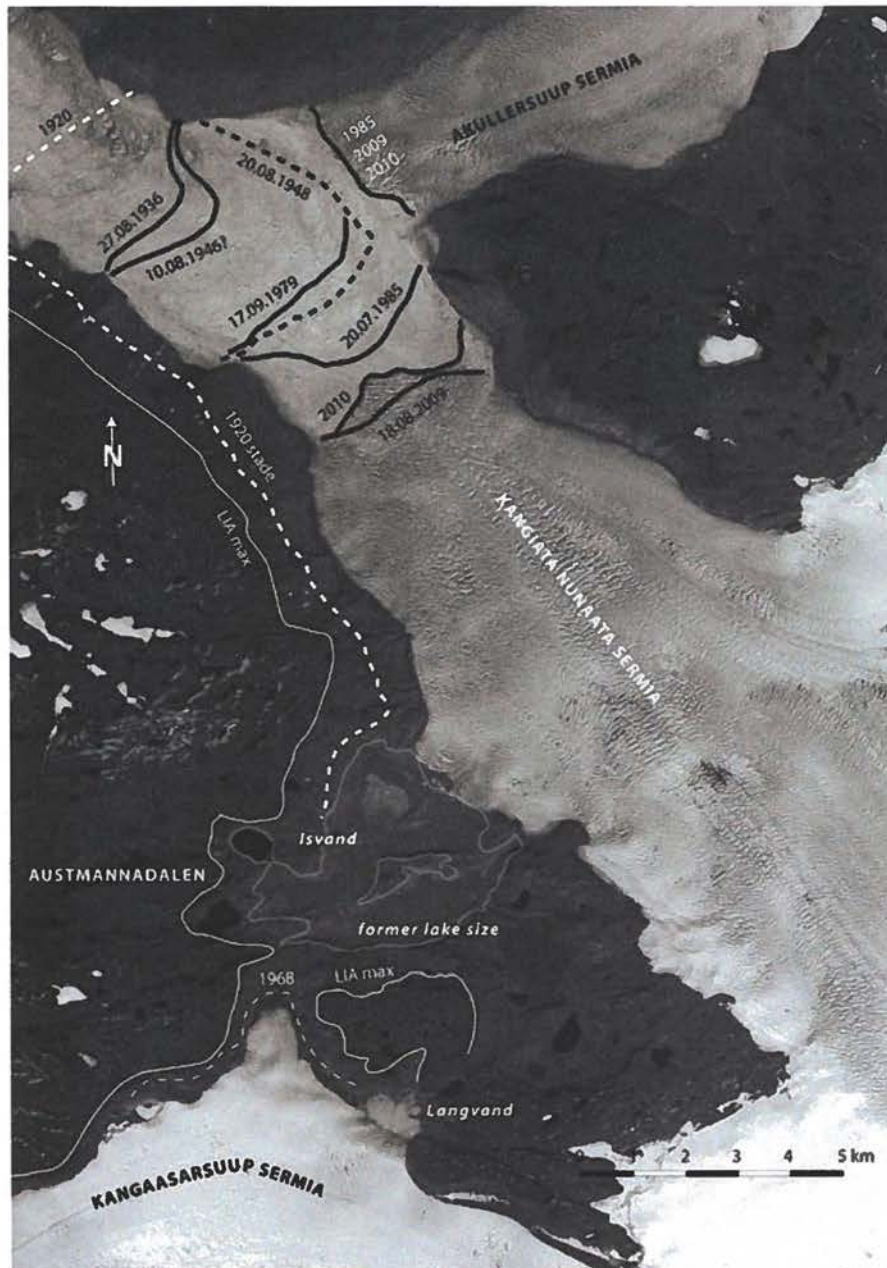


**Figure 44.** An ASTER satellite scene of the area in the front of Kangiata Nunaata Sermia and former areas of Isvand showing the situation in 2010. Contours of former lake Isvand for 1968 are shown with white lines. Approximate positions of the front of Kangiata Nunaata Sermia are shown for the period 1920–2010.

#### **Evaluation of DEM products and satellite laser altimetry datasets**

Glacier surface elevation and elevation changes can be used to measure volume changes, to derive glacier hypsometries and as input datasets for modelling. A number of techniques are available to obtain such information at different levels of accuracy, detail and reliability. The full archive of ICESat/GLAS satellite laser altimeter product has been acquired spanning the entire operational life of the instrument, and preprocessing scripts to subset and reformat the data have been written to enable easy and fast use. Preliminary tests have been carried out to familiarize with the product and to compare it against other ground ele-

vation sources available at GEUS, including the topographic maps from the GeoGreen database described above.

The entire ASTER GDEM coverage of Greenland has also been acquired. This product is the result of mostly automatic stereophotogrammetric extraction of a geolocated tiled digital elevation model based on the stereoscopic capability of the Terra/ASTER sensor. Visual inspection and comparison with reference datasets show that wide areas are affected by mild to severe artifacts, limiting the usefulness of the ASTER GDEM without extensive editing and validation. Above the snow line, this dataset is mostly unusable, as is to be expected given the lack of contrasted surface features required for stereophotogrammetric DEM extraction.

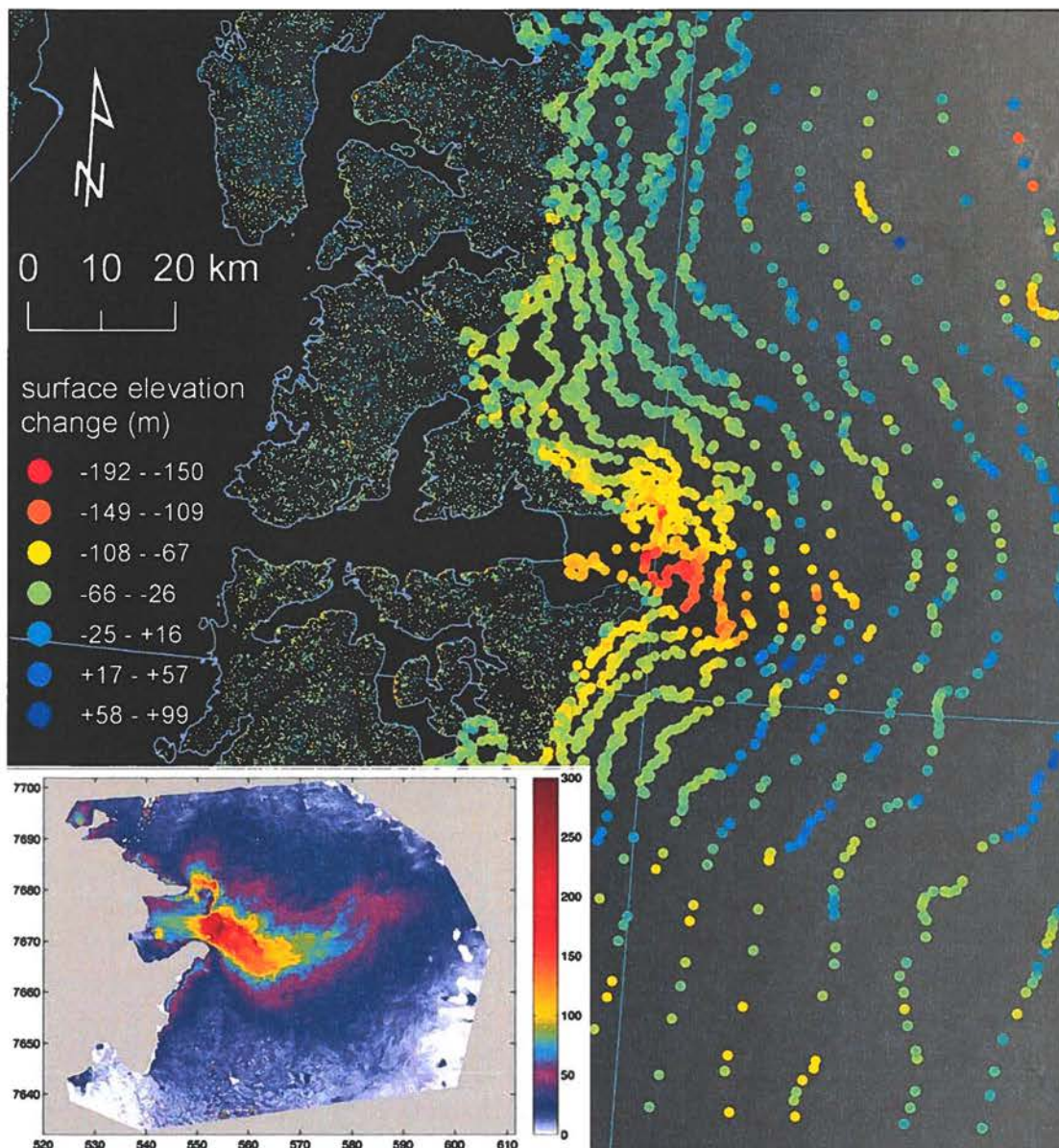


**Figure 45.** Results of a test evaluating the feasibility of estimating surface elevation changes (coloured dots) by comparing the elevation contour lines in the GEUS vector maps and an ASTER derived DEM (greyscale background). The inset reproduces Fig. 43 of (Motyka et al., 2010) showing thinning during a similar timeframe, for comparison.

Finally, a number of individual ASTER scenes have been submitted through the affiliation with GLIMS for on-demand processing into AST14DMO Level 3 DEM and orthorectified raster. Preliminary evaluation of these products show that the quality of selected scenes can be significantly better than the ASTER GDEM, and it is much easier to quality control them and mask out any part of the image affected by artifacts. Accuracy of the geolocation is generally poor, requiring adjustments before the data can be combined with any other elevation source, but a simple affine transformation has been found to work well. A significant systematic vertical shift is normally found and needs to be corrected by fitting with independent elevation data.

A preliminary test has been carried out over Jakobshavn Isbræ (Fig. 45), a target where a strong elevation change signal and relatively benign surface features contrast have been demonstrated by previous studies using high quality SPOT images and DEM (Motyka et al., 2010), showing that over a similar time frame the elevation change is also detectable by comparing the AST18DMO and GEUS elevation contours products. While detail is quite lower (Fig. 45), the magnitude and spatial pattern of the elevation change are remarkably similar to the carefully controlled work by (Motyka et al., 2010), which is encouraging given the availability of data and the straightforward processing.

When combining ICESat, ASTER and the GEUS vector maps, it was found that the amount of data and the required workflow make it inadvisable to rely on unstable desktop GIS packages such as ArcGIS for the analysis. Processing for the preliminary tests was therefore carried out using the GDAL (Geospatial Data Abstraction Library) and Numpy libraries in a python scripting environment, with ArcGIS used for map composition and layout. Upon completion of the glacier mapping task described in the previous subsections it will be possible to apply the experience, tools and datasets acquired during 2010 to prepare derived glacier hypsometry and surface elevation change products. However this will require further development of the workflow and tools.

## Airborne survey of ice sheet elevation and thickness

A Riegl LMS-Q140i-60 near infrared laser scanner and the DTU-developed 60 MHz ice-sounder was flown on a DeHavilland DHC-6 Twin Otter registered under OY-POF chartered from Air Greenland. The ice-sounder uses radio pulses to measure the distance between aircraft and the ice surface and the distance from the ice surface to the bedrock. From those distances the ice thickness is calculated. When the conditions permit acquisition of laser scanner data of the ice surface, the ice-sounder surface measurements are replaced by the laser measurements having much higher accuracy. The aircraft position was recorded by three on-board geodetic GPS receivers sampling at 1 Hz corresponding to a flight distance of approximately 70 m. The three GPS receivers were connected, via splitters, to either the front or the rear aircraft GPS antenna. The sampling frequency of the laser-scanner was 40 scan lines each with 250 measurements per second while the ice-sounder recorded 3.125 samples/second (after pre-processing).

The ice-sounder worked continuously during the complete flight mission, but was not active during the transits between the airport and the ice edge. To optimise the bedrock detection with the radar a low flight altitude is preferred, i.e. about 1,000 ft., and down to 100 ft. in some areas. The radar was not able to detect the bottom in some areas near the ice edge mainly due to heavily crevassed ice and in some areas in the southern part of Greenland probably due to water in the ice. Figure 46 shows the flight track and where a bottom echo was obtained.

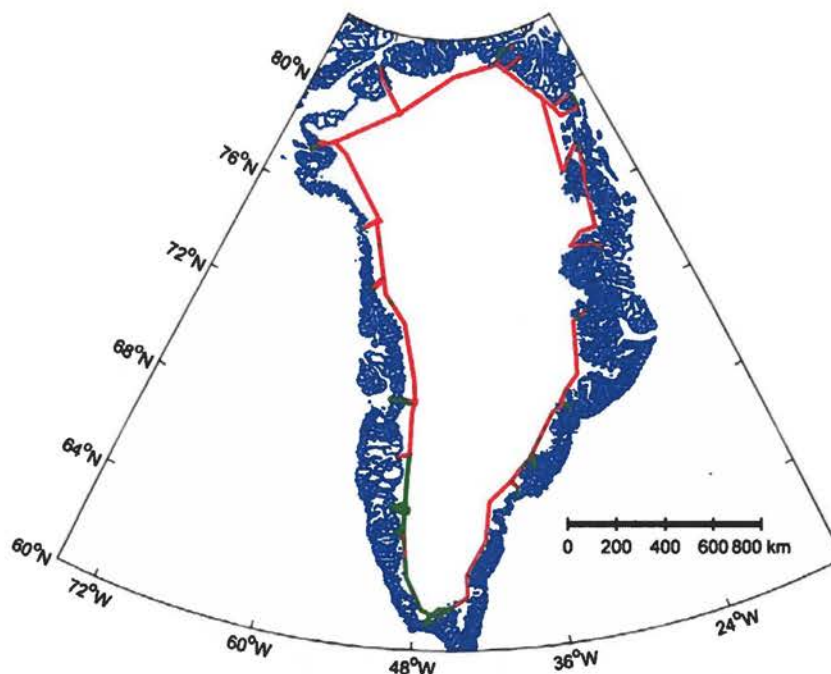


**Figure 46.** The flight path with transits excluded. Green segments show where a bottom echo was detected, while red segments show where a bottom echo was not detected.

## **GPS data**

The GPS position data was processed by using a PPP (Precise Point Positioning) software developed partly at Wuhan University and partly at National Space Institute, DTU Space, providing latitude, longitude and height above the WGS84 ellipsoid of the GPS antennas. The solutions were compared with differential GPS solutions from Trimble GPSurvey 2.35 to evaluate the robustness of the positions. Both PPP and GPSurvey rely on precise GPS products from IGS (International GNSS Service).

Data from the different GPS receivers was compared and quality controlled, and the best solution selected for further use. The GPS data were transferred to the laser scanner and ice-sounder instruments by adding the positions of these instruments inside the aircraft relative to the GPS antenna positions to the GPS data.

## **Lidar data**

Surface elevation data was derived from laser altimeter measurements made concurrently with the radar measurements and using the same INS and GPS set up to derive positioning information. The Riegl scanning laser used to make the elevation measurements provides cross-track scans with a range accuracy better than 5 cm. Absolute elevations are given with a precision of  $\pm 0.3$  m following processing. The laser operates in the near-infrared wavelength band and has a scan angle of  $60^\circ$ , giving a swath width similar to the flight elevation above the ground. Over the glacier surface, a typical value of this distance was 300 m. Roll, pitch, heading, and yaw of the aircraft were recorded at 50 Hz by a Honeywell H764-G, medium-grade INS (Inertial Navigation System). The orientation and the position of the aircraft with respect to the earth fixed reference system are used to exactly map each laser measurement to a position on the surface.

## **Data acquisition and processing - Ice-sheet bottom echo**

The ice-sounder data acquisition consists of transmitting pulses at a pulse repetition frequency of 5kHz (i.e. the sampling in the flight direction) and sampling the returned echo at 75MHz in range producing 4096 samples per transmitted pulse. While internal scattering masks the desired echo, reflection and absorption within the ice-sheet reduces the strength of the returned echo. Substantial processing is therefore required to produce a radargramme that makes detection of the ice-sheet bottom echo possible. This radargramme processing is done both on-line during acquisition and off-line using software developed at the Microwave & Remote Sensing division, DTU-Space. An example of a radargramme obtained by the icesounder is displayed in Figure 47, where the horizontal direction represents the time with a spacing of 320 ms per line (i.e. 22.4 m spacing at aircraft velocity 70 m/s). The vertical direction shows propagation time of the radar pulse with a spacing of 80 ns per line of the radar pulse. This represents vertical distances but not by simple scaling because the speed of light within the ice-sheet is lower than in free air. The

transmit pulse is also visible in the radargramme, because echo data sampling is started before the transmit pulse begins. This early starting of data sampling ensures calibration of the propagation delay.

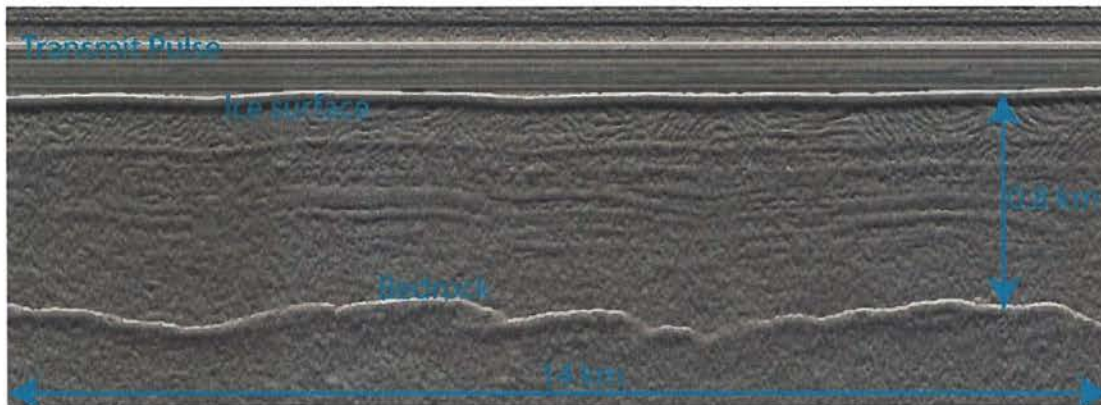


**Figure 47.** Radargramme showing transmit pulse, ice surface, and bedrock echo.

The processing of the ice-sounder data was performed by using a semi-automatic layer (bottom and surface) detection programme developed at the Microwaves & Remote Sensing division, DTU Space. The detection programme detects each layer individually; hence the following detection procedure is performed for both surface and bottom. The detection process is initiated by the user selecting a pixel in the radargramme that is part of the layer to be detected. This pixel is located in one particular vertical line. The automatic part of the programme then selects the pixel (left or right) within a specified search angle in a neighbouring vertical line that shows the strongest contrast to its neighbouring samples in the same line. This second pixel then becomes the basis for the automatic selection of the third pixel and so forth. There may be multiple echoes from the bedrock at some locations with rough bedrock. In such cases it may be impossible to see which echo is from vertical beneath the aircraft and which echo comes from the bedrock slightly off the flight track. This algorithm works well in areas with good layer echoes. In other areas the automatic detection loses track of the layer wherefore the user must manually set the pixel for each vertical line in such areas. As the layer (both bottom and surface) may not be detectable everywhere, the outcome of this process is a number of intervals of consecutive vertical lines with a pixel defining the layer. The positions of all these pixels in terms of UTC-time, GPS position, and propagation time are recorded to a file.

## Ice surface elevation, ice thickness and bottom elevation

UTC-time or GPS-time is recorded by all of the GPS-position-, laser scanner- and ice-sounder instruments and is used as reference for aligning the three different types of observations. At the time of the mission, the GPS-time is given as UTC-time plus 14 seconds.

The calculation of ice thickness and bedrock elevation requires the surface elevation to be known; hence ice thickness and bedrock elevation is not calculated in areas where the ice surface could neither be measured with the scanner nor the radar.

The ice surface elevation can be measured with either the scanner or with the radar, but the two sensors does not detect the same surface. The scanner detects the optical surface usually perceived as the surface while the radar pulse is reflected approximately 12 m below the optical surface. This difference has been measured by comparing measurement over the Kangerlussuaq runway with measurements over the ice. As the scanning laser altimeter is far more accurate than the radar, scanner data has been used for calculating the surface elevation where available. However, due to fog or malfunction scanner data was not available everywhere and radar data was then used instead. As the 12 m difference only applies over ice and as all radar data recordings including parts without ice were requested, no surface elevation correction was applied in areas where radar data was used. Instead the radar data product contains information as to which sensor was used for each calculation of the surface elevation. However, this surface difference was corrected for in the calculation of ice thickness and bottom elevation as shown below.

Replacing scanner data with radar data for ice surface detection poses a special problem when flying close to the ice surface. Oscillations from the radar transmit pulse masks the received echo from the ice surface when the distance from the radar to the ice surface is below approximately 200 m. A new processing technique has reduced this distance to 120 – 150 m. However, when radar data has been used to detect the ice surface and this distance is detected to be below 150 m the ice surface altitude must be considered less reliable and in theory this distance could be anywhere between 0 and 120 m. This uncertainty translates into an uncertainty for the bottom elevation of 52 m.

The ice surface elevation (given as height above the ellipsoid) of a point along the flight track is calculated by subtracting the aircraft to surface distance  $d_{surf}$  measured by the laser scanner from the GPS-measured aircraft ellipsoidal height. The horizontal position of the surface point is given by the horizontal GPS coordinates.

The ice thickness of a point along the flight track is given by

$$d_{ice} = 84.5(T_{bot} - T_{sur}) + 12$$

where  $d_{ice}$  is the thickness of the ice in meters.  $T_{bot}$  is the propagation time (echo delay) in microseconds of the radar signal bottom echo and  $T_{sur}$  is the propagation time in microseconds of the radar signal surface echo.  $T_{bot}$  is measured by the radar.

When laser data are available  $T_{sur}$  is calculated by

$$T_{sur} = T_{pulse} + (d_{surf} + d_{cable} + 12)/150$$

where  $T_{pulse}$  is the propagation time in microseconds of the radar transmit pulse,  $d_{surf}$  is the distance in meters from scanner to ice surface and  $d_{cable}$  is the equivalent free air length of the radar to antenna cable.

When laser data are not available  $T_{sur}$  is taken from the radar measurements and is calculated as

$$d_{surf} = 150(T_{sur} - T_{pulse}) - d_{cable} - 12$$

in order to provide the surface elevation. The bottom elevation is obtained by subtracting the ice thickness from the surface elevation. All elevations are in WGS84 ellipsoid coordinates.

# Ice sheet velocity mapping

## Objectives and Planning

The objectives of the velocity mapping activities within PROMICE were threefold:

1. Preparation of a software processing chain capable of measuring the three-component ice velocity from Synthetic Aperture Radar (SAR) data.
2. Delivery of the software to GEUS and assistance in using it.
3. Operational measurements on a limited number of areas of interest.

The following techniques are well established for objective 1, and were therefore selected for the project:

- SAR Interferometry (InSAR)
- Image correlation techniques, known in literature as speckle-, coherence- and feature-tracking methods. These will be jointly referred to as offset-tracking techniques in the following.

In order to ensure updates to future sensors and algorithms and assistance in using the software, a commercial software package distributed by the Swiss consortium GAMMA Remote Sensing and Consulting AG, was selected to provide the core processing modules. This package is referred to as the “GAMMA software” in the following.

The validated software was delivered to GEUS together with version 1.0 of the Software User Manual (SUM) on December 8<sup>th</sup> 2009. The most recent version of the SUM was delivered on August 8<sup>th</sup> 2010. Operational processing was carried out at DTU and GEUS in 2010.

## Processing chain overview

### Functional Blocks

The architecture of the InSAR/offset-tracking software under development is shown in figure 48.

In a typical processing sequence, the focusing module (FOC) is used to concatenate a certain number of consecutive raw data frames acquired from a single satellite track, and to perform range and azimuth focusing, generating a Single Look Complex product (SLC). Both InSAR and offset tracking techniques require pairs of SLC products to be generated, corresponding to approximately the same ground track.

Each SLC pair is then processed by the offset-tracking module (OTR), which models the registration offsets between non-moving areas in pairs of SLC products with low order pol-

ynomials in each image dimension, and accordingly re-samples each pair to a common master SLC geometry. In all cases, SLC or SLC intensity data patches are correlated on a coarse grid (e.g. 3 km) to refine the re-sampling information derived from the orbit state vectors. Optionally, correlations are subsequently also performed on a fine grid (e.g. 100 m), yielding residual registration offsets in the slant-range and azimuth dimensions. Coarse and fine grid registration offsets form an Offset Tracking Product (OTP).

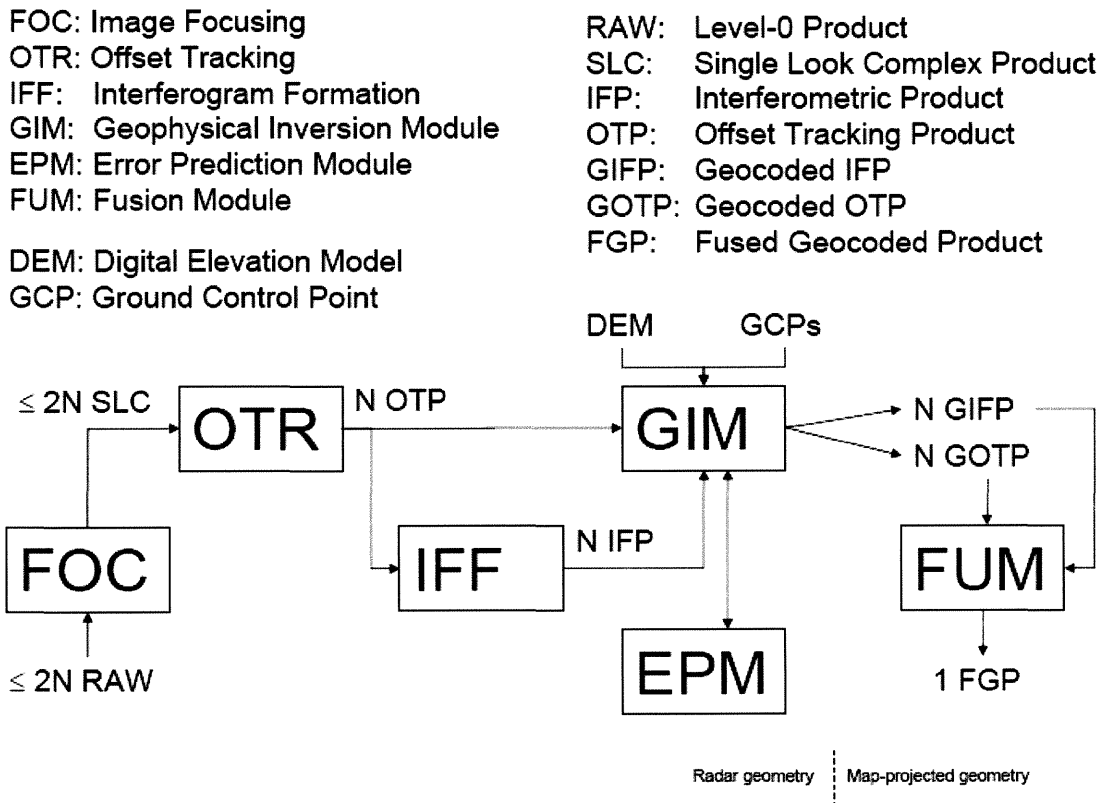


**Figure 48.** Processing chain block diagram

For each SLC pair, if registration offsets were computed only on a coarse grid, the re-sampled SLCs may be input to the Interferogram Formation module (IFF), which will generate an interferometric product (IFP). If SLC registration offsets were computed also on a fine grid, these may be either supplied to the IFF, which will use them to refine the image-registration based on the coarse offsets only, or directly supplied to the Geophysical Inversion module (GIM).

The GIM uses one or more OTP and/or IFP to output map-projected geophysical measurements (displacement and height) and their predicted error measurement standard deviation, generated by the Error Prediction Module (EPM). These form the GIFP (Geophysical Interferometric Product) and the GOTP (Geophysical Offset Tracking) products respectively. The GOTP includes displacement measurements in azimuth and slant-range, whereas the GIFP may contain height and/or slant-range displacement measurements. In general also auxiliary data, namely an external Digital Elevation Model (DEM) and a set of Ground Control Points (GCPs) (points of known height and velocity) will be needed by the GIM to obtain accurate results.

In the FUM, displacement products from single tracks are converted to a coordinate system independent of radar geometry (e.g. east, north, up) and height and displacement measurements from different (and possibly overlapping) tracks are combined to form a Fused Geophysical Product (FGP), which is the processing chain final output.

### **Implementation**

The developed software consists of 5 user-operated Linux executables corresponding to the functional blocks previously described, namely FOC, OTR, IFF, GIM and FUM. The EPM is instead operated internally by the GIM. These executables make use of those included in the GAMMA software packages as well as a suite of ANSI-C programs developed at DTU.

Combination and testing of the GAMMA executables amount to most of the work in WP-1 and WP-2. This is due to the fact that the GAMMA software comes as a set of Linux executables, thought for general InSAR/Offset-tracking applications. The modules of primary interest for this project, namely the MSP (Modular SAR Processor), ISP (Interferometric SAR Processor) and DIFF&GEO (Differential Interferometry and Geocoding) ones include 57, 92 and 56 executables respectively. Therefore a selection of the supported algorithms is required, as well as a determination of appropriate parameter ranges, based on GAMMA documentation, scientific literature and performance on test-cases.

Additional software development is required to provide utility programs needed to combine the GAMMA executables in the desired way, as well as to implement functionalities not included in the commercial package, but essential for PROMICE.

Implementation details and software usage are considered out of the scope of this report, and will be documented in a Software User Manual, as part of WP-4.7.

### **Development data set**

The tests described in the following sections were carried out on an ERS-tandem data set described in 49. It is composed of two ERS-1/ERS-2 tandem acquisitions, referred to as T1 and T2 in 49 and in the following. Each acquisition is composed of 3 consecutive raw data frames, acquired on descending track 325 over north-eastern Greenland.

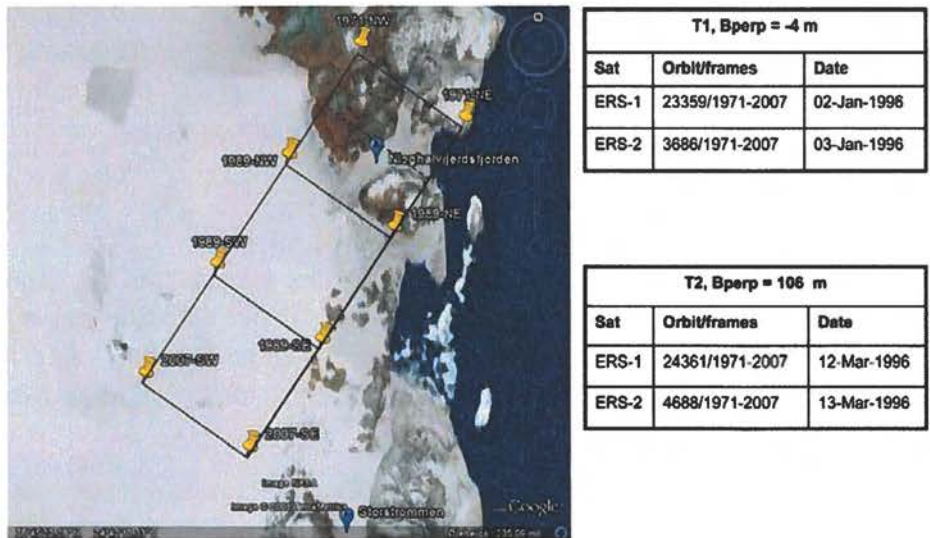


**Figure 49.** Development data set coverage. The dashed line indicates the approximate extent of the reference height and displacement data set of figure 50.

A height and a 2-D displacement map covering most of this area was kindly provided by Ian Joughin, now at the University of Washington, and used as a reference for the testing of the developed processing chain. It is plotted in a geographic equiangular projection in figure 50. The average height and slant-range displacement accuracy of the reference data are expected to be 13 m and 3.0 m/y respectively (Joughin et al., 2000).

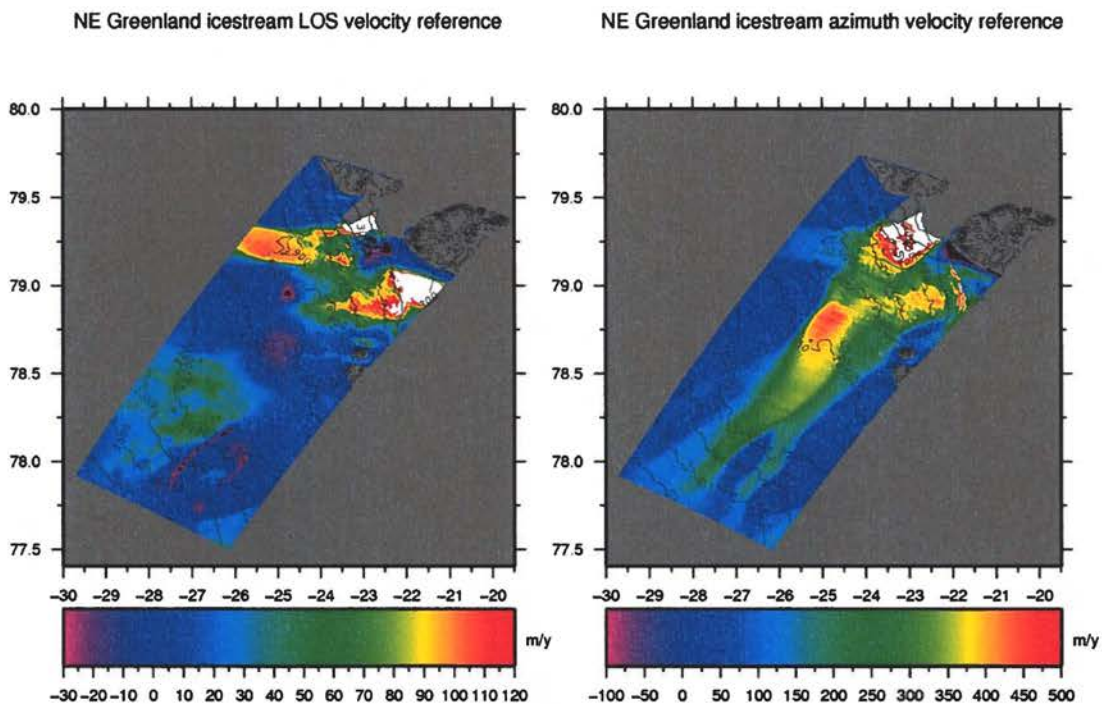


**Figure 50.** Line-of-sight (LOS) displacement [m/y] (left) and azimuth displacement [m/y] (right) with superposed WGS-84 ellipsoidal height contour [m]. Data was provided by Ian Joughin, University of Washington, and re-projected from map-geometry to the reference radar geometry of the development data set. LOS measures are positive towards the radar, azimuth ones are positive from bottom to top of the radar image.

## Processing Chain Performance on the Development Data Set

### Image Focussing

In order to extract geophysical measurements from the development data set, the FOC was run 4 times, once for each raw data strip composing T1 and T2 (see figure 49), obtaining 4 SLC products.

A multi-looked intensity image corresponding to ERS-2 orbit 03686 (denoted E2\_03686 in the following), is shown in figure 51 to the left. The image is in radar geometry, averaged by factors 8 x 40 in slant-range and azimuth respectively, corresponding 160 m x 160 m on ground. Due to the descending track acquisition geometry and to the fact that the SAR “looks” to the right, Lambert Land appears to the left of Nioghalvfjerdingsfjorden, in the near-range of the radar. A higher radar backscatter is observed, as expected, from areas above the equilibrium located at a height of about 800 m for this region (see the height contours in figure 50).



**Figure 51.** *Left: Multi-looked intensity image of E2\_03686 obtained with the FOC module. Right: full resolution resampled SLC magnitude corresponding to area in the white box in the multi-looked image, obtained with the OTR module. From left to right the full-resolution image patches correspond to E2\_03686, E1\_23359, E1\_24361 and E2\_04688 respectively.*

## Registration offset computation

In a first processing run, the OTR was run on each SLC pair composing T1 and T2, with the objective of registering non-moving areas in each SLC to a common reference geometry, chosen as that of E2\_03686.

For each SLC-pair, residual registration offsets compared to orbital information were estimated by computing intensity correlation-peaks on a regular grid (32 x 96 correlations in slant-range and azimuth respectively, corresponding to a 3km x 3km grid on ground). Large correlation windows of size 64 x 256 in slant-range and azimuth respectively were chosen and images were oversampled by a factor 2 prior to correlation. Signal-to-noise-ratio (SNR) was used as a confidence measure for offset estimation. This is defined as the ratio of the correlation peak to the averaged correlation value in a box surrounding the peak. Offsets with an SNR>4.0 were used to estimate 4 polynomial parameters, modelling image misregistration. These were subsequently used to resample each SLC to the reference geometry.

The registered SLC images were visually inspected to verify that point targets in non-moving areas, such as bedrock, had been registered to sub-pixel accuracy. In the case of the T2 SLC pair, the above procedure had to be repeated using an even larger correlation window size of 256 x 1024 pixels, in order to achieve registration with sub-pixel accuracy. Offsets were in this case computed on a coarser grid of 16 x 48 pixels, to improve efficiency.

The magnitude of a small portion of the registered SLC images is shown in figure 51 (right). The area considered (white box in figure 51, left) is on the floating glacier tongue of Nioghalvfjærdsfjorden, and includes co-registered static features (bedrock), as well as mis-registered moving ones (e.g. the white disc feature, which might be a frozen meltwater lake).

In a second processing run, the OTR was used on each re-sampled SLC pair, obtained with the procedure described above, to compute residual offsets related to motion. To this end, two different offset-tracking techniques were tested and are described in the following sub-sections.

## Intensity tracking

Intensity correlations were computed for the T1 SLC pair using windows 8 x 32 pixels in slant range and azimuth respectively (160 m x 130 m on ground), on a 10 x 50 pixel grid (~200 m on ground). Images were oversampled by a factor two prior to correlation.

Subsequently, range and azimuth offsets were culled using an SNR threshold of 4.0, and a threshold based on the maximum expected offset magnitude. Hole-filling was performed through a weighted interpolation of at least 8 neighbouring points in a radius of 8 offset measurements. Finally a moving average window 7 x 9 in size was used to reduce the variance of the estimates, at the price of a reduced spatial resolution of about 1.2 km x 1.2 km. The results are shown in figure 53.

Correlation SNRs above threshold are achieved over almost all the image, including featureless ice-sheet areas, with the highest values located in bedrock areas, and the lowest at the margins of rapidly flowing ice (see figure 50), and where the ice-sheet funnels into the glacier. There is a close relation between SNR and interferometric correlation, figure

54, indicating that correlation peaks are related to correlated intensities, rather than to visible features.

In the slant-range and azimuth offsets of figure 53, the regions of fastest ice-flow can be recognised, as compared to the reference measurements, figure 50. The offsets however require calibration, i.e. removal of a slowly-varying trend, before they can be interpreted as displacement. This step will be carried out within the GIM. In the azimuth offset data, horizontal stripes appear, at a small angle compared to the slant-range direction. These have been observed by several researchers and are known to be due to ionospheric propagation delay (Gray et al., 2000).

The intensity tracking procedure was repeated for the T2 SLC pair. Due to the low coherence of this data, figure 55 (left), very low SNRs were achieved and offsets with a very large variance were obtained. The results are not reported, as useful measurements could not be extracted from this data.

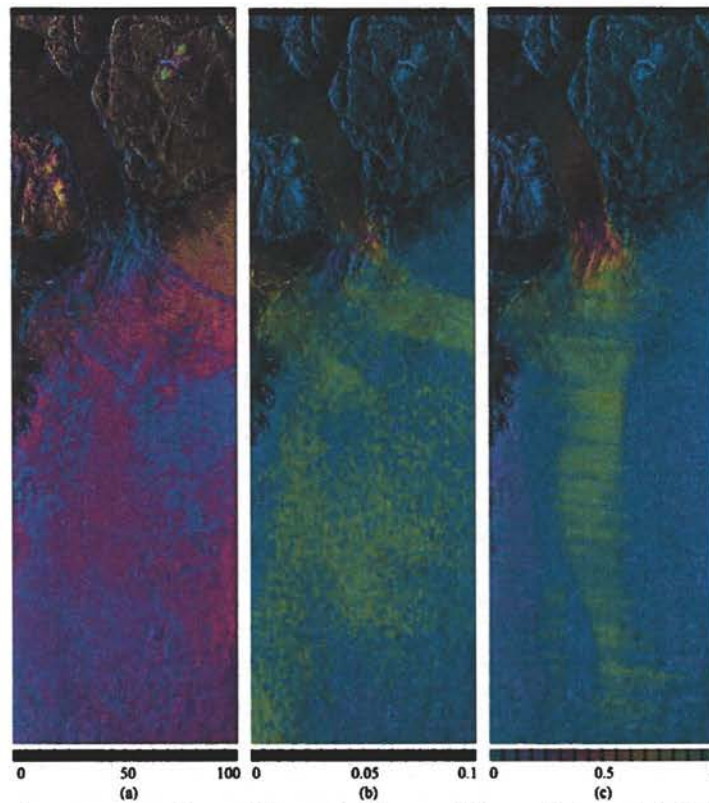


**Figure 52.** *T1 coherence tracking with an 8x16 correlation window. (a) Offset SNR (b) Slant-range offsets [pixels] (c) Azimuth offsets [pixels]. Slant range and azimuth pixel sizes are respectively 8 m and 4 m. Image brightness is based on a multi-looked intensity image of E2\_03686.*

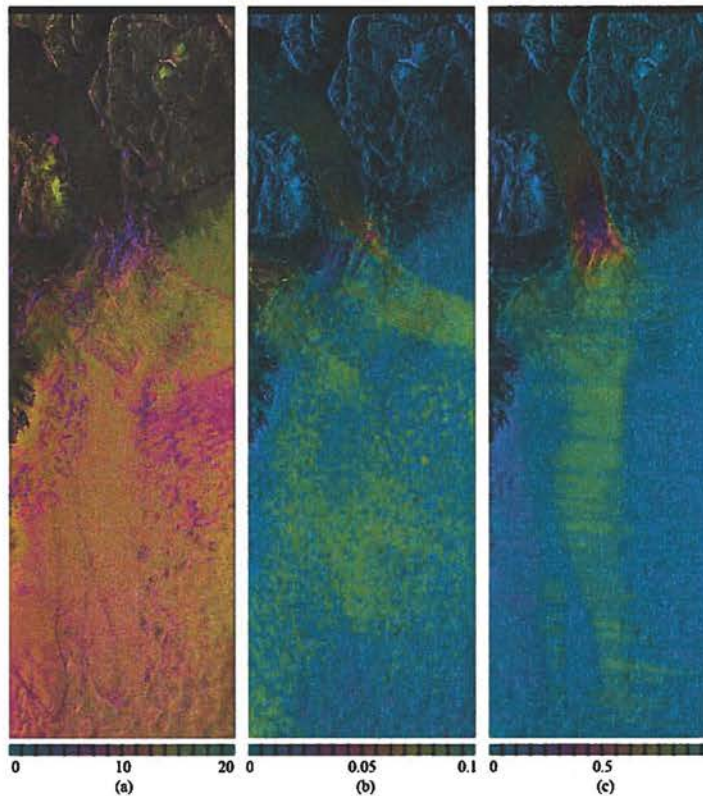


**Figure 53.** *T1 intensity tracking with an 8x32 correlation window. (a) Offset SNR (b) Slant-range offsets [pixels] (c) Azimuth offsets [pixels]. Slant range and azimuth pixel sizes are respectively 8 m and 4 m. Image brightness is based on a multi-looked intensity image of E2\_03686.*

### Coherence tracking

Slant-range and azimuth offsets maximising interferometric coherence were computed using windows 8 x 16 in slant range and azimuth respectively (160 m x 65 m on ground), on a 10x50 pixel grid (~200 m on ground).

Subsequently, range and azimuth offsets were culled using an SNR threshold of 2.5, and a threshold based on the maximum expected offset magnitude. The same hole-filling and moving-averaging parameters used for intensity tracking were chosen.

Results are shown in figure 52. Although the SNR values are much higher than those in Fig. 53, the spatial pattern is very similar and related to coherence. The spatial pattern of range and azimuth offsets are also similar to those obtained for intensity tracking, figure 53, including the ionospheric streaks which appear in the azimuth offsets.

### Interferogram Generation

The IFF was run on the registered T1 and T2 SLC-pairs output by the OTR, obtaining two interferograms.

The IFF performed common-band filtering, phase flattening to the WGS-84 ellipsoid, phase averaging of approximately 22 independent samples (using a 3 x 15 averaging window in slant-range and azimuth respectively) and coherence estimation on approximately 300 independent samples.

For T1, the intensity-tracked offsets were used to refine the SLC resampling performed by the OTR, prior to the above mentioned operations.

The wrapped interferometric phase and coherence estimates are shown in figure 54 for T1.

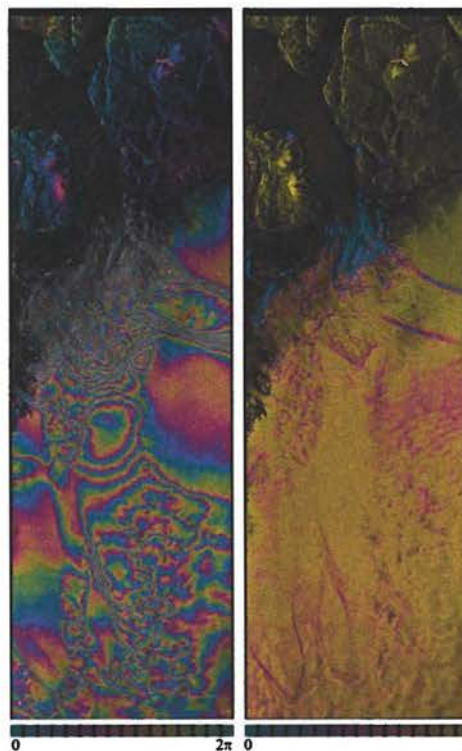


**Figure 54.** *Interferometric phase (left) and coherence (right) for T1, output by the IFF.*

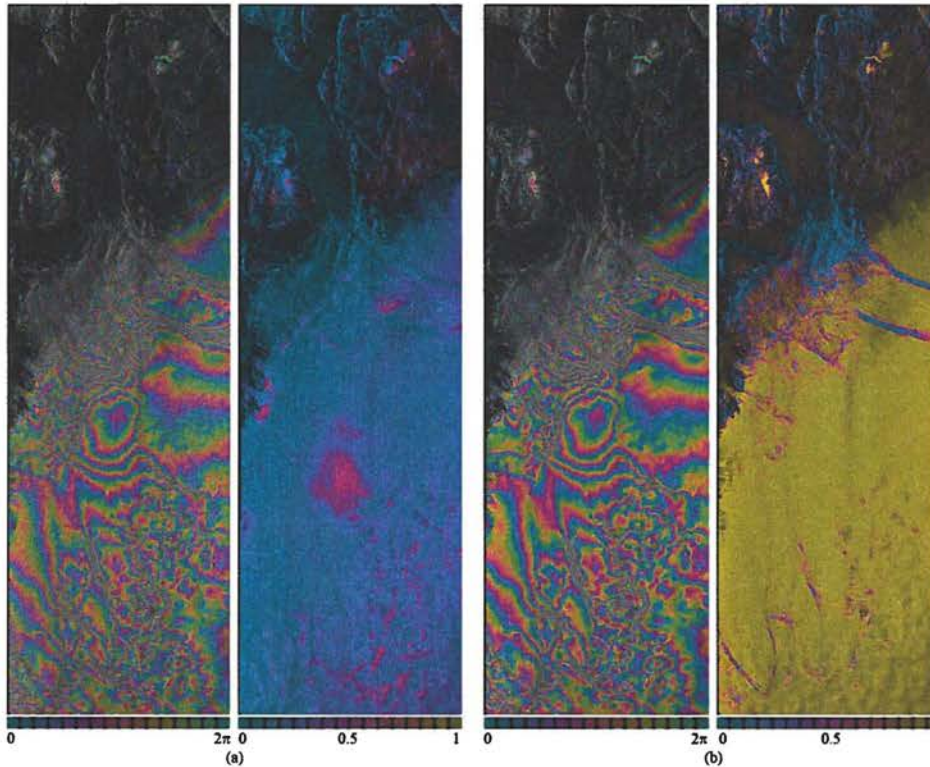


**Figure 55.** *Interferometric phase and coherence output by the IFF for T2 (a) without adaptive filtering (b) after “Goldstein” adaptive filtering.*

Since T2 exhibited a low coherence, processing was repeated using the so-called “Goldstein” adaptive filtering technique (Goldstein and Werner, 1998), which was very effective in reducing the phase noise. Results of both processing runs are shown in figure 55.

For T1, interferometric phase is quite insensitive to topography, due to the small 4 m perpendicular baseline. Therefore phase variations in figure 54 mostly correspond to displacement, although slow-varying trends apparent in the bedrock areas to the top-right of the image (Kronprins Christian Land), very likely due to orbit inaccuracies, and where steep topographic variations occur, as in the bedrock area in the left of the image (Lambert Land).

Coherence for the T1 data set is exceptionally high on average, with expected low values at the shear margins and at the entrance of the fjord, where flow is turbulent and accompanied by topographic variations.

The T2 interferometric phase shows a much higher sensitivity to topography, due to the 105 m baseline, as can be noticed especially on bedrock.

Coherence of the T2 data set, figure 55, is not uniformly low, since some coherent patches are seen. This suggests the cause of decorrelation could be weathering (e.g. a snow-fall) between the two acquisitions, separated by 1 day.

### **Geophysical Inversion**

The GIM was run to obtain height and slant-range displacement measurements from the T1 and T2 interferograms, and azimuth and slant-range displacement from the T1 offsets.

The external DEM from the reference height data set was used, and a set of 20 GCPs was extracted from the reference displacement data set, from areas at the sides of the main icestream.

InSAR measurements were obtained with two techniques, namely DEM elimination, using either T1 or T2 and the external DEM, and Double Difference, using both the T1 and the T2 interferograms.

Offset-tracking displacement measurements were derived from the results of intensity- and coherence-tracking.

The results for each technique are described in the following subsections.

### **InSAR DEM Elimination**

Within the GIM, a synthetic interferogram was generated from the reference DEM, and used to re-flatten the phase of the T1. Subsequently phase-unwrapping was carried out using the algorithm in (Goldstein et al., 1988). A least-square fit to the expected phase from the GCPs was carried out, to calibrate out orbital and atmospheric effects. The resulting phase was converted to line-of-sight displacement, with a positive sign indicating motion towards the radar.

Displacement measures were geocoded to a lat/lon grid (Equiangular projection), at a posting of 9 arcsec and 36 arcsec in latitude and longitude respectively, corresponding to roughly 250 m x 250 m on ground.

The resulting geocoded line-of-sight velocity map is plotted next to the reference displacement map in figure 56.

On the glacier tongue in figure 56, no measurements were available, since unwrapping with the chosen algorithm failed across the low coherence area at the entrance of the fjord (figure 54).

The velocity differences compared to the reference are plotted in figure 57 (left). Some differences are very regular in shape, and are most likely due to the mosaicing process used to generate the reference velocities. These probably cause the distribution of the observed differences to deviate from the Gaussian one, figure 57 (right). Elsewhere most of the differences lie within 4 m/y.

An independent error analysis was done computing the velocity statistics for bedrock areas in the top-left and top-right areas of Fig 56 (left), which are expected to be stationary. Mean biases of -1.39 m/y and -2.71 m/y and standard deviations of 0.28 m/y and 0.42 m/y were found respectively.

The root-mean-square values of both comparisons could be explained by the following error budget:

Decorrelation errors: 0.08 m/y (coherence=0.95) to 0.18 m/y (coherence=0.8), for 22 independent averaged phase samples.

Atmospheric errors: 0.42 m/y ( $\pi/12$  differential phase delay).

Topographic compensation errors: 0.05 m/y ( $B_{\text{perp}} = 4$  m, DEM accuracy = 13 m).

Reference velocity errors: 3.0 m/y.

This would yield an expected displacement measurement error standard deviation in the order of 0.43 m/y.

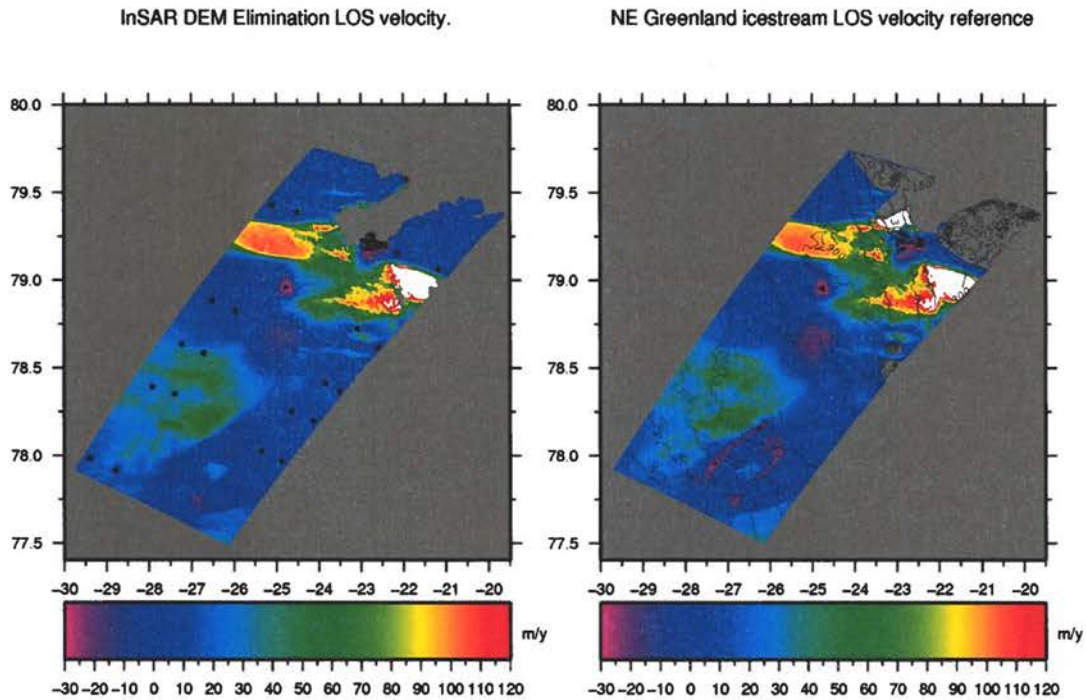


**Figure 56.** Geocoded LOS velocity from GIM DEM elimination (left) and from the reference (right). Latitude and longitude degrees are reported on the y and x axis respectively.

InSAR T1 DEME LOS velocity comparison with reference.

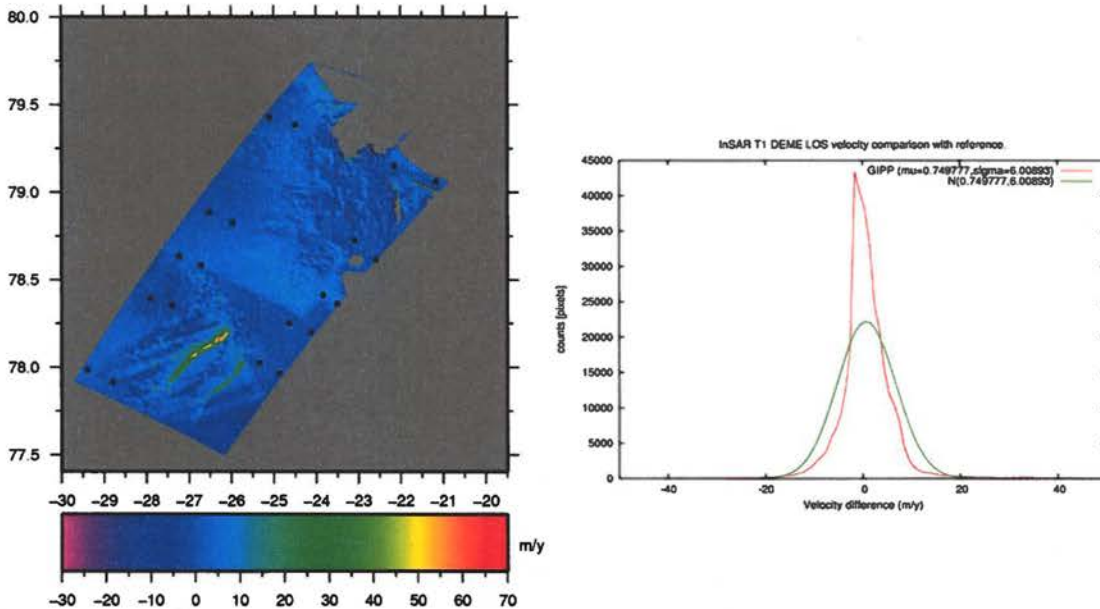


**Figure 57.** Differential LOS velocity compared to the reference (left) and corresponding histogram (right). The red curve in the histogram refers to the actual difference measurements, whereas the superimposed green curve represents a Gaussian distribution with same mean and standard deviation.

## InSAR Double Difference

Interferograms T1 and T2 were processed with the GIM, using the Double Difference technique, obtaining geocode line-of-sight displacement and a height maps.

Processing differs from the DEM elimination method, in that topographic contribution from the interferometric phase is estimated by differencing the two interferograms, assuming a common displacement rate.

For this data-set topography is therefore estimated with a perpendicular baseline of about  $4 \text{ m} - 106 \text{ m} = 110 \text{ m}$ .

In principle no external DEM is required in the processing. However the external reference DEM was used to improve phase flattening, and thus aid phase unwrapping.

The output height and displacement were geocoded to an equiangular projection, at a  $250 \text{ m} \times 250 \text{ m}$  posting, as for the DEM elimination results.

The measured LOS displacement, together with the measured height contours are shown in figure 58 (left). The same plot for the reference data set is provided for comparison. The differences in height and displacement are shown in figure 59. In figure 58 and figure 59 the displacement is positive towards the radar, and elevation is referred to the WGS-84 ellipsoid.

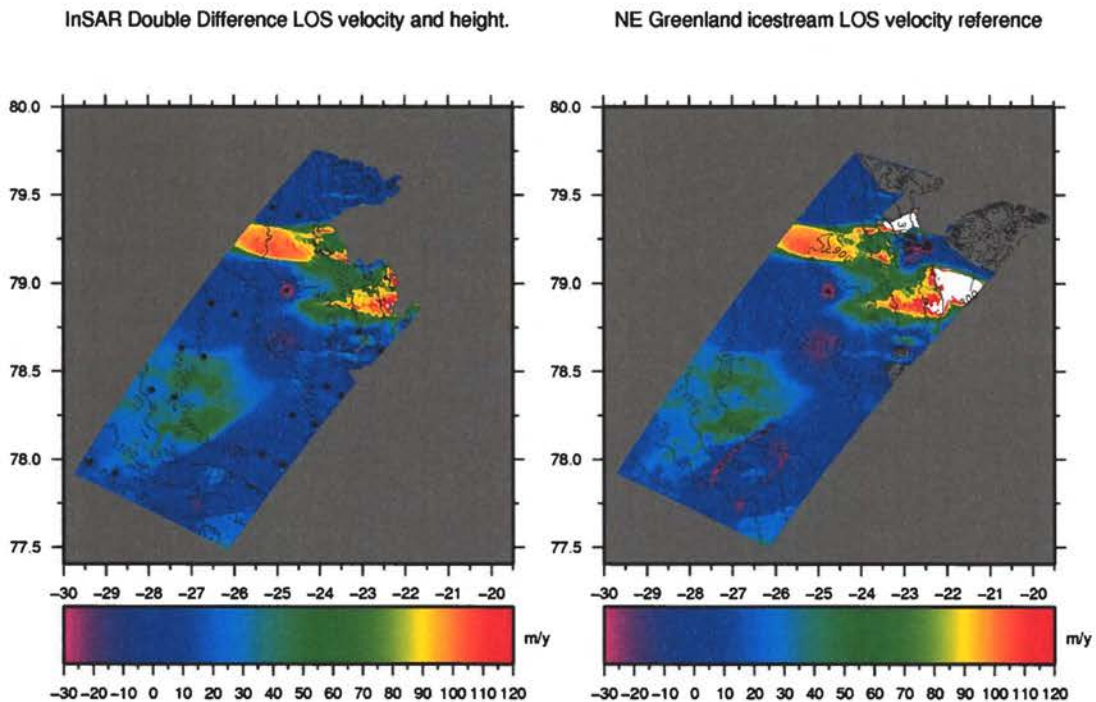


**Figure 58.** DD results: LOS velocity from the GIM (left) and from the reference (right).

The mean differences compared to the reference were  $1.14 \text{ m/y}$  and  $-5 \text{ m}$  respectively, with standard deviations of  $5.55 \text{ m/y}$  and  $39 \text{ m}$ . In both cases the distributions were not Gaussian, as can be seen from the images of figure 59. An error budget based on the sensitivity equations of the Double-Difference method yields an expected height standard deviation of  $21 \text{ m}$ , and an expected displacement error of  $0.58 \text{ m/y}$ . These figures, together with the accuracy of the reference data, were considered sufficient to explain the observed differences.

InSAR DD LOS velocity comparison with reference.

InSAR DD LOS height comparison with reference.

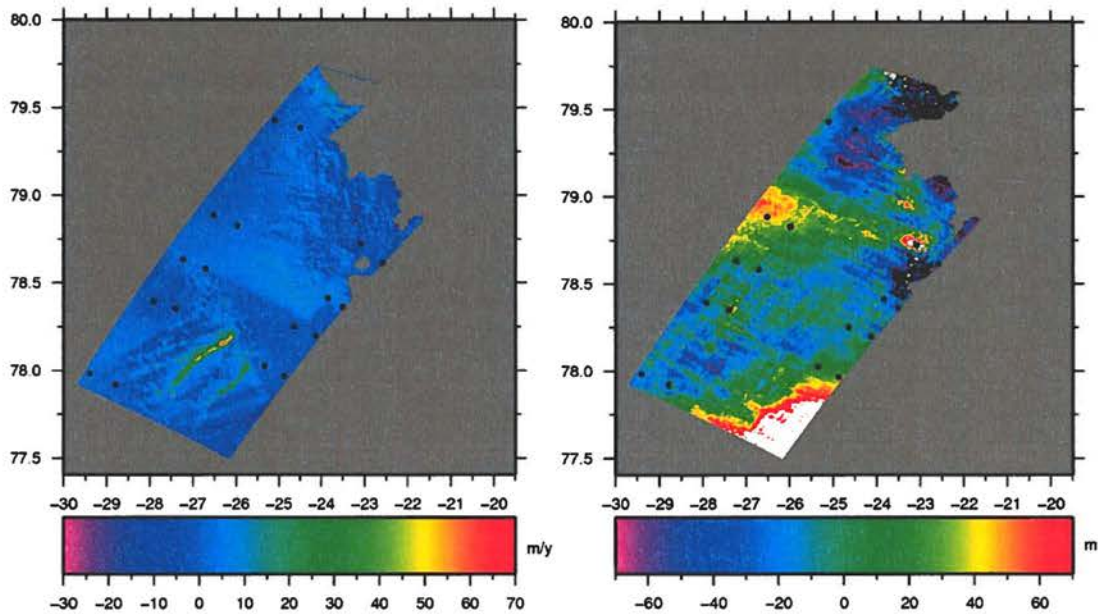


**Figure 59.** DD results: Differential LOS velocity (left) and height (right) with respect to the reference.

### Coherence-Tracking Velocities

The GIM was used on the output of the T1 OTR coherence-tracking run described previously. Geocoded line-of-sight and azimuth displacement maps were generated.

Within the GIM, the slant range and azimuth offsets output by the OTR were calibrated, using ground control points, before being converted to displacement. The azimuth and range offset error throughout the image was modelled as a plane (3 parameters), and the model parameters were estimated in a least-square sense based on the observed and the expected offsets at the control points. An iterative procedure was used to discard points which differed from the median by more than 3.5 times the inter-quartile range. The estimated polynomial corrections were subtracted from the offset measurements. This calibration procedure was not part of the GAMMA software package, and was implemented as an auxiliary C program.

Subsequently the offsets were converted to displacements in the line-of-sight and in azimuth by applying the appropriate scaling factors, depending on pixel size (4 m x 8 m respectively for ERS), grid dimensions (10 x 50) and temporal baseline (1 day for Tandem data).

Finally measurements were geocoded on a 9 x 36 arcsec posting in latitude and longitude respectively. The results are shown in figure 60, whereas a comparison with the reference displacement measures is provided in figure 61 and figure 62.

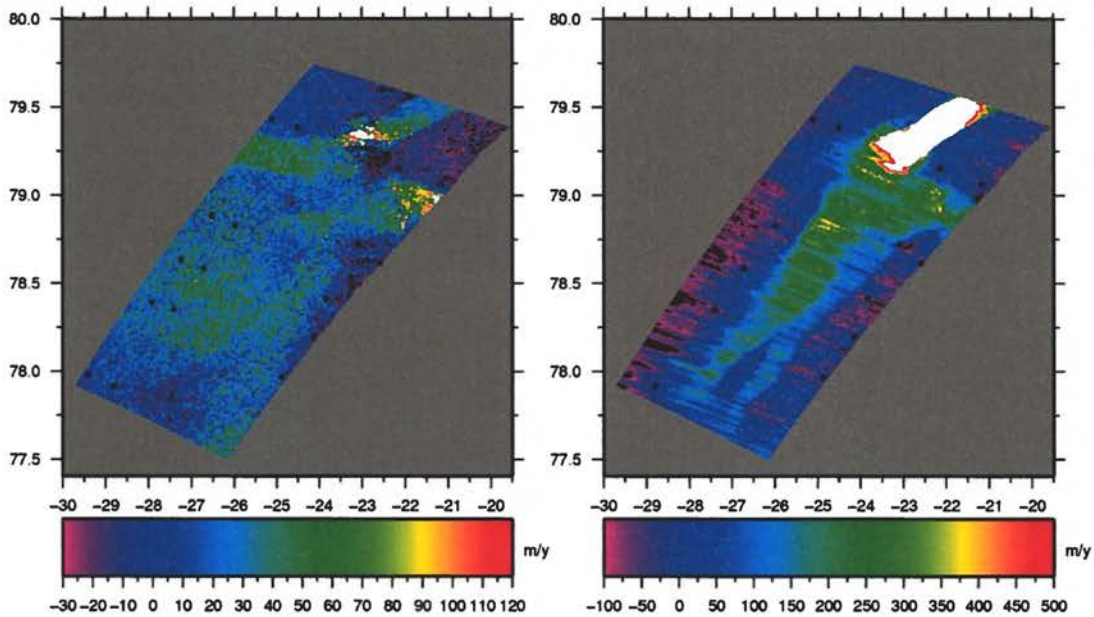


**Figure 60.** Coherence tracking: geocoded LOS velocity (left) and azimuth velocity (right).

The line-of-sight velocity map appears noisy compared to the corresponding ones, derived with InSAR techniques (figure 56 and figure 59). A bias is also apparent in the high-velocity areas in the upper part of the image. This is very likely due to an improper offset-calibration. In fact 3 control points were discarded in the calibration procedure, resulting in a weak conditioning of the right portion of the velocity map. The calibration procedure is not robust in the face of noise, since it does not take error standard deviations or correlations into account. This issue will be addressed in WP-3.

The RMS error in the line-of-sight is in the order of 30 m/y compared to the reference, as seen from figure 62. This value however is somewhat misleading, as the histogram of the differences seems to contain two overlapping Gaussian bells, centred on different mean values. These are likely to correspond to the upper and lower part of the image respectively. On two bedrock areas in the top-left and top-right of figure 60, RMS deviations of 8 m/y were found.

The error budget expected from theory in areas of high coherence ranges between 6.5 m/y and 11.4 m/y for coherences in the range of 0.9 to 0.75 respectively. These values are based on the curves reported in figure 1 in Bamler and Eineder, 2005, and on the correlation windows and averaging factors used in the OTR processing.

These expectations are considered in sufficiently good agreement with the bedrock observations.

The azimuth displacement map, figure 60(right), is dominated by the ionospheric effects already noted in section 0. In this case the latter indirectly cause a large additional bias, by inducing an error in offset calibration. RMS azimuth velocities on bedrock were found to be about 16 m/y. Azimuth displacement accuracy expected theoretically is in the order of 3 to 6 m/y, since the azimuth pixel-spacing is smaller than the slant-range one by a factor 2. It is therefore likely that ionospheric effects contribute the additional unexplained variance of

about 10 to 13 m/y, corresponding roughly to 0.01 azimuth pixels. This error figure agrees with other observations (Joughin, 2002).

Methods have been proposed to remove ionospheric effects (Mattar and Gray, 2002), (Wegmuller et al. 2006), but the procedure requires care, especially when the scene presents a high motion component in the azimuth direction, as is the case at hand. Therefore it was considered out of the scope of this work.

Coherence tracking LOS-reference (win=8x16,ave=7x9). Coherence tracking azimuth-reference (win=8x32,ave=7x9).

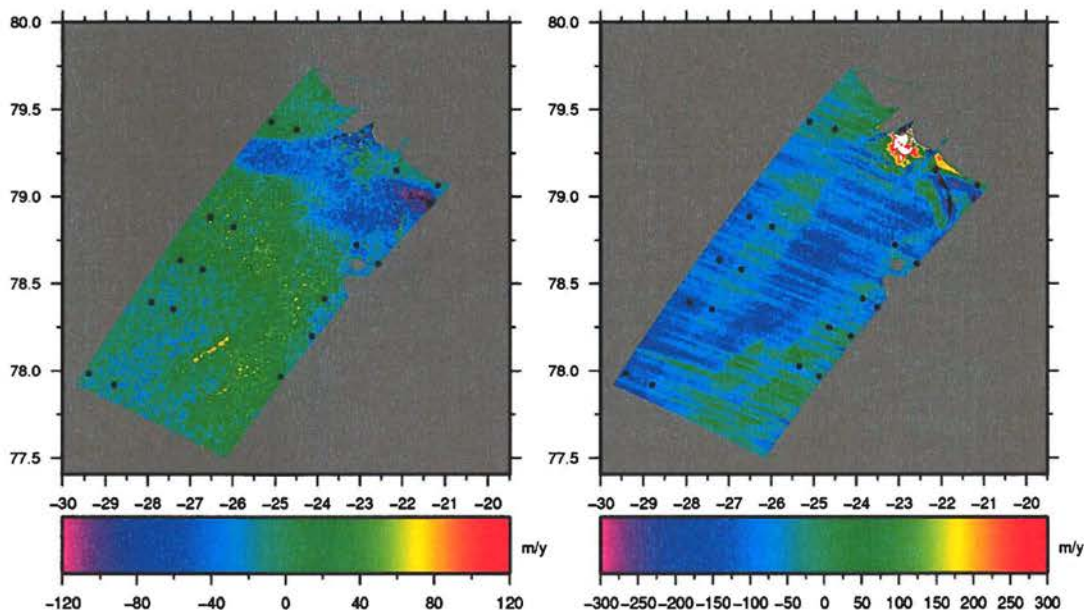


**Figure 61.** Coherence tracking: Differential LOS velocity (left) and azimuth velocity (right) with respect to the reference. Areas in black and white exceed respectively the lower and upper boundary of the colour scale.

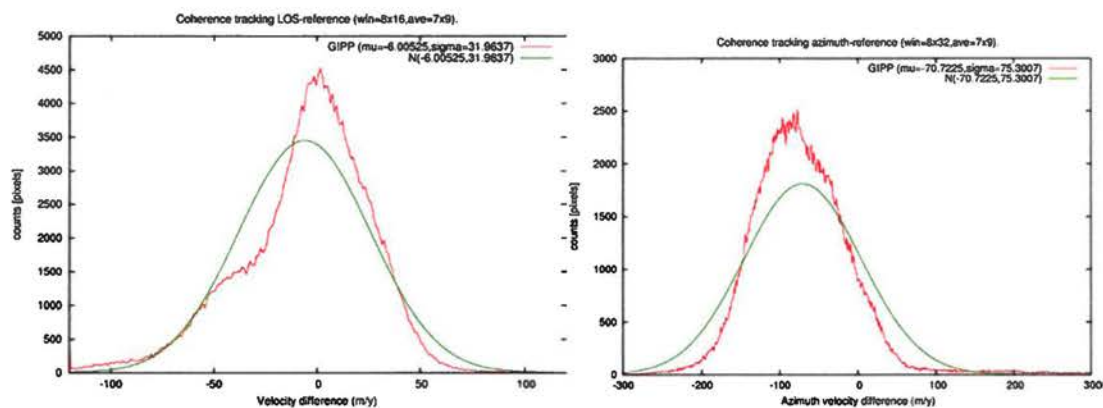


**Figure 62.** Coherence tracking comparison: LOS velocity (left) and azimuth velocity (right) differences compared to the reference data set. The red curve corresponds to the actual differences, whereas the superposed green curve represent a Gaussian distribution with same mean and standard deviation.

### Intensity-Tracking Velocities

The GIM was used on the output of the OTR intensity-tracking run on the T1 SLC-pair, described previously.

The same offset calibration procedure described in the previous section was applied.

Finally measurements were geocoded on a 9 x 36 arcsec posting in latitude and longitude respectively. The results are shown in figure 63, whereas a comparison with the reference displacement measures is provided in figure 64 and figure 65.

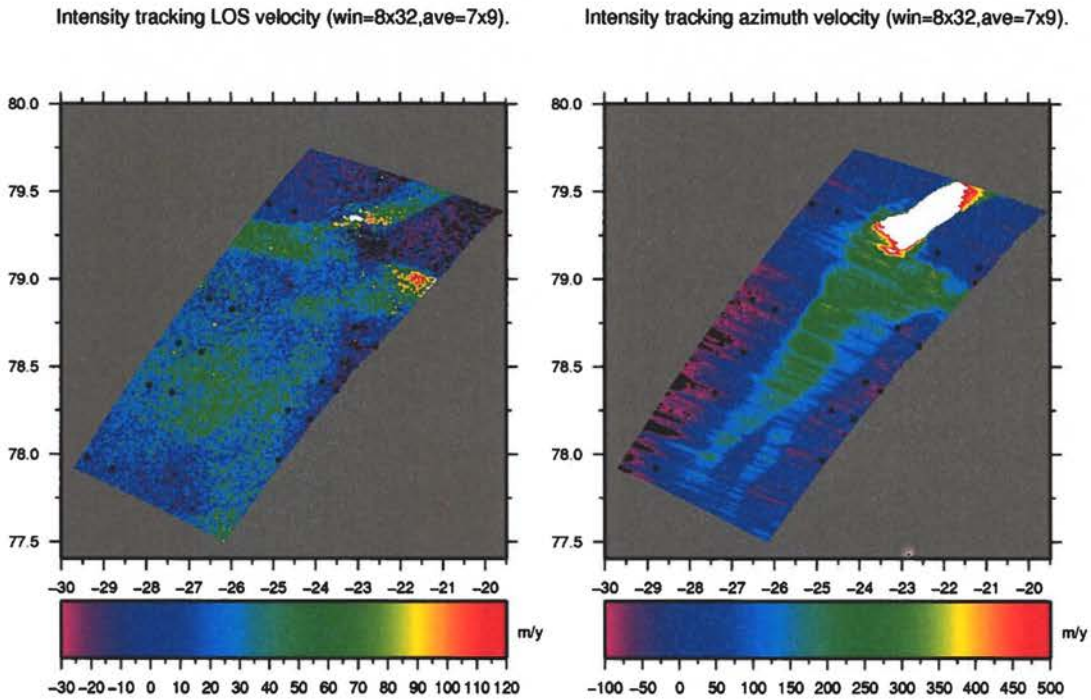


**Figure 63.** Intensity tracking: LOS velocity (left) and azimuth velocity (right)

Similar results compared to coherence-tracking were obtained. RMS velocities on bedrock were found to be around 11 m/y in slant-range and about 20 m/y in azimuth. The expected errors are within 6.5 and 11.3 m/y in slant-range and half of these values in azimuth. The observations on bedrock are explained, assuming ionospheric effects to contribute an additional variance of about 10 to 13 m/y, as for the coherence-tracking results.

Intensity tracking LOS-reference (win=8x32,ave=7x9).

Intensity tracking azimuth-reference (win=8x32,ave=7x9).

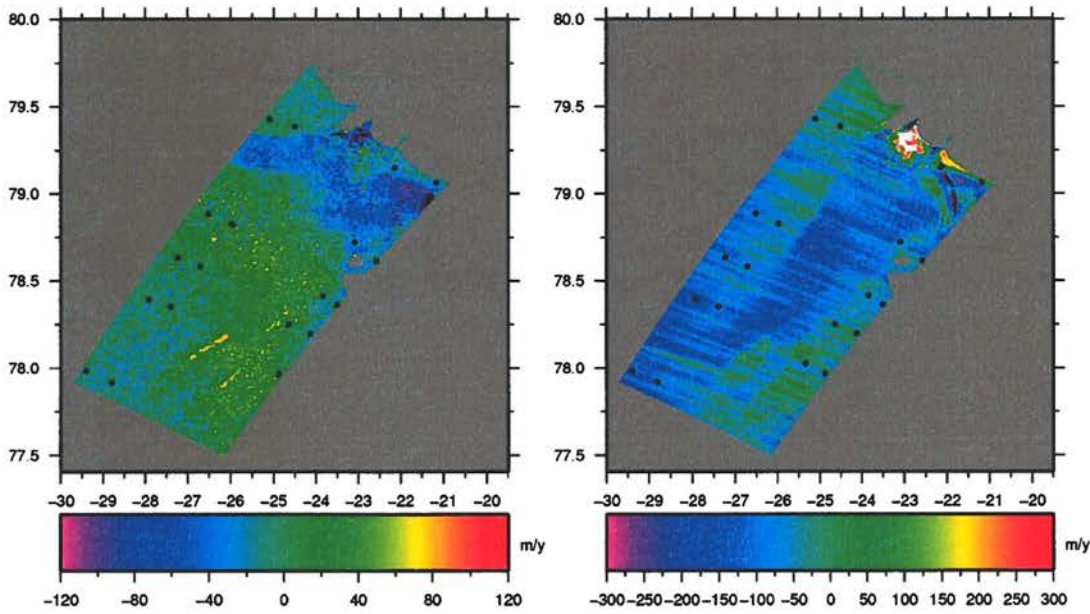


**Figure 64.** Intensity tracking: LOS velocity (left) and azimuth (right) velocity differences with respect to the reference.

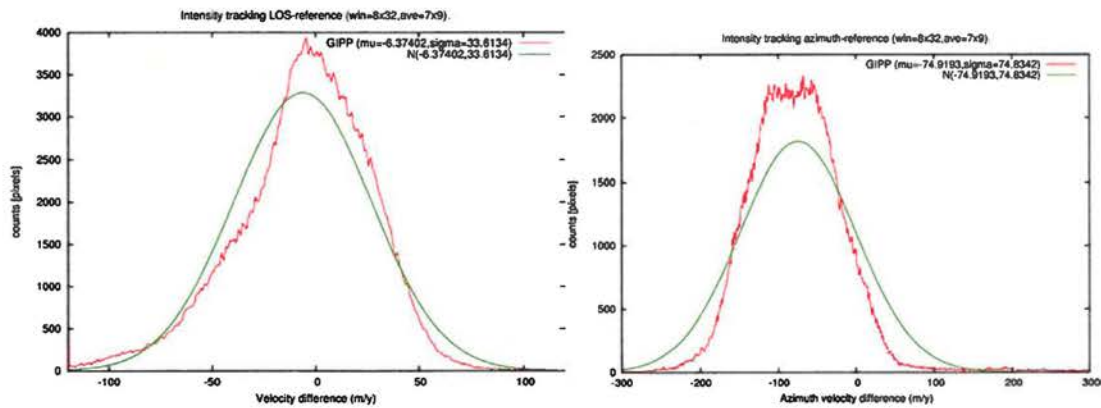


**Figure 65.** Intensity tracking comparison: LOS velocity (left) and azimuth velocity (right) differences compared to the reference data set. The red curve corresponds to the actual differences, whereas the superposed green curve represent a Gaussian distribution with same mean and standard deviation.

### Error prediction

The objective of the error prediction modules is to predict the error standard deviations associated to the geophysical measurements carried out with a specific SAR data processing technique. The geophysical measurements are, potentially, height and slant-range displacement for SAR interferometry (InSAR), and slant-range and azimuth displacement for offset-tracking.

The error prediction framework described in Mohr and Boncori, 2008 was applied to both techniques. It allows to predict a spatially varying error standard deviation, keeping into

account the spatial distribution of the Ground Control Points (GCPs) used for phase (or offset) calibration. In order to do this, second-order statistical error models must be available for the main measurement error sources.

Concerning InSAR, error models describing the main error sources, namely phase unwrapping, decorrelation and atmospheric propagation, were derived in Mohr and Boncori, 2008.

Concerning offset-tracking, error models were developed specifically for PROMICE. The main error sources affecting slant-range and azimuth displacements are due to uncertainties in locating the peak of the cross-correlation function. This may be caused by phase decorrelation, in the case of speckle-tracking, or by low Signal to Clutter ratio, in the case of feature tracking (Bamler and Eineder, 2005). Azimuth displacement fields may also be significantly affected by ionospheric propagation effects on SAR image formation (Mattar and Gray, 2002). Simplified error models for these sources, based on (Joughin, 2002), were implemented for PROMICE. Concerning cross-correlation errors, simplification consists in using the local root-mean-square variation of the measured offsets as a proxy for the local standard deviation, rather than modelling this from phase decorrelation or feature Signal-to-Clutter ratio. Concerning ionospheric errors, instead of considering the spatial correlation of this error source, for which no model is available in literature, a constant user-configurable standard deviation figure for the whole image was used.

### **Measurement fusion (mosaicing)**

The objective of the fusion module is to create height and displacement (velocity) mosaics, with their associated error estimates.

Both InSAR and offset-tracking techniques are typically applicable only between SAR image pairs acquired from the same satellite track, so that mosaicing of the geophysical measurements obtained for several adjacent and partially overlapping tracks is required in general to cover an area of interest.

Fusion of InSAR-derived height maps is carried out by a weighted average of a number of input layers, with weights set to the inverse of the height standard deviation output by the error prediction module.

Fusion of several slant-range and/or azimuth displacement maps is carried out by first creating a number of input layers consisting in the Cartesian components of displacement. These may be obtained in three ways:

1. From two InSAR slant-range displacement measures, assuming Surface Parallel Flow (SPF).
2. From an InSAR slant-range, an offset-tracking azimuth displacement measure and the SPF assumption.
3. From two slant-range and two azimuth displacement measures derived from offset tracking.

Each layer is then fused in the same way as for the height mosaic, again using the error standard deviations output by the error prediction modules to compute error estimates for the fused product.

SAR intensity images are also fused, using a weighted average with unitary weights in overlapping areas.

## Software validation

A detailed description of the validation is given in (Boncori et al., 2009). In this section the most important results are summarised.

### Data

A test-site in west Greenland, near Kangerlussuaq airport, was chosen to validate the processing chain, due to the availability of stakes with GPS positioning in this area (Van de Wal et al., 2008). SAR data for winter 2007/2008 was provided by ESA through CAT-1 project 6288. Two ALOS-PALSAR FBD frames, taken 46 days apart, and four ENVISAT-ASAR IS2 strips, taken 35 days apart, were available. The data coverage is shown in figure 66. The location of the GPS stations within the coverage of the SAR data is shown in figure 67 and named after Van de Wal et al., 2008.

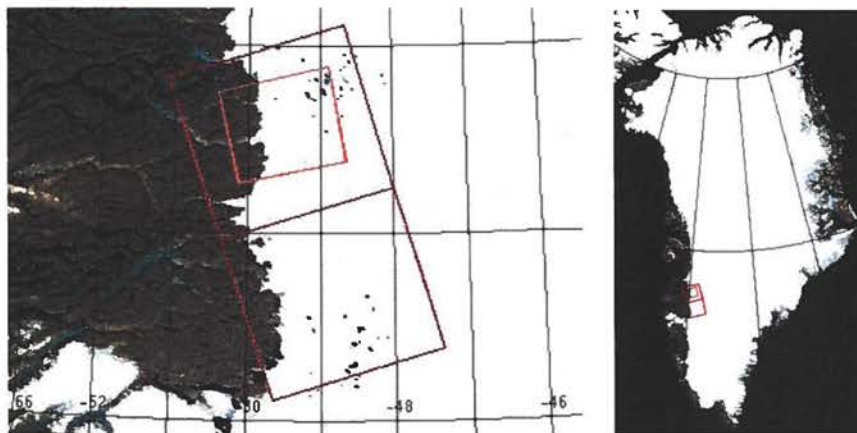


**Figure 66.** SAR data location. ASAR IS2 (two frames) and PALSAR FBD. ASAR acquisition dates: 20071111, 20071216, 20080120, 20080224. PALSAR acquisition dates: 20080203, 20080320.

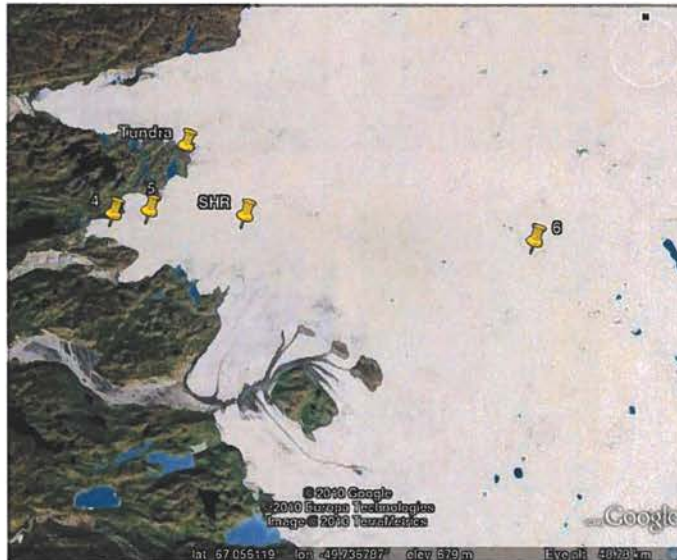


**Figure 67.** Validation data set GPS stations.

### Measurements

The raw data were focused and intensity correlation was carried out on each SLC pair, using correlation windows of 64x256 pixels in slant-range and azimuth respectively (1.2 km x 1.2 km on ground), on a grid of 10x50 pixels (200 m x 200 m on ground). Correlations with SNR lower than 7.0 were rejected. The resulting offsets were box-averaged on a window of size 8x8 to reduce uncorrelated errors. Two examples are shown in figure 68.

The PALSAR FBD offset field has a reduced coverage due to the fact that several lines of calibration data were present in the raw dataset. The azimuth offsets contain some “streaks”, visible on the bedrock area in right image of figure 68a, which are a typical signature of ionospheric propagation effects.

The ASAR image pairs yield correlations with an SNR above threshold only within the ablation area, which corresponds to the darker area in the radar intensity mosaic of figure 69. Useful correlations were derived from two 35-day image pairs and one 70-day one.

All offset images show overall image trends, more clearly visible on the bedrock areas. These are due to orbit errors and propagation through ionosphere and troposphere.

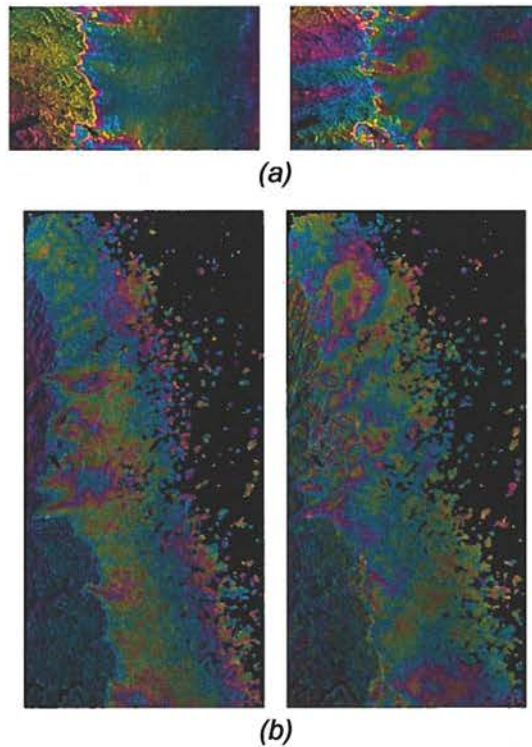


**Figure 68.** Slant-range (left) and azimuth offsets (left) for the PALSAR FBD frame (a) and a 35-day ASAR pair (b). Display is on a cyclic scale of 0.5 pixels. Images are in radar geometry (vertically flipped and rotated with respect to map geometry).

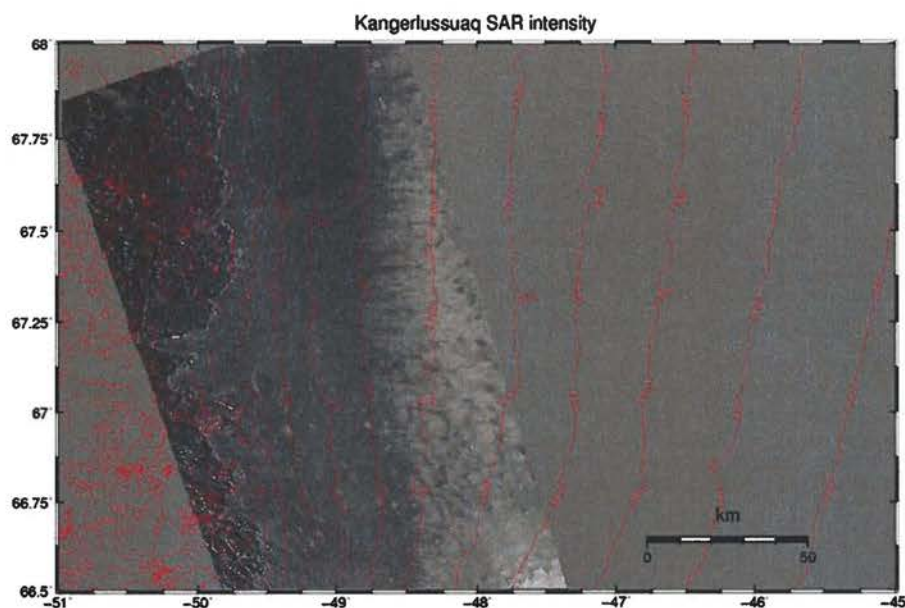


**Figure 69.** SAR intensity mosaic of all processed images. The equilibrium line altitude is expected to be around 1500 m. Radar backscatter is stronger from the non-homogeneous percolation zone compared to the ablation one.

A set of Ground Control Points (GCPs) was extracted from bedrock areas. Heights were derived from the NSIDC Greenland DEM (Di Marzio et al., 2007) and displacements were assumed to be zero. A plane was fitted in a least-square sense to the difference between the observed and the expected offsets at the GCP locations, for the slant-range as well as

for the azimuth datasets. The estimated planar trends were then subtracted for the offset fields in order to calibrate out slowly varying contributions not due to motion.

The calibrated offset fields were converted to slant-range and azimuth displacement measurements, and error standard deviations were estimated. These were subsequently geocoded on a latitude/longitude grid with a 9 x 36 arcsec posting (about 300 m x 300 m on ground). The mean slant-range and azimuth velocities measured from the PALSAR FBD pair and from three ASAR pairs were then converted to easting and northing velocity components under the surface parallel flow assumption and fused into a single mean velocity product through a weighted average. The weights were taken as the inverse of the per-pixel error variances, estimated in the previous processing step. The magnitude of the fused mean velocity product is shown in

Fi 70.

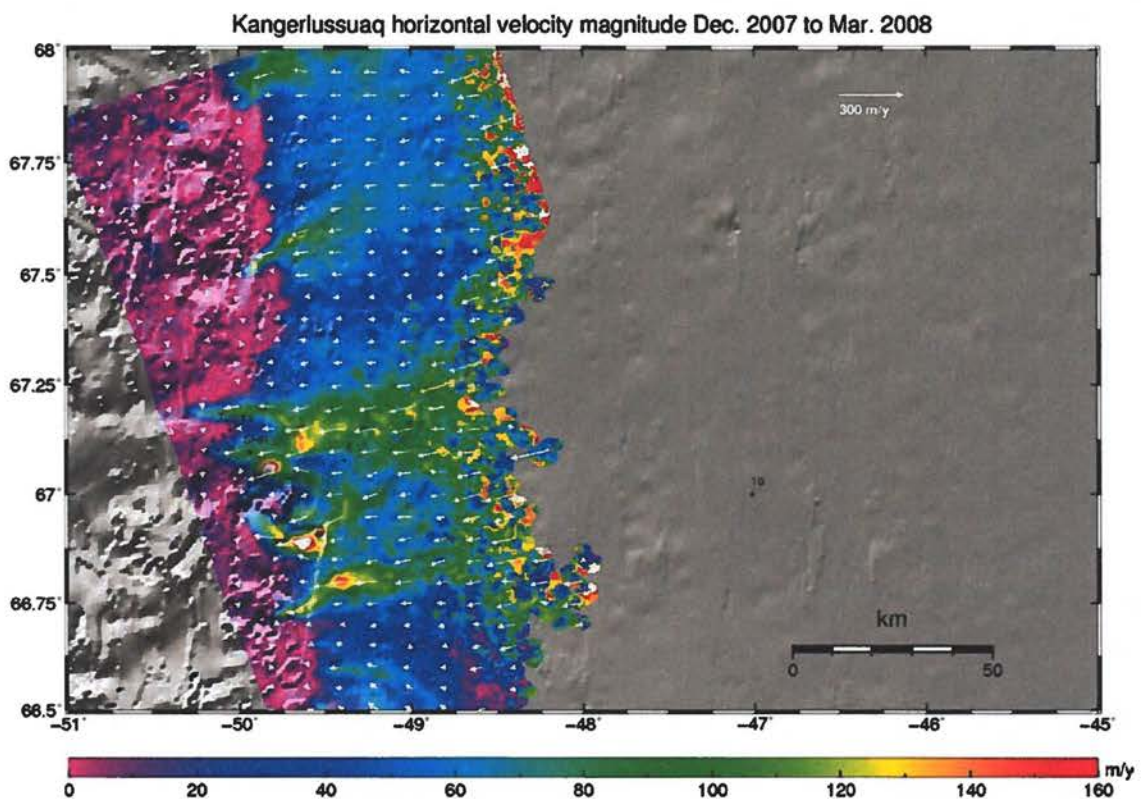


**Figure 70.** Fused mean velocity magnitude and flow directions plotted over a DEM shaded relief. The GPS stations used for comparison are located slightly above the 67<sup>th</sup> parallel and are plotted as black circles.

### Comparison with GPS velocities

Hourly GPS position measurements spanning the acquisition times of the SAR data were provided by R. van de Wal, from the Institute for Marine and Atmospheric Research Utrecht. The GPS stations were within the coverage of the ASAR datasets only. A linear regression of the hourly measurements of each horizontal position component was carried out for each station and is shown in figure 7, yielding mean velocity estimates and an associated error standard deviation.

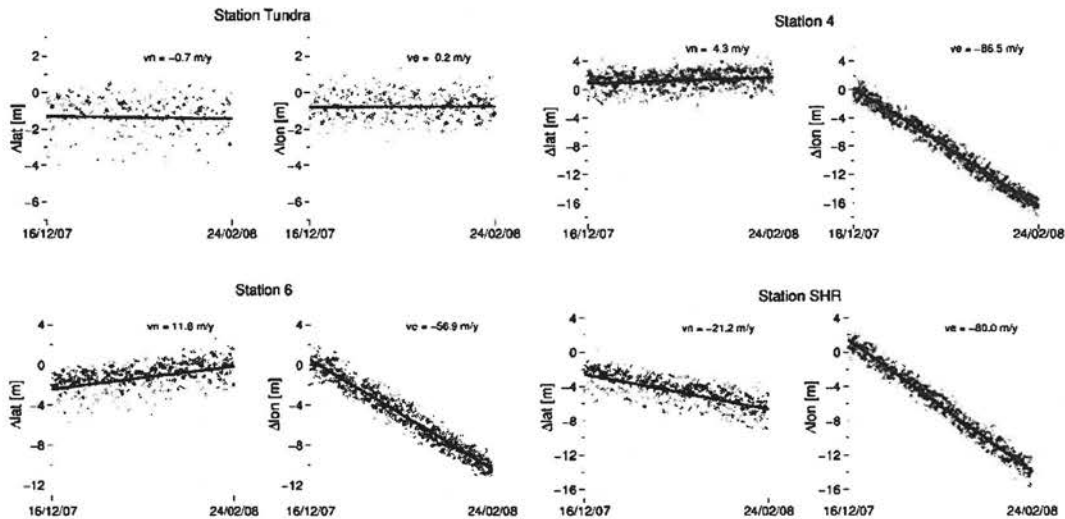


**Figure 71.** Examples of easting and northing mean velocity estimates from GPS hourly position measurements.

It is worth to notice in that the displacement over the considered period has a very linear trend for all stations, an assumption which is made in deriving the mean velocities from SAR data. A comparison of the SAR and GPS mean velocity measurements is given in table 13.

Station	ve_SAR (m/y)	ve_std_SAR (m/y)	vn_SAR (m/y)	vn_std_SAR (m/y)
Tundra	-3.04	1.6	-1.66	1.35
4	-27.62	5.08	5.47	2.59
5	-59.93	2.98	11.8	1.56
6	-58.35	3.49	4.34	2.2
SHR	-86.17	2.68	-20.74	1.46

Station	ve_GPS (m/y)	ve_std_GPS (m/y)	vn_GPS (m/y)	vn_std_GPS (m/y)
Tundra	0.23	1.04	-0.73	1.96
4	-86.5	1.23	4.32	2.15
5	-66.92	1.12	9.63	2.04
6	-56.86	1.24	11.83	2.39
SHR	-80	1.07	-21.18	1.9

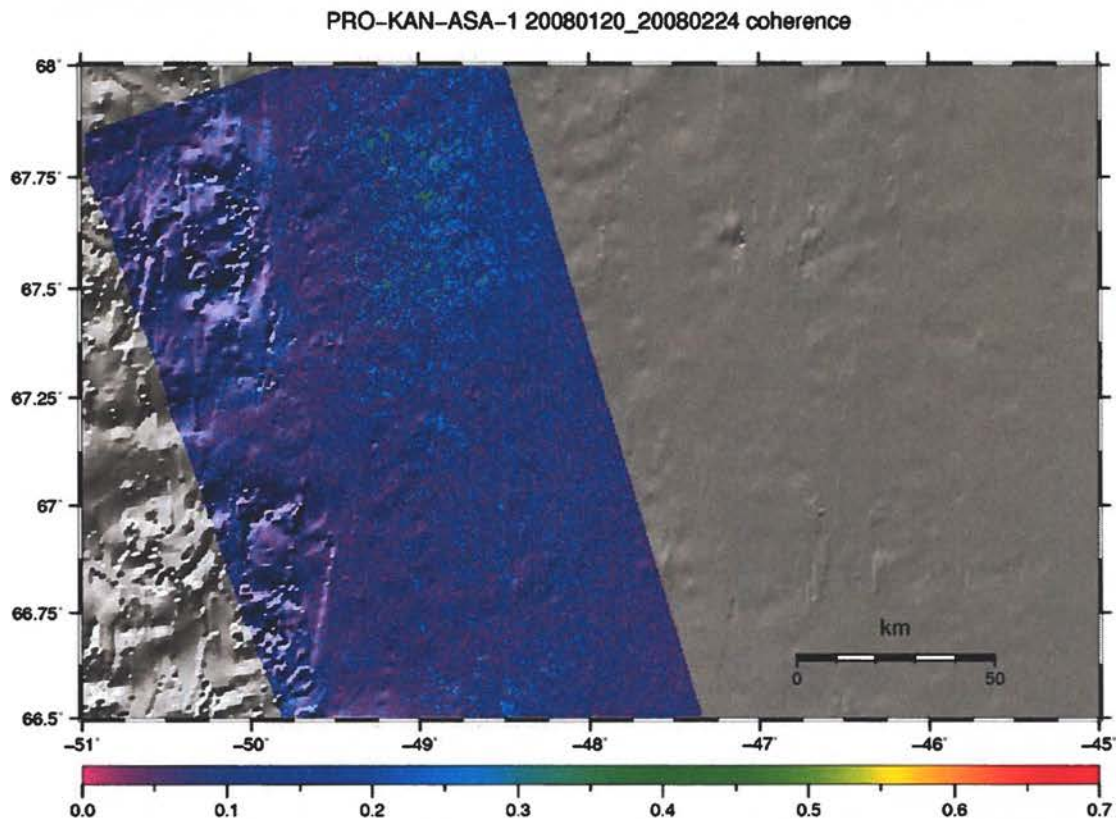
Station	Dve (SAR-GPS) (m/y)	Dve_std (m/y)	Dvn (SAR-GPS) (m/y)	Dvn_std (m/y)
Tundra	-3.27	1.91	-0.93	2.38
4	58.88	5.23	1.15	3.37
5	6.99	3.18	2.17	2.57
6	-1.49	3.7	-7.49	3.25
SHR	-6.17	2.89	0.44	2.4

**Table 13.** Comparison of SAR and GPS mean velocity measurements. *ve* and *vn* indicate easting and northing velocity components respectively, whereas *ve\_std* and *vn\_std* represent the measurement error standard deviations. The SAR and GPS measures are shown on the top and middle rows respectively, whereas their difference is shown in the lower row.

## Discussion

Concerning the comparison of GPS and SAR measurements, as seen from table 13, bottom row, these are in most cases explained by the predicted measurement error standard deviations and are in the order of a few m/y. Only for station 4, do the SAR measurements provide a major underestimate compared to GPS. This is probably due to the fact that station 4 is located in the vicinity of bedrock, as seen from figure 67. The correlation window sizes are such that bedrock and ice are present in the window, leading to an underestimate of the easting velocity in particular. This aspect could be improved by using a land-ice mask in the correlation process.

A second interesting issue is the coverage of the SAR measurements. It is seen that the measurements of figure 70 are noisier in the wet-snow area (the brighter area in 69), and often discarded because below the cross-correlation Signal-to-Noise threshold. This has been found to be unrelated to the coherence of the SAR image pairs used for offset tracking, as can be seen from Fig. The ASAR image pairs show an almost uniformly low level of coherence, whereas the PALSAR pair retains quite a high level of coherence, despite the longer repeat cycle (46 days, compared to 35 days for ASAR). In the ASAR case, this means that the cross-correlation peaks are due to features, rather than to correlated speckle, and that these features are predominant in the ablation area.



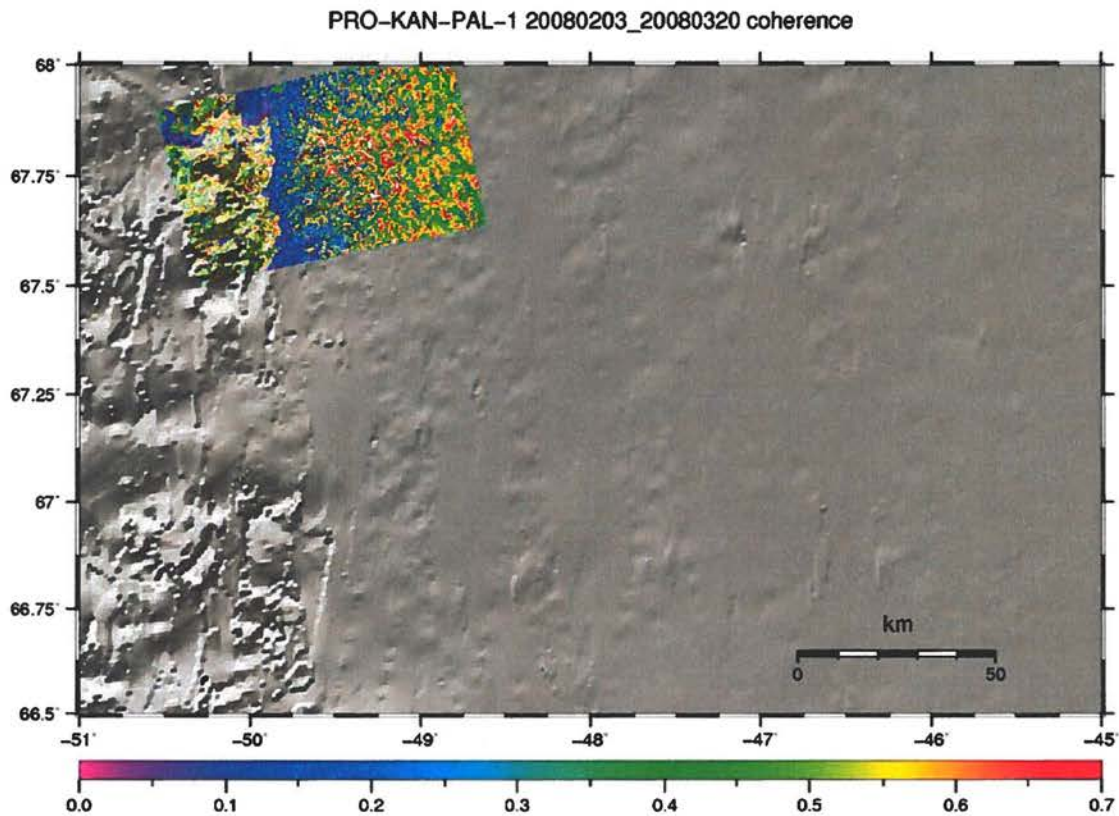


**Figure 72.** Coherence magnitude images for an ASAR pair (top) and the PALSAR pair (bottom).

## Operational measurements

### Overview

Operational mean-velocity measurements were carried out in the following areas, and time-spans:

1. Kangerlussuaq (West), Dec. 2007 – Mar. 2008 (see software validation section)
2. Nuuk area, Sep. 2009 – Feb. 2010
3. Helheim glacier area, Jan. 2009 – Mar. 2009
4. Helheim glacier area, Oct. 2009 – Jan. 2010

The SAR acquisition coverage is shown in Fig. 73.

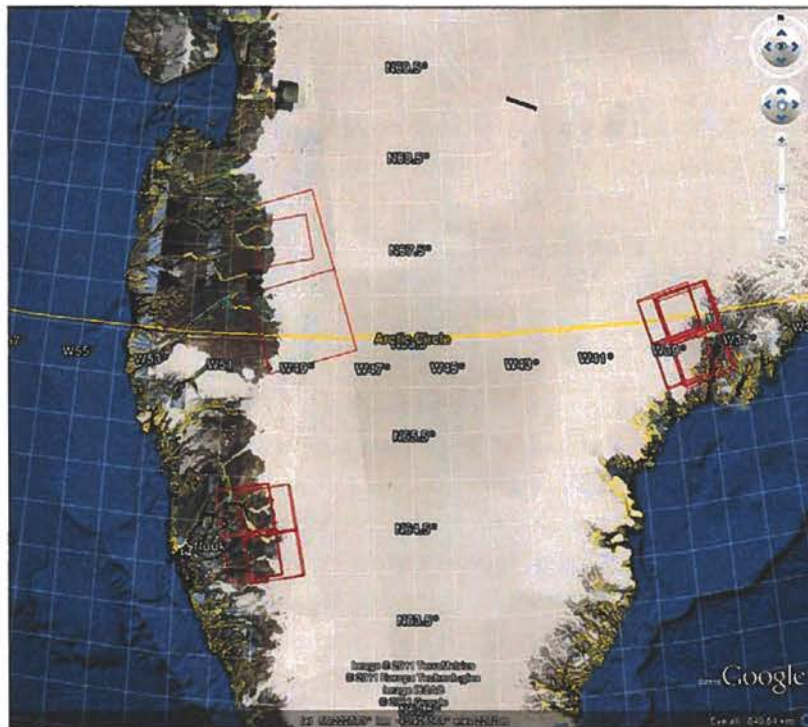


**Figure 73.** Operational measurement sites

Due to the long repeat-cycles of current SAR sensors, and to the availability on most of the sites of a single SAR image pair per season, offset-tracking was applied to derive the mean velocities.

A common processing strategy was followed. Intensity cross-correlations were carried out with windows about 1 km x 1 km in size, on a posting of approximately 200 m x 200 m. A 5 x 5 box-averaging was applied to the resulting offsets. Slant-range and azimuth displacements of each radar track were geocoded on a lat/lon grid corresponding to about 300 m x 300 m on ground and fused.

Two Digital Elevation Models were used to geocode the measurements, namely the NSIDC DEM (Marcio et al,2007), and the ASTER GDEM. These were found to be complementary with respect to accuracy, the NSIDC being more accurate on the inland-ice and the GDEM closer to the ice-sheet margin. The ASTER GDEM was used for the Nuuk area, whereas a fusion of the NSIDC and ASTER GDEM was attempted for the Helheim area.

### Nuuk area

Two ALOS/PALSAR tracks were processed, covering the Kangersuneq fjord and its surroundings. The acquisition dates and sensor modes are listed in table 14.

Acquisition date	Sensor	Mode	Track
20090928	PALSAR	FBD	72
20091130	PALSAR	FBS	73
20100115	PALSAR	FBS	73
20100213	PALSAR	FBS	72

**Table 14.** *Nuuk area SAR dataset*

The magnitude of the mean horizontal velocity and its associated error standard deviation are shown in figure 74. The areas of fastest movement correspond to three calving outlet glaciers, namely, from south to north, Kangiata nunata sermia, Akugdlerussup sermia and Narssap sermia. The predicted error standard deviations range from less than 10 m/y in areas of slow motion to about 50 m/y on the outlet glaciers. These accuracies are still useful, given the high velocities, which range from 700 m/y to 1600 m/y.

A small investigation was carried out to understand whether the cross-correlation peaks were due to coherence or to features in the intensity images. As for the validation dataset case, the uniformly low level of coherence observable in figure 75 suggests that correlation peaks are due to features.

Unlike the validation dataset though, there does not seem to be a strict correspondence between the ablation area and the coverage of the measurements. According to (Weidick, 1995), the snowline is expected to be between 600 and 800 m, whereas many measurements are successful also above this height, as seen from figure 76 and figure 74.

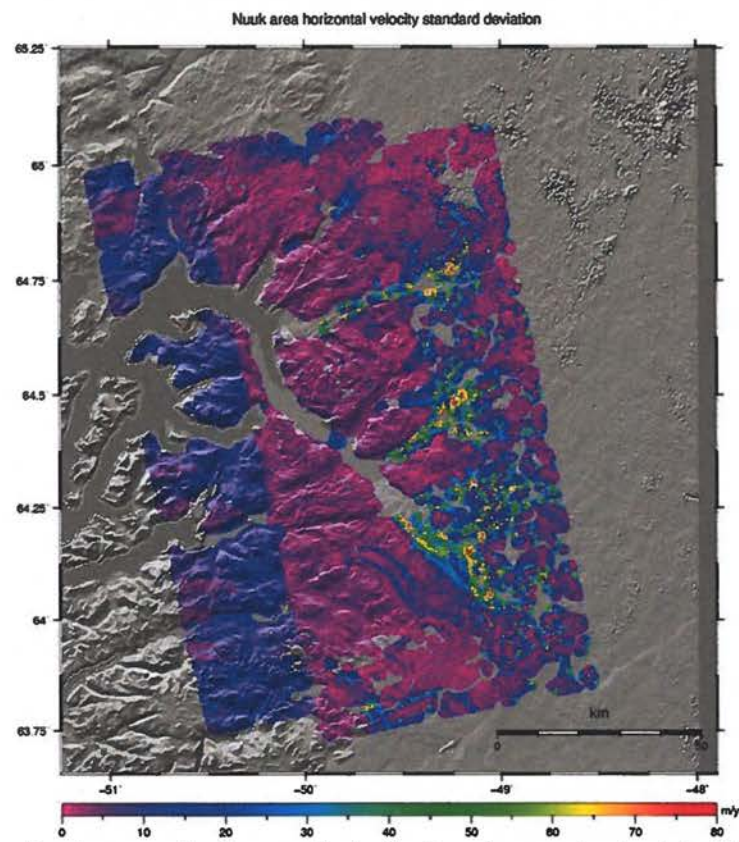
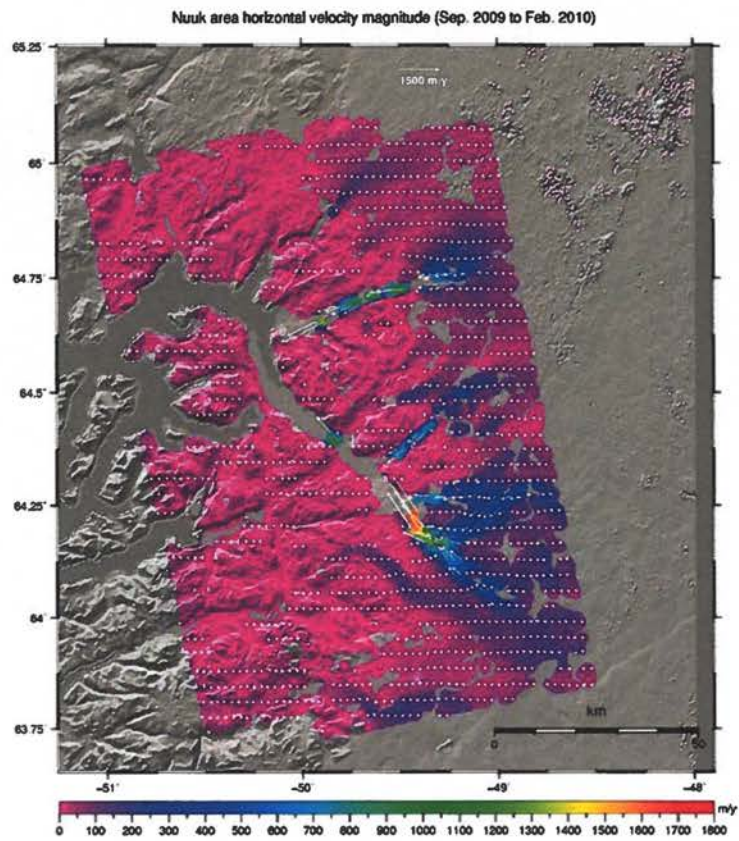
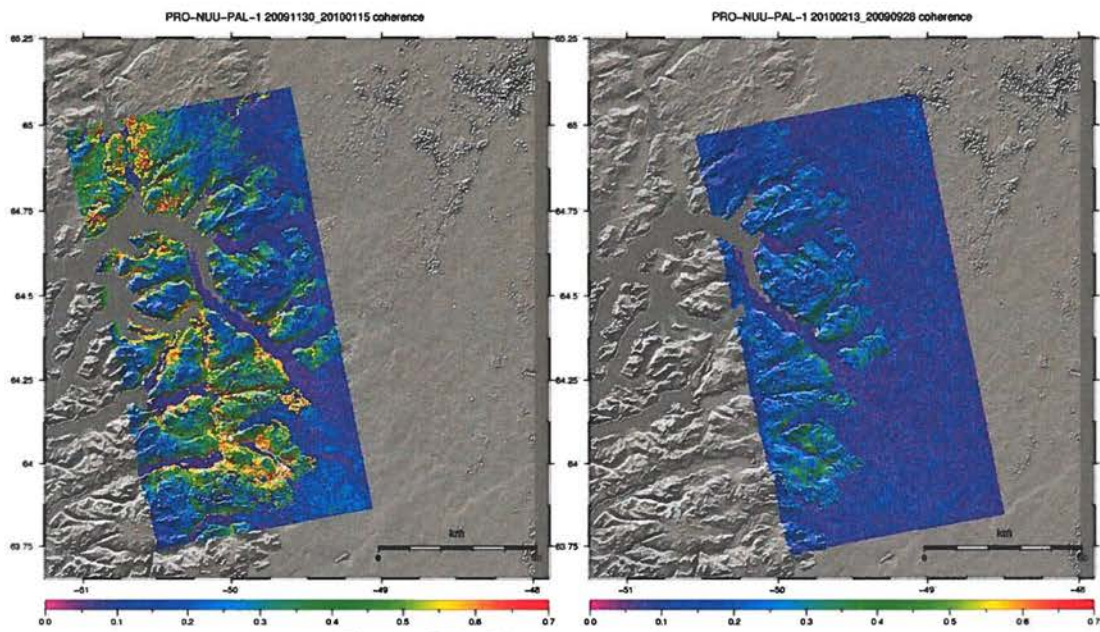
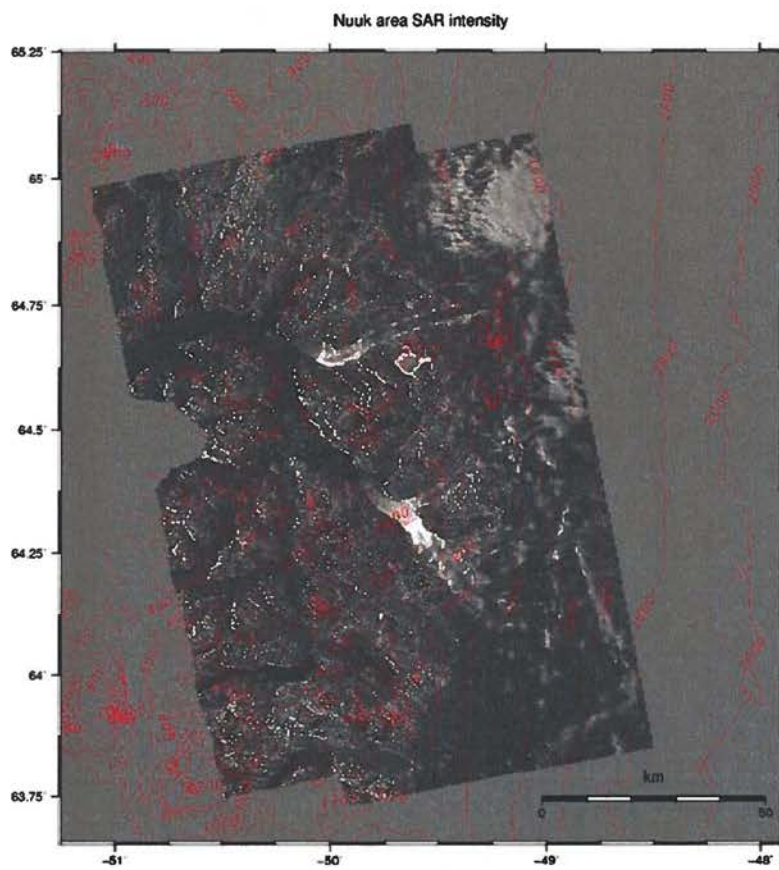


Figure 74. Nuuk area velocity magnitude (top) and error standard deviation (bottom)



**Figure 75.** Nuuk area coherence maps



**Figure 76.** Nuuk area SAR intensity mosaic and height contour

### Helheim Glacier area

Two ALOS/PALSAR tracks were processed, covering Helheimgletscher and its surroundings. The acquisition dates and sensor modes are listed in table 15

Acquisition date	Sensor	Mode	Track
20090118	PALSAR	FBS	49
20090305	PALSAR	FBS	49
20091021	PALSAR	FBD	49
20091206	PALSAR	FBS	49
20091223	PALSAR	FBS	50
20100121	PALSAR	FBS	49
20100207	PALSAR	FBS	50

**Table 15.** Helheim glacier area SAR dataset

A single pair and a single track were available for winter 2008/2009, whereas two tracks and three acquisitions were used for winter 2009/2010.

For winter 2008/2009, the magnitude of the mean horizontal velocity and its associated error standard deviation are shown in figure 77. The areas of fastest movement correspond to the basin of Helheimgletscher and to Fenrisgletscher in the east. As for the Nuuk area, the predicted error standard deviations range from less than 10 m/y in areas of slow motion to about 50 m/y in those of fastest motion.

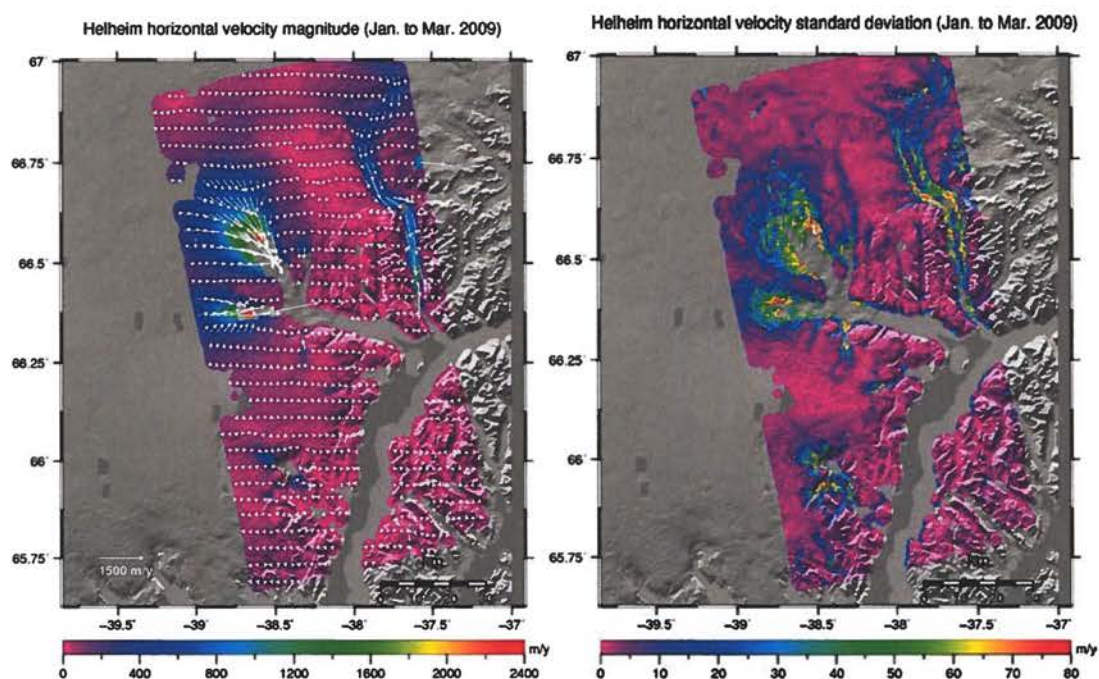


**Figure 77.** Helheim area, winter 2008/2009 horizontal velocity magnitude (left) and error standard deviation (right)

For winter 2009/2010, the magnitude of the mean horizontal velocity and its associated error standard deviation are shown in figure 78.

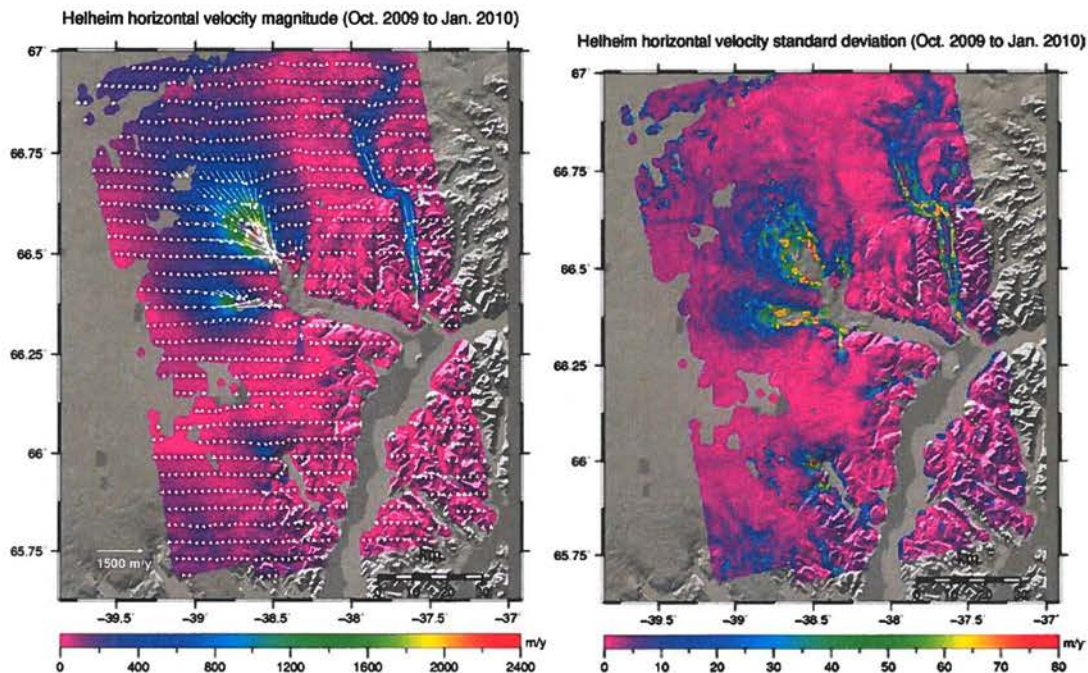


**Figure 78.** Helheim area, winter 2009/2010 horizontal velocity magnitude (left) and error standard deviation (right).

It is noted that velocity measurements could not be made on the tongue of the glacier, where velocities are expected to be in the order of several km/y. This is most likely due to a limitation of the core offset-tracking program, developed by GAMMA Remote Sensing and Consulting, which is not able to measure displacements greater than a fraction of the correlation window size. This fraction is in the order of 10% according to the developers (Wegmuller). The results obtained on Helheim suggest this percentage might be greater, in the order of 25-30%. For correlation window sizes of 1 km and repeat-cycles of 46 days, this poses an upper limit of about 2.5 km/y on the maximum velocity which can be measured by feature tracking.

## Data acquisition strategy

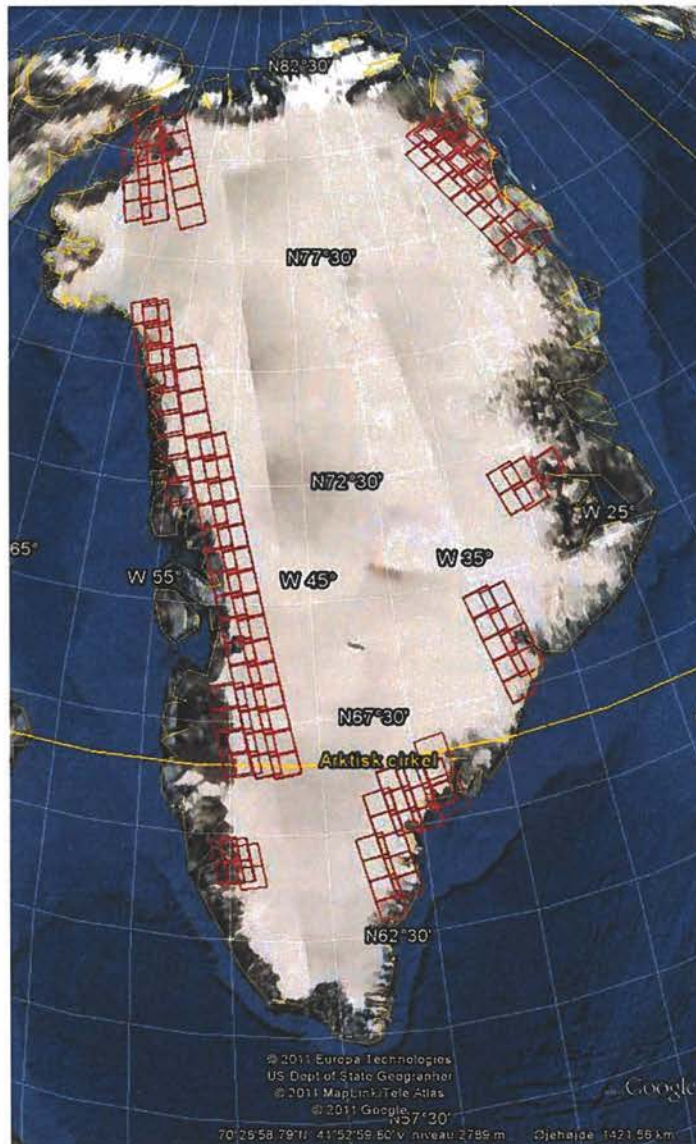
The current SAR-sensors for used for operational velocity mapping in the PROMICE programme are ENVISAT/ASAR and ALOS/PALSAR from which data is available through ESA. Due to the large temporal baseline they are suited only for off-set tracking limiting the resolution to about 1 km. This is however adequate for the purpose of estimating dynamic mass loss.

Figure 79 shows the frames acquired so far for the PROMICE project covering the time period spring 2010. It is under the way of being processed at GEUS during 2011. More frames will be acquired as processing progresses to fill in the gaps such that a velocity map covering Greenland with recent data can be made.

Collaboration with the Environment Canada has been made concerning RadarSat-2 data. RadatSat-2 acquisitions are not directly available to GEUS. However RadarSat-2 scenes

have been ordered by Environment Canada for selected areas over Greenland with the purpose of comparing velocity maps derived from RadarSat-2 and ESA-satellite measurements.

A user consultation has been attended and contact has been made with ESA regarding requirements for Sentinel-1 satellite planned to launch in early 2013. With the Sentinel data it is anticipated there will be complete coverage of the Greenland at an acquisition rate adequate to resolve the seasonal variations in ice surface velocity.



**Figure 79.** SAR data frames acquired for velocity mapping.

## Outlet glacier monitoring

The purpose of PROMICE is to monitor the mass loss from the Greenland Ice Sheet by providing information on, respectively, the surface melt and the ice lost through the great outlet glaciers as icebergs or by submarine melting of the glacier tongue. There is still uncertainty regarding the relative contribution of the two components of the mass loss, but the outlet glaciers have been estimated to contribute between half and two-thirds of the mass loss (Rignot ref, van de Broeke / box ref). The uncertainty is partly due to the lack of a consistent, continuous data series over several years, as the outlet glaciers are prone to large-scale inter-annual variability in ice output due to external forcing mechanisms like warmer ocean currents or changes in atmospheric circulation patterns. Therefore, one cannot assume that the velocity of outlet glaciers in a region at a certain time is representative, no matter the size of the region in question. Glaciers over the whole region may accelerate or decelerate from year to year. Apart from the interannual variability, the outlet glaciers (and indeed the ice margin as a whole) also exhibit a seasonal variability in velocity which is neither well understood nor well documented.

Thus, if one wants to quantify the mass loss from the outlet glaciers of the Greenland Ice Sheet it is necessary to tie the spatial information available from satellite-derived velocity maps to the temporal information which can be retrieved from direct on-site monitoring of individual outlet glaciers. In PROMICE, a new satellite radar data processing chain, SUSIE, has been developed, enabling us to produce velocity maps from both interferometric (for slow-moving ice) and feature-tracking (for fast-moving ice) methods. Combining the velocity maps with the airborne measurements of ice thickness and elevation along the ice margin provides a snapshot in time of the mass loss.

Even with the velocity maps, we will not exactly capture the integrated mass loss over the year, and even less the variation over a number of years. It is well known that the seasonal variation in glacier velocity is not the same from year to year, but depends on factors like the fjord ice cover and the temperature of the ocean water in the fjord that year. To quantify and solve this problem, it is necessary to continuously monitor the velocity of a number of larger outlet glaciers directly.

### Methods for monitoring glacier velocity

Monitoring glacier velocity can be done either by placing GPS-instruments directly on the surface of the glaciers or it can be done by geodetic analysis of time-lapse glacier imagery from a stationary camera. The challenge in the GPS-method is the extremely dynamic nature of the relevant glaciers, meaning that deployment and retrieval of the instruments is far from trivial. The dynamics of the glacier surface also implies that instruments are more prone to failure or risk getting lost in crevasses. It is therefore essential that the GPS-instruments can transmit their position regularly and are not too expensive as they might get lost. For the time-lapse camera method, the challenge lies in the image analysis. It is relatively easy to have a camera take nice pictures, but deriving glacier velocities from these requires advanced digital photogrammetry.

The optimal solution is a combination of the two methods, where the image analysis delivers data from the entire glacier front, with calibration provided by the GPS placed on the glacier surface within the picture frame. In PROMICE we have identified such an opportunity. A research group at Byrd Polar Research Center, Ohio State University has developed and proven a photogrammetric time-lapse camera system over the last few years which has been deployed under the label Extreme Ice Survey (EIS). We have established collaboration between EIS and PROMICE, in which instruments, data, logistical opportunities and image processing are exchanged for mutual benefit. In parallel we have established collaboration with Assoc. Prof. Alberto Behar, NASA/JPL & Arizona State University, who has developed a relatively cheap, extremely robust and power-efficient GPS unit, capable of transmitting its position according to user requirements.

## The EIS system in Greenland

Within EIS, automatic ground-based time-lapse camera stations were installed at major west Greenland marine terminating glaciers and have acquired scenes at daily intervals beginning in year 2007. The collaboration with PROMICE has expanded the coverage to five additional glaciers in East, Southeast, South, Southwest and Northwest Greenland, respectively. We have developed image matching procedures that are significantly advanced from conventional matching approaches (Ahn and Box, submitted). Terrestrial photogrammetry has the advantage of higher spatial and temporal resolution than available from conventional remote sensing techniques. Projection using a terrain model data allows the conversion of pixel displacements to m per hour velocity units. Image processing techniques include: image enhancement; projective transformation for compensating camera instability; registration with multiple base images; and multiple image/chip matching to derive velocities on the glacier at a distance of ~2 km with sub-pixel precision (0.65 pixels).

We are able to retrieve daily velocities at a distance up to 4 kilometres from the camera station with the 10.2 Mpixel camera system. Daily velocity variations are produced, now opening the possibility to relate glacier speed changes to ice dynamical factors and climate.

Camera	Nikon D200
Lens	Nikon 20, 24, 28 mm
Image format	3872 x 2592 pixels, 10.2 Megapixel
Timer	National Geographic Remote Imaging Laboratory
Enclosure	Pelican case with optically natural plastic window custom installed
Power	50Ah gel cel battery, 10 solar panel
Support	Steel cable, rock bolt

**Table 16.** *Time-lapse station hardware specification*

### Image registration

Images from each time lapse camera require stabilization, called registration, before ice displacements and ultimately ice velocity may be calculated. Dr. Yushin Ahn, a specialist in digital photogrammetry, has developed software to achieve image registration automatically for 80% of the imagery we have. The software identifies cases that cannot be registered automatically. Among these, some fraction, roughly half can be registered after manual point selection, performed by students at Ohio State University. Image registration procedure and ice displacement calculation details are provided in Ahn and Box (2010).

### Initial results from EIS

Prior to the PROMICE involvement, the EIS team has so far derived daily ice velocity time series from three sites: Store Glacier, Rink Glacier, and Umiamako Glacier. Daily velocities are illustrated in figure 81 below from the Rink A site. The largest velocity variations are associated with large iceberg calving events. Other speed changes are found to correlate with a) surface air temperature, a proxy of surface melt intensity, and b) supra-glacial melt lake drainage events. Error bars are derived from multiple image / multiple chip matching procedures of Ahn and Box (2010).

Glacier	Lat [N]	Lon [W]	Lens [mm]	Camera Elev. [m]
Jakobshavn	69°10'	49°50'	28, 28	132
Store A	70°23'	50°33'	24	327
Rink A	71°45'	51°36'	20	518
Umiamiko	71°44'	52°24'	20, 20	721
Torsukatat Avannarleq	~70°04'	~50°24'	20	~300
Sermilik Brae	60°59'	46°55'	28	310
Petermann Glacier A	81°09'	61°22'	20, 20	902
Petermann Glacier B	81°03'	62°06'	28	710
Sermeq Avannarleq	69°20'	50°18'	24	~500
Daugaard-Jensen Glacier	71°52'	28°36'	28	1178
Helheim Glacier	66°19'	38°14'	35	718
Qajuutap Sermia	-	-	-	-
Kangiata Nunata Sermia A	-	-	-	-
Upernavik Isstroem	-	-	-	-

**Table 17.** Time-lapse camera station information



**Figure 80.** Extreme Ice Survey (EIS) kamera system sat op ved Umiamiko Bræ i det nordlige Vestgrønland

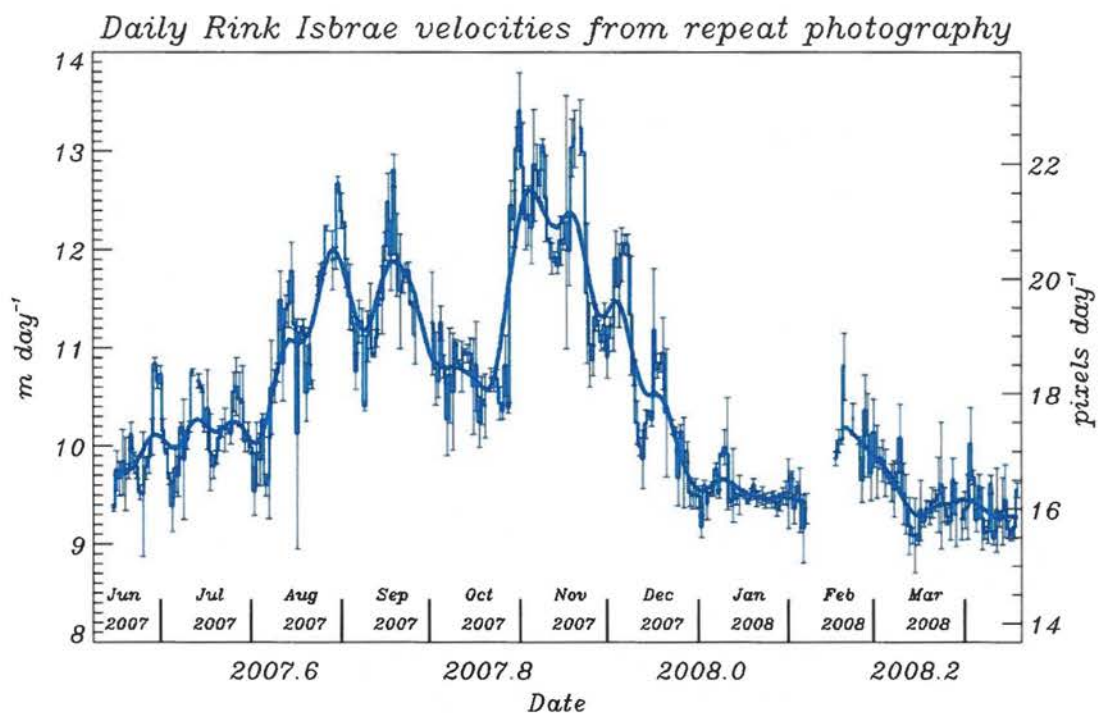


**Figure 81.** Daily velocities at the Rink A site

#### Existing and new EIS sites

In summer 2010, two new EIS systems were installed at Helheim Glacier, Southeast Greenland and Daugaard-Jensen Glacier, East Greenland. Data from these will be re-

trieved in summer 2011, assuming a successful field season. Additional EIS systems are planned for deployment in 2011 at Qajuutap Sermia (South Greenland), Kangiata Nunata Sermia (Southwest Greenland) and Upernavik Isstroem (Northwest Greenland). All these sites are chosen to be in the vicinity of existing PROMICE transects with automatic weather stations, not only to facilitate logistical requirements and cost-efficiency, but also because of the scientific value of combining the outlet glacier monitoring with the surface melt monitoring to establish potential causal relationships.

### **Development of transmitting GPS units**

PROMICE has teamed up with a NASA instrument specialist to solve the problem of on-site glacier velocity monitoring. The developer, Dr. Behar, has 18 years of experience from the Mobility and Robotics Section of the Jet Propulsion Laboratory at NASA and has specialized in developing instrumentation for extreme and remote locations, such as Mars, Antarctica or Greenland. The PROMICE team required the new type of GPS units to be developed specifically to suit the following set of requirements:

1. Long non-maintenance instrument life after deployment (> 2 years)
2. Rugged and robust construction for survival in an extreme environment
3. Capability of measuring the position with an accuracy of a few metres
4. Transmission of data on a daily basis, preferably configurable while deployed
5. Low cost due to risk of loss and the need for many units

All these needs were met by the system now in operation. The GPS units are ruggedized and fixed entirely inside small watertight pelican boxes and mounted on a tripod. The GPS units are simple L1 single-frequency systems, with limited absolute accuracy but with low power consumption and minimal on-site processing needs. Emphasis has been put on selecting the optimal power supply, which consists of a pack of 30 coupled non-toxic D-size battery units. The GPS units transmit position to an internet site twice a day, but are remotely configurable (two-way communication) in case a different measurement frequency becomes attractive (e.g. if the glacier accelerates). The internet display software interfaces with Google Earth and the data retrieved is displayed as latitude/longitude/elevation to ease analysis and readability.

### **Deployment of transmitting GPS units**

The establishment of a network of transmitting GPS units was initiated in summer 2010, with successful deployments on Daugaard-Jensen Glacier (3 units), Helheim Glacier, Qajuutap Sermia and Kangiata Nunata Sermia. In collaboration with the EU-project ice2sea, 5-6 more transmitting GPS units are scheduled for deployment in the summer of 2011, with Upernavik Isstrøm as one of the target glaciers. As Upernavik Isstrøm has by now retreated and consequently split into four individual marine-terminating outlet glaciers, two GPS units might get deployed to better capture the overall ice flux and get an idea of the variation in velocity between the different branches.

# Outreach

## Media strategy

PROMICE is intended as a high-profile activity of national and international importance, showcasing the Danish contribution to monitoring the impact of climate change in the Arctic. To live up to this obligation, public visibility is required on a range of levels. With the strong public interest in the fate of the Greenland Ice Sheet, the PROMICE team has worked towards delivering expert knowledge on the subject directly or via the media. Emphasis has been on striking a sober tone in the otherwise highly polarized climate change debate, often pitched by the inherently conflict-oriented reporting methods of news media in particular. The PROMICE team is often used by Danish and international news media for comments on glaciological aspects of climate change and has actively engaged with science reporters, to the level of taking them on rough fieldwork on the Greenland Ice Sheet. We were very active in supporting the Ministry of Climate and Energy up to and during the COP15-meeting, for example participating as science communicators at a political meeting in Ilulissat prior to COP15. We have likewise assisted the Minister for Climate and Energy directly to answer challenging glaciological questions posed in political fora. The PROMICE team thus serves as a filter for making sense of the international science news stream towards the public and the political system. Appendix A provides documentation on 65 PROMICE appearances in the public arena during the initiation phase 2007-2010.

Another important aspect of PROMICE is the education of future scientists and the general understanding of science in the public, with emphasis on our field of knowledge, glaciology. We have dealt with this obligation as a high priority, actively securing external funding to produce three complete e-learning sites. These have been designed in collaboration with private consulting firms specializing in science communication, to reach a professional level beyond the capabilities of individual scientists. The e-learning sites are described in further detail below.

As PROMICE begins to increasingly produce results of interest to the public, we have designed a pro-active media strategy. News will be disseminated through a PROMICE Newsletter, designed and published by GEUS electronically. To increase the impact in the media, we have established collaboration with the News Section of Experimentarium, an institution devoted to the communication of science to the public. Once we have a draft for a newsletter, we circulate it with our partners at Experimentarium that will attempt to market the contents first to their national newspaper partners, then through their contact to a national news bureau, Ritzau, that delivers stories to all Danish media. Using Experimentarium means that the recipient media can rely on a trusted partner for their story, rather than having to judge the validity and interest of the PROMICE Newsletter specifically. Science projects and institutions release press briefings all the time, competing for space in the media. In this competition, Experimentarium is a perfect partner for us as they serve as a filter and clearinghouse for the media when it comes to science-stories.

## **Webpage & online social media**

In 2010 the PROMICE website ([www.promice.dk](http://www.promice.dk) or [www.promice.org](http://www.promice.org)) was upgraded from a site with the bare necessities such as a short description of our activities, contact information, and the possibility to download AWS data (via the database website) to a full site with:

- an updated introduction
- a one-page description of all different research activities within PROMICE (more to be added in 2011)
- a clear link to an improved database website for data viewing and download
- descriptions of all related projects
- detailed contact information with CVs of all those in / related to PROMICE
- a gallery with photos of PROMICE fieldwork activities
- videos and animations related to the programme
- a list of publications
- a page with links to the PROMICE outreach/e-learning sites
- the PROMICE Newsletters

The PROMICE website will undergo continuous changes to keep up with the current state of affairs. For instance, a recent addition was a link to the new PROMICE Facebook group named 'The Greenland Ice Sheet'. The group was initiated to spread PROMICE news faster, and bring Greenland Ice Sheet researchers in closer connection. The possibilities are endless, since researchers can efficiently announce workshops or conferences, post news, share results, or start a discussion, while anyone can get in touch with the glaciological community with questions.

## **E-learning initiatives**

### **The PROMICE outreach platform**

To present PROMICE to an international as well as national audience prior to the COP15 meeting in Copenhagen, we established an e-learning platform in collaboration with Context Consulting, a firm specialized in web-based science communication. It is an interactive multimedia platform with English speak, driven by the curiosity of the visitor. It is designed to allow a high degree of free navigation allowing the individual visitor to decide on the depth and broadness of the e-learning experience. It is designed with an interested non-specialist in mind as recipient and is unencumbered by the need to read long texts – although the speak is texted, it is never more than a few lines per slide or movie. The PROMICE outreach platform is quite extensive, with literally hundreds of slides, movies and animations, providing a varied, captivating e-learning experience on the relationship between ice sheets and climate as well as knowledge about PROMICE specifically.

The platform thus delivers expert knowledge in an easy-to-follow way and through an information hierarchy that makes it possible to get something out anything from a brief visit

lasting little more than 10 seconds, to an extensive learning experience lasting hours, all at the discretion of the visitor.

### **Isskolen I – e-learning for grades 7-9**

With the aim of educating Danish school children about the Greenland Ice Sheet and Climate Change and attracting their interest for the natural sciences a website [www.isskolen.dk](http://www.isskolen.dk) containing educational material Isskolen (The Ice School) focusing on the PROMICE programme has been developed. The target audiences are teachers and school children, grade 7-10 (age 13-16).

The students are following in the footsteps of a scientist setting up weather stations at the margin of the Greenland ice sheet. From this the students are taught about mass balance of the Greenland ice sheet and sea level rise. The spectacular setting in the nature of Greenland makes it visually appealing and exciting.

The website contains a complete 'education package' including films, animations, e-learning, exercises (in some cases using data from the PROMICE weather stations) and assignments. In addition the website also contains instructions for teachers and suggestions for building lectures based on the material.

The material was developed in 2009-2010 collaboration between GEUS researchers, school teachers from Krebs Skole and Context Consulting with funding from the Danish Ministry of Education - Rådighedspuljen.

The website was launched in May 2010 and has been very well received.

### **Isskolen II – e-learning for grades 4-6**

Following the success of the first 'Isskole' it was decided to try and expand the concept to younger school children, grade 4-6 (10-12 years), by making a website with educational material targeted at this level.

Funding for this was received in September 2010 also from the Danish Ministry of Education - Rådighedspuljen and work on the isskole for younger children is currently proceeding.

This second isskole will be based on the same general concept however simplified and with new exercises. It is expected to be launched in August 2011.

## Research education

A monitoring programme as PROMICE carries an obligation to disseminate results and knowledge to the public it serves, as documented in the former section. In a scientific field as narrow as glaciology, this obligation carries on into university level education. The existence of PROMICE supports a base for PhD and MSc-level education in glaciology that would not otherwise exist in Denmark, apart from within ice-core paleoclimatology. This ensures a strengthened future research environment in an issue believed to be crucial for the impact assessment of climate change on Danish society. PROMICE does not support PhD and MSc-studies directly, but the data collected as well as the logistical platform and research group makes them feasible in the first place. The quality and timeliness of this educational effort is underlined by the fact that the two first PhD-candidates to graduate have both been employed as research scientists at GEUS in the glaciology group in open competition.

### **Abstract from PhD thesis: Robert S. Fausto**

Improving surface boundary conditions for large-scale ice sheet models of Greenland is the main focus of this thesis. Near-surface air temperature (2m) over the Greenland Ice Sheet (GrIS) is parameterized using data from automatic weather stations (AWS) located on land and on the ice sheet. The parameterization is expressed in terms of mean annual temperature and mean July temperature both depending linearly on altitude, latitude and longitude. The temperature parameterization is compared to a previous study and it is shown to have a better agreement with observations. The temperature parameterization is tested in a positive degree day (PDD) model to simulate the present (1996-2006) mean melt area extent of the GrIS. The model accounts for firn warming, rainfall, and refreezing of melt water, with different PDD-factors for ice and snow under warm and cold climate conditions. The simulated melt area extent is found to have a reasonable agreement with satellite-derived observations. Snow pack changes during the melt season are often not incorporated in modelling studies of the surface mass balance (SMB) of the GrIS. Densification of snow accelerates when meltwater is present due to percolation and subsequent refreezing and needs to be incorporated in ice sheet models for ablation calculations. In this thesis, simple parameterizations used to calculate surface melt, snow densification and meltwater retention are included as surface boundary conditions in a large-scale ice sheet model of Greenland. Coupling the snow densification and meltwater retention processes achieves a separation of volume and mass changes of the surface layer in order to determine the surface melt contribution to runoff. Experiments for present-day conditions show that snow depth at the onset of melting, mean annual near-surface air temperature and the mean density of the annual snow layer are key factors controlling the quantity and spatial distribution of meltwater runoff above the equilibrium line on the GrIS.

# Surface melt, dynamics and seismicity at Helheim Glacier, East Greenland

## Abstract from PhD-thesis of Morten Langer Andersen

Understanding the processes that govern the flow of the large outlet glaciers draining the Greenland Ice Sheet is critical for assessing the impact of climate change on sea-level rise. These processes include calving of icebergs and subsurface melt in the fjords, but drainage of surface runoff to the glacier bed also plays a role. How melt water affects the flow of fast outlet glaciers is poorly understood and is the main aim of the three interdisciplinary studies comprising this thesis. First, the extent of melt-water-induced flow speed variability is investigated. An energy balance model is developed for the surface of Helheim Glacier, East Greenland, in order to estimate runoff from surface melt. Melt variations during the summer seasons are compared to GPS observations of surface velocity. Significant correlations are found, with a 12–36 hours delay of velocity relative to melt. Next, the glacier's sensitivity to variations in melt-water input is quantified and found to decrease approximately exponentially with distance from the calving front. Sensitivity to melt generally increases over the melt season. The time-varying sensitivity is interpreted to result from changes in subglacial hydraulic routing caused by the changing volume of melt-water input. Finally, seismic signals associated with calving and ice rupture are considered. Large seismic events are found at Helheim Glacier to be preceded by long-duration rumblings with a characteristic frequency content. A detection algorithm is developed to automatically detect rumblings recorded at a seismic station located close to the glacier. The analysis shows a seasonal variation in the occurrence of rumblings with a peak in mid-September coinciding with the end of the melt season. Further research into understanding the flow dynamics of the fast outlet glaciers of Greenland is crucial in order to accurately predict the increasing contribution of iceberg-calving to sea-level rise.

## Modelling Hydrology of the Greenland Ice Sheet

### PhD-study: Alison Banwell

Ms. Alison Banwell is a UK Natural Environment Research Council funded student, supervised by Dr. Ian Willis and Dr. Neil Arnold with Dr. Andreas Ahlstrøm acting in an important advisory role. The research builds on the expertise, interests and experience of the three senior researchers who have collaborated in an informal way on this project since 2007. This previous collaboration led to a Masters dissertation (Sylvan Long, 2008) and several presentations including at AGU (2008) and EGU (2010). At a more practical level, the research benefits from combining a modelling approach (using a series of numerical models, originally developed at Scott Polar Research Institute, Cambridge University), with empirical data sets (surface elevation, ice thickness and bed elevation) provided by GEUS. The collaboration has also facilitated access to other important data sets (weather and proglacial lake discharge) collected by the Greenlandic Government organisation, ASIAQ Greenland Survey.

The model that is being developed has three components. First, a mass balance model, which uses energy terms to calculate surface melting and which includes effects of conduction and refreezing, calculates patterns of accumulation and melting (Arnold et al., 2007; Rye et al., 2010). Second, a surface hydrology model routes the meltwater vertically through a snowpack and laterally across the snow-covered or snow-free ice surface (Arnold et al., 1998). Key developments of this model component will be its ability to fill surface lakes before they overtop or drain, as well as its ability to therefore calculate hydrographs to lakes or moulins. Third, a subglacial routing model will route the water from lake drainage events or more gradual moulin inputs through a subglacial drainage network of channels, eventually to the ice sheet margin (Arnold et al., 1998). The subglacial component is based on the EXTRAN routines of the US Environmental Protection Agency Storm Water Management Model (SWMM) (Roesner et al., 1988) which has been adapted to account for growth and shrinkage of ice walled conduits (Spring and Hutter, 1981). We are currently developing the model for the Paakitsoq region of the GrIS, where AWS data (GC-Net) are available to drive the model. The mass balance model is being parameterised/tested against data on surface lowering collected at the AWSs and on snowline position derived from satellite imagery. The surface routing model will be parameterised/tested against data on surface lake area and volume derived from satellite imagery and from a few in-situ lake measurements (Box & Ski, 2007; Marco Tedesco, unpublished data). The subglacial routing model will be tested against proglacial discharge data (ASIAQ Greenland Survey).

## **Mass balance on A.P. Olsen Ice Cap**

### **MSc-study: Signe Hillerup Larsen**

A mass balance study of the southeast outlet glacier at AP Olsen Ice Cap in Northeast Greenland using a temperature index model will be conducted. The project will be a part of the Glaciobasis programme which has been running since 2008. Three weather stations at different elevations and 15 stakes along the main flow line, alongside GPR measurements of the snow depth, provide a detailed dataset. Furthermore, weather stations from other projects along the valley have been recording temperatures for up to 15 years and the overall goal of the project will be to produce a 15 year long mass balance record of the outlet glacier. To set up the temperature index model it will be necessary to have a detailed picture of the lapse rate along the valley and glacier including temporal variations. Finally, an energy balance model will be applied using data from the weather stations on the glacier and the two model results will be compared to evaluate the applicability of the simple temperature index model.

### **Sermilik Field Course**

An introduction to our automatic weather station setup was given to a group of Master student from the Institute of Geology and Geography, Copenhagen University on the 9th of August, 2010, on the Mittivakkat glacier in Southeast Greenland.

# Scientific publications & presentations

## Scientific activities

PROMICE has during its initiation phase resulted directly or indirectly in 19 publications in scientific journals subject to international peer-review with PROMICE team members as authors or co-authors. Additionally, PROMICE team members have presented or co-presented their work at scientific conferences 51 times, many of these with published abstracts. Finally, the PROMICE team has published 9 reports with material relating to PROMICE activities. All the scientific activities mentioned are listed for reference in Appendix B.

The peer-reviewed publications can loosely be grouped into the following subjects:

- *Overview papers* (Ahlstrøm et al., 2008; Citterio, 2007; Smelror et al., 2008)
- *Ice-sheet surface mass-balance* (van As et al., 2009; van As, 2010; Mernild et al., 2010; Fausto et al., 2007; Fausto et al., 2009a; Fausto et al., 2009b, Mottram et al., 2009)
- *Outlet glaciers* (Andersen et al., 2010; Nick et al., 2009, Nick et al., 2010; Dawes & van As, 2009; de Juan et al., 2010; Nettles et al, 2008; Weidick & Bennike, 2007)
- *Change of local glaciers and ice caps* (Ahlstrøm et al., 2007; Citterio et al., 2009)

The range of subjects only reflects PROMICE activities to some extent. During the initiation phase of PROMICE, we have developed entirely new tools, e.g. for ice-sheet velocity mapping and outlet glacier velocity monitoring, that are only just now becoming operational. As with any monitoring programme, the data becomes more interesting for publication once the time series become longer and more significant in terms of evaluating trends. Obviously this is also a limiting factor for the publication activity in the upstart of PROMICE. Yet, the high level of activity, including co-authoring, shows that the PROMICE team has successfully engaged in partnering science projects, in effect broadening the impact of the monitoring programme.

## Contribution to SWIPA

The contribution to the report 'Snow, Water, Ice and Permafrost in the Arctic' (SWIPA, 2011) from the PROMICE team has been on two levels. In the initiation phase of the separate report for the Greenland Ice Sheet, scheduled for the COP15 meeting in Copenhagen in 2009, we assisted in the selection of appropriate authors in the science community to ensure the highest scientific level. The direct contribution to the report was to the report on the impact of climate change on hydropower feasibility in Greenland.

## Collaborative activities

### Greenland Ecological Monitoring (GEM)

The existence of PROMICE facilitated the addition of a glaciological sub-programme to the monitoring activities at Zackenberg in Northeast Greenland, namely GlacioBasis. This programme is a sibling to PROMICE and shares concepts and technology, and indeed team members. The more recent addition of a monitoring facility near Nuuk in Southwest Greenland, benefits from PROMICE through the automatic mass-balance station transect on the ice margin nearby, which helps to determine the ice sheet meltwater contribution to the freshwater budget of Godthaabsfjorden.

“As an integrated activity at Zackenberg the long-term monitoring programme, Zackenberg Basic, was initiated in 1995 and fully implemented for the terrestrial part of the ecosystem in 1996.

In 2003, the programme was supplemented with a sub-programme, MarineBasis, taking care of the marine environment. In 2008, it was supplemented with another sub-programme focusing on glaciers (GlacioBasis). The objective of the programme is to provide long time series of data on the natural innate oscillations and plasticity of a high Arctic ecosystem. This is accomplished through monitoring of selected biotic parameters and elements (BioBasis and MarineBasis) as well as climatic (ClimateBasis and GlacioBasis) and other abiotic (GeoBasis and MarineBasis) parameters and elements throughout the year on a long-term basis.” (source: <http://www.zackenberg.dk/monitoring/>)

“GlacioBasis carries out quantitative glaciological field observations from the A. P. Olsen Ice Cap (74.6° N, 21.5° W) and from the outlet glacier discharging into the Zackenberg River drainage basin. Since March 2008, two Automatic Weather Stations (AWS) have been providing data for surface energy balance and ablation modelling from different elevations in the ablation zone. The main AWS transmits real-time data to Copenhagen year-round, and the second AWS provides data to obtain gradients of physical parameters.

GlacioBasis also maintains a network of ablation stakes, and in co-operation with GeoBasic carries out Ground Penetrating Radar (GPR) surveys of snow depth, calibrating accumulation with density profiles from snow pits”

(source: <http://www.zackenberg.dk/monitoring/glaciobasis/>)

### Ice2sea

The ice2sea programme has obtained €10M in funding from the EU Framework 7 (FP7) for four years of research. The 24 institutional partners in ice2sea work together to quantify the contribution of continental ice to sea-level rise over the next 200 years.

This is accomplished through an integrated programme that includes:

- targeted studies of key processes in mountain glacier systems and ice caps (e.g. Svalbard, Patagonia), and in ice sheets in both polar regions (Greenland and Antarctica)
- improved satellite determinations of changes in continental ice mass
- development and implementation of ice-sheet/glacier models to generate detailed projections of the contribution of continental ice to sea-level rise over the next 200 years

Results are made available in forms accessible to scientists, policy-makers and the general public, including clear presentations of the sources of uncertainty.

Ice2sea has been set the task of providing input to the up-coming Fifth Assessment of the Intergovernmental Panel on Climate Change (IPCC).

This report is due to be finalised in late-2012, with publication planned for early-2013.

In brief, ice2sea will provide the following elements that may be used to inform the report:

1. Improved understanding of the key processes that control how glacial systems respond to atmospheric and oceanic climate change
2. New methodologies for the prediction of global sea-level rise based on improved models of the response of ice sheets and mountain glacier to climate change.
3. Updated assessments of the likely contribution of the cryosphere to sea-level rise over the next 200 years, based on two emissions scenarios.
4. A collective view of the likelihood of catastrophic sea-level rise, due collapse of either Greenland or Antarctic ice sheets.
5. A clearer view of where the uncertainties in predicting future sea-level rise arise, and how these may be reduced in future.

PROMICE is closely linked with ice2sea, and delivers to the IPCC process through this project. The connection is firm as the chief scientist on PROMICE, Dr. Andreas P. Ahlstrøm, is also heading Work Package 3 in ice2sea, entitled 'Foundation and validation data'. This work package will provide the basic observational data for building and validating the glaciological models applied in Work Package 2 (Key processes) and Work Package 5 (Ice-response modelling). This will be accomplished by building on existing remote sensing and field programmes, with a focus on making these datasets available for and useful to, the modelling work packages. New data collection activities are supported to fill crucial data gaps. The main focus is on the decadal timescale (observational and satellite era), except for the ice-sheet accumulation, which is on a centennial time scale.

Work Package 3 contains four sub-work packages, which are listed to illustrate direct the relevance to the PROMICE aims:

- Past and recent accumulation on ice sheets
- Mass balance time series for the ice sheets
- Inventories of glaciers and ice caps
- Sensitivity to change in near-polar ice caps

The GEUS Glaciology Group also contributes directly to the science in ice2sea through the application of a numerical model (in Work Package 2) partly developed as part of PROMICE (and described under 'Numerical modelling – development of a new calving model [...]'). In the same vein, PROMICE also contributes with outlet glacier velocity measurements, supplementing similar measurements (also carried out by GEUS) funded directly through ice2sea.

The application of the previously developed 1D outlet glacier flow model (Nick et al., 2009) is carried out in collaboration with Dr. Faezeh Nick, Université Libre de Bruxelles (ULB). The purpose of the collaboration is to quantify the ice flux from the large outlet glaciers, draining the ice sheet, into the sea in a 100-year perspective. A specific group of marine-terminating outlet glaciers has been selected, based on the volume of ice drained, and their potential for rapid changes. These include Jakobshavn Isbræ, Upernavik Isstrøm (West Greenland), Helheim, Kangerlussuaq, Daugaard-Jensen Glaciers (East Greenland), Petermann Glacier (North West Greenland), and 79 Fjord Glacier (North East Greenland). So far, data sets have been compiled for a number of these glaciers, including surface and bed elevation, flow velocity (both from remote sensing observations) and surface mass balance (regional climate modelling). Presently the model runs are being produced. These will be calibrated against in-situ data collected from most of the glaciers in the form of GPS based velocity measurements. The work is expected to result in several publications in the near future.

## **Stability and Variations of Land Ice (SVALI)**

The Nordic Centre of Excellence SVALI will study basic cryospheric processes using remote sensing, airborne and in-situ measurements, and carry out advanced Earth System Modelling with focus on land ice in the Arctic/North-Atlantic area. The ultimate goal is to answer these key questions: How fast is land ice volume in the Arctic and North-Atlantic area changing, and why? Will these processes continue to accelerate? What are the consequences for sea-level and ocean circulation? What are the implications for society? GEUS will be involved in leading the Theme 1 'Observing the present state of the cryosphere, process studies on surface mass balance, surface properties and calving and head the outreach activity of the centre.

**Period:** 2010 - 2015

**Project leader:** Signe Bech Andersen

**Funders:** Norden - Top Level Research Initiative

**Collaborators:** University of Oslo, Norwegian Polar Institute, CSC - IT Center for Science Ltd., University of Copenhagen, Danish Meteorological Institute, Uppsala University, Norwegian University of Life Sciences, University Centre in Svalbard, Finnish Meteorological Institute, Icelandic Meteorological Office, University of Iceland, Arctic Centre - University of Lapland, Climate Research Centre Greenland, Norwegian Water Resources and Energy, University of Stockholm

**Website:** <http://ncoe-svali.org>

## **Greenland Analogue Project (GAP)**

Near the south-western town of Kangerlussuaq in Greenland, the Greenland Analogue Project (GAP) set out to determine the level of meltwater penetration into the bedrock. The five-year project runs from 2008 to 2013 and is funded by the Swedish, Finnish and Canadian nuclear waste management agencies SKB, Posiva Oy, and NWMO. Since this project is based in a sector of the Greenland ice sheet where PROMICE is not represented with weather stations, GAP financed three stations of PROMICE-design, which will be carried over into PROMICE after the project's end. Based on the weather station measurements, GEUS delivers ice sheet surface melt maps to the project, using the melt modelling technique developed in PROMICE.

## **FreshLink**

In 2007 the FreshLink project was initiated by the Nature Institute, in the south-western region of the Greenland ice sheet near the town of Nuuk. The project combined various disciplines, with the ultimate goal of assessing the freshwater budget of the entire Nuuk fjord. GEUS was involved to determine the meltwater influx into the fjord from the ice sheet, using weather station measurements and melt modelling techniques developed in PROMICE. The two PROMICE weather stations NUK\_L and NUK\_U were placed in 2007, and were co-financed by FreshLink. The project came to an end in 2010, but GEUS continued similar activities in the region within the Imglaco project.

## **ImGlaCo**

The Impact on Glaciers near the Coast (Imglaco) project is from GEUS' perspective a continuation of the FreshLink project, in which the freshwater budget of the Nuuk fjord was determined. Under the umbrella of the Greenland Climate Research Centre, one additional weather station was placed in the Nuuk region of the Greenland ice sheet, financed by Imglaco, adding to the PROMICE network, and benefitting from PROMICE expertise and logistics. This weather station (NUK\_N) was erected on the north end of the ice sheet sector that drains into the Nuuk fjord, in order to determine the along-slope gradients in meteorological variables, in addition to the cross-slope gradients known from the two NUK stations already in place since 2007.

## **SEDIMICE**

The SEDIMICE project is focused on climate variability in the region around Sermilik fjord and Helheim glacier in East Greenland. The aim is to investigate the processes behind past fluctuations in the Greenland ice sheet and in local glaciers - qualitatively and quantitatively. Climate variability is investigated on short time scales by monitoring and modelling the ice sheet and by the local glacier mass balance and also by estimating sediment production. Climate variability on longer time scales is investigated by a palaeoclimatic reconstruction based on

- Marine fjord sediment cores
- Lake sediment cores
- Moraine deposits

The project is financed by Geocenter Denmark and involves the National Geological Survey of Denmark and Greenland (GEUS), the Department of Geography and Geology at University of Copenhagen, Geological Museum (at Natural History Museum of Denmark) and the Department of Earth Sciences at University of Aarhus.

From the glaciological side, SEDIMICE was envisioned as a research effort to better understand the processes causing the mass loss fluctuations observed in PROMICE. The glaciologists contributing to SEDIMICE are also affiliated with PROMICE ensuring the integration of the research results into the monitoring effort.

Webpage:

<http://www.geus.dk/geuspage-dk.htm?http://www.geus.dk/program-areas/nature-environment/greenland/sedimice-dk.htm>

## **Greenland Climate Network (GC-Net)**

An inspiration to the PROMICE Network was (and is) the Greenland Climate Network (abbreviated GC-Net), primarily covering the accumulation zone of the Greenland Ice Sheet with more than 20 automatic weather stations currently in operation. GC-Net was established mainly during the PARCA project by Prof. Konrad Steffen and co-workers. In his own words: "The GC-Net was established in spring 1995 with the intention of monitoring climatological and glaciological parameters at various locations on the ice sheet over a time period of at least 10 to 15 years. The first AWS was installed in 1990 at the Swiss Camp, followed by four AWS in 1995, four in 1996, five in 1997, four in 1999, and two in 2000. Our objectives for the Greenland weather station (AWS) network are to measure daily, annual and inter-annual variability in accumulation rate, surface climatology and surface energy balance at selected locations on the ice sheet, and to measure near-surface snow density at the AWS locations for the assessment of snow densification, accumulation, and metamorphosis." (Steffen et al., 2004).

PROMICE was from the onset closely linked with GC-Net and designed to cover the part of the ice sheet not covered by the existing network, i.e. the ablation zone (apart from the region close to Jakobshavn Isbræ). PROMICE and GC-Net both support an open data policy and works together to maximize the observational coverage of the ice sheet. The link is strengthened by personal contacts, and an extended research visit is envisaged in 2011 by Dirk van As (senior scientist in the PROMICE team with responsibility for the AWS network) to CIRES in Boulder, Colorado, to further explore the synergy between the two monitoring efforts.

## Global Land Ice Measurements from Space (GLIMS)

PROMICE participates in and contributes to the global umbrella project Global Land Ice Measurements from Space (GLIMS) through the effort to utilize the digital maps produced at GEUS and the National Survey and Cadastre (KMS) for climate change science and make the data available to the global scientific community. Additionally, we engage in the effort to map the ice sheet margin as well as the local glaciers and ice caps in Greenland with satellite imagery and actively support or join projects with similar aims, such as the EU-project ice2sea and the ESA-project GlobGlacier.

“GLIMS (*Global Land Ice Measurements from Space*) is a project designed to monitor the world's glaciers primarily using data from optical satellite instruments, such as [ASTER](#) (Advanced Spaceborne Thermal Emission and reflection Radiometer).

GLIMS began as an ASTER Science Team project. Through this connection, we have guided the ASTER instrument to acquire imagery of Earth's glaciers that is optimized (best season and instrument gain settings) for glacier monitoring. We have also put together a network of international collaborators who analyze imagery of glaciers in their regions of expertise. Analysis results include digital glacier outlines and related metadata, and can also include snow lines, center flow lines, hypsometry data, surface velocity fields, and literature references. Results from analysis done by the Regional Centers are sent for archive to the National Snow and Ice Data Center ([NSIDC](#)).

We continue to develop tools to aid in glacier mapping and for transfer of analysis results to NSIDC. These include [GLIMSVIEW](#), documented procedures for GLIMS analysis, and [web-based tools](#) for data formatting and quality control.” (source: <http://www.glims.org/>).

## World Glacier Monitoring System

PROMICE contributes to the World Glacier Monitoring System by providing a national representative from the PROMICE team.

“Since this beginning of internationally coordinated systematic observations on glacier variations in 1894, a valuable and increasingly important data basis on glacier changes has been built up. In 1986 the World Glacier Monitoring Service (WGMS) started to maintain and continue the collection of information on glacier changes, when the two former ICSI services PSFG (Permanent Service on Fluctuations of Glaciers) and TTSWG (Temporal Technical Secretariat/World Glacier Inventory) were combined.

Today, the World Glacier Monitoring Service (WGMS) collects standardized observations on changes in mass, volume, area and length of glaciers with time (glacier fluctuations), as well as statistical information on the distribution of perennial surface ice in space (glacier inventories). Such glacier fluctuation and inventory data are high priority key variables in climate system monitoring; they form a basis for hydrological modelling with respect to possible effects of atmospheric warming, and provide fundamental information in glaciology, glacial geomorphology and quaternary geology. The highest information density is found for

the Alps and Scandinavia, where long and uninterrupted records are available.” (source: <http://www.wgms.ch/about.html>)

Through WGMS and GLIMS, PROMICE also contributes to the Global Terrestrial Network for Glaciers (GTN-G).

“The Global Terrestrial Network for Glaciers (GTN-G) is the framework for the internationally coordinated monitoring of glaciers and ice caps in support of the United Nations Framework Convention on Climate Change (UNFCCC). The network, authorized under the Global Climate/Terrestrial Observing System ([GCOS](#), [GTOS](#)), is jointly run by the World Glacier Monitoring Service (WGMS), the U.S. National Snow and Ice Data Center (NSIDC), and the Global Land Ice Measurements from Space initiative (GLIMS).” (source: <http://www.gtn-g.org/>)

## **GlobGlacier - Glacier Monitoring Service using Data from Space**

PROMICE participates in the GlobGlacier project as an active member of the user group, with the obligation to evaluate the products of the project.

“The **GlobGlacier** project will attempt to establish a service for glacier monitoring from space that is based on user requirements and builds upon, complements and strengthens the existing network for **global glacier monitoring** (GTN-G). The project will help to establish a global picture of glaciers and ice caps, and their role as **Essential Climate Variables** (ECVs) as defined in the GCOS implementation plan for the UNFCCC (GIP, 2004). With this respect, the most requested issue is to complete the **world glacier inventory** (WGI) from the 1970s by producing glacier outlines in regions where actually is nothing and to complement the point information already stored in the WGI by 2D information to allow change assessment. Moreover, **GlobGlacier** will integrate satellite data from various sensors to create value added products for a wide range of user communities. A close cooperation with major user groups (e.g. WGMS) and related projects (e.g. GLIMS) will ensure a maximum benefit of the generated products from a global perspective.

The project will provide new information on **three major topics**:

1. **identification of key regions** for each product to be generated based on a survey of the currently available databases, their gaps, and the earth observation (EO) data holdings
2. well **documented processing workflows** for individual sensors and products as well as for their combined and synergetic use in a set of document deliverables
3. **raw data of the required glacier products in open standard formats** for easy public access (e.g. through the GLIMS and WGMS database)

The quality of the generated products and documents will be evaluated by the members of the user group to ensure the best possible service.”

(source:

<http://www.globglacier.ch/content.html?menuitem=sub1&contentItem=projectObjectives>)

## Conclusion & Outlook

The timeliness and necessity of the Programme for Monitoring of the Greenland Ice Sheet becomes evident when reading the recently released 'Executive Summary' of the report 'Snow, Water, Ice and Permafrost in the Arctic' (SWIPA, 2011) which states that one of the four biggest unanswered questions identified is:

*'How quickly could the Greenland Ice Sheet melt?' (SWIPA, 2011)*

...and further:

*'To reduce the uncertainty in future assessments, more robust observational networks are needed. [...] Observational networks need to be expanded to provide a robust set of cryospheric data for monitoring, model improvement and satellite product validation.'* (SWIPA, 2011)

The focus of these statements is on assessments of the future fate of the Greenland Ice Sheet in a changing climate. It is imperative to understand that until PROMICE was initiated, there was no observational network measuring the melt on the ice sheet. Without such ground truth observations, mass balance modelling becomes a theoretical exercise. The scientific community is only now reaching a point where the *present-day* mass balance of the Greenland Ice Sheet can be evaluated at sufficient spatial resolution to capture the relatively narrow ablation zone along the ice margin. The PROMICE network provides the means to not only validate such evaluations, but also provide crucial direct input data into the near real-time regional climate models in the part of the ice sheet that matters the most and is the hardest to get right.

We need to *first* manage to combine observations and models to produce reliable estimates of *present-day* mass balance, validated by the direct ablation measurements of the PROMICE network. Once this aim is accomplished, we are in a much better position to improve assessments of the *future* mass balance of the Greenland Ice Sheet.

This point is relevant both for the ice lost through melt at the surface and that lost at the interface between the ice sheet and the ocean. PROMICE provides new consistent observational data series to improve the modelling of both. As is evident from this report, this is not a simple task, as the ablation zone and the outlet glaciers remains the most hostile region of the ice sheet to operate an observational campaign in. The ice melts away underneath the stations at a rate up to nearly 9 metres per year, crevasses open up swallowing the instruments, extreme winds destroy the stations, scattering parts over hundreds of metres, and heavy snow breaks the stations as it compacts in the spring, forming thick ice lenses. Conditions as these explain the need to visit most stations once a year, although some stations in more quiet parts of the ice sheet margin have been operating for up to 4 years without a visit.

Data from the PROMICE station network have formed the basis of several scientific publications already and served as input to regional melt modelling. However, to take the step

towards a full mass balance model of the Greenland Ice Sheet, it is necessary to combine observations with a regional climate model. This step is necessary in order to include the accumulation of snow as well as reliably predict the values of melt model input parameters in between the automatic weather stations. Collaboration with the US Greenland Climate Network (GC-Net) stations ensure a good observational coverage of the central parts of the ice sheet and DMI stations along the coast provide the perimeter off the ice sheet.

Thus, in order to fulfil the first of the aims of PROMICE, collaboration has been established with DMI that runs a prognostic regional climate model at high resolution over Greenland several times a day. PROMICE and GC-Net data is now provided in near real-time to DMI (to be distributed to the World Meteorological Organisation (WMO) from there) and the challenge is now to provide a modelled mass balance estimate that utilizes these observations, even if they can never be as consistent as traditional weather data from safer locations off the ice sheet. It is expected that we will have such an observation-driven mass-balance model system running before the end of 2012.

The second component of the mass loss, namely that from outlet glaciers calving and melting into the ocean is likewise a key focus of PROMICE. As documented in this report, a new processing system to derive ice sheet velocity maps is now operational. This system has been designed for monitoring purposes, meaning that emphasis has been on providing flexibility to ingest data from future sensors rather than focussing only on existing satellite datasets.

Producing velocity maps over a region as large as the Greenland Ice Sheet is a major undertaking, relying on the existence and availability of radar remote sensing data. Regarding availability, we actively pursue a collaboration policy to obtain data or derived products from colleagues that might have access to data that would otherwise not be available to a Danish governmental programme as PROMICE. Foreign research groups and international research projects have produced ice sheet velocity maps in parallel to the efforts in PROMICE, but we cannot rely solely on such efforts to continuously assess changes in the Greenland Ice Sheet on a monitoring basis. The future existence of satellite radar data over Greenland is not a given fact. PROMICE team members actively engage in hearings on future satellite missions organized by the European Space Agency to stress the need for radar data over the Greenland Ice Sheet. Without this data, assessing changes in the ice sheet contribution to sea level change ends up relying on even more peripheral satellite missions aimed at altimetry and gravity measurement. These have proven useful in highlighting ice sheet volume and mass changes, but crucially lack the explanatory power needed to improve our future modelling capabilities.

Velocity maps provide an excellent overview of the ice movement for a particular point in time. However, the outlet glaciers tend to change their pace over time. Indeed, the recent accelerated mass loss from the ice sheet has been largely due to an acceleration of the outlet glaciers. To provide the temporal change in the mass loss between velocity map dates, we initiated the deployment of rugged, transmitting GPS-trackers on a number of outlet glaciers. As these trackers move along with the fast-flowing ice, they need to be repositioned or replaced every 1-2 years, imposing severe financial limitations on the extent of such a network. Currently, we have aimed at outlet glaciers near our station transects to

minimize logistical costs. Again, we collaborate with international partners to increase the total amount of available velocity data.

The final step is to calculate the total annual ice flux towards the sea. This requires knowledge of the ice thickness, preferably close to the ice margin. To obtain this, PROMICE successfully carried out an airborne campaign in 2007 along the entire margin of the Greenland Ice Sheet, including flights down the 20 largest outlet glaciers, providing ice sheet surface elevation from laser altimetry and basal elevation from ice-sounding radar. A sector in SW Greenland proved impenetrable for the ice-sounding radar and will be targeted with an alternative radar system in spring 2011. The airborne survey will be repeated in late summer 2011, as close to the dates of the data collection in 2007. This specifically optimizes the comparison of the surface elevation data, as the noise from seasonal snow fall is minimized. It is intended to include elevation data from other sources, such as ICE-Sat/GLAS and US airborne surveys to evaluate the ice sheet elevation change in order to provide an independent control on the mass budget method employed in PROMICE.

With a flux gate established from the airborne survey along the majority of the ice margin, it becomes feasible to calculate the amount of ice passing by assuming a velocity profile from the surface towards the base of the ice sheet. Data from the GPS-trackers will assist in quantifying the variability of the ice flux seasonally and from year to year. To assess the loss of ice to the ocean, it is necessary to deduct the runoff from surface melting between the flux gate and the ice margin. This means that the melt maps are needed to assess the ice loss directly to the ocean through calving and bottom melting of floating glaciers. Even with velocity maps, melt maps and ice thickness data available, flux-gate calculations are inherently complicated to set up due to the complex topography of the marginal region of the Greenland Ice Sheet. We have scheduled the first calculations for 2012.

An issue that is not directly related to the mass loss of the Greenland Ice Sheet proper, but yet extremely important in our assessment of the contribution of ice loss from Greenland to sea level rise, is that of ice mapping. The seemingly straightforward task of mapping the extent and elevation of ice in Greenland is in reality a difficult problem and a key challenge to PROMICE. The extent and remoteness of Greenland has implied that producing maps required major airborne campaigns collecting orthophotos and decades to analyse the data subsequently. GEUS has been a strong force in this work and high quality digital maps were available at the onset of PROMICE. Yet, the low contrast of snow and ice covered regions means that elevation contours are sparse and that the maps require manual editing to identify ice masses correctly. The airborne orthophoto campaigns were not carried out everywhere at the same time, implying that no complete Greenland ice extent map can be produced from these data for a certain year, but even then *any* map of the ice extent in Greenland is better than what is currently available. It is hard to model the expected sea level rise from ice masses in Greenland if you have only a vague idea about the present-day extent. Thus, in previous studies, the ice caps and glaciers outside the ice sheet to be either considered part of the ice sheet despite large differences in mass loss mechanisms or simply discarded from calculations due to lack of data. Area estimates have varied dramatically, especially as there has not been a consensus on how to delineate local ice caps and glaciers from the ice sheet proper.

In 2011, PROMICE will deliver a map of the ice extent based on the orthophoto campaigns of the late 1970s and 80s, providing much-needed baseline data for the modelling community.

The next step is of course to assess the change in ice cover and volume, also for local ice masses. To this end, the PROMICE team has actively pursued participation in, or collaboration with, international research projects and currently acts as a clearing-house for all glacier-mapping efforts in Greenland in the global umbrella-project Global Land Ice Measurements from Space (GLIMS). The GLIMS mapping methodology is based primarily on ASTER and LandSat satellite data in an attempt to provide a baseline map from a specific period, facilitating future change assessments. Large sectors of Greenland are being processed, primarily by partners at the University of Zürich, through funding from the European Space Agency and the European Union. Change assessments have already been carried out (and published) within PROMICE for a test area covering Disko Island, Nuussuaq Peninsula and Svartenhuk Peninsula in West Greenland, proving the concept.

The activities described so far have to some extent resembled the kind of work that is also carried out sequentially in short-term research projects. What really makes PROMICE stand out as a *monitoring* programme is the additional dual emphasis on data storage and public outreach. The PROMICE database is designed as a full-scale system in terms of data security, quality assurance, data availability and ease of use. PROMICE has benefited from the expertise at GEUS in building databases for storage of data of national importance, such as oil & gas data. Constructing a working database with easy access from the internet, that lives up to the highest standards is no simple endeavour. Yet, as this report testifies, we have come a long way, particularly with the automatic weather station data. The AWS data received highest priority because this type of data is the hardest to handle and also benefits the most from being stored and treated in a standardized system. Other products from PROMICE, like data from airborne surveys or derived remote-sensing products like velocity maps or ice extent maps are simpler to store and will be included in the online database as they are produced.

Public outreach is another central effort. Although only partly financed through PROMICE, the activities have laid the ground for obtaining funding for outreach projects from other sources. So far, three major projects have been initiated as multimedia e-learning platforms aimed at different audiences, with an external funding of nearly 1 mio. DKK. The first project (in English) presents PROMICE broadly to the international public audience and was launched for the COP15 meeting in Copenhagen in 2009. The two following projects have been directly aimed at primary school children, ages 10-12 years and 13-16 years, respectively, complete with exercises and teachers manuals. Apart from these dedicated activities, the PROMICE team participates in the public debate nationally and internationally, disseminating results and providing expert opinions on issues related to glaciers and ice sheets. The PROMICE Newsletter will be the next step to actively engage with the press and the public and is central to the pro-active media strategy of the programme, establishing collaboration with the News Department of Experimentarium, an institution devoted to, and specialized in, popular science outreach.

This report sums up the initialization phase of PROMICE from 2007-2010 as laid out in the original plan from 2006. An evaluation of the initialization phase pinpoints the difficulty in planning or predicting the course of scientific activities several years into the future. Some activities, like the automatic weather station network were not only ahead of schedule, but has also been strengthened by additional stations financed by parallel research, commercial or monitoring activities. This means that the PROMICE team can currently draw on data from no less than 24 stations, rather than just the 14 supported directly by PROMICE. Not all this data is available to the public due to contractual obligations, but the majority can be obtained from the PROMICE database. Another success has been the public outreach effort, particularly in terms of utilizing PROMICE to recruit future potential scientists. With three substantial, and externally financed, projects dedicated to outreach, we have lived up to our ambitious aim of redefining the relationship between science and outreach on an institutional as well as personal level. On top of this prioritized type of outreach, PROMICE has also made its impact on the national and international debate through a large number of appearances in news media on TV, radio and in national and international newspapers. PROMICE has also starred in science programmes on TV and radio, with reporters participating in the fieldwork on the ice sheet. A long series of talks in all foras from groups of international journalists to 5<sup>th</sup> grade pupils, as well as PROMICE appearances in cultural events and down to the level of answering direct calls from concerned farmers on the issue of the impact of local sea level rise on their fields tops up the outreach effort.

On other fronts, the PROMICE plan has turned out to be harder to follow. The central issue of modelling the mass balance of the entire Greenland Ice Sheet turned out to require a substantial extension of the original scope, as a regional climate model has been deemed necessary to do the work properly. This has caused part of the delay in the delivery of a mass balance number for the ice sheet, but now has the potential to not only provide a great step forward in reliability of present-day mass-balance estimates, but also to feed much more directly into similar climate models producing future scenarios for mass balance. This combination serves both the immediate and ultimate aims of PROMICE simultaneously.

Building the capability to produce ice sheet surface velocity maps on a large scale has also turned out to be a major feat, with obstacles extending beyond what was originally anticipated. Particularly the issue of data existence and availability has proven difficult to tackle. The PROMICE team has worked from the international diplomatic level down to grass-root science contacts to obtain the necessary data or derived products to carry out this work without running into unacceptable commercial data costs. The sheer scale of the Greenland Ice Sheet is a challenge when it comes to satellite coverage and even data that is provided for research at a nominal cost ends up as a major expense in the budget. Likewise, we have realized the urgent need of lobbying for future data availability within the framework of the European Space Agency and of supporting similar activities towards other space agencies.

Despite these apparent disparities between the original plan and the current status, we consider the initialization phase an outright success. PROMICE has succeeded in establishing a research and monitoring capacity in Denmark on the current state of the Greenland Ice Sheet, an issue of urgent interest to the Danish society, feeding directly into policy-

making nationally as well as internationally. With large-scale mitigation efforts underway, it becomes increasingly important to know exactly what climate change effects we need to mitigate. As pointed out, the contribution of the Greenland Ice Sheet to sea level rise has been singled out as one of the major unknowns. PROMICE delivers on exactly this issue – *quantification and attribution of causes*. All this while serving the raw data directly to the international scientific community and keeping the public updated with sober reporting from the frontline of climate change science.

The Programme for Monitoring of the Greenland Ice Sheet has firmly reinstated Denmark in a central position regarding climate change research and monitoring in the Arctic, particularly within the Arctic Monitoring and Assessment Programme under the auspices of the Arctic Council. As with any monitoring effort, the impact of PROMICE will only increase over the years as the need for observations and long-term datasets becomes more and more urgent. The impact of human activities on the global climate is becoming increasingly apparent and over time it will only become more important to understand exactly *how*.

## References

- ACIA, 2005. Arctic Climate Impact Assessment. *Cambridge University Press*, 1042p. <http://www.acia.uaf.edu>
- Ahlstrøm, A.P., S.B. Andersen, D. Van As, M. Citterio, R.S. Fausto, S. Nielsen, H.F. Jepsen, S.S. Kristensen, E.L. Christensen, L. Stenseng, R. Forsberg, S. Hanson and D. Petersen, 2008. A new programme for monitoring the Greenland ice sheet mass loss, *GEUS Bulletin Series: Review of Survey activities, Geological Survey of Denmark and Greenland Bulletin* 15, 61-64.
- Ahlstrøm, A.P., C.E. Bøggild, O.B. Olesen, D. Petersen and J.J. Mohr, 2007. Mass balance of the Amitsulôq ice cap. Glacier Mass Balance Changes and Meltwater Discharge, *IAHS Red Books* 318, 107-115 *International Association of Hydrological Sciences. IAHS Press*.
- Ahn, Y and J. E. Box, 2010. Glacier velocities from time-lapse photos: technique development and first results from the Extreme Ice survey (EIS) in Greenland, *Journal of Glaciology*, Vol. 56, No. 198, p.723-734.
- Andersen, M.L., T.B. Larsen, M. Nettles, P. Elosegui, D. van As, G.S. Hamilton, L.A. Stearns, J.L. Davis, A.P. Ahlstrøm, J. de Juan, G. Ekström, L. Stenseng, S.A. Khan, R. Forsberg and D. Dahl-Jensen, 2010. Spatial and temporal melt variability at Helheim Glacier East Greenland, and its effect on ice dynamics, *Journal of Geophysical Research* 115, 18 pp. doi:10.1029/2010JF001760.
- Arctic Climate Impact Assessment Policy Document, 2004. *Issued by the Fourth Arctic Council Ministerial Meeting Reykjavík, 24 November 2004*, [http://www.acia.uaf.edu/PDFs/ACIA\\_Policy\\_Document.pdf](http://www.acia.uaf.edu/PDFs/ACIA_Policy_Document.pdf)
- Arnold N, K. Richards, I. Willis and M. Sharp, 1998. Initial results from a semi-distributed, physically-based model of glacier hydrology. *Hydrological Processes* 12: 191–219.
- Arnold, N. S., W.G. Rees, A.J. Hodson, and J. Kohler, 2006. Topographic controls on the energy balance of a high Arctic glacier. *Journal of Geophysical Research*. 111 F02011, doi:10.1029/2005JF000426.
- Bahr, D.B., M.F. Meier and S.D. Peckham, 1997. The physical basis of glacier volume-area scaling. *J. Geophys. Res* 102, 355–362.
- Bamber, J. L., R.B. Alley and I. Joughin, 2007. Rapid response of modern day ice sheets to external forcing. *Earth and Planetary Science Letters* 257, 1–13.
- Bamler, R. and M. Eineder, 2005. Accuracy of differential shift estimation by correlation and split-bandwidth interferometry for wideband and Delta-k SAR systems", *IEEE Geosc. Rem. Sens. Lett.*, Vol. 2, No. 2.

Boncori, J.P.M., J. Dall, A.P. Alstrøm and S.B. Andersen, 2009. Development and preliminary validation of a SAR ice-motion processing chain in support of PROMICE (Programme for the Monitoring of the Greenland Ice-Sheet). *in Proc. Fringe'09*, Frascati (Italy).

Boncori, J.P.M., J. Dall, A.P. Alstrøm and S.B. Andersen, 2010. Validation and operational measurements with SUSIE – a SAR ice motion processing chain developed within PROMICE. *In proc. ESA Living Planet Symposium*, Bergen (Norway).

Bougamont, M., J.L. Bamber, J.K. Ridley, R.M. Gladstone, W. Greuell, E. Hanna, A.J. Payne and I. Rutt, 2007. Impact of model physics on estimating the surface mass balance of the Greenland ice sheet, *Geoph. Res. Lett.*, 34, L17501, doi:10.2929/2007GL030700.

Box, J.E., D.H. Bromwich, B.A. Veenhuis, L. Bai, J.C. Stroeve, J.C. Rogers, K. Steffen, T. Haran and S. Wang, 2006. Greenland Ice Sheet Surface Mass Balance Variability (1988-2004) from Calibrated Polar MM5 Output, *J. Clim.*, 19(12), 2783-2800.

Box, J.E., J. Cappelen, D. Decker, X. Fettweis, T. Mote, M. Tedesco and R. S. W. van de Wal, 2010. Greenland, *Arctic Report Card 2010*, <http://www.arctic.noaa.gov/reportcard>

Box, J.E. and A.E. Cohen, 2006. Upper-air temperatures around Greenland: 1964-2005, *Geoph. Res. Lett.*, 33, L12706.

Box J. E and K. Ski, 2007. Remote sounding of Greenland supraglacial melt lakes: implications for subglacial hydraulics, *Journal of Glaciology*, Vol. 53, 257-265.

Braithwaite, R.J., 1984. Calculation of degree-days for glacier-climate research, *Polarforschung*, 20, 1–8.

Braithwaite, R.J., 1995. Positive degree-day factors for ablation on the Greenland ice sheet studied by energy-balance modelling, *J. Glaciol.*, 41, 153-160.

Bøggild, C.E., N. Reeh and H. Oerter, 1994. Modelling ablation and mass-balance sensitivity to climate change of Storstrømmen, North-east Greenland, *Global and Planetary Change*, 9, 79-90.

Citterio, M., 2007. Immagini da satellite e bilanci energetici [om Overvågning af Grønlands indlandsis]. Valle d'Aosta figlia dei ghiacci. Fondazione Montagna Sicura - Montagne Sûre. Quart, Aosta. *Musumeci*, 117-118.

Citterio, M., F. Paul, A.P. Ahlstrom, H.F. Jepsen and A. Weidick, 2009. Remote sensing of glacier change in West Greenland: accounting for the occurrence of surge-type glaciers. *Annals of Glaciology* 50, 70–80.

Cogley, J.G., 2009. A more complete version of the World Glacier Inventory. *Annals of Glaciology* 50, 32–38.

Dawes, P.R. and D. van As, 2009. An advancing glacier in a recessive ice regime: Berlingske Bræ, North-West Greenland. In: Bennike, O., Garde, A.A. & Watt, W.S. (eds): Review of Survey activities 2009. *Geological Survey of Denmark and Greenland Bulletin* 20, 79-82.

de Juan, J., P. Elosegui, M. Nettles, T.B. Larsen, J.L. Davis, G.S. Hamilton, L.A. Stearns, M.L. Andersen, G. Ekström, A.P. Ahlstrøm, L. Stenseng, S.A. Khan and R. Forsberg, 2010. Sudden increase in tidal response linked to calving and acceleration at a large Greenland outlet glacier. *Geophysical Research Letters* 37 (12501), 5 pp., doi:10.1029/2010GL043289.

Di Marzio, J., A. Brenner, R. Schutz, C. A. Shuman, and H. J. Zwally, 2007. *GLAS/ICESat 1 km laser altimetry digital elevation model of Greenland*, Boulder, Colorado USA: National Snow and Ice Data Center. Digital media.

Dyrgerov, M.B. and M.F. Meier, 2005. Glaciers and the changing Earth system: a 2004 snapshot, *INSTAAR occasional paper 58*, Institute of Arctic and Alpine Research, University of Colorado Boulder, CO.

Fausto, R.S., A.P. Ahlstrom, D. Van As, C.E. Boggild and S.J. Johnsen, 2009a. A new present-day temperature parameterization for Greenland. *J. Glaciol.*, 55(193), 869–878.

Fausto, R.S., A.P. Ahlstrom, D. Van As, C.E. Boggild and S.J. Johnsen, 2009b. Improving surface boundary conditions with focus on coupling snow densification and meltwater retention in large-scale ice-sheet models of Greenland, *J. Glaciol.*, 55(189), 95–105.

Fausto, R.S., C. Mayer and A.P. Ahlstrøm, 2007. Satellite-derived surface type and melt area of the Greenland Ice Sheet using MODIS data from 2000-2005, *Ann. Glaciol.*, 46, 35-42.

Fettweis, X., 2007. Reconstruction of the 1979-2006 ice sheet surface mass balance using the regional climate model MAR, *The Cryosphere*, 1, 21-40.

Fettweis, X., J.P. van Ypersele, H. Gallée, F. Lefebvre and W. Lefebvre, 2007. The 1979-2005 ice sheet melt extent from passive microwave data using an improved version of the melt retrieval XPGR algorithm, *Geoph. Res. Lett.*, 34, L05502, doi:10.1029/2006GL028787.

Goldstein, R.M. and C.L. Werner, 1998. Radar interferogram filtering for geophysical applications, *Geophys. Res. Lett.*, Vol. 25, No. 21, pp. 4035-4038.

Goldstein, R.M., H.A. Zebker and C.L. Werner, 1988. Satellite radar interferometry two-dimensional phase unwrapping, *Radio Sci.*, Vol. 23, No. 4, pp. 713-720.

Gray, A.L., K.E. Mattar and G. Sofko, 2000. Influence of ionospheric electron flux on satellite radar interferometry, *Geophys. Res. Lett.*, Vol. 27, No. 10, pp. 1451-1454.

Greve, R., 2005. Relation of measured basal temperature and the spatial distribution of the geothermal heat flux for the Greenland Ice Sheet, *Ann. Glaciol.*, 42, 424-432.

Grotjahn, R., 1993. Global atmospheric circulations: Observations and Theories, *Oxford University Press*, 1, 1-417.

Hock, R., 2003. Temperature index melt modelling in mountain areas, *J. Hydrol.*, 282, 104-115.

Huybrechts, P. and J. de Wolde, 1999. The dynamic response of the Greenland and Antarctic ice sheets to multiple-century climatic warming, *J. Clim.*, 12, 2169-2188.

IPCC, 2007. Climate Change 2007: The Physical Science Basis. Contribution of Working Group I to the Fourth Assessment Report of the Intergovernmental Panel on Climate Change [Solomon, S., D. Qin, M. Manning, Z. Chen, M. Marquis, K.B. Averyt, M. Tignor and H.L. Miller (eds.)]. *Cambridge University Press*, Cambridge, United Kingdom and New York, NY, USA, 996 pp.

Joughin, I., 2002. Ice-sheet velocity mapping: a combined interferometric and speckle-tracking approach, *Ann. Glaciol.*, 34, pp. 195-201.

Joughin, I., W. Abdalati, and M. Fahnestock, 2004. Large fluctuations in speed on Greenland's Jakobshavn Isbræ glacier. *Nature* 432, 608-610.

Joughin, I.R., M.A. Fahnestock and J.L. Bamber, 2000. Ice flow in the northeast Greenland ice stream, *Ann. Glaciol.*, 31, pp. 141-146.

Lefebvre, F., H. Gallee, J. Van Ypersele and P. Huybrechts, 2002. Modelling of large-scale melt parameters with a regional climate model in south Greenland during the 1991 melt season, *Ann. Glaciol.*, 35, 391-397.

Marshall, S.J., M.J. Sharp, D.O. Burgess and F.S. Anslow, 2007. Near-surface-temperature lapse rates on the Prince of Wales icefield, Ellesmere Island, Canada: Implications for regional downscaling of temperature., *J. Geophys. Res.*, 27, 385-398.

Mattar, K.E. and A.L. Gray, 2002. Reducing ionospheric electron density errors in satellite radar interferometry applications, *Can J. Rem. Sens.*, Vol. 28, No. 4, pp. 593-600.

McGranahan, G., D. Balk and B. Anderson, 2007. The rising tide: assessing the risks of climate change and human settlements in low elevation coastal zones, *Environment and Urbanization*, vol. 19, no. 1, p.17-37.

Meier, M.F., 2005. Comment on "The potential for sea level rise: New estimates from glacier and ice cap area and volume distribution" by S. C. B. Raper and R. J. Braithwaite, *Geophys. Res. Lett.* 32.

Meier, M.F., M.B. Dyurgerov, U.K. Rick, S. O'Neel, W.T. Pfeffer, R.S. Anderson, S.P. Anderson and A.F. Glazovsky, 2007. Glaciers Dominate Eustatic Sea-Level Rise in the 21st Century, *Science* 317, 1064-1067.

- Mernild, S.H., I.M. Howat, Y. Ahn, G.E. Liston, K. Steffen, B.H. Jakobsen, B. Hasholt, B. Fog, and D. van As, 2010. Freshwater flux to Sermilik Fjord, SE Greenland. *Cryosphere* 4, 453-465.
- Mohr, J.J. and J.P. Merryman Boncori, 2008. An error prediction framework for interferometric SAR data, *IEEE Trans. Geosc. Rem. Sens.*, Vol. 46.
- Mottram, R., C. Nielsen, A.P. Ahlstrøm, N. Reeh, S.S. Kristensen, E.L. Christensen, R. Forsberg, and L. Stenseng, 2009. A new regional high-resolution map of basal and surface topography for the Greenland ice sheet margin at Paakitsoq, West Greenland, *Annals of Glaciology* 50 (51), 105-111.
- Motyka, R.J., M. Fahnestock and M. Truffer, 2010. Volume change of Jakobshavn Isbrae, West Greenland:: 1985-1997-2007, *Journal of Glaciology* 56, 635–646.
- Nettles, M., T.B. Larsen, P. Elosegui, G.S. Hamilton, L.A. Stearns, A.P. Ahlstrøm, J.L. Davis, M.L. Andersen, J. de Juan, S.A. Khan, L. Stenseng, G. Ekström and R. Forsberg, 2008. Step-wise changes in glacier flow speed coincide with calving and glacial earthquakes at Helheim Glacier, Greenland, *Geophysical Research Letters* 35, L24503, 5 pp. doi:10.1029/2008GL036127.
- Nick, F.M., C.J. van der Veen, A. Vieli, and D.I. Benn, 2010. A physically based calving model applied to marine outlet glaciers and implications for the glacier dynamics. *Journal of Glaciology* 56 (199), 781-794.
- Nick, F.M., A. Vieli, I.M. Howat, and I. Joughin, 2009. Large-scale changes in Greenland outlet glacier dynamics triggered at the terminus. *Nature Geoscience* 2, 110-114.
- Oerlemans, J., 2001. Glacier and climate change. A. A. Balkema, Amsterdam, *Taylor & Francis*.
- Ohmura, A., 1987. New temperature distribution maps for Greenland, *Z. Gletscherkd. Glazialgeol.*, 23(1), 1-45.
- Ohmura, A., 2001. Physical basis for the temperature-based melt-index method, *J. App. Meteo.*, 40, 753-761.
- Paterson, W.S.B., 1994. The Physics of Glaciers, *Butterworth-Heinemann*, 3, 1-420.
- Pepin, N. and M. Losleben, 2002. Climate change in the colorado rocky mountains: Free air versus surface temperature trends, *Int. J. Climatol.*, 22, 311-329.
- Radić, V., R. Hock, 2010. Regional and global volumes of glaciers derived from statistical upscaling of glacier inventory data, *J. Geophys. Res.* 115.

Raper, S.C.B., 2005. Reply to comment by M. F. Meier et al. on The potential for sea level rise: New estimates from glacier and ice cap area and volume distributions, *Geophys. Res. Lett.* 32.

Raper, S.C.B. and R.J. Braithwaite, 2005. The potential for sea level rise: New estimates from glacier and ice cap area and volume distributions, *Geophysical research letters* 32, L05502.

Raper, S.C.B. and R.J. Braithwaite, 2006. Low sea level rise projections from mountain glaciers and icecaps under global warming, *Nature* 439, 311-313.

Raup, B., A. Racoviteanu, S.J.S. Khalsa, C. Helm, R. Armstrong and Y. Arnaud, 2007. The GLIMS geospatial glacier database: a new tool for studying glacier change. *Global and Planetary Change* 56, 101–110.

Reeh, N., 1991. Parameterization of melt rate and surface temperature on the Greenland Ice Sheet, *Polarforschung*, 59(3), 113-128.

Rignot, E., D. Braaten, S.P. Gogineni, W.B. Krabill, and J.R. McConnell, 2004. Rapid ice discharge from southeast Greenland glaciers, *Geophysical Research Letters* 31, L10401, doi: 10.1029/2004GL019474.

Rignot, E. and P. Kanagaratnam, 2006. Changes in the velocity structure of the Greenland Ice Sheet, *Science*, 311, 986-990.

Ritz, C., A. Fabre and A. Letreguilly, 1997. Sensitivity of a Greenland Ice Sheet model to ice flow and ablation parameters: Consequences for the evolution through the last climate cycle, *Climate Dyn.*, 13(1), 11-24.

Roesner, L.A., J.A. Aldrich, and R.E. Dickinson, 1988. Storm Water Management Model User's Manual version 4; EXTRAN Addendum. *US Environmental Protection Agency, Athens, Georgia*. 188 p.

Rye, C. J., N. S. Arnold, I. Willis, and J. Kohler, 2010. Modelling the surface mass balance of a High Arctic glacier using the ERA-40 Reanalysis, *Journal of Geophysical Research (Earth Surface)*. doi:10.1029/2009JF001364.

Serreze, M.C., A.P. Barrett and J.J. Cassano, 2011. Circulation and surface controls on the lower tropospheric air temperature field of the Arctic, *Journal of Geophysical Research*, Vol. 116, D07104, doi:10.1029/2010JD015127.

Smelror, M., A. Ahlstrøm, L. Ekelund, J.M. Hansen, K. Nenonen and A.K. Mortensen, 2008. The Nordic geological surveys: Geology for society in practice. *Episodes* 31(1), 193-200.

Spring, U. and K. Hutter, 1981. Numerical studies of Jökulhlaups', *Cold Reg. Sci. Technol.*, 4, 227-244.

- Steffen, K. and J.E. Box, 2001. Surface climatology of the Greenland ice sheet: Greenland Climate Network 1995-1999, *J. Geophys. Res.*, 106(D24), 33951-33964.
- Steffen, K., J.E. Box and W. Abdalati, 1996. Greenland Climate Network: GC-Net, in Colbeck, S. C. Ed. *CRREL 96-27 Special Report on Glaciers, Ice Sheets and Volcanoes, trib. to M. Meier*, 1, 98-103.
- Steffen, K., J.E. Box, N.J. Cullen, R. Huff, 2004. Greenland Climate Network (GC-Net), In: 'Automatic Weather Stations on Glaciers – Lessons to be learned Extended abstracts', *Workshop 28-31 March 2004, Pontresina (Switzerland)*, 100-102.
- Steffen, K., S.V. Nghiem, R. Huff and G. Neumann, 2004. The melt anomaly of 2002 on the Greenland Ice Sheet from active and passive microwave satellite observations, *Geoph. Res. Lett.*, 31, L20402, doi:10.1029/2004GL020444.
- Tarasov, L. and W. Richard Peltier, 1999. Impact of thermomechanical ice sheet coupling on a model of the 100 kyr ice age cycle, *J. Geophys. Res.*, 104(D8), 9517-9545.
- van As, D. 2010. Changes in temperature and glacier melt from weather station observations in the Melville Bay region of North-West Greenland, *J. Glaciol.* 57 (202), 208-220.
- van As, D., C.E. Bøggild, S. Nielsen, A.P. Ahlstrøm, R.S. Fausto, S. Podlech and M.L. Andersen, 2009. Climatology and ablation at the South Greenland ice sheet margin from automatic weather station observations, *Cryosphere Disc.* 3 (1), 117-158.
- Van de Wal, R.S.W., W. Boot, M.R. Van den Broeke, C.J.P.P Smeets, C.H. Reijmer, J.J.A. Donker and J. Oerlemans, 2008. Large and rapid melt-induced velocity changes in the ablation zone of the Greenland Ice Sheet, *Science*, Vol. 321 (5885), pp. 111-113.
- Van de Wal, R.S.W., 1996. Mass-balance modelling of the Greenland Ice Sheet: A comparison of an energy-balance and degree-day model, *Ann. Glaciol.*, 23, 36-45.
- Van de Wal, R.S.W., W. Greuell, M.R. Van den Broeke, C.H. Reijmer and J. Oerlemans, 2005. Surface mass-balance observations and automatic weather station data along a transect near Kangerlussuaq, West Greenland, *Ann. Glaciol.*, 42, 311-316.
- Van der Veen, C.J., 1999. Fundamentals of Glacier Dynamics, *A.A. Balkema/ Rotterdam/ Brookfield*.
- Van der Veen, C.J., 2002. Calving glaciers, *Progr. Phys. Geogr.*, 26(1), 96–122.
- Vieli, A. and A.J. Payne, 2005. Assessing the ability of numerical ice sheet models to simulate grounding line migration, *J. Geophys. Res.*, 110(F1), F01003. (10.1029/2004JF000202.)

Wang, L., M. Sharp, B. Rivard and K. Steffen, 2007. Melt season duration and ice layer formation on the Greenland ice sheet, 2000-2004, *J. Geophys. Res.*, 112, F04013, doi:10.1029/2007JF000760.

A. Weidick, 1995. Satellite image atlas of glaciers of the world - Greenland, *U.S. geological survey professional paper* 1386-C.

Weidick, A. and O. Bennike, 2007. Quaternary glaciation history and glaciology of Jakobshavn Isbræ and the Disko Bugt region, West Greenland: a review, *Geological Survey of Denmark and Greenland Bulletin* 14, 78 pp.

Weidick, A., C.E. Boggild and N.T. Knudsen, 1992. Glacier inventory and atlas of West Greenland, *Rapp./Gronlands geol. undersogelse*.

Weidick, A. and M. Citterio, 2011. The ice-dammed lake Isvand, West Greenland, has lost its water, *Journal of Glaciology* 57, 186–188.

Weidick, A. and E. Morris, 1998. Local glaciers surrounding the continental ice sheets, *Studies and reports in hydrology* 56, 197–207.

Wegmuller, U., GAMMA Remote Sensing and Consulting, *personal communication*.

Wegmuller, U., C.L. Werner, T. Strozzi and A. Wiesmann, 2006. Ionospheric electron concentration effects on SAR and InSAR", *In Proc. IGARSS'06*.

## Appendix A – PROMICE in the public arena

The list below features 65 individual non-scientific public appearances by PROMICE team members in the public arena. The entries describe widely different efforts, ranging from extensive popular papers to brief interviews on the phone, from appearing in BBC World News HARDtalk program to an interview by 7<sup>th</sup> grade pupils for their school assignment. The list specifically excludes presentations at scientific conferences and scientific publications which are listed elsewhere. The list is intended to document and testify the gravity of the outreach effort in PROMICE.

1. Ahlstrøm, A.P. 2010: PROMICE - Freezing the retreat of ice. International Innovation Magazine. Research Media. International Innovation Magazine - Featured Project, 90-92.
2. Siewertsen, B., Pedersen, L.T., Adalgeirsdottir, G., Andersen, K.K. & Ahlstrøm, A.P. 2010: Orientering om knækket istunge fra Petermann gletsjeren i Nordvestgrønland- RØD. 13/08-2010. Cover - til Klima og Energiminister Lykke Friis.
3. Ahlstrøm, A. P. 2010: Climate Change Effects - the Danish Monitoring Programme for the Greenland Ice Sheet [Foredrag for UN-FCCC delegation - review af Danmarks 5. indberetning]. 23. juni, 2010. Copenhagen. Energistyrelsen.
4. Ahlstrøm, A.P. 2010: PROMICE - Status for overvågningen af Grønlands indlandsis [Foredrag for ansatte på Geocenter Danmark]. 10. maj, 2010. København. GEUS.
5. Ahlstrøm, A.P. 2010: Overvågning af Indlandsisen i praksis [Demonstration for Klima og Energiminister Lykke Friis, Departementschef Thomas Egebo, DMU Direktør Henrik Sandbech, Rektor ved Aarhus Universitet Lauritz B. Holm-Nielsen, m.fl., 17. august, 2010].
6. Ahlstrøm, A.P. 2010: PROMICE - Overvågningsprogrammet for Grønlands Indlandsis. 07 december, 2010. København. GEUS.
7. Ahlstrøm, A.P., Andersen, S.B., van As, D., Citterio, M. & Fausto, R.S. 2010: PROMICE - Klima og Energiministeriets overvågningsprogram for indlandsisen [Foredrag for Klima og Energiminister Lykke Friis, Departementschef Thomas Egebo, DMU Direktør Henrik Sandbech, Rektor ved Aarhus Universitet Lauritz B. Holm-Nielsen, m.fl., 18. august, 2010].
8. Ahlstrøm, A.P., Andresen, C.S., Pedersen, N.N., Citterio, M., Andersen, S.B., van as, D., Fausto, R.S. 2010: GEUS Glaciological Activities in Greenland 2010 and 2011 [Seminar om Indlandsisen for forskere i Københavnsområdet med interesse for Indlandsisen]. 25 november, 2010. DMI.

9. Ahlstrøm, A.P. (Interview-person) 2010: Gigantisk isflage er brækket løs i Grønland. 11. august, 2010. Hvilsom, F. (Journalist) Politikens netavis.
10. Ahlstrøm, A.P. (Interview-person) 2010: Kæmpe isbjerg knækker af Petermann Gletsjeren. 7. august, 2010. Kaldan, J. (Journalist) DR Radioavisen 12-nyhederne.
11. Ahlstrøm, A.P. (Interview-person) 2010: Hvorfor bliver sne tungere i tøvejr? Vestergård, G.L. (Journalist) Videnskab.dk.
12. Ahlstrøm, A.P. 2009: Grønlands Indlandsis og klimaet - hvad sker der? Geoviden - Geologi og Geografi 2009 (3), Geocenter Danmark., 8-15.
13. Ahlstrøm, A.P. 2009: Vandkraft i Grønland. Geoviden - Geologi og Geografi 2009 (3), Geocenter Danmark., 16-17.
14. Ahlstrøm, A.P. 2009: Verdensarv - Ilulissat [Undervisningsmateriale til Gymnasierne fra Danmarks Radio - dr.dk/gymnasium].
15. Andersen, S.B. 2009: Hvordan kommer temperaturstigningerne til at påvirke Grønland? In: Ingeniøren, 7. maj, 2009. Ingeniøren, Spørg Scientariat.
16. Ahlstrøm, A.P. 2009: Ice ages and the Greenland Ice Sheet [DIS undervisning af amerikanske college-studerende]. 15 Sep., 2009.
17. Ahlstrøm, A.P. 2009: Klimaprojekt for 7. klasse [Omkring klimaforandringer og indlandsisen. Interview af Line og Signe fra 7.kl., Marbækskolen, Skibby]. 7. dec., 2009
18. Ahlstrøm, A.P. 2009: The Greenland Ice Sheet and Jakobshavn Isbræ in a global warming perspective [Pressebriefing]. 3 July, 2009. Udsendt af Klima og Energiministeriet.
19. Ahlstrøm, A.P. (Interview-person) 2009: Meet the Danes [Optræder som fotostat og med filmklip]. COP15. 7-18 December, 2009. Copenhagen, Denmark. Udenrigsministeriet.
20. Ahlstrøm, A.P. (Interview-person) 2009: Greelands Ice Sheet Melting Faster Than Ever. 13-NOV-09. Seidler, C. (Journalist) Spiegel Online International.
21. Ahlstrøm, A.P. (Interview-person) 2009: Greenland's glaciers under threat from climate change. Allagui, S. (Journalist), AFP.
22. Ahlstrøm, A.P. (Interview-person) 2009: Grönlands Eisschild ist ein erwachender Riese. Seidler, C. (Journalist), Spiegel Online Wissenschaft [http://www.spiegel.de/wissenschaft/natur/0,1518,634515,00.html].

23. Ahlstrøm, A.P. (Interview-person) 2009: Grönlands Eisschild schmilzt so schnell wie nie. 13 Nov. 2009. Seidler, C. (Journalist) Spiegel Online Wissenschaft.
24. Ahlstrøm, A.P. (Interview-person) 2009: Grønlandsk klimasucces for Hedegaard - Klimaministre skal lære af gletsjer. Springborg, S.(Journalist), Berlingske - Web-TV.
25. Ahlstrøm, A.P. (Interview-person) 2009: HARDtalk on the road. Sackur, S. (Journalist), BBC World News – HARDtalk.
26. Ahlstrøm, A.P. (Interview-person) 2009: The Greenland Ice Sheet Is an Awakening Giant. Seidler, C. (Journalist), Spiegel Online International [<http://www.spiegel.de/international/world/0,1518,634629,00.html>].
27. Ahlstrøm, A.P. (Interview-person) 2009: Verdensarv - Gletsjeren 1. Munk, A. (Journalist), DR Aktualitet Web. [[http://www.dr.dk/Undervisning/verdensarv/dk\\_verdensarv/20090827163444.htm?play=%2FForms%2FPublished%2FPlaylistGen.aspx%3Fqid%3D1120057](http://www.dr.dk/Undervisning/verdensarv/dk_verdensarv/20090827163444.htm?play=%2FForms%2FPublished%2FPlaylistGen.aspx%3Fqid%3D1120057)].
28. Ahlstrøm, A.P. (Interview-person) 2009: Verdensarv - Is fortæller om fortiden! Munk, A. (Journalist), DR Aktualitet Web [[http://www.dr.dk/Undervisning/verdensarv/dk\\_verdensarv/20090827163444.htm?play=%2FForms%2FPublished%2FPlaylistGen.aspx%3Fqid%3D1120056](http://www.dr.dk/Undervisning/verdensarv/dk_verdensarv/20090827163444.htm?play=%2FForms%2FPublished%2FPlaylistGen.aspx%3Fqid%3D1120056)].
29. Ahlstrøm, A.P. (Interview-person) 2009: Verdensarv - 12 km is!. Munk, A. (Journalist), DR Aktualitet Web [[http://www.dr.dk/Undervisning/verdensarv/dk\\_verdensarv/20090827163444.htm?play=%2FForms%2FPublished%2FPlaylistGen.aspx%3Fqid%3D1120057](http://www.dr.dk/Undervisning/verdensarv/dk_verdensarv/20090827163444.htm?play=%2FForms%2FPublished%2FPlaylistGen.aspx%3Fqid%3D1120057)].
30. Ahlstrøm, A.P. (Interview-person) 2009: Vores land i forandring. Nyborg, K. (Journalist), KNR.
31. Andersen, S.B. (Interview-person) 2009: Ugens Spørgsmål: Hvorfor stiger verdenshavene? (5) 30. jan., 2009. Ingeniøren, 2.
32. Ahlstrøm, A.P. 2008: A new programme for monitoring the Greenland Ice Sheet [Gæstelærerforedrag i kursus for amerikanske studerende]. University of Washington.
33. Ahlstrøm, A.P. 2008: Den levende indlandsis [Webpræsentation P1 Natursyn. Tilrettelægger: Line Friis Møller].
34. Ahlstrøm, A.P. (Interview-person) 2008: Den levende indlandsis. Møller, L.F. (Journalist) DR- P1 Natursyn.
35. Ahlstrøm, A.P. (Interview-person) 2008: Grønland smelter - en grøn ø i fremtiden. Lykke, K. (Journalist) Kanal København.

36. Ahlstrøm, A.P. (Interview-person) 2008: Verdt å vite spesial Grønlandsisen litt for lang. Tarjem, G. (Journalist) NRK (Radioprogram), 31. december, 2008.
37. Andersen, S.B. 2008: Hvorfor er gletschere blå? Ingeniøren, "Spørg Scientariatet", 2. februar, 2008.
38. Andersen, S.B. 2008: Hvorfor stiger verdenshavene, når isen smelter? Ingeniøren, "Spørg scientariatet" - webside, 4. december, 2008.
39. Andersen, S.B. 2008: Var den lille istid global? Ingeniøren, "Spørg Scientariatet", 13. juni 2008 nr. 24.
40. Ahlstrøm, A.P. 2007: Indlandsisen - en forhistorisk kæmpe på rystende ben. 5. oktober, 2007. Krebs Skole, København.
41. Ahlstrøm, A.P. 2007: Indlandsisen - en forhistorisk kæmpe på rystende ben. 21 marts, 2007. Taarbæk Skole. Taarbæk Kulturförening.
42. Ahlstrøm, A.P. 2007: Indlandsisen - en forhistorisk kæmpe på rystende ben. 10. oktober, 2007. Frederikssund. AOF Frederikssund.
43. Ahlstrøm, A.P. 2007: Indlandsisen - en forhistorisk kæmpe på rystende ben. 2. november, 2007. København. Institut for Geografi og Geologi, Københavns Universitet.
44. Ahlstrøm, A.P., Andersen, S.B., Nielsen, S., Citterio, M. & Mottram, R. 2007: Overvågning af indlandsisen på Grønland. Kulturnatten 2007. 12. oktober, 2007. Geologisk Museum. Kulturnatten 2007 / Geocenteret.
45. Ahlstrøm, A.P., Forsberg, R. & Gravesen, P. 2007: PROMICE - et overvågningsprogram for Grønlands indlandsis [Orienteringsmøde/workshop]. 26. februar, 2007.
46. Thomsen, H.H., Ahlstrøm, A., Larsen, T. & Bennike, O. 2007: Is i opbrud [Oplevelsesarrangement under Kulturnat København]. 12. oktober 2007. Geologisk Museum, København.
47. Ahlstrøm, A.P. & Larsen, T.B. (Interview-person) 2007: Spurtende gletschere kan udløse jordskælv. Willumsen, G. (Journalist) MiljøDanmark 1/2007, 34-37.
48. Ahlstrøm, A.P. & Larsen, T.B. (Interview-personer) 2007: Natursyn - Indlandsis på skrump. 24 februar, 2007. Olesen, J. (Journalist) Danmarks Radio P1.
49. Ahlstrøm, A.P. & Yde, J.C. Interview-personer) 2007: Indlandsisen forsvinder. 6 marts, 2007. Steen, M. (Journalist) MetroXpress, 30-31.
50. Ahlstrøm, A.P., Forsberg, R. & Gravesen, P. (Interview-personer) 2007: Usikker på isen. 2 marts, 2007. Vestergaard, F. (Journalist) Weekendavisen, s. 6.

51. Ahlstrøm, A.P. (Interview-person) 2007: Interview 27. april, 2007. Madsen, K. (Journalist) DR P1 Miljømagasinet.
52. Ahlstrøm, A.P. (Interview-person) 2007: Det underlige vejr. 20 marts, 2007. Borenhoff, P. (Journalist) Det Grønne Område, Forsiden, 2. sektion.
53. Ahlstrøm, A.P. (Interview-person) 2007: Glacier retreat in Greenland - new islands appear. Latham, H. (Journalist) BBC World Service Newshour.
54. Ahlstrøm, A.P. (Interview-person) 2007: Globale klimaforandringer og Indlandsisen [Filmet interview - Skoleprojekt]. 14 marts, 2007.

55. Ahlstrøm, A.P. (Interview-person) 2007: Grønland smelter - Danmark drukner. 17 april, 2007. Rasmussen, R. (Journalist) DR1 TV-Avisen.
56. Ahlstrøm, A.P. (Interview-person) 2007: Grønlands klimabombe under lup. 11 marts, 2007. Andersen, P. (Journalist) Berlingske Tidende, Magasin s. 22.
57. Ahlstrøm, A.P. (Interview-person) 2007: Havene stiger hurtigere end tidligere antaget. 17 april, 2007. Johansen, L. & Eggen, A. (Journalister) DR2 Deadline.
58. Ahlstrøm, A.P. (Interview-person) 2007: Indlandsisens bidrag til det globale havniveau [Telefoninterview - Skoleprojekt]. 14 marts, 2007.
59. Ahlstrøm, A.P. (Interview-person) 2007: Interview om Jakobshavn Gletscher og PROMICE overvågningen af indlandsisen. 26. juni, 2007. TV2 News.
60. Ahlstrøm, A.P. (Interview-person) 2007: Isbjergfabrikken går amok. 3. februar, 2007. Pedersen, M. (Journalist) Ekstrabladet.
61. Ahlstrøm, A.P. (Interview-person) 2007: Løft til Polarforskningen. 18. januar, 2007. Høxbroe, A. (Journalist) DR Radioavisen.
62. Ahlstrøm, A.P. (Interview-person) 2007: Ny ø i Østgrønland. Strøm, J. (Journalist) KNR Grønlands Radio.
63. Ahlstrøm, A.P. (Interview-person) 2007: Polarforskning. 18. januar, 2007. Bo, A. (Journalist) TV2 Nyhederne.
64. Ahlstrøm, A.P., Larsen, T.B. & Khan, S.A. (Interview-personer) 2007: Viden Om - Klimaets Kanarifugl [Deltager i programmet]. Marker, A. & Bendtsen, J. (Journalister) DR2 Viden Om.
65. Ahlstrøm, A.P. (Interview-person) 2007: Gennembrud af isdæmmede sø ved Søndre Strømfjord. 6 september, 2007. Rosing, K. (Journalist) DR Radioavisen.

## Appendix B – Science from the PROMICE team

This appendix details the scientific results produced by PROMICE team members with relation to their activities in PROMICE. This means that commercial activities apart from that dealing with the climate change-hydropower relationship have not been listed. The appendix is divided in three, showing 19 peer-reviewed scientific publications, 52 scientific conference contributions and 9 reports.

### Scientific publications with international peer-review

1. Ahlstrøm, A.P. & the PROMICE project team 2008: A new programme for monitoring the mass loss of the Greenland ice sheet. In: Bennike, O. & Higgins, A.K.(eds): Review of Survey activities 2007. Geological Survey of Denmark and Greenland Bulletin 15, 61-64.
2. Ahlstrøm, A.P., Bøggild, C.E., Olesen, O.B., Petersen, D. & Mohr, J.J. 2007: Mass balance of the Amitsulôq ice cap. Glacier Mass Balance Changes and Meltwater Discharge. IAHS Red Books 318, 107-115 International Association of Hydrological Sciences. IAHS Press.
3. Andersen, M.L., Larsen, T.B., Nettles, M., Elosegui, P., van As, D., Hamilton, G.S., Stearns, L.A., Davis, J.L., Ahlstrøm, A.P., de Juan, J., Ekstrøm, G., Stenseng, L., Khan, S.A., Forsberg, R. & Dahl-Jensen, D. 2010: Spatial and temporal melt variability at Helheim Glacier East Greenland, and its effect on ice dynamics. Journal of Geophysical Research 115, 18 pp. doi:10.1029/2010JF001760.
4. Citterio, M. 2007: Immagini da satellite e bilanci energetici [om Overvågning af Grønlands indlandsis]. Valle d'Aosta figlia dei ghiacci. Fondazione Montagna Sicura - Montagne Sûre. Quart, Aosta. Musumeci, 117-118.
5. Citterio, M., Paul, F., Ahlstrøm, A.P., Jepsen, H.F. & Weidick, A. 2009: Remote sensing of glacier change in West Greenland: accounting for the occurrence of surge-type glaciers. Annals of Glaciology 50(53), 70-80.
6. Dawes, P.R. & van As, D. 2009: An advancing glacier in a recessive ice regime: Berlingske Bræ, North-West Greenland. In: Bennike, O., Garde, A.A. & Watt, W.S. (eds): Review of Survey activities 2009. Geological Survey of Denmark and Greenland Bulletin 20, 79-82.
7. de Juan, J., Elosegui, P., Nettles, M., Larsen, T.B., Davis, J.L., Hamilton, G.S., Stearns, L.A., Andersen, M.L., Ekstrøm, G., Ahlstrøm, A.P., Stenseng, L., Khan, S.A. & Forsberg, R. 2010: Sudden increase in tidal response linked to calving and acceleration at a large Greenland outlet glacier. Geophysical Research Letters 37 (12501), 5 pp., doi:10.1029/2010GL043289.

8. Fausto, R.S., Ahlstrøm, A.P., van As, D., Bøggild, C.E. & Johnsen, S.J. 2009: A new present-day temperature parameterization for Greenland. *Journal of Glaciology* 55(189), 95-105.
9. Fausto, R.S., Ahlstrøm, A.P., van As, D., Johnsen, S.J., Langen, P.L. & Steffen, K. 2009: Improving surface boundary conditions with focus on coupling snow densification and meltwater retention in large-scale ice-sheet models of Greenland. *Journal of Glaciology* 55(193), 869-878.
10. Fausto, R.S., Mayer, C. & Ahlstrøm, A.P. 2007: Satellite derived surface type and melt area of the Greenland ice sheet using MODIS data from 2000 to 2005. *Annals of Glaciology* 46, 35-42.
11. Mernild, S.H., I.M. Howat, Y. Ahn, G.E. Liston, K. Steffen, B.H. Jakobsen, B. Hasholt, B. Fog, and D. van As. 2010. Freshwater flux to Sermilik Fjord, SE Greenland. *Cryosphere* 4, 453-465.
12. Mottram, R., C. Nielsen, A.P. Ahlstrøm, N. Reeh, S.S. Kristensen, E.L. Christensen, R. Forsberg, and L. Stenseng. 2009. A new regional high-resolution map of basal and surface topography for the Greenland ice sheet margin at Paakitsoq, West Greenland. *Annals of Glaciology* 50 (51), 105-111.
13. Nettles, M., Larsen, T.B., Elosegui, P., Hamilton, G.S., Stearns, L.A., Ahlstrøm, A.P., Davis, J.L., Andersen, M.L., de Juan, J., Khan, S.A., Stenseng, L., Ekström, G. & Forsberg, R. 2008: Step-wise changes in glacier flow speed coincide with calving and glacial earthquakes at Helheim Glacier, Greenland. *Geophysical Research Letters* 35, L24503, 5 pp. doi:10.1029/2008GL036127.
14. Nick, F.M., C.J. van der Veen, A. Vieli, and D.I. Benn. 2010. A physically based calving model applied to marine outlet glaciers and implications for the glacier dynamics. *Journal of Glaciology* 56 (199), 781-794.
15. Nick, F.M., A. Vieli, I.M. Howat, and I. Joughin. 2009. Large-scale changes in Greenland outlet glacier dynamics triggered at the terminus. *Nature Geoscience* 2, 110-114.
16. Smelror, M., Ahlstrøm, A., Ekelund, L., Hansen, J.M., Nenonen, K. & Mortensen, A.K. 2008: The Nordic geological surveys: Geology for society in practice. *Episodes* 31(1), 193-200.
17. van As, D. 2010. Changes in temperature and glacier melt from weather station observations in the Melville Bay region of North-West Greenland. *J. Glaciol.* 57 (202), 208-220.

18. van As, D., C.E. Bøggild, S. Nielsen, A.P. Ahlstrøm, R.S. Fausto, S. Podlech, M.L. Andersen. 2009. Climatology and ablation at the South Greenland ice sheet margin from automatic weather station observations. *Cryosphere Disc.* 3 (1), 117-158.
19. Weidick, A. & Bennike, O. 2007: Quaternary glaciation history and glaciology of Jakobshavn Isbræ and the Disko Bugt region, West Greenland: a review. *Geological Survey of Denmark and Greenland Bulletin* 14, 78 pp.

## Scientific presentations & abstracts at conferences

1. Ahlstrøm, A.P. 2007: Monitoring of the Greenland Ice Sheet [Talk: AMAP Coordination Group Meeting]. 2 February, 2007.
2. Ahlstrøm, A.P. 2007: PROMICE - A new monitoring programme for the Greenland Ice Sheet. Nordic Branch Meeting of the International Glaciological Society 2007. 25 October, 2007. Uppsala, Sweden. Uppsala University.
3. Ahlstrøm, A.P. 2007: PROMICE - a new monitoring programme for the Greenland Ice Sheet. GLIMS Workshop. 6 July, 2007. Perugia, Italy. Global Land Ice Monitoring from Space.
4. Ahlstrøm, A.P. 2007: PROMICE - a new programme for monitoring of the Greenland ice sheet. Zackenberg Basic Strategy Workshop. 28 March, 2007. Roskilde. Dansk Polarcenter.
5. Ahlstrøm, A.P. 2007: Results from the AMAP Expert Group on Climate, UV and Ozone [Talk: AMAP Coordination Group Meeting]. 2 February, 2007.
6. Ahlstrøm, A.P. 2010: Ice2sea WP3 Report [Presentation before the Steering Committee]. 27 October, 2010.
7. Ahlstrøm, A.P. 2010: WP3 Foundation and Validation Data. Ice2sea First Open Forum. 16-18 March, 2010. Krakow, Poland. FP7 EU-project Ice2sea.
8. Ahlstrøm, A.P. 2009: Danish Glaciology in Greenland. PARCA Meeting. 30 September - 1 October, 2009. Seattle, U.S.A. National Aeronautics and Space Administration (NASA).
9. Ahlstrøm, A.P., Andersen, S.B., van As, D., Citterio, M, Fausto, R., Forsberg, R., Kristensen, S.S., Stenseng, L., Dall, J., Merryman Boncori, J.P., Christensen, E.L., Petersen, D. & Hanson, S. 2010: Programme for Monitoring of the Greenland Ice Sheet - Recent Developments. IASC Network for Arctic Glaciology Annual Workshop. 8-10 March, 2010. Obergurgl, Austria. Innsbruck University & GEUS.

10. Ahlstrøm, A.P., As, D.v., Andersen, S.B., Boncori, J.M., Citterio, M., Forsberg, R., Kristensen, S.S., Dall, J., Stenseng, L., Petersen, D., Christensen, E.L., Fausto, R.S. & Hanson, S. 2010: Programme for Monitoring of the Greenland Ice Sheet. In: International Glaciological Society Nordic Branch Meeting 2010. 28-30 October, 2010. Copenhagen. Geological Survey of Denmark and Greenland (GEUS). Andersen, S.B. (ed.): Nordic Glaciology. Abstract from Glaciological Society Nordic Branch Meeting, 28-30 October 2010. Danmark og Grønlands Geologiske Undersøgelse Rapport 2010/94, ?.
11. Ahlstrøm, A.P., Mottram, R.H., Nielsen, C., Reeh, N., Andersen, S.B., Kristensen, S.S., Christensen, E.L., Stenseng, L., Forsberg, R. & Stendel, M. 2009: Estimating the future ice sheet hydropower potential in Pakitsq, Ilulissat, West Greenland. Climate and Energy Systems Workshop. 11-12 May, 2009. Copenhagen. DONG Energy. Abstract volume, 1 p.
12. Ahlstrøm, A.P., Mottram, R.H., Nielsen, C., Reeh, N., Andersen, S.B., Kristensen, S.S., Christensen, E.L., Stenseng, L. & Forsberg, R. 2008: Estimating the future ice sheet hydropower potential in Paakitsoq, Ilulissat, West Greenland. AGU Fall Meeting 2008. 15-19 December, 2008. San Francisco, U.S.A. American Geophysical Union. Eos Trans. AGU, 89(53), Fall Meet. Suppl. Abstracts, C23A-0588 only.
13. Ahlstrøm, A.P., Paul, F., Jepsen, H., Citterio, M., Solgaard, A.M. & Andersen, S.B. 2007: Glacier retreat on Disko Island, West Greenland. IUGG 2007 Perugia, XXIV IUGG General Assembly. 2-13 July, 2007. Perugia, Italy. International Union of Geodesy and Geophysics, 1 p.
14. Ahlstrøm, A.P., van As, D., Citterio, M., Andersen, S.B., Fausto, R.S., Andersen, M.L., Forsberg, R., Stenseng, L., Christensen, E.L., Kristensen, S.S. & Hanson, S. 2008: A new programme for monitoring the mass loss of the Greenland ice sheet. IASC-WAG Meeting. 28 January - 1 February, 2008. Obergurgl, Austria. IASC Working group on Arctic Glaciology. Abstract volume, 1 p.
15. Ahlstrøm, A.P., van As, D., Citterio, M., Andersen, S.B., Fausto, R.S., Andersen, M.L., Forsberg, R., Stenseng, L., Christensen, E.L., Kristensen, S.S. & Hanson, S. 2007: A new Programme for Monitoring the Mass Loss of the Greenland Ice Sheet. AGU Fall Meeting 2007. 10-14 December, 2007. San Francisco, U.S.A., American Geophysical Union. Eos Trans. AGU, 88(52), Fall Meet. Suppl., Abstract, C11A-0083.
16. Ahlstrøm, A.P., van As, D., Citterio, M., Gravesen, P., Forsberg, R., Christensen, E.L., Kristensen, S.S., Petersen, D., Andersen, S.B., Stenseng, L., Fausto, R.S. & Hanson, S. 2009: Monitoring the mass loss of the Greenland ice sheet. Climate Change: Global Risks, Challenges & Decisions. 10-12 March, 2009. Copenhagen. University of Copenhagen & International Alliance of Research Universities (IARU). IOP Conference Series: Earth and Environmental Science 6, 012003.

17. Ahlstrøm, A.P., van As, D., Merryman, J.P., Citterio, M., Forsberg, R., Kristensen, S.S., Andersen, S.B., Dall, J., Stenseng, L., Petersen, D., Christensen, E.L., Fausto, R.S. 2010: PROMICE - Monitoring the mass loss of the Greenland Ice Sheet. IASC Network on Arctic Glaciology, Workshop and GLACIODYN meeting. 16-19 februar, 2009. Kananaskis, Canada. IASC Network on Arctic Glaciology. In: Ahlstrøm, A.P. & Sharp, M. (eds): The Dynamics and Mass Budget of Arctic Glaciers. Danmarks og Grønlands Geologiske Undersøgelse Rapport 2010/127, 16-18.
18. Ahlstrøm, A.P., van As, D., Merryman Boncori, J.P., Citterio, M., Forsberg, R., Kristensen, S.S., Andersen, S.B., Dall, J., Stenseng, L., Petersen, D., Christensen, E.L., Fausto, R.S. & Hanson, S. 2009: Monitoring the Mass Loss of the Greenland Ice Sheet. Changes of the Greenland Cryosphere. 25-27 August, 2009. Nuuk, Greenland. National Space Institute, DTU. Abstract volume, 1 p.
19. Ahlstrøm, A.P. & Vieli, A. 2009: Inspiration & Insight – a tribute to Niels Reeh. AGU Fall Meeting 2009. 14-18 December, 2009. San Francisco, U.S.A. American Geophysical Union. Eos Trans. AGU, 90(52), Fall Meet. Suppl., Abstracts, C34A-01.
20. Andersen, M.L., Larsen, T.B., Nettles, M., Elosegui, P., Ahlstrøm, A.P., Stearns, L.A., Hamilton, G.S., Schild, K., Davis, J.L., de Juan, J., Ekstrøm, G., Forsberg, R., Khan, S.A. & Stenseng, L. 2008: Surface Energy Balance Model of Helheim Glacier, Southeast Greenland. AGU Fall Meeting 2008. 15-19 December, 2008. San Francisco, U.S.A. American Geophysical Union. Eos Trans. AGU, 89(53), Fall Meet. Suppl. Abstracts, C42A-05 only.
21. Andersen, M.L., Larsen, T.B., Nettles, M., Elósegui, P., Dahl-Jensen, D. & Ahlstrøm, A. 2008: Analysis of a regional seismic signal from a glacial earthquake at the Helheim glacier, Southeast Greenland. EGU General Assembly 2008. 13-18 April, 2008. Vienna, Austria. European Geosciences Union. Geophysical Research Abstracts 10 [Available on CD-Rom only], 1 p.
22. Andersen, S.B., Ahlstrøm, A., van As, D., Citterio, M., Nielsen, S. & Thomsen, C.T. 2009: The new 'Programme for Monitoring of the Greenland Ice Sheet' data base. AGU Fall Meeting 2009. 14-18 December, 2009. San Francisco, U.S.A. American Geophysical Union. Eos Trans. AGU, 90(52), Fall Meet. Suppl., Abstracts, C31A-0433.
23. Andersen, S.B., van As, D., Citterio, M., Fausto, R., Merryman, J.P., Dall, J., Kristensen, S.S., Forsberg, R., Christensen, E.L. & Petersen, D. 2010: Programme for Monitoring of the Greenland Ice Sheet. Helheim Workshop. 25-26 March, 2010. Copenhagen. Geocenter Danmark / Geologisk Museum. Abstract volume, 20 only.
24. Andresen, C.S. Andersen, T.J., Kuijpers, A., Massé, G., Weckstrøm, K., Ahlstrøm, A.P., Nørgaard-Pedersen, N., Bjørk, A. & Kjær, K.H. 2010: Reconstruction of the latest 100 years of iceberg calving from Helheim Glacier, Southeast Greenland, on basis of marine sediment cores from Sermilik Fjord. AGU Fall Meeting 2010. 13-17

December, 2010. San Francisco, California, U.S.A. American Geophysical Union. [Abstracts - Available on the internet], 1 p.

25. Boncori, J.P.M., Dall, J., Ahlstrøm, A.P. & Andersen, S.B. 2010: Validation and operational measurements with SUSIE - A SAR ice motion processing chain developed within PROMICE. Living Planet Symposium. 28 June, 2010. Bergen, Norway. ESA. Proceedings, 5 only.
26. Bøggild, C.E., Rysgaard, S., Mortensen, J., Kallenborn, R., Truffer, M., Forsberg, R., Ahlstrøm, A.P. & Petersen, D. 2008: Linking Ice Sheet Freshwater Discharge and Marine production in Greenland via Fiord Circulation. 'FreshLink', an Interdisciplinary Project Involving Researchers from Multiple Countries. AGU Fall Meeting 2008. 15-19 December, 2008. San Francisco, U.S.A. American Geophysical Union. Eos Trans. AGU, 89(53), Fall Meet. Suppl. Abstracts, C51B-07.
27. Citterio, M. 2008: Meteorologia glaciale in Groenlandia: dalla ricerca sul cambiamento climatico alle applicazioni nei settori idroelettrico e minerario. Milano, Italy. Università di Milano and Comitato Glaciologico Italiano, 19. June, 2008.
28. Citterio, M., Paul, F., Ahlstrom, A.P., Jepsen, H.F. & Weidick, A. 2008: Remote sensing of glacier change on Disko Island, Nuussuaq Peninsula and Svartenhuk Halvø (West Greenland) since the Little Ice Age. 33rd International Geological Congress 2008. 6-14 August, 2008. Oslo, Norway. International Geological Congress Committee (IGCC). Abstract volume (CD-Rom only), 1 p.
29. Davis, J.L., Elosegui, P., de Juan, J., Nettles, M., Ahlstrøm, A., Andersen, M.L., Ekström, G., Forsberg, R., Hamilton, G., Khan, A., Larsen, T., Stearns, L. & Stenseng, L. 2008: Determining the Timing of Helheim Glacial Earthquakes from Glacier-Based GPS Time Series. AGU Fall Meeting 2008. 15-19 December, 2008. San Francisco, U.S.A. American Geophysical Union. Eos Trans. AGU, 89(53), Fall Meet. Suppl. Abstracts, G53C-03 only.
30. de Juan, J., Elosegui, P., Nettles, N., Davis, J.L., Larsen, T., Ahlstrøm, A., Andersen, M.L., Ekström, G., Forsberg, R., Hamilton, G.S., Khan, S.A., Schild, K.M., Stearns, L.A. & Stenseng, L. 2009: Ocean tides modulation of flow at Helheim Glacier, East Greenland, observed using GPS. AGU Fall Meeting 2009. 14-18 December, 2009. San Francisco, U.S.A. American Geophysical Union. Eos Trans. AGU, 90(52), Fall Meet. Suppl., Abstracts, C11A-01.
31. de Juan, J., Elosegui, P., Nettles, M., Larsen, T.B., Davis, J.L., Ahlstrøm, A. P., Andersen, M.L., Ekström, G., Forsberg, R., Hamilton, G.S., Khan, S.A., Schild, K.M., Stearns, L.A. & Stenseng, L. 2008: Sub-daily glacier flow variations at Helheim Glacier, East Greenland, using GPS. AGU Fall Meeting 2008. 15-19 December, 2008. San Francisco, U.S.A. American Geophysical Union. Eos Trans. AGU, 89(53), Fall Meet. Suppl. Abstracts, C31C-0518, 1 p.

32. Elosegui, P., Davis, J.L., Nettles, M., Larsen, T.B., Ahlstrøm, A.P., de Juan, J., Ekstrøm, G., Forsberg, R., Hamilton, G., Khan, S.A., Andersen, M., Stearns, L. & Stenseng, L. 2007: Geodetic Measurements and Analysis of Glacier Kinematics in East Greenland. AGU Fall Meeting 2007. 10-14 December, 2007. San Francisco, U.S.A., American Geophysical Union. Eos Trans. AGU, 88(52), Fall Meet. Suppl. Abstracts, G33C-02.
33. Elosegui, P., Nettles, M., Davis, J.L., Hamilton, G.S., Larsen, T.B., Gonzalez, I., Malikowski, E., Stearns, L.A., de Juan, J., Hill, E.M., Ahlstrøm, A.P., Andersen, M.L., Ekstrøm, G., Forsberg, R., Khan, S.A., Stenseng, L., Schild, K.M., Okal, M. & Johns, B. 2008: Determining glacier flow with novel polar GPS systems. AGU Fall Meeting 2008. 15-19 December, 2008. San Francisco, U.S.A. American Geophysical Union. Eos Trans. AGU, 89(53), Fall Meet. Suppl. Abstracts, G13B-0657, 1 p.
34. Fausto, R.F., Ahlstrøm, A.P., Bøggild, C.E. & Johnsen, S.J. 2007: New present day temperature parameterization and degree day model for Greenland. AGU Fall Meeting 2007. 10-14 December, 2007. San Francisco, U.S.A., American Geophysical Union. Eos Trans. AGU, 88(52), Fall Meet. Suppl. Abstracts, C51A-0103.
35. Fausto, R.S., Ahlstrøm, A.P. & Johnsen, S.J. 2008: Coupling snow densification and melt-water retention in a large-scale ice sheet model. AGU Fall Meeting 2008. 15-19 December, 2008. San Francisco, U.S.A. American Geophysical Union. Eos Trans. AGU, 89(53), Fall Meet. Suppl. Abstracts, C31B-0488.
36. Hamilton, G.S., Khan, S.A., Schild, K.M., Stearns, L.A., Nettles, M., Ahlstrøm, A.P., Andersen, M.L., Davis, J.L., Ekstrøm, G., Elosegui, P., Forsberg, R., de Juan, J., Larsen, T.B. & Stenseng, L. 2008: Iceberg Calving and flow dynamics at Helheim Glacier, East Greenland, from time-lapse photography. AGU Fall Meeting 2008. 15-19 December, 2008. San Francisco, U.S.A. American Geophysical Union. Eos Trans. AGU, 89(53), Fall Meet. Suppl. Abstracts, C13A-0565, 1 p.
37. Jiskoot H., St.Pierre H., Juhlin D., Citterio M. (2010) – Tidewater Margin Dynamics in Central East Greenland Over two Decades. Eos Trans AGU, Fall Meet. 2010, Suppl, Abstract C23C-0633.
38. Larsen, T.B., Andersen, M.L., Nettles, M., Elosegui, P., Ahlstrøm, A.P., Davis, J.L., de Juan, J., Ekstrøm, G., Forsberg, R., Hamilton, G.A., Khan, S.A., Stearns, L.A. & Stenseng, L. 2008: Glacial earthquakes in Greenland. EGU General Assembly 2008. 13-18 April, 2008. Vienna, Austria. European Geosciences Union. Geophysical Research Abstracts 10 [Available on CD-Rom only], 1 p.
39. Larsen, T.B., Nettles, M., Elosegui, P., Andersen, M.L., Ahlstrøm, A.P., Davis, J.L., de Juan, J., Ekstrøm, G., Forsberg, R., Hamilton, G.S., Khan, S.A., Stearns, L.A., Stensen, L. 2008: East Greenland Glacier Dynamics: An Interdisciplinary study of Helheim Glacier. AGU Fall Meeting 2008. 15-19 December, 2008. San Francisco, U.S.A. American Geophysical Union. Eos Trans. AGU, 89(53), Fall Meet. Suppl. Abstracts, C41A-0479, 1 p.

40. Larsen, T.B., Andersen, M.L., Nettles, M., Elosegui, P., Ahlstrøm, A. P., Davis, J.L., Juan, D. de, Ekstrøm, G., Forsberg, R., Hamilton, G.S., Khan, S.A., Stearns, L.A. & Stenseng, L. 2007: Regional rumble: a seismological study of glacial earthquakes in Greenland. AGU Fall Meeting 2007. 10-14 December, 2007. San Francisco, U.S.A., American Geophysical Union. Eos Trans. AGU, 88(52), Fall Meet. Suppl. Abstracts, G23A-02, 1 p.
41. Larsen, T.B., Jørgensen, T.M., Nettles, M., Ahlstrøm, A.P., Krüger, J., Hanka, W. & Ekstrøm, G. 2007: Regional rumble: glacial eaerthquakes in Greenland. EGU General Assembly 2007. 16-20 April, 2007. Vienna, Austria. European Geosciences Union. Geophysical Research Abstracts 9 [Available on CD-Rom only], 1 p.
42. Long, S.M., Willis, I., Arnold, N. & Ahlstrøm, A.P. 2008: Subglacial Meltwater Drainage at Paakitsoq, West Greenland: Insights From a Distributed, Physically Based Numerical Model. AGU Fall Meeting 2008. 15-19 December, 2008. San Francisco, U.S.A. American Geophysical Union. Eos Trans. AGU, 89(53), Fall Meet. Suppl. Abstracts, C42A-03.
43. Merryman Boncori, J.P., Dall, J., Ahlstrøm, A.P. & Andersen, S.B. 2009: A SAR Ice-Motion Processing Chain in Support of PROMICE (Programme for Monitoring of the Greenland Ice-Sheet). 6th International Workshop on Advances in the Science and Application of SAR Interferometry - Fringe 2009 Workshop. 30 November - 4 December, 2009. Frascati, Italy. European Space Agency. ESA Special Publication SP-677, 1 p.
44. Nettles, M., Elosegui, P., Larsen, T., Davis, J.L., Hamilton, G.S., Stearns, L.A., Andersen, M.L., de Juan, J., Malikowski, E., Gonzalez, I., Okal, N., Johns, B., Ekstrom, G., Ahlstrøm, A., Stenseng, L., Khan, S.A., Schild, K.M., Forsberg, R. & Veitch, S.A. 2009: Geodetic observations of short-time-scale changes in glacier flow at Helheim and Kangerdlugssuaq Glaciers, East Greenland. AGU Fall Meeting 2009. 14-18 December, 2009. San Francisco, U.S.A. American Geophysical Union. Eos Trans. AGU, 90(52), Fall Meet. Suppl., Abstracts, C11A-02.
45. Nettles, M., Larsen, T.B., Elósegui, P., Ahlstrøm, A.P., Davis, J.L., de Juan, J., Ekstrøm, G., Forsberg, R., Hamilton, G.S., Khan, S.A., Andersen, M.L., Stearns, L.A. & Stenseng, L. 2008: Short-time-scale variations in flow speed observed at Helheim Glacier, East Greenland. EGU General Assembly 2008. 13-18 April, 2008. Vienna, Austria. European Geosciences Union. Geophysical Research Abstracts 10 [Available on CD-Rom only], 1 p.
46. Nettles, M., Larsen, T.B., Elosegui, P., Hamilton, G.S., Stearns, L.A., Ahlstrøm, A. P., Davis, J.L., Andersen, M.L., de Juan, J., Khan, S.A., Stenseng, L., Ekstrøm, G., Forsberg, R. & Schild, K.M. 2008: Glacier acceleration, glacial earthquakes, and ice loss at Helheim Glacier, Greenland. AGU Fall Meeting 2008. 15-19 December, 2008. San Francisco, U.S.A. American Geophysical Union. Eos Trans. AGU, 89(53), Fall Meet. Suppl. Abstracts, G23A-02 only.

47. Nettles, M., Larsen, T.B., Elósegui, P., Ahlstrøm, A.P., Davis, J.L., de Juan, J., Ekström, G., Forsberg, R., Hamilton, G.S., Khan, S.A., Andersen, M.L., Stearns, L. & Stenseng, L. 2007: Short-time-scale variations in flow speed and behavior, Helheim Glacier, East Greenland. AGU Fall Meeting 2007. 10-14 December, 2007. San Francisco, U.S.A., American Geophysical Union. Eos Trans. AGU, 88(52), Fall Meet. Suppl. Abstracts, C13A-08.
48. Nick, F.M., C.J. van der Veen, A. Vieli, D. Benn. 2008: A calving law for ice sheet models; Investigating the role of surface melt on dynamics of Greenland outlet glaciers. AGU Fall Meeting 2008. 15-19 December, 2008. San Francisco, U.S.A. American Geophysical Union. Eos Trans. AGU, 89(53), Fall Meet. Suppl. Abstracts, C31C-0513.
49. Paul, F., Citterio, M., Ahlstrom, A.P., Jepsen, H.F. & Weidick, A. 2008: A new inventory of local glaciers and ice caps for part of West Greenland: methods, challenges and change assessment. International Workshop on World Glacier Inventory. 20-21 September, 2008. Lanzhou, China. International Glaciological Society. Abstract volume, 1 p.
50. Petach, T.A., Davis, J.L., Nettles, M., Elosegui, P., de Juan, J., Hamilton, G.S., Larsen, T., Ahlstrøm, A.P., Andersen, M.L., Ekstrom, G., Forsberg, R., Khan, S.A., Schild, K.M., Stearns, L.A. & Stenseng, L. 2009: A Kinematic Model of the Surface Velocity of Helheim Glacier, Greenland. AGU Fall Meeting 2009. 14-18 December, 2009. San Francisco, U.S.A. American Geophysical Union. Eos Trans. AGU, 90(52), Fall Meet. Suppl., Abstracts, C23B-0501.
51. van As, D. & Ahlstrøm, A.P. 2007: A Long-Term Network of Automatic Weather and Ice Monitoring Stations in the Ablation Zone of the Greenland Ice Sheet. AGU Fall Meeting 2007. 10-14 December, 2007. San Francisco, U.S.A., American Geophysical Union. Eos Trans. AGU, 88(52), Fall Meet. Suppl. Abstracts, C11A-0084.
52. van As, D. & Ahlstrøm, A.P. 2008: Mass-balance measurements from a network of automatic weather stations in the ablation zone of the Greenland Ice Sheet. AGU Fall Meeting 2008. 15-19 December, 2008. San Francisco, U.S.A. American Geophysical Union. Eos Trans. AGU, 89(53), Fall Meet. Suppl. Abstracts, C31B-0494.

## Reports

1. Ahlstrøm, A.P. 2010: Previous glaciological activities relating to hydropower in Johan Dahl Land, South Greenland. Glaciological investigation. Danmarks og Grønlands Geologiske Undersøgelse Rapport 2010/97, 56 pp.

2. Ahlstrøm, A.P. 2007: Previous glaciological activities related to hydropower at Paakitsoq, Ilulissat, West Greenland. Danmarks og Grønlands Geologiske Undersøgelse Rapport 2007/25, 42 pp.
3. Ahlstrøm, A.P., Mottram, R., Nielsen, C., Reeh, N. & Andersen, S.B. 2008: Evaluation of the future hydropower potential at Paakitsoq, Ilulissat, West Greenland. Danmarks og Grønlands Geologiske Undersøgelse Rapport 2008/31, 16 pp.
4. Ahlstrøm, A.P., Mottram, R., Nielsen, C., Reeh, N. & Andersen, S.B. 2008: Evaluation of the future hydropower potential at Paakitsoq, Ilulissat, West Greenland. Technical Report. Danmarks og Grønlands Geologiske Undersøgelse Rapport 2008/37, 50 pp.
5. Ahlstrøm, A.P. & Sharp, M. (eds) 2010: The Dynamics and Mass Budget of Arctic Glaciers. Extended abstracts Workshop and Glaciodyn meeting, 16-19 Feb 2009, Kananaskis (Canada) IASC Network on Arctic Glaciology. Danmarks og Grønlands Geologiske Undersøgelse Rapport 2010/127, 73 pp.
6. Ahlstrøm, A.P., van As, D., Citterio, M., Andersen, S.B., Nick, F.M., Gravesen, P., Edelvang, K., Fausto, R.S., Kristensen, S.S., Christensen, E.L., Merryman Boncori, J.P., Dall, J., Forsberg, R., Stenseng, L., Hanson, S., Petersen, D. 2009: PROMICE 2007 - 2008. Status Report for the first two years of the Programme for Monitoring of the Greenland Ice Sheet. Danmarks og Grønlands Geologiske Undersøgelse Rapport 2009/77, 74 pp.
7. Andersen, S.B. (ed.) 2010: Nordic Glaciology. Abstract from Glaciological Society Nordic Branch Meeting, 28-30 October 2010. Danmarks og Grønlands Geologiske Undersøgelse Rapport 2010/94, 81 pp.
8. Bergström, S., Jóhannesson, T., Adalgeirsdóttir, G., Ahlstrøm, A., Andreasson, L.M., Andréasson, J., Beldring, S., Björnsson, H., Carlsson, B., Crochet, P., de Woul, M., Einarsson, B., Elvehøy, H., Flowers, G.E., Graham, P.L., Gröndal, G.O., Gudmundsson, S., Hellström, S., Hock, R., Holmlund, P., Jónsdóttir, J.F., Pálsson, F., Radic, V., Reeh, N., Roald, L.A. & Rogozova, S., 2007: Impacts of climate change on river runoff, glaciers and hydropower in the Nordic area. Joint final report from the CE Hydrological Models and Snow and Ice Groups, CE-6. Hydrological Service - National Energy Authority, Reykjavík, Iceland, 40 pp.
9. Mottram, R., Hanson, S., Kristensen, S.S., Ahlstrøm, A.P., Hvidegaard, S.M., Skourup, H., Sørensen, L.S., Nielsen, J.E. & Stenseng, L. 2009: Ice sheet surface and basal topography from radar and lidar, West Greenland. Danmarks og Grønlands Geologiske Undersøgelse Rapport 2009/24, 25 pp.